Title
The Role of the Tumor Microenvironment and Epithelial-Mesenchymal Plasticity in Prostate Cancer Progression and Metastasis

Author
Ruscetti, Marcus Andrew

Publication Date
2015

Peer reviewed|Thesis/dissertation

UNIVERSITY OF CALIFORNIA

Los Angeles

The Role of the Tumor Microenvironment and Epithelial-Mesenchymal Plasticity in Prostate Cancer Progression and Metastasis

A dissertation submitted in partial satisfaction of the

requirements for the degree Doctor of Philosophy

in Molecular Biology

by

Marcus Andrew Ruscetti

2015

ABSTRACT OF THE DISSERTATION

The Role of the Tumor Microenvironment and Epithelial-Mesenchymal Plasticity in Prostate Cancer Progression and Metastasis

by

Marcus Andrew Ruscetti

Doctor of Philosophy in Molecular Biology

University of California, Los Angeles, 2015

Professor Lily Wu, Co-Chair

Professor Hong Wu, Co-Chair

PTEN is one of the most commonly deleted tumor suppressor genes in human prostate cancer. Our group previously demonstrated that *Pten* deletion in the murine prostate epithelium recapitulates the disease progression seen in human prostate cancer, culminating in invasive adenocarcinoma. In addition to *Pten* loss endowing prostate cells with enhanced proliferative capacity, we found that *Pten* loss also led to the upregulation of inflammatory pathways, including *Csf-1* and *Il1b* expression, within the prostate epithelium. These inflammatory cytokines recruit myeloid-derived suppressor cells (MDSCs) into the prostate, which subsequently promote an immune-suppressive tumor microenvironment and thereby facilitate tumor progression. Targeting immune-responsive pathways with the CSF-1R inhibitor GW2580 successfully inhibits MDSC infiltration and delays tumor progression.

As *Pten* deletion alone does not produce distant macrometastasis, we surveyed additional pathways altered in human metastatic prostate cancer, and found that the RAS/MAPK pathway was significantly elevated in metastatic lesions. Indeed, when we combined *Pten* deletion with *Kras* activation in the prostate epithelium (*Pb-Cre*$^{+/-}$*;Pten*$^{L/L}$*;Kras*$^{G12D/+}$) (*CPK*), we observed macrometastasis to the lungs and liver. Interestingly, within the prostate, we observed an epithelial-mesenchymal transition (EMT) phenotype, accompanied by significant upregulation of the EMT transcription factor Snail. Importantly, genetic deletion of *Snail* in *CPK* mice prevented distant macrometastasis, providing a mechanistic link between EMT and metastasis.

To study the dynamic regulation of the EMT process, we crossed *CPK* mice with *Vimentin-GFP* reporter mice (*CPKV*), and were able to isolate populations of epithelial, EMT, and mesenchymal-like prostate tumor cells. We demonstrate that EMT and mesenchymal-like tumor cells have enhanced stem-like and tumor-initiating capacities and exhibit cellular plasticity *in vivo*. HMGA2, a chromatin remodeling protein, is significantly upregulated in EMT and mesenchymal-like tumor cells, as well as in human metastatic castration-resistant prostate cancer (mCRPC). Knockdown of Hmga2, or suppressing Hmga2 expression with the HDAC inhibitor LBH589, inhibits epithelial-mesenchymal plasticity and stemness activities *in vitro* and dramatically reduces prostate tumor burden and distant metastasis *in vivo*. Importantly, LBH589 in combination with castration significantly prolongs survival by targeting castration-resistant mesenchymal-like tumor cells and preventing mCRPC. LBH589 treatment in combination with androgen deprivation therapy may therefore be a promising treatment for patients with mCRPC.

The dissertation of Marcus Andrew Ruscetti is approved.

Robert E. Reiter

Steven M. Dubinett

Owen N. Witte

John J. Colicelli

Lily Wu, Committee Co-Chair

Hong Wu, Committee Co-Chair

University of California, Los Angeles

2015

DEDICATION

To my parents, Drs. Sandra and Francis Ruscetti, for providing me with the tools necessary to pursue my wildest dreams and conquer the depths of my imagination, and for teaching me to respect everyone but question everything.

To Alyson, for believing in me even when I had forgotten how to believe in myself.

TABLE OF CONTENTS

LIST OF FIGURES

Chapter 1

Chapter 2

Chapter 3

Chapter 4

Chapter 6

ACKNOWLEDGEMENTS

I would like to first and foremost thank my advisor and mentor, Dr. Hong Wu, for all of her support over the past 5 years. Hong pushed me to become the very best scientist I could be, and taught me to not be afraid to address and pursue the hardest and most important scientific problems. Her enthusiasm for science and discovery is infectious and inspiring, and she has been a great role model for me to emulate. Hong successfully prepared me for my future in academia, and I will always remain eternally grateful for the training she has given me.

I want to thank my committee members, Drs. Lily Wu, Robert Reiter, Steven Dubinett, Owen Witte, and John Colicelli for their insightful comments and support of my research and career goals over the years. I have benefited greatly from your expertise.

One of the most important lessons I learned from graduate school is that great science does not exist without great collaboration. I owe a great deal of my scientific and technical knowledge to current and former members of the Hong Wu lab, especially to Dr. David Mulholland, who was my mentor in the lab for my first few years of graduate school. Thank you for showing me how to do mouse work, enlightening me on the important problems in the prostate cancer field, and listening to my ideas, the good, the bad, and the ugly alike. I would also like to thank Dr. Mulholland, Dr. Alex Garcia, and Dr. Naoko Kobayashi for providing me with expert training in flow cytometry, cell culture, and a variety of surgical techniques, as well as for leading the research studies in Chapters 2, 3, and 4, respectively. Special thanks are also in order to Linh Tran and Suzanne Schubbert, who provided me with invaluable and lasting scientific and career

advice over the years, and to Ying Wang for being our lab/mouse Mom and reminding me to always “believe.” To the rest of the group, it has been a pleasure to work alongside you.

I am grateful to my two exceptional undergraduate students, Bill Quach and Eman Dadashian, for their dedication, hard work, reliability, and enthusiasm. I could not have asked for two better students or people. They both went above and beyond what was asked of them, and greatly contributed to the success of my research. I could not have accomplished this without either of them. I hope they have learned as much from me as I have learned from them. When you both are famous physicians, please remember me.

To my former lab mates at NCI-Frederick and at Oxford University, thanks for teaching me how much fun science can be. It was with you that my passion for science first originated.

Importantly, I would like to also thank my friends and family for the tremendous support and encouragement they have given me over the past 5 years, especially my fellow graduate student colleagues who I have endured the successes and failures of graduate school life alongside.

Chapter 1 is a version of “Ruscetti, M. & Wu, H. (2013). PTEN in Prostate Cancer. In D.J. Tindall, *Prostate Cancer: Biochemistry, Molecular Biology, and Genetics, Protein Reviews, 16* (pp. 87-137). New York: Springer.”

Chapter 2 is a reprint of “Garcia, A.J., Ruscetti, M., Arenzana, T.L., Tran, L.M., Bianchi-Frias, D., Sybert, E., Priceman, S.J., Wu, L., Nelson, P.S., Smale, S.T., and Wu, H. (2014). *Pten null*

prostate epithelium promotes localized myeloid-derived suppressor cell expansion and immune suppression during prostate cancer initiation and progression. *Mol. Cell Biol.* 34: 2017-28." H. Wu was the PI. A.J. Garcia and M. Ruscetti contributed to the concept and design, the development of the methodology, and writing, reviewing, and revising the manuscript. A.J. Garcia, M. Ruscetti, T.L. Arenzana, D. Bianchi-Frias, E. Sybert, and S.J. Priceman contributed to the acquisition of data. A.J. Garcia, M. Ruscetti, T.L. Arenzana, L.M. Tran, and S.J. Priceman contributed to analysis and interpretation of the data.

Chapter 3 is a reprint of "Mulholland, D.J., Kobayashi, N., Ruscetti, M., Zhi, A., Tran, L.M., Huang, J., Gleave, M., and Wu, H. (2012). *Pten* loss and RAS/MAPK activation cooperate to promote EMT and metastasis initiated from prostate cancer stem/progenitor cells. *Cancer Res*. 72:1878-89." H. Wu was the PI. D.J. Mulholland contributed to the concept and design, the development of the methodology, and writing, reviewing, and revising the manuscript. D.J. Mulholland, N. Kobayashi, M. Ruscetti, A. Zhi, L.M. Tran, and M. Gleave contributed to the acquisition of data. D.J. Mulholland, N. Kobayashi, M. Ruscetti, L.M. Tran, and J. Huang contributed to analysis and interpretation of the data.

Chapter 4 is a version of "Kobayashi, N., Ruscetti, M., Tran, L.M., Mulholland, D.J., Li, Y., Wang, Y., Quach, B., Huang, J., Gridley, T., and Wu, H. The PI3K and MAPK pathways promote prostate cancer metastasis by inducing SNAIL-mediated epithelial-mesenchymal transition (EMT). (Manuscript submitted for publication)" H. Wu was the PI. N. Kobayashi and M.Ruscetti contributed to the concept and design, the development of the methodology, and writing, reviewing, and revising the manuscript. N. Kobayashi, M. Ruscetti, D.J. Mulholland, Y.

Li, Y. Wang, and B. Quach contributed to the acquisition of data. N. Kobayashi, M. Ruscetti, L.M. Tran, D.J. Mulholland, and J. Huang contributed to analysis and interpretation of the data.

Chapter 5 is a version of "Ruscetti, M., Quach, B., Dadashian, E.L., Mulholland, D.J., and Wu, H. (2015) Tracking and functional characterization of epithelial-mesenchymal transition and mesenchymal tumor cells during prostate cancer metastasis. *Cancer Res.*, 10.1158/0008-5472.CAN-14-3476." H. Wu was the PI. M. Ruscetti contributed to the concept and design, the development of the methodology, and writing, reviewing, and revising the manuscript. M. Ruscetti, B. Quach, E.L. Dadashian, and D.J. Mulholland contributed to the acquisition, analysis, and interpretation of the data.

Chapter 6 is a version of "Ruscetti, M., Dadashian, E.L., Guo, W., Quach, B., Mulholland, D.J., Park, J.W., Tran, L.M., Kobayashi, N., Bianchi-Frias, D., Xing, Y., Nelson, P.S., and Wu, H. HDAC inhibition impedes HMGA2-controlled epithelial-mesenchymal plasticity and suppresses metastatic, castration-resistant prostate cancer. (Manuscript submitted for publication)" H. Wu was the PI. M.Ruscetti contributed to the concept and design, and the development of the methodology. M.Ruscetti, E.L. Dadashian, and W. Guo contributed to writing, reviewing, and revising the manuscript. M. Ruscetti, E.L. Dadashian, W. Guo, B. Quach, D.J. Mulholland, J.W. Park, N. Kobayashi, and D. Bianchi-Frias contributed to the acquisition, analysis, and interpretation of the data.

I would like to finally thank my funding source, the NIH T32 CA009056 Training Grant, for supporting my research and travel to scientific conferences.

VITA

Education

University of Virginia, College of Arts & Sciences

2004-2008 Bachelor of Arts in Biology

Johns Hopkins University, School of Education

2008-2010 Master of Arts in Teaching (MAT) in Secondary Science

Positions

2003-2005 Research student, Laboratory of Dr. Kathy Jones, National Cancer Institute-Frederick, Frederick, Maryland

2007 Research student, Laboratory of Dr. Sten-Erik Jacobsen, Weatherall Institute, Oxford University, UK

2008-2009 Science teacher, Collington Square School, Baltimore, Maryland

2010 Biology/Chemistry teacher, Milford Mill Academy, Baltimore, Maryland

2010-2015 Graduate Student Researcher, Laboratory of Dr. Hong Wu, Molecular Biology Institute, UCLA

2012-2013 Teaching Assistant, UCLA

2012-2015 Committee Member, IMED Seminar Committee, UCLA

Honors/Award

2012-2015 NIH T32 CA009056 Grant Recipient

2014 Paul D. Boyer Outstanding Teaching Award

Publications

1. Mulholland, D.J., Kobayashi, N., **Ruscetti, M.**, Zhi, A., Tran, L.M., Huang, J., Gleave, M., and Wu, H. (2012). *Pten* loss and RAS/MAPK activation cooperate to promote EMT and metastasis initiated from prostate cancer stem/progenitor cells. *Cancer Res*. 72:1878-89.

2. **Ruscetti, M.** & Wu, H. (2013). PTEN in Prostate Cancer. In D.J. Tindall, *Prostate Cancer: Biochemistry, Molecular Biology, and Genetics, Protein Reviews, 16* (pp. 87-137). New York: Springer.

3. Garcia, A.J.*, **Ruscetti, M.***, Arenzana, T.L., Tran, L.M., Bianchi-Frias, D., Sybert, E., Priceman, S.J., Wu, L., Nelson, P.S., Smale, S.T., and Wu, H. (2014). *P*ten null prostate epithelium promotes localized myeloid-derived suppressor cell expansion and immune suppression during prostate cancer initiation and progression. *Mol. Cell Biol.* 34: 2017-28.

4. **Ruscetti, M.**, Quach, B., Dadashian, E.L., Mulholland, D.J., and Wu, H. (2015) Tracking and functional characterization of epithelial-mesenchymal transition and mesenchymal tumor cells during prostate cancer metastasis. *Cancer Res.*, 10.1158/0008-5472.CAN-14-3476.

5. Kobayashi, N., **Ruscetti, M.**, Tran, L.M., Mulholland, D.J., Li, Y., Wang, Y., Quach, B., Huang, J., Gridley, T., and Wu, H. PI3K and MAPK pathways promote prostate cancer metastasis by inducing SNAIL-mediated epithelial-mesenchymal transition (EMT). (Manuscript submitted for publication)

6. **Ruscetti, M.**, Dadashian, E.L., Guo, W., Quach, B., Mulholland, D.J., Park, J.W., Tran, L.M., Kobayashi, N., Bianchi-Frias, D., Xing, Y., Nelson, P.S., and Wu, H. HDAC inhibition impedes HMGA2-controlled epithelial-mesenchymal plasticity and suppresses metastatic, castration-resistant prostate cancer. (Manuscript submitted for publication)

***** Both authors contributed equally to this work

Chapter 1:

Pten in Prostate Cancer

Introduction

Although partial or complete loss of chromosome 10 in brain, bladder, and prostate cancers was identified as early as 1984 (1), it was not until 1997 that three independent groups, through mapping of mutations on chromosome 10 and cloning of a novel phosphatase, identified a tumor suppressor gene at the 10q23.31 locus named by different laboratories as the phosphatase and tensin homolog (PTEN), mutated in multiple advanced cancers 1 (MMAC1) and TGF-β-regulated and epithelial cell-enriched phosphatase 1 (TEP1) (2-4). PTEN is a non-redundant phosphatase that antagonizes the phosphatidylinositol 3-kinase (PI3K)/AKT signaling pathway, one of the most important and well-studied cancer promoting pathways. As PTEN is the only known 3' phosphatase counteracting the PI3K/AKT pathway, it is not unexpected that loss of PTEN has a significant impact on prostate cancer progression. Indeed, loss of heterozygosity (LOH) of *PTEN* occurs frequently in many advanced stage sporadic tumors, including approximately 60% of advanced prostate cancers (2). Germline PTEN gene mutations account for the majority (80%) of cases of Cowden Syndrome, an autosomal dominant multiple hamartoma syndrome that leads to an increased propensity for patients to develop breast (5), endometrial (5, 6), and thyroid cancers (7-9). However, prostate cancer has not been associated with Cowden Syndrome and germline PTEN loss (10, 11), perhaps providing credence to the understanding that loss of PTEN is a late event in prostate carcinogenesis (12, 13).

In this chapter, we will review PTEN structure, function and regulation. The consequences of loss of PTEN regulation and function in different stages of prostate cancer development, as well as the potential use of PTEN loss as a biomarker for prostate cancer

prognosis and prediction of patient responses to PI3K/AKT/mTOR pathway inhibitors, will also be addressed.

PTEN Structure and Function

PTEN Structure

The *PTEN* gene comprises nine exons and encodes a protein of 403 amino acids (14). The amino acid sequence of the PTEN tumor suppressor is considerably homologous to dual-specific protein phosphatases and tensin, a chicken cytoskeletal protein (2). The crystal structure of PTEN revealed an expanded active site pocket for binding to its substrates and a C2 domain, which mediates membrane attachment of cell signaling proteins. Three other functional domains have also been identified: a short phosphatidylinositol-4,5-bisphosphate (PIP2) binding domain on the N-terminus, and PEST sequences and a PDZ interaction motif on the C-terminal tail that regulate protein stability and binding to PDZ domain-containing proteins, respectively (15). The binding of PIP2 to PTEN produces a conformational change in the enzyme, leading to allosteric activation (16). The positive charge of PTEN's substrate binding pocket is also important for accommodating larger acidic substrates such as phosphoinositides. The PTEN phosphatase domain is evolutionarily conserved, and is the recipient of 40% of its cancer-associated mutations, which occur most commonly through either a C124S mutation that abolishes both lipid and protein phosphatase activity, or a G129E mutation that abrogates only its lipid phosphatase activity (17-19). Although the phosphatase domain is responsible for PTEN's physiological activity, other PTEN tumorigenic mutations occur on the C-terminal C2 domain

and tail sequence, highlighting an important role of the C-terminus in maintaining PTEN protein stability (20, 21). The fact that tumor-associated mutations occur in all PTEN functional domains indicates that each of these regions is biologically relevant to PTEN function. In prostate cancer, PTEN loss most commonly results from a somatic mutation generated through copy number loss rather than point mutation (22), although recent exome sequencing has identified several recurrent mutations in the PTEN gene (23, 24).

PTEN and Regulation of the PI3K/AKT/mTOR Pathway

PI3K/AKT signaling plays a critical role in regulating growth responses, homeostasis and longevity. At the cellular level, the PI3K/AKT pathway controls cell growth, migration, differentiation, and survival. Activation of the PI3K/AKT pathway is also frequently detected in human cancers (25). PTEN is a unique lipid phosphatase that removes the phosphate from the D3 position of phosphatidylinositol-3,4,5-triphosphate (PIP3), a product of PI3K, thus directly antagonizing the action of PI3K (19, 26, 27). PIP3 accumulation at the plasma membrane through PI3K activity results in recruitment and activation of important kinases involved in cell growth and survival, including phosphoinositide-dependent kinase-1 (PDK1) and AKT family members, via their pleckstrin homology (PH) domains (19, 26, 27). In this manner, PTEN negatively regulates the PI3K/AKT pathway by inhibiting downstream AKT activation.

AKT isoforms (AKT1, AKT2, AKT3) are activated by phosphorylation at two different residues: Thr308 by PDK1 (28), and Ser473 by mammalian target of rapamycin complex 2 (mTORC2) (29). Activated AKT drives cell survival, proliferation, growth, angiogenesis, and

metabolism by phosphorylating downstream signaling proteins, which include inhibitory phosphorylation of GSK3β, FOXO, BAD, p21, p27, and PGC1, and activating phosphorylation of mammalian target of rapamycin complex 1 (mTORC1), IKK-β, MDM2, ENTPD5, SREBP1C, AS160, and SKP2 (29, 30). AKT promotes cell cycle progression and proliferation by directly inhibiting p21 and p27 and alleviating GSK3β-induced cyclin D1 degradation. Moreover, inhibition of GSK3β has been shown to prevent the degradation of β-catenin, which can further stabilize cyclin D1 mRNA and promote G_1-phase/S-phase progression (30, 31). Activation of AKT also helps evade apoptosis directly by phosphorylation of the pro-apoptotic protein BAD (32). In this regard, it is not surprising that re-expression of WT PTEN in *PTEN* null prostate cancer cell lines leads to apoptosis (33).

AKT directly activates the mTOR pathway by phosphorylating TSC2, which dismantles the TSC1/TSC2 complex that normally inhibits Rheb. Rheb, now free from TSC1/TSC2 inhibition, can stimulate the phosphotransferase activity of mTORC1 (34). AKT may also activate mTORC1 by phosphorylating and inhibiting PRAS40, a negative regulatory subunit of the mTORC1 complex (29, 35). Active mTORC1 phosphorylates p70 ribosomal protein S6 kinase (S6K) and 4E-binding protein (4EBP1), which in turn initiates cap-dependent protein translation (36). Therefore, as a consequence of PTEN inactivation, PI3K/AKT/mTOR pathway activation leads to enhanced translation of mRNAs involved in protein synthesis, cell growth and proliferation.

Interestingly, mTORC1 signaling also triggers a negative feedback loop that inhibits the PI3K/AKT pathway. This occurs through the phosphorylation and degradation of insulin

receptor substrate 1 (IRS1), a crucial effector of insulin signaling, by S6K (37, 38). Conversely, inhibition of mTORC1 results in hyperactivation of the PI3K/AKT pathway, as well as increased signaling through the Ras/MAPK pathway. The growth factor receptor GRB10 is a novel mTORC1 substrate that mediates feedback inhibition of the PI3K/AKT and Ras/MAPK pathways by direct inhibition of IRS proteins (39, 40). In contrast, PTEN loss can reverse mTORC1-mediated negative feedback inhibition of the PI3K/AKT/mTOR pathway by activating both the upstream and downstream arms of the PI3K/AKT/mTOR pathway. Therefore, effective inhibition of tumors with PTEN loss will require inhibition of both mTORC1 and other signaling molecules upstream in the pathway, including PI3K and AKT.

PTEN and metabolism

Recent studies have suggested that metabolic reprogramming is a requirement for the rapid cell proliferation of cancer cells. As opposed to differentiated and non-proliferating cells, which primarily utilize mitochondrial oxidative phosphorylation to generate the ATP needed for cellular processes, rapidly proliferating cells, including stem cells and cancer cells, tend to convert most glucose to lactate, even in the presence of oxygen, through aerobic glycolysis and a phenomenon known as the Warburg effect (41). In this way, cancer cells exhibit high rates of glycolysis with increased glucose and glutamine uptake and lactate production, as well as increased biosynthesis of lipids, amino acids, and nucleic acids, macromolecules that are needed to compensate for anabolic growth (42).

The PI3K/AKT pathway plays a key role in the regulation of glucose metabolism given its position downstream of the insulin receptor. The PI3K/AKT pathway enhances insulin-mediated glucose uptake and membrane translocation of the glucose transporter GLUT1, which has been positively correlated with higher tumor grades and Gleason scores (43), by way of mTORC1 activation and cap-dependent translation (44), and GLUT4, by way of inhibition of AS160 (45). As PI3K/AKT signaling leads to increased production of HIF1α (46, 47), a transcription factor that regulates the transcription of the *Glut-1* gene (48), it is likely that both the PI3K/AKT pathway and HIF1α activation contribute to higher levels of GLUT1 and enhanced glucose uptake (49). Increased HIF1α expression also upregulates expression of vascular endothelial growth factor (VEGF), a potent stimulator of angiogenesis that may further promote tumor metabolism by facilitating access to nutrients in the blood (50). Conversely, stimulation of the PI3K/AKT pathway blocks gluconeogenesis by preventing both FOXO and PGC1α activation (51, 52). AKT may indirectly activate glycolysis as well by directly phosphorylating PKF2, whose product, Fru-1,6-P2, is a potent allosteric activator of the glycolysis rate-controlling enzyme PFK1 (28, 53). A recent study using siRNA mediated gene silencing in metastatic prostate cancer cell lines revealed that PFKFB4, an isoform of PFK2 that is required for glycolysis, is essential for survival of prostate tumor cells, and that ablation of PFKFB4 inhibits tumor growth in a xenograft model (54).

In comparison to other epithelial cancers, primary prostate cancers are less glycolytic and, therefore, not sensitive to FDG-PET imaging until reaching the metastatic stage (55, 56). On the other hand, prostate cancer is known to be lipogenic, and C-11-acetate and F18-choline have been used, although in limited scale, in prostate cancer imaging (55, 57). Recent studies suggest

that the PI3K/AKT pathway can regulate lipid metabolism as well to further promote anabolic growth through the Warburg effect. Upon PTEN loss and through inhibition of GSK3β, the PI3K/AKT axis activates the transcription factor SREBP1C, which in turn transcribes genes involved in cholesterol and fatty acid biosynthesis (58, 59). PTEN has also been shown to regulate the synthesis of long chain saturated fatty acids by inducing the downregulation of fatty acid synthase (FAS), a lipogenic enzyme overexpressed in many human cancers, including prostate cancer, in a lipid-phosphatase dependent manner (60). Therefore, PTEN loss in prostate cancer cells may increase FAS protein expression, which is elevated in tumors with a poor prognosis (61). Collectively, these data indicate that both upstream and downstream components of the PTEN regulated PI3K/AKT/mTOR pathway are involved in the metabolic reprogramming required to sustain the rapid growth and proliferation of tumor cells by 1) increasing glucose metabolism via aerobic glycolysis and 2) promoting macromolecule biosynthesis via lipogenesis.

The recent creation of a mouse model with global PTEN overexpression, the "Super-PTEN" model, has demonstrated that PTEN elevation at the organism level results in diminished glucose and glutamine uptake and increased mitochondrial oxidative phosphorylation, resulting in a reversion to a more healthy metabolism (62). PTEN elevation in this model coordinates this metabolic shift by negatively regulating both PI3K/AKT-dependent pathways, such as mTORC1 activation of PKM2, a controller of glycolytic flux (63), and PI3K/AKT–independent pathways, such as degradation of PFKFB3, a key regulator of glycolysis (64), through APC/Cdh1 activation (62). Interestingly, these "Super-PTEN" mutants are resistant to oncogenic transformation, demonstrating that inhibition of the metabolic reprogramming to aerobic glycolysis through PTEN expression or inactivation of the PI3K/AKT pathway may be sufficient

to obstruct tumor propagation (62). These outcomes suggest that PTEN elevation may indeed be an attractive option for cancer prevention and therapy.

PTEN in the Nucleus

It was initially assumed that PTEN is exclusively localized in the cytoplasm. However, following the discovery that PTEN contains dual nuclear localization signal-like sequences (65), it has been well recognized that PTEN can localize to the nucleus, and recent studies have illustrated the important functions of nuclear PTEN in regulating cell cycle progression and genomic integrity. Indeed, not only is there a marked reduction in nuclear PTEN in rapidly cycling cancer cell lines in comparison to resting or differentiated cells (66-69), but absence of nuclear PTEN has also been associated with reduced overall survival in prostate cancer patients (70).

Oxidative stress is one of the physiological stimuli that regulates the accumulation of nuclear PTEN (71). Oxidative stress inhibits PTEN nuclear export, a process dependent on phosphorylation at Ser380. Nuclear PTEN, independent of its phosphatase activity, can regulate p53 stability and transcriptional activity (72, 73), leading to p53-mediated G_1 growth arrest, cell death and reduction of reactive oxygen species (ROS) production (71). Nuclear PTEN is also sufficient to reduce human prostate cancer xenograft growth *in vivo* in a p53-dependent manner (71), suggesting a unique role of nuclear PTEN to arrest and protect cells following oxidative damage and to regulate prostate cancer development.

Nuclear PIP3, unlike cytoplasmic PIP3, is insensitive to the lipid phosphatase activity of PTEN, implying nuclear functions for PTEN beyond its role as a negative regulator of the PI3K/AKT pathway (74). This is at odds with another finding that forced nuclear expression of PTEN can reduce nuclear levels of P-AKT, although it was not demonstrated whether this mechanism occurred through a PI3K-dependent or independent pathway (75). One proposed function of PTEN in the nucleus is to induce G_1 cell cycle arrest in part by reducing cyclin D1 levels through its protein phosphatase activity (76), or through controlling MAPK signaling (77). Nuclear PTEN maintains chromosomal stability by physically associating with centromeres through docking onto CENP-C, a centromeric binding protein (78). Moreover, nuclear PTEN, through a phosphatase-independent mechanism, enhances DNA repair through increasing the activity of RAD51, a protein implicated in double strand break (DSB) repair (78). Not surprisingly, PTEN-null cells develop spontaneous DNA DSBs at a higher rate (78). Cytoplasmic PTEN can also contribute to DSB repair by inhibiting AKT-dependent sequestration of the cell cycle regulator CHK1 in the cytoplasm (79). In this fashion, PTEN helps maintain the G_2/S cell cycle checkpoint, and likewise prevents genomic instability and DSBs. As PTEN loss leads to homologous recombination defects in human tumor cells through downregulation of RAD51 and CHK1 in the nucleus, tumor cells display increased sensitivity to inhibitors of the PARP (80-82). These findings provide evidence for the use of PARP inhibitors in patients with PTEN deficient prostate cancer. However, a recent study of clinical prostate cancer specimens suggests that PTEN loss is not associated with reduced RAD51 mRNA or protein expression in primary prostate cancer, and that PTEN-deficient cells only exhibit mild sensitivity to PARP inhibition, casting doubt on whether PTEN is a useful biomarker for response to PARP inhibitors in prostate cancer (83).

Nuclear PTEN directly increases the anti-tumor and E3 ligase activity of APC/C through a phosphatase independent mechanism by promoting the association of APC/C with its activator CDH1 (84). The APC/C-CDH1 complex contains tumor suppressive activities that degrade oncogenic proteins such as PLK1 and Aurora kinases (85, 86). In this regard, combining PLK and Aurora kinase inhibitors with PI3K/AKT inhibitors may provide increased efficacy in treating PTEN-deficient prostate cancer. Altogether, these findings suggest that the tumor suppressive functions of PTEN are in part due to its functions within the nucleus. New insights into the regulation of PTEN subcellular localization and the functions of PTEN in the nucleus may shed light on novel biomarkers and therapeutics for the treatment of prostate cancer.

PI3K/AKT/mTOR-independent Functions of PTEN

Although most phenotypes associated with PTEN loss can be accounted for by the activation of the PI3K/AKT pathway, transgenic models with prostate-specific overexpression of p110β or a constitutively active form of AKT develop only localized, pre-cancerous PIN lesions, suggesting that PTEN possesses other tumor suppressor functions independent of the PI3K/AKT pathway (87-89). Similarly, while conditional deletion of *p110β* or *Rictor*, in addition to *Pten* conditional deletion, prevents the progression of tumor development from PIN to adenocarcinoma, they do not completely prevent prostate cancer initiation (90, 91).

One example of a PI3K/AKT/mTOR-independent mechanism of PTEN regulation is the interaction between PTEN and p53 (92). While PTEN inactivation is known to increase the

expression (93) and activation of the p53 repressor MDM2 (94) by a PI3K/AKT-dependent pathway (95) and upregulate p53 through translational mechanisms mediated by mTORC1 (96, 97), the PTEN C2 domain, which lacks phosphatase activity, can also regulate cell motility (98). Interestingly, the same C2 domain interacts directly with p53 in a phosphatase-independent manner to enhance p53-mediated cell cycle arrest and apoptosis by promoting the stabilization, acetylation, and tetramerization of p53 (71, 72, 99). Conversely, p53 can also regulate PTEN at the transcription level (100). In the *Pten*-null mouse model, deletion of p53 accelerates *Pten*-null prostate cancer by reducing cellular senescence (101). Concomitant mutations of PTEN and p53 have been detected within individual human tumors, supporting a selective advantage for combined inactivation of both tumor suppressors. However, whether the cooperation of PTEN and p53 loss in overriding cellular senescence promotes human prostate cancer progression needs to be further investigated.

PTEN can also regulate the expression of other tumor suppressors whose functions are commonly lost as an early event in prostate cancer initiation, such as Nkx3.1 (102). Not only is Nkx3.1 expression downregulated in the PTEN-null murine prostate cancer model, but forced expression of Nkx3.1 in the PTEN-null prostate epithelium prevents prostate cancer initiation and progression (102). Moreover, while a transcriptional profiling study has indicated that the JNK pathway is activated following PTEN loss in an AKT-independent manner (103), a recent report elucidated that JNK deficiency collaborates with PTEN loss in promoting CRPC (104).

Though the lipid phosphatase activity of PTEN is central to its role as a tumor suppressor, other, phosphatase-independent functions of PTEN are also important. PTEN is a dual-

specificity protein phosphatase with activity towards acidic substrates. PTEN is capable of dephosphorylating phosphorylated serine, threonine, and tyrosine residues on peptide substrates *in vitro* (105), as well as protein substrates such as FAK (106), CREB (107), eIF2 (108), and SRC (109) *in vivo,* thereby directly inhibiting cell survival, proliferation and migration. The activation of these PI3K/AKT-independent pathways after PTEN loss suggests that combining PI3K/AKT inhibitors with inhibitors of these other pathways may improve efficacy in treating patients with PTEN-deficient prostate cancer.

PTEN Regulation

Genetic Regulation

Germline PTEN mutations do not predispose men to prostate cancer (10, 11). However, the 10q23 gene locus is a frequent target for somatic heterozygous deletion in primary, and, more frequently, in metastatic prostate tumors, where loss of heterozygosity (LOH) is found in 20-60% of tumors (110). However, the finding that the rate of PTEN LOH and mutations are far less frequent than the detected rate of PTEN loss at the protein level suggests that other, non-genomic alterations may occur that inactivate the second PTEN allele.

Epigenetic Regulation by DNA Methylation

Supporting its important physiological functions, PTEN is constitutively expressed in normal tissues, including infant and adult human prostates. However, PTEN expression can be

downregulated on many levels in various physiological settings. Epigenetic inactivation of the PTEN promoter has been described in prostate cancer xenografts, where loss of PTEN protein is a result of promoter methylation (111); however, this has yet to be shown in primary prostate cancer specimens. Additionally, the zinc-finger transcription factor SALL4 represses PTEN transcription in embryonic stem cells by recruiting an epigenetic repressor complex called the Mi-2/NuRD complex to the PTEN locus (112). Despite these discoveries, epigenetic silencing of PTEN in prostate cancer has not been demonstrated in the *in vivo* and clinical setting.

Transcriptional Regulation

Suppression of *PTEN* transcription may have an important and understated role in prostate cancer initiation and progression. PTEN was originally cloned as a gene transcriptionally regulated by transforming growth factor β (TGFβ) (4), which both suppresses and induces PTEN expression depending on the activation status of the Ras/MAPK pathway. When Ras/MAPK is activated, as is common in aggressive, late stage disease, TGFβ suppresses PTEN expression through a Smad4-independent pathway (113). Alternatively, when the Ras/MAPK pathway is blocked, TGFβ induces PTEN expression through its canonical Smad-dependent pathway (114). The Ras/MAPK pathway also suppresses PTEN levels through the transcription factor c-Jun (115). Moreover, the MEK-JNK pathway suppresses PTEN transcription via activation of NF-kB, which directly binds to and suppresses the PTEN promoter (116). Expression of PTEN is also negatively regulated by the epithelial-to-mesenchymal transition (EMT) transcription factor SNAIL, which is itself activated by PI3K/AKT and RAS/MAPK pathways (117-119). SNAIL competes for binding to the PTEN promoter with p53, which is a transcriptional activator of

PTEN and leads to activation of PTEN transcription during p53-mediated apoptosis (92). Activated NOTCH1 both positively and negatively regulates PTEN expression through MYC and CBF1, respectively (120, 121). PTEN transcription can also be upregulated through several other transcription factors, including PPARγ (122) and EGR1 (123), as well as downregulated by BMI1 (124), which regulates prostate stem cell self-renewal and malignant transformation (125). All in all, transcriptional control of PTEN lies within a network of tumor suppressors and oncogenes controlling various signaling and development programs within normal and cancerous prostate cells.

Post-transcriptional Regulation

PTEN mRNA is also post-transcriptionally regulated by PTEN-targeting microRNAs (miRNAs), a class of endogenous 20-25 nucleotide non-coding RNAs that repress mRNA translation through imperfect base pairing between the seed sequence of the miRNA and the complementary seed match sequence in the 3' untranslated region of the target mRNA (126). A number of miRNAs have been reported to promote tumorigenesis by downregulating PTEN expression. For example, miR-22 and the miR-106b-25 cluster, both PTEN-targeting miRNA loci, are aberrantly over-expressed in human prostate cancer, and are capable of initiating prostate tumorigenesis *in vitro* and *in vivo* (127). The identification of these and other prospective PTEN-targeting miRNAs in serum of prostate cancer patients may be valuable as surrogate markers for PTEN-status, and hence could correlate with both disease progression and the potential efficacy of PI3K/AKT inhibitor treatment.

In a newly emerging field of research, the PTEN pseudogene 1 (PTENP1) was found to influence PTEN expression through a coding-independent function, uncovering a new mechanism of gene regulation (128). Since the PTENP1 mRNA transcript shares vast homology with PTEN mRNA, PTENP1 acts as a decoy for PTEN-targeting miRNAs, and can thereby sequester and inhibit the negative regulatory effects of miRNAs on PTEN expression (129). PTENP1 can, therefore, be considered a competing endogenous RNA, or ceRNA. Recent research has uncovered a large network of ceRNA transcripts in prostate cancer that can control PTEN expression by blocking the action of PTEN-targeting miRNAs. These discoveries fortify the existence of a large and complex PTEN tumor suppressor network that can be regulated by coding and non-coding RNAs, and can be used to explain the observance of partial or incomplete PTEN inactivation in human prostate cancer (130-132).

Post-translational Regulation

PTEN stability is regulated by various post-translational modifications. When inactivated, PTEN is phosphorylated at various serine and threonine residues on its C-terminal tail, which, in turn, increases PTEN stability (133-135). This C-terminal phosphorylation results in a more stable yet "closed" state of PTEN, which reduces its plasma membrane localization (136) and its ability to form a complex with PDZ domain-containing proteins (135), thereby reducing its PIP3 lipid phosphatase activity (137-139). As PTEN is activated, dephosphorylation of its C-terminal tail opens its phosphatase domain, increasing PTEN activity and enhancing its interactions with binding partners, but in turn making PTEN increasingly unstable (140). Also located in the C-terminal tail, Ser370 can be phosphorylated by a downstream effector of SRC, CK2 (141), while

Thr366 appears to be phosphorylated by GSK3β (142); however, the function of phosphorylation at these sites still remains unclear (143). The targeting of PTEN to the plasma membrane can also be orchestrated through phosphorylation at Ser 229 and Thr321 on its C2 domain by the protein kinase ROCK (144-146). Tyr336 of PTEN can also be phosphorylated by RAK, which can act as a tumor suppressor in its own right by regulating PTEN stability and function (147). Future research may unveil other known and unknown kinases that are capable of phosphorylating PTEN and thereby regulate specific PTEN functions.

The open state of PTEN is also more prone to ubiquitin-mediated proteasomal degradation. Lys13 and Lys289 are conserved sites for PTEN ubiquitination, and monoubiquitination is necessary for the movement of PTEN from the cytoplasm to the nucleus (75). NEDD4-1 is a recently identified E3 ligase of PTEN that induces both PTEN mono- and poly-ubiquitination (148). However, NEDD4-1 knockout mice contain no differences in the expression level and subcellular localization of PTEN, hinting that other E3 ligases may be involved in the regulation and localization of PTEN (149). Along these lines, two other E3 ligases, XIAP and WWP2, have been proposed to mediate PTEN ubiquitination (150, 151).

Similar to other phosphatases, the cysteine residues in the bottom of the PTEN catalytic pocket are very sensitive to oxidation (152). The catalytic activity of PTEN is attenuated by reactive oxygen species (ROS) through the development of a disulphide bond between Cys71 and Cys124 that is induced during oxidative stress (153, 154). Furthermore, PTEN can also be acetylated at Lys125 through Lys128 by PCAF and at Lys402 by CBP, inhibiting its catalytic activity while facilitating interactions with PDZ domain-containing proteins (155). Finally, other

forms of PTEN redox regulation have been suggested by research demonstrating the inactivation of PTEN through nitrosylation of cysteine residues in its phosphatase domain (156). Together, these findings highlight the potential to manipulate mechanisms of PTEN post-translational modifications for use as therapeutics to enhance the tumor suppressive functions of PTEN.

Protein-Protein Interactions

A number of PTEN interacting proteins regulate the tumor suppressive abilities of PTEN by altering its conformation, stability, and subcellular localization. PTEN contains a 3 amino acid C-terminal region that binds to PDZ domain-containing proteins, and these PDZ domains are involved in multi-protein complex assembly (134, 157). Indeed, the PDZ domain of PTEN mediates interactions with NHREF, which binds to and recruits PTEN to PDGFR to inhibit the activation of the PI3K-AKT pathway (158). The PTEN PDZ-binding domain binds to several other proteins, including MAGI-2 and MAST205, which appear to enhance the stabilization of PTEN (157, 159, 160). As PTEN can be found in high molecular mass complexes through size-exclusion chromatography, it was hypothesized that the PDZ binding domain may be required for such complex formation (161). However, mutagenesis studies demonstrated that neither PTEN's catalytic activity nor its PDZ binding domain are absolutely required for its complex formation. Instead, PTEN phosphorylation status has a significant role in its complex assembly (162). Using two-dimensional gel electrophoresis and mass spectrometry analysis, hnRNPC was identified as a novel PTEN interacting protein (162). Indeed, PTEN and hnRNPC are co-localized in the nucleus and may be involved in RNA regulation (162, 163).

Additional proteins are capable of binding to other domains on the PTEN protein. PICT-1 interacts with PTEN by binding to and promoting phosphorylation of the C-terminal tail, conferring PTEN stabilization (164). Through a yeast two-hybrid screen, β-arrestin was identified as a PTEN binding partner, binding to PTEN's C2 domain (165). When PTEN is dephosphorylated at Thr383, this increases the binding affinity of β-arrestin to PTEN, which in turn allows PTEN to negatively regulate cell proliferation through its lipid phosphatase activity, as well as enhance cell migration by reversing the inhibitory effect of the C2 domain (165). Furthermore, PTEN can directly interact with the regulatory subunit of PI3K, p85, which increases its lipid phosphatase activity and subsequent capability of downregulating the PI3K-AKT pathway (138, 166). Therefore, p85 can regulate the PI3K/AKT pathway by both negatively regulating PI3K through direct binding to its catalytic subunit, p110, and by positively regulating PTEN activity. Under oxidative stress conditions, DJ-1, which was identified in Drosophila melanogaster, can also directly bind to PTEN, an action that is associated with increased P-AKT levels (167, 168). Recent screens have identified novel PTEN regulators, including PREX2a (169) and SIPL1 (170), which bind to PTEN directly and inhibit its phosphatase activity against PIP3. MAN2C1 also binds to PTEN and inhibits its function in both prostate cancer cell lines and primary human prostate tumors (171). Intriguingly, one study found that, of 60% of primary human prostate tumors that were PTEN-positive, 80% displayed overexpression of MAN2C1, uncovering a possible new mechanism of PTEN downregulation without genomic loss of PTEN (171). Despite the discovery of various PTEN protein-binding partners, further investigation is necessary to understand the physiological and clinical relevance of these interactions.

Subcellular Localization

The function of PTEN is also regulated by its subcellular localization. At the plasma membrane, PTEN can regulate directional chemotaxis. PTEN recruitment to the plasma membrane relies on electrostatic interactions with acidic lipids in the membrane, such as phosphatidylserine, PIP2, PIP3, and phosphatidic acid (172), as well as additional protein-protein interactions (140, 173). PTEN interacts with several membrane-anchored proteins in its dephosphorylated form, including MAGI-2 (157), MAST205 (159), hDLG (135), MVP (174), PDGFR and NHERF (158), which are thought to be potentially part of a larger PTEN complex, via its C-terminal PDZ domain. NEP has been shown to recruit PTEN to the plasma membrane, which in turn enhances its catalytic activity and subsequently hinders AKT activity (175). Similarly, the motor protein myosin V regulates the migration of PTEN to the membrane by directly binding to PTEN (176).

PTEN is predominantly localized to the nucleus in differentiated and resting cells in comparison to rapidly cycling cancer cells (68). The nuclear localization of PTEN is also dependent upon the cell cycle stage, with nuclear PTEN levels highest at the G_1 phase and lowest at the S phase (67). While some studies have shown that PTEN nuclear localization is dependent upon noncanonical nuclear localization sequences on PTEN and major vault protein-mediated nuclear transport (65), others have shown that nuclear localization of PTEN occurs through passive diffusion through the nuclear membrane (177). It has been further suggested that PTEN contains a type of cytoplasmic localization signal (CLS) in its N-terminal region that, when mutated, induces the nuclear import of PTEN (178). Other so-called nuclear exclusion motifs and NLS sequences have been identified that control PTEN localization through a RAN-

dependent mechanism (179); however, how they regulate the shuttling of PTEN between the nucleus and the cytoplasm is not understood. More conclusively, PTEN monoubiquitination by the E3 ligase NEDD4-1 induces the nuclear localization of PTEN (148), while the deubiquitinase HAUSP controls PTEN deubiquitination and nuclear exclusion (180). Oxidative stress induces the accumulation of PTEN in the nucleus, where it associates with p53 to trigger cell cycle arrest and reduce ROS (71). Nevertheless, mechanisms involved in the nuclear export of PTEN are still waiting to be uncovered. The use of models utilizing PTEN proteins with mutations that disrupt PTEN localization but maintain PTEN phosphatase activity may provide new understandings into the role of nuclear PTEN.

PTEN Loss as a Biomarker for Human Prostate Cancer

Despite recent and past findings firmly establishing loss of *PTEN* as one of the most common somatic genetic alterations in prostate cancer, prostate cancer specimens are not routinely screened for PTEN loss in the clinical setting. Fluorescence in situ hybridization (FISH) has been used to identify genomic *PTEN* loss, which is found in 9-23% of high-grade prostatic intraepithelial neoplasia (PIN) lesions (181, 182) and 10-70% of prostate cancers (12, 13, 183-187), and is correlated with an overall poor prognosis (22, 70, 187-190). Loss of PTEN expression in the cytoplasm as well as in the nucleus, as determined by FISH and immunohistochemistry (IHC) analysis, is independently associated with decreased disease specific survival (70, 191). Part of the reason for these variations may be due to the subjective nature and tediousness of counting the number of fluorescent signals and positive antibody stains relative to control signals and stains to quantify PTEN expression. FISH analysis also lacks the

sensitivity to identify minor mutations/perturbations in the PTEN gene locus, as well as other epigenetic and post-transcriptional changes that may influence PTEN expression (13, 192). Moreover, current research, through the use of "break apart" FISH technology, has revealed that gross chromosomal rearrangements of the PTEN locus occur in prostate cancer, which could very well explain the absence of PTEN expression in tumors designated as harboring genomic loss of one PTEN allele using conventional single probe FISH (193).

Despite discrepancies in reported rates of genomic *PTEN* loss, a general finding of these studies is that loss of one *PTEN* allele is significantly more frequent than loss of both *PTEN* alleles, although homozygous deletions are associated with advanced disease and metastasis (194, 195). Haploinsufficiency for PTEN, as well as inactivation of the second *PTEN* allele through non-genomic alterations, may explain why heterozygous *PTEN* deletions outnumber homozygous *PTEN* deletions in human prostate cancer and also result in poor outcomes (181, 187, 196). Indeed, nearly 70% of primary human prostate tumors do not contain inactivation of both copies of *PTEN* (101). In terms of disease progression, the frequency of *PTEN* loss is higher in surgical cohorts enriched for high Gleason grades and aggressive disease stages (189). *PTEN* loss is more common in hormone refractory and metastatic prostate cancer than in hormone dependent primary tumors, with homozygous *PTEN* loss in 10% and 50% of hormone dependent and metastatic/hormone refractory cases, respectively (70, 181, 182, 186-188, 190, 197, 198). Therefore, PTEN could serve as a prognostic marker for hormone refractory and metastatic disease. *PTEN* genomic loss is also associated with the TMPRSS2-ERG fusion (22, 182), and recent reports have concluded that these events cooperate to stratify patients with a poorer prognosis in the clinic (189). A close association between PTEN loss and therapeutic resistance,

as demonstrated by a decreased time to biochemical recurrence after radical prostatectomy, adjuvant docetaxel treatment, and radiotherapy, has also been observed (70, 187, 188, 199, 200).

The possibility that FISH and other genomic analyses may fail to detect some cases of PTEN inactivation calls for alternative methods to detect PTEN loss. Considering the role of post-transcriptional and post-translational modifications in PTEN protein expression and subcellular localization as discussed above, quantification of PTEN protein levels using immunohistochemistry (IHC) may be a better indicator of PTEN expression. In a recent study using a rabbit monoclonal antibody against PTEN for IHC analysis, PTEN protein loss was detected in 75%-86% of samples with genomic PTEN loss, and was even discovered at times in the absence of genomic *PTEN* loss (191). Interestingly, 45% and 37% of tumors with PTEN protein loss did not show genomic deletions measureable by FISH or SNP microarray analysis, respectively, further suggesting that alternative mechanisms of PTEN inactivation exist beyond the genomic level (191). Moreover, IHC analysis has correlated PTEN protein loss with high Gleason scores, as well as decreased time to metastasis in a cohort of patients having undergone surgical resection (191). Other studies using large prostate cancer cohorts combining genomic analysis, through comparative genomic hybridization (CGH) and whole-exome sequencing, and transcriptosome analysis have uncovered frequent alterations of the PI3K/AKT pathway in prostate cancer (22-24), which correlated with 42% and 100% of human primary and metastatic prostate cancer, respectively, as well as high-risk disease (22). Using network component analysis, 20 transcription factors have been identified whose activities, as deduced from their target gene expression, are immediately altered upon the re-expression of PTEN in a PTEN-inducible system (201). Notably, the activity of these transcription factors can be used to predict

PTEN functional status in human prostate, breast and brain tumor samples with increased reliability when compared to basic expression-based analysis (201). With improved mechanisms for detecting PTEN functional status, PTEN loss could be used not only as a prognostic biomarker for men with prostate cancer, but also as a potential predictive marker to identify patients who could benefit from emerging PI3K/AKT pathway therapies.

PTEN in Prostate Cancer Initiation, Progression, CRPC, and Metastasis

Mouse Models of Prostate Cancer

Prostate cancer research has been limited, in part, by the lack of animal models that develop spontaneous prostate tumors in a manner that mimics human prostate cancer. Mouse xenograft models reconstituted from primary human metastatic prostate cancer cells and cell lines have been developed and used extensively in research as preclinical models. However, these xenograft models cannot be used for studying the underlying mechanisms involved in prostate cancer initiation and progression since they are derived from late stage disease. Moreover, many of the key features of the disease, especially the resident tumor microenvironment and the stromal and immune cells that occupy it, are lacking in this immune incompetent system and, therefore, engrafted tumors cannot recapitulate the whole spectrum of human prostate cancer (202). Genetically engineered mouse (GEM) models of prostate cancer have advanced significantly over the past decade (203-207), and the strong implication of PTEN loss in prostate cancer progression in humans has prompted the expansion of GEM models based on PTEN inactivation. Greater knowledge of the role of PTEN loss as an individual and cooperative agent in prostate

cancer development, including initiation, progression and invasion, castration-resistant prostate cancer (CRPC), and metastasis, has been uncovered using mouse models that recapitulate the human disease through genetic loss of the murine homolog of the *Pten* gene (Fig. 1).

PTEN Dosage in Mouse Models of Prostate Cancer

PTEN dosage appears to be an important determinant in the development of many epithelial cancers, as demonstrated in various mouse models of *Pten* loss (208). In the prostate, a hypomorphic PTEN allele, which leads to approximately 20% reduction of PTEN levels, shows no sign of neoplastic lesions in the prostate epithelium, while conditional or conventional deletion of one Pten allele causes a 50% reduction of PTEN levels and leads to pre-cancerous PIN lesions but not cancer, indicating that inactivation of one allele of *Pten* is sufficient to initiate tumorigenesis but not tumor progression (72, 209-213) . Interestingly, by combining a hypomorphic allele with a knockout allele, and thereby reducing PTEN levels by 70-80%, these mice progress to invasive adenocarcinoma of the prostate (211), indicating that a more profound downregulation of PTEN is needed for cancer progression to occur in the prostate (214). These findings counter the canonical “two-hit hypothesis” of cancer, and suggest that slight variations in PTEN expression, induced through genetic alterations as well as non-genetic changes in PTEN expression, are able to recapitulate varying stages of prostate tumor initiation and progression (215). Despite the evidence for PTEN haplosufficiency in the mouse, evidence for this in humans still remains to be determined.

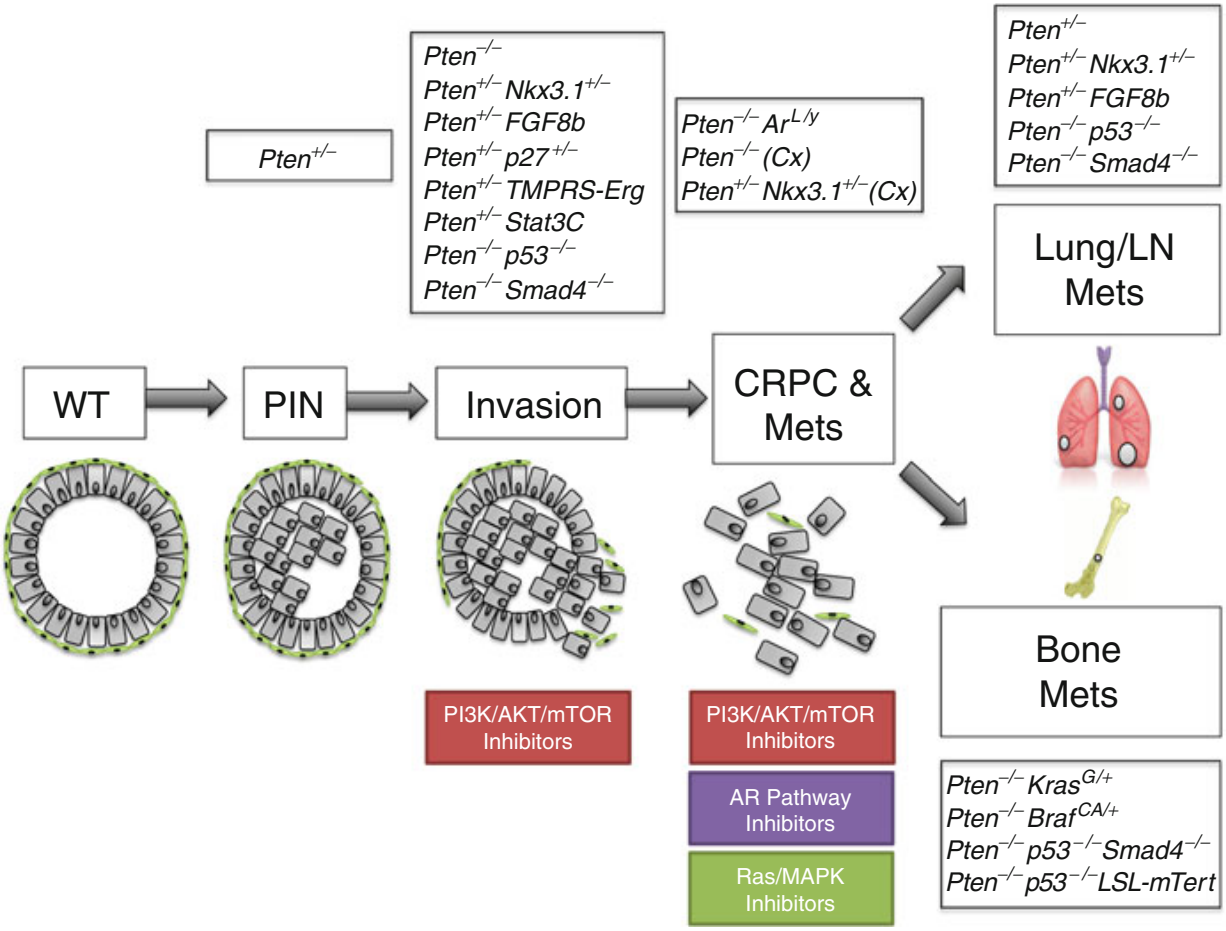

Figure 1. Pten knockout mouse models of prostate cancer. *Pten* heterozygous (*Pten*$^{+/-}$) or homozygous (Pten$^{-/-}$) loss, alone or in combination with other pathway alterations, is able to recapitulate all stages of human prostate cancer, including initiation (PIN), cancer progression/invasion, CRPC, and metastasis. Studies in these murine models provide credence for the use of PI3K/AKT/mTOR, AR, and Ras/MAPK inhibitors for the treatment of metastatic CRPC. In the figure, *gray squares* represent luminal cells, while *green ovals* represent basal cells. *Cx*, castration, *PIN* prostatic intraepithelial neoplasia, *LN* lymph nodes, *Mets*, metastases, *WT* wild type, *CRPC* castration-resistant prostate cancer.

Phenotypes associated with homozygous deletion of Pten in the prostate epithelium

A number of studies have been performed through the use of conditional mutants with prostate-specific deletion of one or both *Pten* alleles (208, 210-212, 216-218). Conditional homozygous *Pten* deletion (*Pten*$^{-/-}$) driven by the *PB-Cre4* promoter results in invasive adenocarcinoma in

100% of mice at 9-12 weeks (212). Importantly, the *Pten*$^{-/-}$ prostate cancer model mimics the course of human prostate cancer formation, progressing from hyperplasia to PIN to invasive adenocarcinoma with defined kinetics (212). Interestingly, homozygous deletion of other tumor suppressors in the murine prostate, including *p53* (219), *retinoblastoma* (*Rb*) (220), and *Nkx3.1* (221), leads to PIN lesions but never an adenocarcinoma phenotype, solidifying the importance of PTEN function in the prostate gland. Moreover, although *Pten*-null tumors are initially responsive to androgen ablation, eventually the animals will develop CRPC, as is commonly seen in human prostate cancer (212). *Pten* homozygous deletion driven by other promoters in the mouse, including *PSA*^{Cre}, *MMTV*^{Cre}, and *Nkx3.1*^{CreERT2}, also results in the development of invasive adenocarcinoma, albeit over a longer latency (222-225).

Compound Pten Knockout Transgenic Mouse Models of Prostate Cancer

Pten loss combined with alterations in other tumor suppressors

Several studies carried out with compound transgenic mice have shown that monoallelic or biallelic deletion of tumor suppressor genes such as *Nkx3.1* (226, 227), *p27*^{KIP1} (228), and *p53* (101) can cooperate with *Pten* loss in promoting prostate cancer (Fig. 1). While loss of a single allele of *Nkx3.1* (221, 229) and *p27*^{KIP1} (230), both of which occurrences have been implicated in advanced stage prostate cancer and poor disease-free survival in humans (231, 232), is sufficient to promote prostate cancer initiation and PIN lesions, concomitant loss of *Pten* is needed to promote prostate tumorigenesis and cancer progression (208, 227, 228, 233). Moreover, while the TRAMP mouse model alone, which contains inactivation of the *p53* and *Rb* tumor suppressor

genes through expression of the large/small SV40 tumor T antigens under the *probasin* promoter, is capable of inducing the development of aggressive prostate tumors (206), loss of heterozygosity of *Pten* in TRAMP mice demonstrated an increased rate of tumor development, with a subsequent decrease in overall survival from 245 days to 159 days (234). In the same way, conditional ablation of one or two alleles of *p53* leads to the development of PIN lesions, while $Pten^{-/-}$;$p53^{-/-}$ double mutants exhibit invasive prostate cancer as early as two weeks after puberty that is invariably lethal by 7 months of age (101, 235). Also, deletion of *Smad4*, a tumor suppressor known to regulate the TGF-β signaling pathway, cooperates with *Pten* deletion in the prostate to enhance tumor cell proliferation and drive invasion to produce fully penetrant prostate cancer and metastases to the lymph nodes and lungs (236). Finally, combining *Pten* and *p53* loss with loss of *Smad4* or reactivation of murine telomerase (*mTert*) produces prostate cancer metastases in the bone (237), indicating that additional pathway alterations are necessary to drive prostate tumor cells to form metastases in the microenvironment of the bone, an important feature of human prostate cancer.

Pten loss combined with alterations in oncogenes and oncogenic signaling pathways

Activation of oncogenes and oncogenic signaling pathways cooperates with PTEN loss to promote invasive prostate cancer. In prostate cancer, the *ERG* gene is frequently translocated to the *TMPRSS2* promoter region, with the resulting *TMPRSS2-ERG* fusion protein expressed in 50% of human prostate cancer specimens (238-240). Whereas mice expressing *TMPRSS2-ERGa* under the control of the *ARR2Pb* promoter only develop PIN lesions (239), this translocation collaborates with *Pten* haplosufficiency to cause invasive adenocarcinoma of the prostate (241).

Similarly, cooperation between *FGF8b* overexpression and *Pten* haplosufficiency in a murine model leads to adenocarcinoma of the prostate, as well as lymph node metastases, in comparison to *FGF8b* overexpression alone, which leads to only hyperplastic and PIN lesions (242). The 8q24 chromosomal region comprising the *MYC* oncogene is somatically amplified in a cohort of advanced human prostate tumors (243). While mice engineered to express high levels of human *c-Myc* in the prostate (*PB-Cre4 Myc^{hi}*) develop invasive adenocarcinomas with 100% penetrance (244), focal expression of *c-Myc* specifically in luminal epithelial cells of the prostate of mice (*PB-Cre4 Z-Myc*) results in only a mild pathology (245). However, when combined with deletion of *Pten*, *PB-Cre4 Z-Myc* mice develop high grade PIN and prostate cancer (245). Although further investigation is needed to fully understand the synergistic effect of *c-Myc* activation and *Pten* loss in prostate cancer, evidence from this study and others suggests that loss of *Pten* may have differential effects depending on the cell types and regions/lobes/zones of the prostate where genetic deletion occurs. With the advent of cell type specific promoters in the prostate, future murine models will be able to tease out the effects of PTEN loss in specific cells in the prostate. For now, these models confirm that concomitant loss of *Pten* and genetic activation of oncogenes such as *ERG, FGF8b*, and *Myc* accelerate initiation and progression in human prostate cancer (Fig. 1).

Pten loss combined with alterations in inflammatory pathway regulators

Various lines of evidence suggest that chronic inflammation is linked to prostate tumorigenesis (246-248). Indeed, expression of specific cytokines can be used as a prognostic indicator of biochemical recurrence in human prostate cancer (249). One of the most prevalent inflammatory

mediators clearly implicated in prostate cancer is IL-6, a cytokine that has not only been associated with tumor growth, proliferation, and angiogenesis in many cancers (250), but whose high levels in the circulating plasma of prostate cancer patients have also been correlated with advanced stages of the disease, therapeutic resistance, and an overall poor prognosis (251). Although the foremost effect of IL-6 is activation of the JAK/STAT3 pathway (252), the PI3K/AKT pathway can also directly activate and phosphorylate STAT3 at Ser727 (253), which induces metastatic behavior of prostate cancer cells both *in vitro* and *in vivo* through stimulation of angiogenesis and suppression of antitumor immune responses (254). While transgenic mice that constitutively express *Stat3* under the control of the *ARR2Pb* promoter develop only PIN lesions, when crossed with $Pten^{+/-}$ mice, the subsequent compound mutants develop invasive prostate tumors (255).

Many inflammatory cytokines and chemokines promote tumor progression by converging on and stimulating the IKK2/NF-κB signaling axis (256). The main function of IKK2 is the phosphorylation of IκB molecules, which act as inhibitors of NF-κB, thus rendering them subject to degradation and allowing NF-κB to remain activated. Constitutive activation of the transcription factor NF-κB in prostate cancer has been correlated with disease progression (257), and inhibition of NF-κB activity in prostate cancer cells can suppress angiogenesis and subsequent tumor invasion and metastasis by downregulating expression of downstream NF-κB targets such as VEGF and MMP9 (258). Interestingly, while a mouse model containing a constitutively active version of IKK2 alone is insufficient in promoting prostate tumorigenesis, in combination with heterozygous loss of *Pten*, IKK2 activation leads to an increase in tumor size, accompanied by increased inflammation (259). These studies demonstrate that

inflammatory cytokines secreted from the stromal microenvironment of the prostate cooperate with PTEN loss to drive epithelial prostate tumor cells towards invasive disease.

PTEN and Tumor Cell Migration and Invasion

As demonstrated in various models of conditional *Pten* deletion in the prostate, homozygous *Pten* loss leads to progression from PIN lesions to invasive adenocarcinoma, a process that requires disruption of the basement membrane and junctional integrity in epithelial acinar structures to allow the invasion of tumor cells through the surrounding basement membrane and into the stromal microenvironment (Fig. 1). PTEN and PIP3 play conserved roles in the determination of cell polarity in diverse cell types. From data first obtained in *Dictyostelium discoideum* (260-263), a unicellular amoeba, and later from neutrophils undergoing chemotaxis (264, 265), enrichment of PIP3 at the leading edge of migrating cells and localization of PTEN in the lateral and trailing edges of the cell has been observed. The PI3K pathway also promotes membrane ruffling, cell motility, and cellular spreading through downstream effectors such as RHO, RAC1, and CDC42 (266). Consequently, forced expression of PTEN in tumor cell lines inhibits tumor cell invasiveness *in vitro* and in xenografts *in vivo* through both phosphatase-dependent (106, 267) and phosphatase-independent (98) mechanisms. In normal glandular development, PTEN concentrates to the apical plasma membrane during epithelial morphogenesis, where it catalyzes the conversion PIP3 into PIP2, which recruits ANX2, CDC42, and aPKC to the membrane to establish cellular polarity (268). In this regard, loss of PTEN expression may block the development of the apical surface and lumen of epithelial structures. Therefore, activation of the PI3K/AKT pathway upon PTEN loss may lead to the loss of

epithelial features, and thereby increase the likelihood of cells developing the properties of increased motility and invasive capacity through an epithelial-to-mesenchymal transition (EMT) (124). In all, these findings raise the possibility that the considerable increase in the *PTEN* mutation/deletion rate in metastatic tumors might result from a selective metastatic advantage acquired through the loss of PTEN regulation of motility and invasion.

Pten Loss in Metastatic Prostate Cancer Mouse Models

It is clear from these models that *Pten* LOH is required for cancer progression and invasive adenocarcinoma development, as well as CRPC upon androgen deprivation. Although biallelic *Pten* deletion, alone or in combination with homozygous deletion of *p53* (101, 235), *Nkx3.1* (227)*, or Smad4 (236)* or activation of *FGF8b* (242), does lead to the occurrence of small micrometastases in the lymph nodes and lungs, it fails to produce significant metastatic burden, particularly in the bone (212). Therefore, other genetic alterations and signaling pathway abnormalities must collaborate with activation of the PI3K/AKT pathway to promote metastatic prostate cancer to the bone.

Although *Ras* mutations (269-271) and *Ras* fusion events (272) in prostate cancer are uncommon, strong evidence suggests that Ras/MAPK activation plays a substantial role in human prostate cancer progression, particularly in metastasis and CRPC development. Indeed, the Ras/Raf/MAPK pathway has been recently shown to be altered in 43% and 90% of primary and metastatic lesions, respectively (22). P-MAPK levels, as assessed in tumor microarrays (TMAs) from human prostate cancer samples, are significantly elevated in neo-adjuvant treated,

recurrent, and CRPC patients as compared to benign prostatic hyperplasia (BPH) specimens, corresponding with a significant reduction in PTEN expression (118). These findings have prompted the development of two recent murine models of prostate cancer that combine homozygous *Pten* loss with activation of the Ras/Raf/MAPK pathway: the *PbCre;Pten*$^{L/L}$*;Kras*$^{G12D/+}$ model (118), and the *Nkx3.1*$^{CE2/+}$*;Pten*$^{f/f}$*;Braf*$^{CA/+}$ model (273). In both models, activation of the MAPK pathway through either *Braf* or *Kras* conditional overexpression resulted in overt macrometastases to the lymph nodes, lungs, liver, and, importantly, the bone marrow, in around 30% (273) and 100% (118) of cases, respectively. In the *PbCre;Pten*$^{L/L}$*;Kras*$^{G12D/+}$ model, treatment with a MEK inhibitor alone was able to fully ablate metastatic spread to the lungs and other distant organs, implicating the RAS/RAF/MAPK pathway as a driver of metastasis in *Pten*-deficient prostate cancer (118). Interestingly, an EMT phenotype is also observed at the primary tumor site in the *PbCre;Pten*$^{L/L}$*;Kras*$^{G12D/+}$ model (118). As EMT has been postulated to play a critical role in the process of metastasis (274), this new model provides a unique opportunity to study the impact of EMT in prostate cancer metastasis *in vivo* in the context of *Pten* loss and Ras/MAPK activation. With these novel metastatic models of prostate cancer, a better understanding of the contribution of PTEN to the metastatic cascade, including localized invasion, intravasation into the blood stream, survival as circulating tumor cells (CTCs), extravasation out of the blood stream, and metastatic seeding to distant organ sites, can be further uncovered. Overall, past and present murine models of prostate cancer induced by *Pten* loss have demonstrated that loss of PTEN, to varying degrees and in combination with other genetic alterations, can recapitulate the entire spectrum of prostate cancer, from initiation (heterozygous *Pten* loss), through progression (homozygous *Pten* loss), and, finally, to metastasis (homozygous *Pten* loss and Ras/MAPK activation) (Fig. 1).

PTEN and Castration-Resistant Prostate Cancer (CRPC)

Androgens are indispensable for prostatic glandular development and homeostasis and contribute to prostate cancer development through activation of the androgen receptor (AR). Androgen deprivation therapy remains the most common treatment for advanced prostate cancer. However, therapeutic effects are short lived, and patients usually succumb to CRPC within 18-24 months, leaving the disease essentially untreatable (275). New generation androgen deprivation therapies (ADTs), such as abiraterone (276) and MDV3100 (277), that more effectively ablate androgen production and AR signaling, are rapidly being developed and approved for patients with metastatic CRPC. Similar to human prostate cancers, while castration initially results in massive apoptosis of the prostate epithelium in the *Pten*-null murine model of prostate cancer, the ki67 proliferation index remains constant, indicating that a select population of cells remains resistant to androgen withdrawal (212).

AR is expressed in CRPC and may function through autocrine signaling or crosstalk with other pro-survival and proliferation pathways (278, 279), including the PI3K/AKT pathway, which has been shown to induce AR expression in the absence of PTEN (280-282). Multiple studies have found an association between the loss of PTEN and the development of CRPC (198, 212, 283, 284). Moreover, loss of PTEN and AR expression has been correlated clinically with increased mortality in CRPC patients (190). aCGH analysis on metastatic prostate cancer samples has also demonstrated frequent amplification of AR (73%), coinciding with aberrant deletion of PTEN (87%) (285).

While some studies have proposed that PTEN deletion activates AR through PI3K-mediated stabilization of AR protein levels or AKT-mediated phosphorylation and activation of the AR (228, 286, 287), other reports have revealed that PI3K/AKT pathway stimulation promotes degradation of AR and inhibits AR transcriptional activity (288). Supporting the later claim, levels of AR are heterogeneous, and, in many cases, absent in late stage, metastatic disease (289-292). These observations raise the possibility that loss of AR expression and activity may serve as a means of evading androgen withdrawal through simultaneous activation of other signaling pathways. Indeed, two independent laboratories have recently demonstrated that PTEN loss inhibits androgen-responsive gene expression by regulating AR activity (293, 294), indicating that castration-resistant growth is an intrinsic property of *Pten* null prostate cancer cells regardless of cancer stage (293). These studies further suggest a reciprocal feedback loop that exists between AR and PTEN in prostate cancer, in which conditional deletion of *Ar* in the prostate epithelium promotes the proliferation of *Pten* deficient cancer cells in *PbCre;Pten*$^{L/L}$*;Ar*$^{L/Y}$ mice through the downregulation of the androgen-responsive gene *Fkbp5* and preventing PHLPP-mediated AKT inhibition (293). Moreover, inhibition of the PI3K/AKT pathway was shown to upregulate the receptor tyrosine kinase HER3 (294). As suppression of HER2/HER3 heterodimers has been linked to inhibition of AR transcriptional activity through an AKT-independent mechanism (295), it is plausible that PI3K/AKT inhibition upregulates AR transcriptional activity by increasing HER3 expression.

In all, it is probable that AR suppresses the PI3K/AKT pathway in order to promote differentiation of the prostate epithelium and keep prostate cancer cells sensitive to androgens.

When AR activity is downregulated upon ADT treatment, the PI3K/AKT pathway takes over to promote cell proliferation and cell survival in the absence of androgen or AR activity, further driving tumor progression towards metastatic CRPC (293, 294). These findings may explain why clinical trials that inhibit the activation of the PI3K/AKT signaling axis, as well as its downstream effector mTOR, failed to have a substantial effect on tumor progression in men (296, 297), as inhibition of the PI3K/AKT/mTOR pathway causes an upregulation of AR transcriptional activity that promotes cell survival (294). Since, in the background of PTEN-deficient prostate cancer, AKT regulates proliferation, while AR regulates survival, inhibition of both signaling pathways is necessary for effective tumor reduction. Indeed, combined therapy targeting both PI3K and AR pathways reduces tumor growth in *Pten*-null mice (293, 294), suggesting the possible efficacy of combined PI3K/AKT and AR inhibitor treatment in the clinic (Fig. 1).

PTEN and the Maintenance of Prostatic Stem Cells/Cancer Stem Cell (CSCs)

Stem Cells in the Normal and Tumorigenic Prostate

Stem cells are important not only in the development of the prostate, but also in the maintenance of adult prostatic glandular structure. The growth of the prostate is dependent upon levels of the steroid hormone androgen, as the prostate undergoes involution upon androgen withdrawal but can completely regenerate upon androgen restoration, suggesting the existence of long-lived prostate stem cell populations in the prostate gland (298-300). Similarly, in prostate cancer patients, there exists a unique population of prostate tumor cells with the ability to survive

therapy, such as ADT, and eventually reconstitute the tumor in its entirety. These cells, which harbor stem cell-like characteristics such as indefinite self-renewal, are thus referred to as cancer stem cells (CSCs) (301, 302). Although it is widely believed that the majority of tumors develop from CSCs, the term CSC does not exclude that the cell-of-origin could be from non-stem cells, including progenitor and more differentiated cell types. Indeed, previous reports have suggested that prostate luminal cells, transit amplifying cells and basal cells can serve as the cell-of-origin for human prostate cancer (303). Therefore, the unique population of cells within the normal epithelium that acquire the initial genetic or pathway alterations to initiate prostate cancer are referred to as tumor initiating cells (TICs) (304). Although a number of experimental systems have been designed over the past decade to prospectively identify prostate stem cells, TICs, and CSCs and quantitatively measure their self-renewal capacity, including *in vitro* 2-dimensional colony or 3-dimensional Matrigel sphere forming assays (303, 305, 306) and *in vivo* kidney capsule reconstitution assays (307, 308), to date, the relationship between TICs and CSCs in prostate cancer has yet to be resolved.

PTEN loss in Cancer Stem Cell (CSC) and Tumor Initiating Cell (TIC) Formation and Activation in Prostate Cancer

PTEN has been shown to be essential for the maintenance of hematopoietic stem cell (HSC) function and prevention of leukaemogenesis (309, 310), as well as negatively regulate neural stem cell self-renewal by modulating G_0-G_1 cell cycle entry (311), suggesting that PTEN possesses broader roles in the maintenance of normal stem cell function and inhibition of malignant transformation in adult stem cells. Various cell surface markers, including CD133

(301), CD117 (312), Sca-1 (313), CD49f (303), CD44 (314), Trop2 (315), p63 (316) and CD166 (317) have been tested for enriching for prostate stem cell activities. sh-RNAi knockdown of PTEN in PTEN-positive DU145 cells leads to a further increase in cells positive for $CD44^+/CD133^+$, putative cell surface markers for human prostate stem cells (301, 314), accompanied by enhanced sphere forming ability, clonal outgrowths and tumorigenic potential (318). Conversely, pharmacological inhibition of PI3K/AKT signaling using NVPBEZ235 (319) had the ability to reverse the expansion of $CD44^+/CD133^+$ cells, a mechanism potentially mediated by increased nuclear expression of FoxO (318). More recent studies also demonstrate the collaboration of the JNK and the PI3K/AKT pathway in prostate cancer development. Downregulation of the JNK signaling pathway by way of conditional deletion of both JNK1/2 or upstream kinases Mkk4/Mkk7 in the *Pten*-null prostate epithelium leads to the expansion of $p63^+$ basal cells and $CD44^+$ cells and enhanced disease progression (104). BMI-1, a polycomb family member whose elevated expression in low grade prostate cancer samples has been correlated with biochemical recurrence (320) and poor clinical outcome (321), was demonstrated to be required for the self-renewal activity and maintenance of $p63^+$ stem cells (125). While overexpression of BMI-1 in the murine prostate leads to invasive adenocarcinoma when combined with *Pten* haplosufficiency, alternatively, BM1-1 inhibition slows the growth of aggressive *Pten* deletion-induced prostate cancer (125). *In vitro* observations reveal that AKT phosphorylates and activates BMI-1(322), and that PTEN negatively regulates BMI-1 function (323), providing an additional link between PTEN function and stem cell self-renewal. These data provide direct evidence that alteration of pathways regulated by the PI3K/AKT axis can directly influence CSC activity in prostate tumorigenesis.

Prostate stem cells can be isolated from both WT mouse and benign human prostate tissue by fluorescence-activated cell sorting (FACS) using the antigenic profile $Lin^{-}Sca\text{-}1^{+}CD49f^{hi}$ (LSC^{hi}) (303) or $Lin^{-}Trop2^{+}CD49f^{hi}$ (LTC^{hi}) (315), respectively. Both LSC^{hi} and LTC^{hi} populations have also been demonstrated to be a cell-of-origin for murine and human prostate cancer (313, 324, 325). These cells possess a basal cell phenotype, primarily reside in the region of the prostate proximal to the urethra, and are further enhanced by androgen withdrawal (300, 303, 312, 313). In the *PbCre4;Pten*$^{Lox/Lox}$ murine model, it was identified that PTEN loss can lead to increased stem/progenitor cell proliferation, and that this in turn may be associated with prostate tumor initiation and progression (212). During prostate cancer progression, a significant increase in the number of $p63^{+}CK5^{+}$ basal cells and $CK5^{+}CK8^{+}$ transient amplifying cells is observed in the proximal region of the dorsolateral lobe of *Pten*-null mice (216). Such observations parallel the finding that PSCA, a marker associated with late-stage transient amplifying prostate epithelial cells in human prostate disease (326), is also increased in *Pten*-null prostates (212, 327). Moreover, in *Pten*-null prostate mutants, the LSC^{high} population, which marks the basal population, increases during tumor progression and harbors the majority of stem/progenitor function, as measured by its high sphere-forming activity, as well as its capacity to be both necessary and sufficient for tumor initiation (328). Recently, CD166/ALCAM, which was identified as a cell surface marker highly upregulated in human and murine CRPC samples, was shown to enrich for a subpopulation of LSC^{hi} cells with an even higher sphere-forming activity ($LSC^{hi};CD166^{hi}$) (317). Not surprisingly, upregulation of the PI3K/AKT pathway, along with increased AR expression in human basal LTC^{hi} cells, the human equivalent of murine LSC^{hi} cells, is also necessary and sufficient for the initiation of human prostate cancer (324). LSC^{hi} cell populations also have the capacity to generate differentiated

luminal cells upon transplantation, an important feature for modeling prostate cancer, as the human disease is marked clinically by the loss of the basal cell marker p63 (118, 315, 324, 328). On the other hand, the LSC^{lo} population, containing luminal epithelial cells, did not demonstrate any tumor initiating capacity (328). The LSC^{hi} stem/progenitor cell population is also increased after castration in *Pten*-null animals, indicating that this population harbors an androgen-independent and castration-resistant phenotype that allows it to persist after hormone withdrawal and possibly contribute to CRPC (328). Collectively, these data indicate that PTEN negatively regulates basal and transient amplifying cell proliferation, and thus PTEN loss mediates changes in the stratification of the prostate epithelium leading to expansion of cells that may function as TICs and potential initiators of CRPC.

Various laboratories have generated a number of different *Pten* conditional deletion lines (101, 212, 222, 223), with not all models eliciting the same phenotype. For example, *PSA-*Cre^{+}*;Pten*$^{loxP/loxP}$ mutants do no exhibit pathology in the proximal region of the prostate, but rather display the accumulation of cells positive for the luminal marker CK8, as well as rare Clu^{+};$Tacstd2^{+}$;$Sca\text{-}1^{+}$ cells that may constitute luminal TICs (329). Additionally, deletion of *Pten* driven by the *Nkx3.1-*Cre^{ER} promoter in Castration Resistant Nkx3.1 expressing cells (CARNs), a rare population of cells identified to have self-renewal capacity and the ability to give rise to both basal and luminal lineages, leads to the formation of adenocarcinoma *in vivo*, suggesting that these CARN cells may be TICs upon activation of the PI3K/AKT pathway (225). More recent studies have compared the potential of basal and luminal TICs for their ability to propagate prostate tumors. Using basal (CK5, CK14) and luminal (CK8) promoters, it was observed that both cellular compartments are capable of transformation upon PTEN disruption

and that each is independently self-sustained in vivo (330). Iterating previous observations made in the *Pten*-null murine model, the *K14-Pten* model demonstrates that oncogenic signals like *Pten* loss can alter the differentiation program of basal cells (330). Strikingly, although PTEN was disrupted specifically only in prostate basal cells, the initiation of cancer did not start until the emergence of P-AKT-expressing luminal cells (330). As it takes at least 3 months for *K14-Pten* mouse prostate basal cells to differentiate into luminal cells, trans-differentiation of basal cells into luminal cell lineages may be a rate-limiting step in prostate cancer progression (330). Overall, these data suggest that multiple stem/progenitor cells can serve as the cell-of-origin of prostate cancer initiated by PTEN loss; however, more defined systems, via lineage-tracing and cell type-specific deletion, are needed to address which cell types are responsible for prostate cancer progression, castration resistance and metastasis.

PI3K/AKT/mTOR Pathway Inhibition as a Treatment for Prostate Cancer

Current Prostate Cancer Treatment

Treatment resistance is a major issue in the management of prostate cancer, as it is estimated that 30,000 men in the United States will die in 2012 alone from metastatic and castration-resistant prostate cancer, for which there is currently no cure. Although androgen-deprivation therapy (ADT) remains the standard treatment of metastatic prostate cancer, progression to castration resistant disease occurs in the majority of patients (331-333). Among available therapeutic approaches for the treatment of CRPC, conventional chemotherapy with docetaxel and other agents has limited efficacy and has yet to produce long-term benefits (334, 335). Although

agents that specifically inhibit the AR, androgen synthesis, and/or AR-regulated pathways, such as MDV3100 and Abiraterone, have recently entered the clinic and have shown promising results (276, 277), their therapeutic effects are short lived, and patients eventually develop CRPC (275). Another novel therapy, sipuleucel-T, which is the first ever FDA-approved therapeutic cancer vaccine for the treatment of metastatic prostate cancer, also only modestly improves the survival of late-stage patients by a few months (336, 337).

The current trend in medicine has been to exercise a personalized treatment approach that is based on molecular and genetic profiling of individual patients to determine the best therapeutic strategy. A considerable number of novel therapeutics are presently undergoing clinical trials, including small molecules that target common genetic or pathway alterations found in human cancers. These inhibitors have been FDA-approved for treatment of various solid tumors including, renal, GIST, breast, pancreatic, colorectal, and NSCLC cancer (338-344), and thus hold promise for the treatment of prostate cancer. As it is clear that PI3K/AKT/mTOR pathway activation plays a prominent role in prostate cancer initiation and progression, CRPC, and metastatic disease, the loss of PTEN expression in individuals with prostate cancer could be used as a biomarker to stratify populations of patients that may benefit from treatment with PI3K/AKT/mTOR pathway inhibitors.

PI3K Inhibitors

Class I PI3Ks are heterodimers composed of one catalytic subunit of p110α, p110β, or p110δ, collectively known as p110, and a regulatory subunit, p85. PI3K isoform selectivity may be

essential to boost therapeutic efficacy and minimize off-target toxicity. Recent research suggests a dominant role for the PI3K isoform p110β in PTEN-deficient tumors. In the *Pten*-null prostate cancer model, loss of p110β, but not p110α, decreased PI3K signaling and prevented prostate carcinogenesis (90). In a similar fashion, inducible depletion of p110β, but not p110α, using shRNA in PTEN-deficient human cancer cell lines quenches PI3K-mediated signaling and inhibits growth both *in vitro* and *in vivo* (345).

The most studied PI3K inhibitors to date are the first-generation PI3K inhibitors LY294002 and wortmannin. LY294002 treatment results in cell-cycle arrest and sensitizes the LNCaP prostate cancer cell line to radiation therapy, decreases the invasive properties of LNCaP, PC-3, and DU145 prostate cancer cell lines, and inhibits angiogenesis in PC-3 prostate cancer cells by way of decreased levels of HIF1-α and VEGF. Similarly, wortmannin induces apoptosis and radiosensitizes DU145 cells (346, 347). However, both wortmannin and LY294004 show limited selectivity for individual PI3K isoforms, non-specifically target multiple other signaling molecules (348-351), and demonstrate significant toxicity in animals (347, 352), limiting their effectiveness *in vivo*.

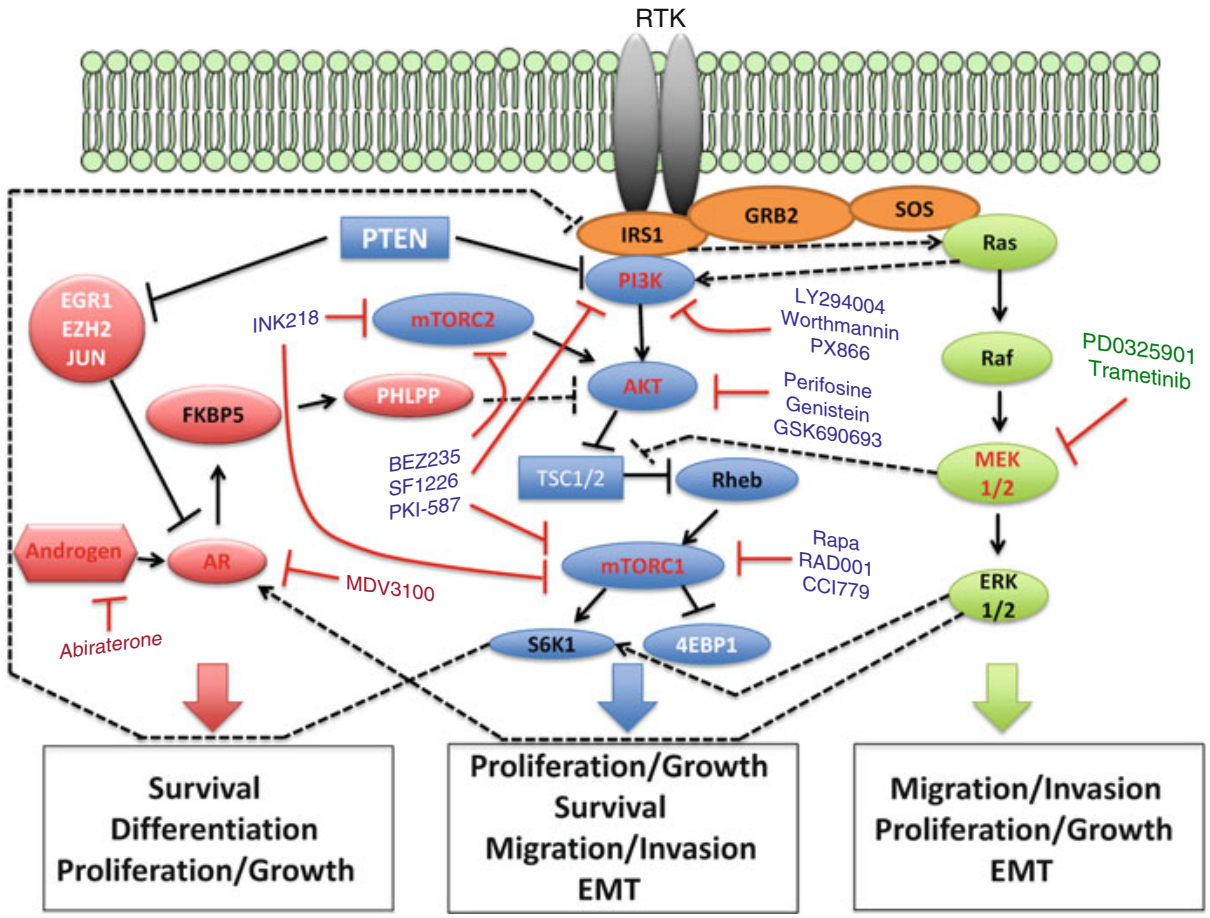

Figure 2. PI3K/AKT/mTOR, Ras/MAPK, and AR signaling pathways converge to promote prostate cancer development. Although all three pathways promote cell proliferation/growth, AR signaling maintains prostate cells in a differentiated state, while PI3K/AKT/mTOR and Ras/MAPK signaling promotes EMT and cell migration/invasion. *Red*, *blue*, and *green ovals* represent AR, PI3K/AKT/mTOR, and Ras/MAPK signaling molecules, respectively. *Orange ovals* denote adaptor molecules. Pathway activators are in *black letters*, and pathway suppressors are in *white letters*. *Solid black lines* depict signaling within a pathway, and *dotted black lines* depict crosstalk between pathways or feedback loops. *Red lines* denote the drug targets. Signaling molecules in these pathways that are the targets of drug inhibitors are in *red letters*.

One potential consequence and side effect of PI3K pathway inhibition is the development of insulin resistance in patients. While both p110α and p110β play specific roles in insulin signaling, research suggests that glucose homeostasis is predominantly mediated by p110α (90, 353). Indeed, p110α inhibitors, but not p110β or p110δ inhibitors, alter insulin-dependent glucose regulation in mice (353). Thus, in the setting of PTEN-deficient tumors, p110β-specific inhibitors, in contrast to pan-PI3K inhibitors, may offer enhanced efficacy with a reduced

likelihood of insulin resistance. Together, these studies suggest that effective treatment of PTEN-deficient prostate tumors may necessitate the use of therapeutic agents that successfully target p110β. However, even in cancers that may be specifically reliant on either p110α or p110β, there remains the possibility that other, non-inhibited p110 isoforms may make up for the decreased activity of the targeted isoform. Moreover, not all tumors that are driven by PTEN loss are dependent on p110β, and the presence of other genetic modifications and pathway alterations is likely to change the PI3K-isoform reliance of these tumors. Interestingly, PTEN loss appears to be a predictive marker for sensitivity to PX-866, an oral derivative of wortmannin, despite the fact that PX-866 displays a high efficacy against p110α and p110δ but not p110β (354). Therefore, although PI3K signaling is an obvious target for therapy, especially in PTEN deficient prostate cancer, given the redundancy and complex feedback regulation existing in the PI3K/AKT/mTOR pathway, as well as a need for a more in depth understanding of the pathway, the clinical efficacy of using PI3K inhibitors as single agents is modest (Fig. 2).

AKT Inhibitors

The significance of the individual AKT isoforms in prostate cancer has yet to be fully uncovered, despite findings that AKT-1 isoform expression may be a prognostic marker for biochemical recurrence in patients with prostate cancer (355). There are several classes of AKT inhibitors currently in development, including isoform-selective AKT catalytic–domain inhibitors and inhibitors of its PH domain, and many have been tested in prostate cancer. Perifosine, an alkylphospholipid that targets the PH domain of AKT and prevents it from binding to PIP3, decreases AKT phosphorylation, inhibits growth, and induces cell-cycle arrest of PC-3 cells

(356). Although there are no published pre-clinical studies investigating perifosine activity against prostate cancer, perifosine has gone to clinical trials for patients with CRPC. Though generally well tolerated, perifosine showed no evidence of significant inhibitory activity (297, 357). Genistein, a non-specific AKT inhibitor, causes significant growth inhibition and apoptosis of cancer cells (358, 359). While genistein has demonstrated significant potential *in vivo*, decreasing the incidence of lung metastasis in an orthotopic model using PC-3 cells (360) and inhibiting tumor growth when combined with docetaxel in an experimental model of bone metastasis (361), another report claimed that genistein increased the size of metastatic lymph nodes in a PC-3 orthotopic model (356). Concomitant targeting of AKT-1 and AKT-2 with ATP-competitive inhibitors, such as GSK690693, has been shown to be more effective than inhibition of single isoforms for the induction of apoptosis in tumor cells, suggesting that these Pan-AKT inhibitors are likely to have more promise in the clinic, although increased toxicity may be a potential issue (362). However, AKT inhibitors will not block the non-AKT effectors downstream of PI3K signaling. Paradoxically, AKT inhibitors could increase upstream receptor tyrosine kinase activities by alleviating downstream negative feedback loops (363). Therefore, the importance of AKT-independent effectors of PI3K signaling and downstream negative feedback loops in the pathway might considerably affect the clinical effectiveness of AKT inhibitors (Fig. 2).

mTOR Inhibitors

mTOR inhibitors have been the most effective among the inhibitors of the PI3K/AKT/mTOR pathway in treating solid tumors, and have received the most consideration in the treatment of

prostate cancer. Rapamycin, the prototypical mTOR inhibitor, associates with its intracellular receptor, FKBP12, which then binds directly to mTORC1 and suppresses mTOR-mediated phosphorylation of its downstream effectors, S6K and 4EBP1. Rapamycin induces cell cycle arrest in PC-3 and DU145 prostate cancer cell lines in *vitro* (364-367), and reduces tumor volume and blocks growth and proliferation in tumors with activated AKT or loss of PTEN *in vivo* (368, 369). Although limited, there have been reports on *in vitro* and pre-clinical studies demonstrating the efficacy of the rapamycin analogs (rapalogs) CCI-779 and RAD001 in the treatment of prostate cancer. CCI-779 inhibits growth of PC-3 and DU145 cells *in vitro*, and, *in vivo*, and reduces tumor volumes in PC-3 and DU145 xenografts (370). Likewise, RAD001 treatment decreases proliferation of prostate cancer cells *in vitro* (371, 372), and reverses PIN lesions in AKT-1 transgenic mice (373).

Despite these preclinical findings, mTORC1 inhibitors, including rapamycin and rapalogs, have demonstrated little success as single agent treatments in the clinic (296, 374, 375). Although rapamycin and rapalogs are effective at inhibiting mTORC1 kinase activity, inhibition of mTORC1 eventually leads to AKT activation and increased P-AKT levels due to the loss of the S6K to IRS-1 feedback loop and reactivation of PI3K signaling (37, 375, 376). Moreover, while mTORC1 is sensitive to rapamycin treatment, mTORC2 is generally considered to be resistant to rapamycin. In this regard, mTORC2 phosphorylation and activation of AKT may further limit the efficacy of mTORC1 inhibitors like rapamycin (34). Therefore, the use of rapamycin and rapalogues as single treatments could potentially cause the hyperactivation of the PI3K/AKT pathway (Fig. 2).

To achieve a significant clinical effect, mTORC1 inhibition with rapamycin and rapalogs may require the addition of upstream inhibitors, such as insulin-like growth factor signaling or PI3K signaling inhibitors (319, 377-379), or, alternatively, more effective inhibition of both TORC1 and TORC2 activity. mTOR catalytic site inhibitors, which are currently in clinical development, target the kinase domain of mTOR and have the advantage of blocking the activity of both mTORC1 and mTORC2. The additional inhibition of mTORC2 provides the benefit of blocking AKT activation through S473 phosphorylation, and therefore, these catalytic site inhibitors would be expected to inhibit the mTOR pathway more effectively than rapamycin. Current research has described torkinibs and torin1, two selective ATP-competitive inhibitors of mTOR that impede cellular growth and proliferation more effectively than rapamycin (380, 381). Interestingly, however, the enhanced activity of these mTOR kinase inhibitors seems to be due to more complete inhibition of mTORC1 activity rather than mTORC2 inhibition, as measured by decreased levels of 4EBP1 phosphorylation and cap-dependent translation compared to rapamycin treatment (380, 381). In support of the efficacy of these mTOR catalytic site inhibitors, a recent preclinical study with the mTOR catalytic site inhibitor INK218 in the *Pten*-null murine prostate cancer model demonstrated that INK218 is able to inhibit AKT and 4E-BP1 phosphorylation in addition to S6K1 phosphorylation, leads to a 50% decrease in PIN lesions, reduce overall tumor volume, and promotes tumor cell apoptosis, as opposed to RAD0001 treatment, which results in inhibition of S6K1 but not AKT and 4E-BP1 phosphorylation, only partial regression of PIN lesions, and no significant effect on tumor cell apoptosis (382). Remarkably, treatment with INK218 blocks progression of invasive prostate cancer locally in the prostate, and even inhibits the total number and size of distant metastases (382). Although new generation mTOR catalytic site inhibitors have the capacity to reduce prostate tumor invasion

and metastasis by more effectively disabling mTORC1 signaling and inhibiting mTORC2 activation, treatment with these inhibitors alone does not inhibit PI3K activity, and, therefore, would need to be combined with other PI3K antagonists to fully ablate distant metastasis and lead to complete tumor regression (Fig. 2).

Dual PI3K-mTOR Inhibitors

The use of multiple inhibitors to target the PI3K/AKT/mTOR pathway may be of particular importance to alleviate the issue of negative-feedback loops in the pathway. As the catalytic domains of the p110 subunits and mTOR are similar in structure, there are a number of small molecule inhibitors currently being tested that can block both PI3K and mTOR. Compared to other PI3K pathway inhibitors, dual PI3K-mTOR inhibitors, which include NVP-BEZ235, BGT-226, XL765, SF11256, PKI-402, and PKI587, have the possible advantage of inhibiting all PI3K isoforms, as well as both mTORC1 and mTORC2. Therefore, these inhibitors should effectively turn off the PI3K/AKT/mTOR pathway completely and overcome feedback inhibition normally observed with mTORC1 inhibitors such as rapamycin and other rapalogs (377). BEZ235 is capable of simultaneously inhibiting multiple class I PI3K isoforms and mTOR kinase activity by binding to their respective catalytic sites (319). BEZ235, unlike PI3K inhibitors alone, is able to lower levels of both P-S6 and P-AKT, demonstrating that dual inhibition of both mTOR and PI3K is capable of preventing an increase in P-AKT levels (319, 379). BEZ235 exhibits greater anti-proliferative effects compared with rapamycin treatment in cancer cell lines *in vitro*, and slows tumor growth and vasculature development in PTEN-deficient cell line engrafted mice, where it is well tolerated with no significant changes in body weight (319, 379, 383). In

preclinical studies, SF1126, a conjugate of LY294002, reduces cell growth, proliferation, and angiogenesis, and exhibits lower toxicity than LY294002 (384). Furthermore, PKI-587, another dual PI3K/mTOR inhibitor, induces tumor regression in several cancer cell line xenograft models, and has a favorable drug safety profile in toxicology studies (385). Importantly, in contrast to PI3K inhibitors that cause cytostatic effects through tumor cell G_0-G_1 arrest (386-388), PKI-587 inhibition of PI3K and mTOR can fully ablate AKT activation and cause the induction of apoptosis, the preferred outcome against tumor cells (385). Despite these preclinical findings, a major issue with dual PI3K/mTOR inhibitors is their efficacies *in vivo* in the clinical settings.

Combination therapy with PI3K/AKT/mTOR and Ras/MAPK inhibitors

One explanation behind the limited success of PI3K/AKT/mTOR pathway inhibition in the clinic is that blockade of PI3K signaling may shift the tumor survival signaling to a Ras/MAPK dependent pathway (389). Analyzes of human prostate cancer microarrays have demonstrated that the PI3K/AKT and Ras/MAPK pathways are often coordinately dysregulated during prostate cancer progression in humans (118, 390). Although BEZ235 is effective against PI3K-driven tumors as a single agent, the inhibitor responds poorly to tumors harboring Kras mutations (379). Indeed, BEZ235 is only effective against Kras-driven tumors when combined with a MEK inhibitor (391). Humans with advanced prostate cancer treated with RAD001 experience increased activation of MAPK signaling, probably due to the loss of the S6K-IRS1 feedback loop that leads to Ras activation (389) (Fig. 2). In addition, neoadjuvant hormone therapy can lead to increased P-MAPK activation and N-cadherin expression, both of which have been

implicated in the induction of the EMT program and metastatic prostate cancer (118, 392). Ras activation can also play a direct role in moving prostate cancer cell lines towards decreased androgen dependence (393). Indeed, PI3K/AKT and Braf/ERK pathway activation acts combinatorially in a mouse model of CRPC (394). These studies suggest the importance for combined PI3K/AKT and Ras/MAPK pathway blockade in the treatment of CRPC and metastatic prostate cancer.

A number of studies conducted with *Pten* knockout mice have shown that combined pharmacological targeting of mTOR and MEK may lead to reduced primary prostate tumor progression (118, 390). Combination therapy using the mTORC1 inhibitor rapamycin and the MEK inhibitor PD0325901 inhibits not only growth in prostate cancer cell lines (390), but also reduces tumor burden in castrated, androgen-insensitive prostate tumors in the $Nkx3.1^{-/-};Pten^{+/-}$ murine model (394). Dual mTOR and MEK inhibition also, remarkably, completely ablates the dissemination of distant metastases in the $PbCre;Pten^{L/L};Kras^{G12D/+}$ murine prostate cancer model, which exhibits 100% penetrable macrometastasis (118), as well as reduces tumor and metastatic burden in $Nkx3.1^{Cre\text{-}ER};Pten^{f/f};Braf^{CA/+}$ mice (273). Thus, in late stage, metastatic prostate cancer, dual PI3K/AKT and Ras/MAPK inhibition may be necessary to reduce metastasis, as well as slow primary tumor growth (Fig. 1).

Combination therapy with PI3K/AKT/mTOR and AR Pathway inhibitors

Recent studies using the *Pten*-null murine model of prostate cancer have demonstrated a reciprocal feedback loop that exists between AR and PI3K pathways in the prostate cancer,

whereby inhibition of the PI3K pathway in *Pten* deficient prostate cancer results in reactivation of AR signaling by modulating AR co-repressor activities or through feedback signaling to the receptor tyrosine kinase HER2/HER3 (293, 294). Therefore, the efficacy of PI3K inhibitors for the treatment of *PTEN* deficient prostate cancer may be improved through combined AR pathway inhibition. Another recent study utilizing surgical castration in *Pten*-null mice to model CRPC demonstrated that dual targeting of both AKT and mTOR with inhibitors MK-2206 and MK-8869, respectively, is highly effective at inhibiting CRPC *in vivo* (395). Moreover, the AR agonist MDV3100, which has shown promise in the clinic, has improved efficacy in combination with BEZ235 (379), a dual inhibitor of PI3K and mTORC1/2, in castration resistant GEM mice (294). Other laboratories have also documented beneficial effects of combined AR and mTORC1 inhibition with rapamycin in $Pten^{-/-}$ models (293, 396). Thus, more effective inhibition of the AR signaling axis with new generation inhibitors such as abiraterone and MDV3100 in combination with mTOR or PI3K/mTOR dual inhibitors may prove to be more beneficial in treating CRPC patients displaying alterations in PI3K/AKT pathway signaling (Fig. 2).

In all, although dual PI3K/mTOR inhibitors now offer the advantage of complete PI3K/AKT/mTOR pathway inhibition, with signaling feedback loops present in the PI3K/AKT/mTOR pathway that negatively control both Ras/MAPK and AR signaling, it is likely that PI3K inhibition alone will not be able to achieve full regression of tumors in patients with prostate tumors driven by PTEN loss. A better understanding of pathway dynamics gained from recent preclinical studies prompts the rationale for combining inhibition of the PI3K/AKT/mTOR pathway with inhibition of either the Ras/MAPK or AR signaling pathways for the treatment of metastatic CRPC. However, better surrogate biomarkers that predict patient

responses to PI3K inhibitors, as well as more high-throughput systems to molecularly profile and detect PTEN loss or PI3K/AKT/mTOR activation in patients, will be needed to accurately assess the efficacy of PI3K/AKT/mTOR inhibition as a treatment in individual patients.

Conclusions and Perspectives

In the 15 years since the discovery of PTEN as a frequently mutated gene in cancer, great progress in understanding the function and regulation of PTEN has been made. While PTEN was first identified as a lipid phosphatase with tumor suppressive activity against the PI3K/AKT pathway, recent studies have revealed that PTEN has additional protein-phosphatase and lipid phosphatase-independent activities, as well as functions in the nucleus. Further understanding of the mechanisms behind PTEN post-transcriptional regulation, post-translational modifications, and protein-protein interactions offers novel therapeutic opportunities, as well as explanations of why, clinically, loss of PTEN expression can occur without genetic deletion or mutations at the *PTEN* locus. With improved methods for detecting PTEN status, such as CGH, whole-exome sequencing, and transcriptome analysis, PTEN loss can more readily and more accurately be used as a prognostic biomarker for men with prostate cancer, as well as a potential predictive marker to identify patients who could benefit from emerging PTEN/PI3K/Akt pathway therapies. Moreover, studies with large human prostate cancer cohorts have revealed that alterations in the PI3K/AKT/mTOR pathway are more common in advanced, metastatic prostate cancer and CRPC compared to primary, androgen-dependent tumors, and are associated with a poorer overall prognosis and increased chance of biochemical recurrence. Recent works using *Pten* mouse models have helped to reveal the role of PTEN dosage on prostate tumorigenesis and the

collaborative effects of PTEN loss and other genetic and pathway alterations in prostate cancer initiation, progression, and metastasis, which recapitulate all stages of human prostate cancer. A better understanding of the interactions between the PI3K/AKT pathway and Ras/MAPK, p53, and TGF-β–Smad pathways has facilitated the development of metastatic models of prostate cancer with bone metastasis potential, an important feature of human prostate cancer. As bone tropism of prostate cancer metastasis is not well understood, these mouse models should provide better insights into the cell types and molecular pathways involved in metastasis to the bone. Better systems, via lineage-tracing and cell type-specific deletion, are needed to address which cell types are responsible for different stages of the disease, including prostate cancer progression, castration resistance and metastasis. As previous studies have suggested that prostate luminal, transit amplifying (TA), and basal cells can serve as a cell-of-origin and as cancer stem cell (CSC) populations in prostate cancer (303), it will be important for future models to employ more restrictive prostate specific promoters allowing the potential for tumor initiation from basal, TA, neuorendocrine, and luminal cell types. Two recent reports have also elucidated a reciprocal feedback loop between the PI3K/AKT and AR signaling pathways that directly regulates CRPC, offering an explanation for how loss of androgen-dependence may further strengthen PI3K/AKT signaling in PTEN deficient prostate cancer, as well as a rationale for the combined use of AR signaling and PI3K/AKT/mTOR inhibitors in the treatment of CRPC.

Although beyond the scope of this review, emerging research in other solid tumors has demonstrated that the tumor microenvironment itself may play a defined role in tumor propagation and progression, and it will be interesting to see if aberrations in the

PI3K/AKT/mTOR signaling in stromal specific subtypes themselves in the prostate may contribute to tumorigenesis. Moreover, PTEN alterations in the tumor epithelium, which have been demonstrated to induce the release of paracrine signals, including chemokines and cytokines that may attract immune cell types to the prostate and contribute to the development of a tumor-permissive rather than a tumor-suppressive microenvironment, suggest that immunotherapy may be a possible treatment for prostate cancer patients. Again, the specific stromal cells and immune cells that contribute to the prostate tumor microenvironment will need to be further pursued with the use of lineage-specific promoters and tracking systems in immune competent models that preserve the tumor's native microenvironment.

Finally, while past clinical trials using rapamycin and rapalogues to treat human prostate cancer have shown little efficacy, due in part to an inability to inhibit PI3K and AKT signaling, dual PI3K/mTOR inhibitors have the capacity to completely inhibit all strands of the PI3K/AKT/mTOR pathway, and thus deserve further study in preclinical models of prostate cancer. However, with signaling feedback loops present in the PI3K/AKT/mTOR pathway that negatively control both Ras/MAPK and AR signaling, it is unlikely that PI3K inhibition alone will be able to achieve full regression of PTEN deficient prostate tumors. Further understanding of pathway dynamics gained from recent preclinical studies prompts the rationale for combining inhibition of the PI3K/AKT/mTOR pathway with inhibition of either the Ras/MAPK or AR signaling pathways for the treatment of metastatic CRPC. In the end, though much progress has been made in understanding the role PTEN and its regulation of the PI3KAKT/mTOR pathway in prostate cancer, in the future, more basic and pre-clinical mechanistic studies that further elucidate the complexity of the PI3K/AKT/mTOR signaling pathway and can be translated from

bench to bedside will help to design better treatment options for patients with metastatic castration-resistant prostate cancer, for which there is still no cure.

References

1. Bigner SH, Mark J, Mahaley MS, Bigner DD. Patterns of the Early, Gross Chromosomal Changes in Malignant Human Gliomas. Hereditas. 1984;101:103-13.

2. Li J, Yen C, Liaw D, Podsypanina K, Bose S, Wang SI, et al. PTEN, a putative protein tyrosine phosphatase gene mutated in human brain, breast, and prostate cancer. Science. 1997;275:1943-7.

3. Steck PA, Pershouse MA, Jasser SA, Yung WK, Lin H, Ligon AH, et al. Identification of a candidate tumour suppressor gene, MMAC1, at chromosome 10q23.3 that is mutated in multiple advanced cancers. Nat Genet. 1997;15:356-62.

4. Li DM, Sun H. TEP1, encoded by a candidate tumor suppressor locus, is a novel protein tyrosine phosphatase regulated by transforming growth factor beta. Cancer Res. 1997;57:2124-9.

5. Gustafson S, Zbuk KM, Scacheri C, Eng C. Cowden syndrome. Semin Oncol. 2007;34:428-34.

6. Blumenthal GM, Dennis PA. PTEN hamartoma tumor syndromes. Eur J Hum Genet. 2008;16:1289-300.

7. Lloyd KM, 2nd, Dennis M. Cowden's disease. A possible new symptom complex with multiple system involvement. Ann Intern Med. 1963;58:136-42.

8. Dahia PL, Marsh DJ, Zheng Z, Zedenius J, Komminoth P, Frisk T, et al. Somatic deletions and mutations in the Cowden disease gene, PTEN, in sporadic thyroid tumors. Cancer Res. 1997;57:4710-3.

9. Halachmi N, Halachmi S, Evron E, Cairns P, Okami K, Saji M, et al. Somatic mutations of the PTEN tumor suppressor gene in sporadic follicular thyroid tumors. Genes Chromosomes Cancer. 1998;23:239-43.

10. Xie CC, Lu L, Sun J, Zheng SL, Isaacs WB, Gronberg H, et al. Germ-line sequence variants of PTEN do not have an important role in hereditary and non-hereditary prostate cancer susceptibility. J Hum Genet. 2011;56:496-502.

11. Cooney KA, Tsou HC, Petty EM, Miesfeldt S, Ping XL, Gruener AC, et al. Absence of PTEN germ-line mutations in men with a potential inherited predisposition to prostate cancer. Clin Cancer Res. 1999;5:1387-91.

12. Feilotter HE, Nagai MA, Boag AH, Eng C, Mulligan LM. Analysis of PTEN and the 10q23 region in primary prostate carcinomas. Oncogene. 1998;16:1743-8.

13. Cairns P, Okami K, Halachmi S, Halachmi N, Esteller M, Herman JG, et al. Frequent inactivation of PTEN/MMAC1 in primary prostate cancer. Cancer Res. 1997;57:4997-5000.

14. Denu JM, Stuckey JA, Saper MA, Dixon JE. Form and function in protein dephosphorylation. Cell. 1996;87:361-4.

15. Lee JO, Yang H, Georgescu MM, Di Cristofano A, Maehama T, Shi Y, et al. Crystal structure of the PTEN tumor suppressor: implications for its phosphoinositide phosphatase activity and membrane association. Cell. 1999;99:323-34.

16. Redfern RE, Redfern D, Furgason ML, Munson M, Ross AH, Gericke A. PTEN phosphatase selectively binds phosphoinositides and undergoes structural changes. Biochemistry. 2008;47:2162-71.

17. Liaw D, Marsh DJ, Li J, Dahia PL, Wang SI, Zheng Z, et al. Germline mutations of the PTEN gene in Cowden disease, an inherited breast and thyroid cancer syndrome. Nat Genet. 1997;16:64-7.

18. Tonks NK, Cicirelli MF, Diltz CD, Krebs EG, Fischer EH. Effect of microinjection of a low-Mr human placenta protein tyrosine phosphatase on induction of meiotic cell division in Xenopus oocytes. Mol Cell Biol. 1990;10:458-63.

19. Maehama T, Dixon JE. The tumor suppressor, PTEN/MMAC1, dephosphorylates the lipid second messenger, phosphatidylinositol 3,4,5-trisphosphate. J Biol Chem. 1998;273:13375-8.

20. Waite KA, Eng C. Protean PTEN: form and function. Am J Hum Genet. 2002;70:829-44.

21. Georgescu MM, Kirsch KH, Kaloudis P, Yang H, Pavletich NP, Hanafusa H. Stabilization and productive positioning roles of the C2 domain of PTEN tumor suppressor. Cancer Res. 2000;60:7033-8.

22. Taylor BS, Schultz N, Hieronymus H, Gopalan A, Xiao Y, Carver BS, et al. Integrative genomic profiling of human prostate cancer. Cancer Cell. 2010;18:11-22.

23. Grasso CS, Wu YM, Robinson DR, Cao X, Dhanasekaran SM, Khan AP, et al. The mutational landscape of lethal castration-resistant prostate cancer. Nature. 2012;487:239-43.

24. Barbieri CE, Baca SC, Lawrence MS, Demichelis F, Blattner M, Theurillat JP, et al. Exome sequencing identifies recurrent SPOP, FOXA1 and MED12 mutations in prostate cancer. Nat Genet. 2012;44:685-9.

25. Vivanco I, Sawyers CL. The phosphatidylinositol 3-Kinase AKT pathway in human cancer. Nat Rev Cancer. 2002;2:489-501.

26. Stambolic V, Suzuki A, de la Pompa JL, Brothers GM, Mirtsos C, Sasaki T, et al. Negative regulation of PKB/Akt-dependent cell survival by the tumor suppressor PTEN. Cell. 1998;95:29-39.

27. Sun H, Lesche R, Li DM, Liliental J, Zhang H, Gao J, et al. PTEN modulates cell cycle progression and cell survival by regulating phosphatidylinositol 3,4,5,-trisphosphate and Akt/protein kinase B signaling pathway. Proc Natl Acad Sci U S A. 1999;96:6199-204.

28. Manning BD, Cantley LC. AKT/PKB signaling: navigating downstream. Cell. 2007;129:1261-74.

29. Zoncu R, Efeyan A, Sabatini DM. mTOR: from growth signal integration to cancer, diabetes and ageing. Nat Rev Mol Cell Biol. 2011;12:21-35.

30. de la Taille A, Rubin MA, Chen MW, Vacherot F, de Medina SG, Burchardt M, et al. Beta-catenin-related anomalies in apoptosis-resistant and hormone-refractory prostate cancer cells. Clin Cancer Res. 2003;9:1801-7.

31. Lee HK, Kwak HY, Hur J, Kim IA, Yang JS, Park MW, et al. beta-catenin regulates multiple steps of RNA metabolism as revealed by the RNA aptamer in colon cancer cells. Cancer Res. 2007;67:9315-21.

32. Grunwald V, DeGraffenried L, Russel D, Friedrichs WE, Ray RB, Hidalgo M. Inhibitors of mTOR reverse doxorubicin resistance conferred by PTEN status in prostate cancer cells. Cancer Res. 2002;62:6141-5.

33. Wu X, Senechal K, Neshat MS, Whang YE, Sawyers CL. The PTEN/MMAC1 tumor suppressor phosphatase functions as a negative regulator of the phosphoinositide 3-kinase/Akt pathway. Proc Natl Acad Sci U S A. 1998;95:15587-91.

34. Guertin DA, Sabatini DM. Defining the Role of mTOR in Cancer. Cancer Cell. 2007;12:9-22.

35. Vander Haar E, Lee S, Bandhakavi S, Griffin TJ, Kim DH. Insulin signalling to mTOR mediated by the Akt/PKB substrate PRAS40. Nature Cell Biology. 2007;9:316-U126.

36. Ma XM, Blenis J. Molecular mechanisms of mTOR-mediated translational control. Nat Rev Mol Cell Biol. 2009;10:307-18.

37. Um SH, Frigerio F, Watanabe M, Picard F, Joaquin M, Sticker M, et al. Absence of S6K1 protects against age- and diet-induced obesity while enhancing insulin sensitivity. Nature. 2004;431:200-5.

38. Harrington LS, Findlay GM, Gray A, Tolkacheva T, Wigfield S, Rebholz H, et al. The TSC1-2 tumor suppressor controls insulin-PI3K signaling via regulation of IRS proteins. J Cell Biol. 2004;166:213-23.

39. Hsu PP, Kang SA, Rameseder J, Zhang Y, Ottina KA, Lim D, et al. The mTOR-regulated phosphoproteome reveals a mechanism of mTORC1-mediated inhibition of growth factor signaling. Science. 2011;332:1317-22.

40. Yu G, Xiao CL, Lu CH, Jia HT, Ge F, Wang W, et al. Phosphoproteome profile of human lung cancer cell line A549. Mol Biosyst. 2011;7:472-9.

41. Warburg O. On respiratory impairment in cancer cells. Science. 1956;124:269-70.

42. Tong X, Zhao F, Thompson CB. The molecular determinants of de novo nucleotide biosynthesis in cancer cells. Curr Opin Genet Dev. 2009;19:32-7.

43. Stewart GD, Gray K, Pennington CJ, Edwards DR, Riddick AC, Ross JA, et al. Analysis of hypoxia-associated gene expression in prostate cancer: lysyl oxidase and glucose transporter-1 expression correlate with Gleason score. Oncol Rep. 2008;20:1561-7.

44. Taha C, Liu Z, Jin J, Al-Hasani H, Sonenberg N, Klip A. Opposite translational control of GLUT1 and GLUT4 glucose transporter mRNAs in response to insulin. Role of mammalian target of rapamycin, protein kinase b, and phosphatidylinositol 3-kinase in GLUT1 mRNA translation. J Biol Chem. 1999;274:33085-91.

45. Eguez L, Lee A, Chavez JA, Miinea CP, Kane S, Lienhard GE, et al. Full intracellular retention of GLUT4 requires AS160 Rab GTPase activating protein. Cell Metab. 2005;2:263-72.

46. Jiang BH, Jiang G, Zheng JZ, Lu Z, Hunter T, Vogt PK. Phosphatidylinositol 3-kinase signaling controls levels of hypoxia-inducible factor 1. Cell Growth Differ. 2001;12:363-9.

47. Gordan JD, Simon MC. Hypoxia-inducible factors: central regulators of the tumor phenotype. Curr Opin Genet Dev. 2007;17:71-7.

48. Zelzer E, Levy Y, Kahana C, Shilo BZ, Rubinstein M, Cohen B. Insulin induces transcription of target genes through the hypoxia-inducible factor HIF-1alpha/ARNT. EMBO J. 1998;17:5085-94.

49. Majumder PK, Sellers WR. Akt-regulated pathways in prostate cancer. Oncogene. 2005;24:7465-74.

50. Zundel W, Schindler C, Haas-Kogan D, Koong A, Kaper F, Chen E, et al. Loss of PTEN facilitates HIF-1-mediated gene expression. Genes Dev. 2000;14:391-6.

51. Sundqvist A, Bengoechea-Alonso MT, Ye X, Lukiyanchuk V, Jin J, Harper JW, et al. Control of lipid metabolism by phosphorylation-dependent degradation of the SREBP family of transcription factors by SCF(Fbw7). Cell Metab. 2005;1:379-91.

52. Li X, Monks B, Ge Q, Birnbaum MJ. Akt/PKB regulates hepatic metabolism by directly inhibiting PGC-1alpha transcription coactivator. Nature. 2007;447:1012-6.

53. Deprez J, Vertommen D, Alessi DR, Hue L, Rider MH. Phosphorylation and activation of heart 6-phosphofructo-2-kinase by protein kinase B and other protein kinases of the insulin signaling cascades. J Biol Chem. 1997;272:17269-75.

54. Ros S, Santos CR, Moco S, Baenke F, Kelly G, Howell M, et al. Functional metabolic screen identifies 6-phosphofructo-2-kinase/fructose-2,6-biphosphatase 4 as an important regulator of prostate cancer cell survival. Cancer Discov. 2012;2:328-43.

55. Plathow C, Weber WA. Tumor cell metabolism imaging. J Nucl Med. 2008;49 Suppl 2:43S-63S.

56. Jadvar H. Molecular imaging of prostate cancer with 18F-fluorodeoxyglucose PET. Nat Rev Urol. 2009;6:317-23.

57. Oyama N, Akino H, Kanamaru H, Suzuki Y, Muramoto S, Yonekura Y, et al. 11C-acetate PET imaging of prostate cancer. J Nucl Med. 2002;43:181-6.

58. Stiles B, Wang Y, Stahl A, Bassilian S, Lee WP, Kim YJ, et al. Liver-specific deletion of negative regulator Pten results in fatty liver and insulin hypersensitivity [corrected]. Proc Natl Acad Sci U S A. 2004;101:2082-7.

59. Horie Y, Suzuki A, Kataoka E, Sasaki T, Hamada K, Sasaki J, et al. Hepatocyte-specific Pten deficiency results in steatohepatitis and hepatocellular carcinomas. J Clin Invest. 2004;113:1774-83.

60. Van de Sande T, De Schrijver E, Heyns W, Verhoeven G, Swinnen JV. Role of the phosphatidylinositol 3'-kinase/PTEN/Akt kinase pathway in the overexpression of fatty acid synthase in LNCaP prostate cancer cells. Cancer Res. 2002;62:642-6.

61. Li JN, Gorospe M, Chrest FJ, Kumaravel TS, Evans MK, Han WF, et al. Pharmacological inhibition of fatty acid synthase activity produces both cytostatic and cytotoxic effects modulated by p53. Cancer Res. 2001;61:1493-9.

62. Garcia-Cao I, Song MS, Hobbs RM, Laurent G, Giorgi C, de Boer VC, et al. Systemic elevation of PTEN induces a tumor-suppressive metabolic state. Cell. 2012;149:49-62.

63. Christofk HR, Vander Heiden MG, Harris MH, Ramanathan A, Gerszten RE, Wei R, et al. The M2 splice isoform of pyruvate kinase is important for cancer metabolism and tumour growth. Nature. 2008;452:230-3.

64. Telang S, Yalcin A, Clem AL, Bucala R, Lane AN, Eaton JW, et al. Ras transformation requires metabolic control by 6-phosphofructo-2-kinase. Oncogene. 2006;25:7225-34.

65. Chung JH, Ginn-Pease ME, Eng C. Phosphatase and tensin homologue deleted on chromosome 10 (PTEN) has nuclear localization signal-like sequences for nuclear import mediated by major vault protein. Cancer Res. 2005;65:4108-16.

66. Gimm O, Perren A, Weng LP, Marsh DJ, Yeh JJ, Ziebold U, et al. Differential nuclear and cytoplasmic expression of PTEN in normal thyroid tissue, and benign and malignant epithelial thyroid tumors. Am J Pathol. 2000;156:1693-700.

67. Ginn-Pease ME, Eng C. Increased nuclear phosphatase and tensin homologue deleted on chromosome 10 is associated with G0-G1 in MCF-7 cells. Cancer Res. 2003;63:282-6.

68. Lachyankar MB, Sultana N, Schonhoff CM, Mitra P, Poluha W, Lambert S, et al. A role for nuclear PTEN in neuronal differentiation. J Neurosci. 2000;20:1404-13.

69. Perren A, Weng LP, Boag AH, Ziebold U, Thakore K, Dahia PL, et al. Immunohistochemical evidence of loss of PTEN expression in primary ductal adenocarcinomas of the breast. Am J Pathol. 1999;155:1253-60.

70. McCall P, Witton CJ, Grimsley S, Nielsen KV, Edwards J. Is PTEN loss associated with clinical outcome measures in human prostate cancer? Br J Cancer. 2008;99:1296-301.

71. Chang CJ, Mulholland DJ, Valamehr B, Mosessian S, Sellers WR, Wu H. PTEN nuclear localization is regulated by oxidative stress and mediates p53-dependent tumor suppression. Mol Cell Biol. 2008;28:3281-9.

72. Freeman DJ, Li AG, Wei G, Li HH, Kertesz N, Lesche R, et al. PTEN tumor suppressor regulates p53 protein levels and activity through phosphatase-dependent and -independent mechanisms. Cancer Cell. 2003;3:117-30.

73. Li Y, Guessous F, Kwon S, Kumar M, Ibidapo O, Fuller L, et al. PTEN has tumor-promoting properties in the setting of gain-of-function p53 mutations. Cancer Res. 2008;68:1723-31.

74. Lindsay Y, McCoull D, Davidson L, Leslie NR, Fairservice A, Gray A, et al. Localization of agonist-sensitive PtdIns(3,4,5)P3 reveals a nuclear pool that is insensitive to PTEN expression. J Cell Sci. 2006;119:5160-8.

75. Trotman LC, Wang X, Alimonti A, Chen Z, Teruya-Feldstein J, Yang H, et al. Ubiquitination regulates PTEN nuclear import and tumor suppression. Cell. 2007;128:141-56.

76. Weng LP, Brown JL, Eng C. PTEN coordinates G(1) arrest by down-regulating cyclin D1 via its protein phosphatase activity and up-regulating p27 via its lipid phosphatase activity in a breast cancer model. Hum Mol Genet. 2001;10:599-604.

77. Chung JH, Ostrowski MC, Romigh T, Minaguchi T, Waite KA, Eng C. The ERK1/2 pathway modulates nuclear PTEN-mediated cell cycle arrest by cyclin D1 transcriptional regulation. Hum Mol Genet. 2006;15:2553-9.

78. Shen WH, Balajee AS, Wang J, Wu H, Eng C, Pandolfi PP, et al. Essential role for nuclear PTEN in maintaining chromosomal integrity. Cell. 2007;128:157-70.

79. Puc J, Keniry M, Li HS, Pandita TK, Choudhury AD, Memeo L, et al. Lack of PTEN sequesters CHK1 and initiates genetic instability. Cancer Cell. 2005;7:193-204.

80. Mendes-Pereira AM, Martin SA, Brough R, McCarthy A, Taylor JR, Kim JS, et al. Synthetic lethal targeting of PTEN mutant cells with PARP inhibitors. EMBO Mol Med. 2009;1:315-22.

81. McEllin B, Camacho CV, Mukherjee B, Hahm B, Tomimatsu N, Bachoo RM, et al. PTEN loss compromises homologous recombination repair in astrocytes: implications for glioblastoma therapy with temozolomide or poly(ADP-ribose) polymerase inhibitors. Cancer Res. 2010;70:5457-64.

82. Dedes KJ, Wetterskog D, Mendes-Pereira AM, Natrajan R, Lambros MB, Geyer FC, et al. PTEN deficiency in endometrioid endometrial adenocarcinomas predicts sensitivity to PARP inhibitors. Sci Transl Med. 2010;2:53ra75.

83. Fraser M, Zhao H, Luoto KR, Lundin C, Coackley C, Chan N, et al. PTEN deletion in prostate cancer cells does not associate with loss of RAD51 function: implications for radiotherapy and chemotherapy. Clin Cancer Res. 2012;18:1015-27.

84. Hu Z, Gu Y, Han B, Zhang J, Li Z, Tian K, et al. Knockdown of AGR2 induces cellular senescence in prostate cancer cells. Carcinogenesis. 2012;33:1178-86.

85. Song MS, Carracedo A, Salmena L, Song SJ, Egia A, Malumbres M, et al. Nuclear PTEN regulates the APC-CDH1 tumor-suppressive complex in a phosphatase-independent manner. Cell. 2011;144:187-99.

86. Liu XS, Song B, Elzey BD, Ratliff TL, Konieczny SF, Cheng L, et al. Polo-like kinase 1 facilitates loss of Pten tumor suppressor-induced prostate cancer formation. J Biol Chem. 2011;286:35795-800.

87. Blanco-Aparicio C, Renner O, Leal JF, Carnero A. PTEN, more than the AKT pathway. Carcinogenesis. 2007;28:1379-86.

88. Majumder PK, Yeh JJ, George DJ, Febbo PG, Kum J, Xue Q, et al. Prostate intraepithelial neoplasia induced by prostate restricted Akt activation: the MPAKT model. Proc Natl Acad Sci U S A. 2003;100:7841-6.

89. Lee SH, Poulogiannis G, Pyne S, Jia S, Zou L, Signoretti S, et al. A constitutively activated form of the p110beta isoform of PI3-kinase induces prostatic intraepithelial neoplasia in mice. Proc Natl Acad Sci U S A. 2010;107:11002-7.

90. Jia S, Liu Z, Zhang S, Liu P, Zhang L, Lee SH, et al. Essential roles of PI(3)K-p110beta in cell growth, metabolism and tumorigenesis. Nature. 2008;454:776-9.

91. Guertin DA, Stevens DM, Saitoh M, Kinkel S, Crosby K, Sheen JH, et al. mTOR complex 2 is required for the development of prostate cancer induced by Pten loss in mice. Cancer Cell. 2009;15:148-59.

92. Stambolic V, MacPherson D, Sas D, Lin Y, Snow B, Jang Y, et al. Regulation of PTEN transcription by p53. Mol Cell. 2001;8:317-25.

93. Chang CJ, Freeman DJ, Wu H. PTEN regulates Mdm2 expression through the P1 promoter. J Biol Chem. 2004;279:29841-8.

94. Mayo LD, Donner DB. A phosphatidylinositol 3-kinase/Akt pathway promotes translocation of Mdm2 from the cytoplasm to the nucleus. Proc Natl Acad Sci U S A. 2001;98:11598-603.

95. Mayo LD, Dixon JE, Durden DL, Tonks NK, Donner DB. PTEN protects p53 from Mdm2 and sensitizes cancer cells to chemotherapy. J Biol Chem. 2002;277:5484-9.

96. Alimonti A, Nardella C, Chen Z, Clohessy JG, Carracedo A, Trotman LC, et al. A novel type of cellular senescence that can be enhanced in mouse models and human tumor xenografts to suppress prostate tumorigenesis. J Clin Invest. 2010;120:681-93.

97. Nardella C, Carracedo A, Alimonti A, Hobbs RM, Clohessy JG, Chen Z, et al. Differential requirement of mTOR in postmitotic tissues and tumorigenesis. Sci Signal. 2009;2:ra2.

98. Raftopoulou M, Etienne-Manneville S, Self A, Nicholls S, Hall A. Regulation of cell migration by the C2 domain of the tumor suppressor PTEN. Science. 2004;303:1179-81.

99. Zhou M, Gu L, Findley HW, Jiang R, Woods WG. PTEN reverses MDM2-mediated chemotherapy resistance by interacting with p53 in acute lymphoblastic leukemia cells. Cancer Res. 2003;63:6357-62.

100. Cully M, You H, Levine AJ, Mak TW. Beyond PTEN mutations: the PI3K pathway as an integrator of multiple inputs during tumorigenesis. Nat Rev Cancer. 2006;6:184-92.

101. Chen Z, Trotman LC, Shaffer D, Lin HK, Dotan ZA, Niki M, et al. Crucial role of p53-dependent cellular senescence in suppression of Pten-deficient tumorigenesis. Nature. 2005;436:725-30.

102. Lei Q, Jiao J, Xin L, Chang CJ, Wang S, Gao J, et al. NKX3.1 stabilizes p53, inhibits AKT activation, and blocks prostate cancer initiation caused by PTEN loss. Cancer Cell. 2006;9:367-78.

103. Vivanco I, Palaskas N, Tran C, Finn SP, Getz G, Kennedy NJ, et al. Identification of the JNK signaling pathway as a functional target of the tumor suppressor PTEN. Cancer Cell. 2007;11:555-69.

104. Hubner A, Mulholland DJ, Standen CL, Karasarides M, Cavanagh-Kyros J, Barrett T, et al. JNK and PTEN cooperatively control the development of invasive adenocarcinoma of the prostate. Proc Natl Acad Sci U S A. 2012;109:12046-51.

105. Myers MP, Stolarov JP, Eng C, Li J, Wang SI, Wigler MH, et al. P-TEN, the tumor suppressor from human chromosome 10q23, is a dual-specificity phosphatase. Proc Natl Acad Sci U S A. 1997;94:9052-7.

106. Tamura M, Gu J, Matsumoto K, Aota S, Parsons R, Yamada KM. Inhibition of cell migration, spreading, and focal adhesions by tumor suppressor PTEN. Science. 1998;280:1614-7.

107. Gu T, Zhang Z, Wang J, Guo J, Shen WH, Yin Y. CREB is a novel nuclear target of PTEN phosphatase. Cancer Res. 2011;71:2821-5.

108. Mounir Z, Krishnamoorthy JL, Robertson GP, Scheuner D, Kaufman RJ, Georgescu MM, et al. Tumor suppression by PTEN requires the activation of the PKR-eIF2alpha phosphorylation pathway. Sci Signal. 2009;2:ra85.

109. Zhang S, Huang WC, Li P, Guo H, Poh SB, Brady SW, et al. Combating trastuzumab resistance by targeting SRC, a common node downstream of multiple resistance pathways. Nat Med. 2011;17:461-9.

110. Sansal I, Sellers WR. The biology and clinical relevance of the PTEN tumor suppressor pathway. J Clin Oncol. 2004;22:2954-63.

111. Whang YE, Wu X, Suzuki H, Reiter RE, Tran C, Vessella RL, et al. Inactivation of the tumor suppressor PTEN/MMAC1 in advanced human prostate cancer through loss of expression. Proc Natl Acad Sci U S A. 1998;95:5246-50.

112. Lu J, Jeong HW, Kong N, Yang Y, Carroll J, Luo HR, et al. Stem cell factor SALL4 represses the transcriptions of PTEN and SALL1 through an epigenetic repressor complex. PLoS One. 2009;4:e5577.

113. Mukhopadhyay NK, Cinar B, Mukhopadhyay L, Lutchman M, Ferdinand AS, Kim J, et al. The zinc finger protein ras-responsive element binding protein-1 is a coregulator of the androgen receptor: implications for the role of the Ras pathway in enhancing androgenic signaling in prostate cancer. Mol Endocrinol. 2007;21:2056-70.

114. Chow JY, Quach KT, Cabrera BL, Cabral JA, Beck SE, Carethers JM. RAS/ERK modulates TGFbeta-regulated PTEN expression in human pancreatic adenocarcinoma cells. Carcinogenesis. 2007;28:2321-7.

115. Hettinger K, Vikhanskaya F, Poh MK, Lee MK, de Belle I, Zhang JT, et al. c-Jun promotes cellular survival by suppression of PTEN. Cell Death Differ. 2007;14:218-29.

116. Xia D, Srinivas H, Ahn YH, Sethi G, Sheng X, Yung WK, et al. Mitogen-activated protein kinase kinase-4 promotes cell survival by decreasing PTEN expression through an NF kappa B-dependent pathway. J Biol Chem. 2007;282:3507-19.

117. Escriva M, Peiro S, Herranz N, Villagrasa P, Dave N, Montserrat-Sentis B, et al. Repression of PTEN phosphatase by Snail1 transcriptional factor during gamma radiation-induced apoptosis. Mol Cell Biol. 2008;28:1528-40.

118. Mulholland DJ, Kobayashi N, Ruscetti M, Zhi A, Tran LM, Huang J, et al. Pten loss and RAS/MAPK activation cooperate to promote EMT and metastasis initiated from prostate cancer stem/progenitor cells. Cancer Res. 2012;72:1878-89.

119. Thiery JP, Acloque H, Huang RY, Nieto MA. Epithelial-mesenchymal transitions in development and disease. Cell. 2009;139:871-90.

120. Palmero I, Pantoja C, Serrano M. p19ARF links the tumour suppressor p53 to Ras. Nature. 1998;395:125-6.

121. Whelan JT, Forbes SL, Bertrand FE. CBF-1 (RBP-J kappa) binds to the PTEN promoter and regulates PTEN gene expression. Cell Cycle. 2007;6:80-4.

122. Patel L, Pass I, Coxon P, Downes CP, Smith SA, Macphee CH. Tumor suppressor and anti-inflammatory actions of PPARgamma agonists are mediated via upregulation of PTEN. Curr Biol. 2001;11:764-8.

123. Virolle T, Adamson ED, Baron V, Birle D, Mercola D, Mustelin T, et al. The Egr-1 transcription factor directly activates PTEN during irradiation-induced signalling. Nat Cell Biol. 2001;3:1124-8.

124. Song LB, Li J, Liao WT, Feng Y, Yu CP, Hu LJ, et al. The polycomb group protein Bmi-1 represses the tumor suppressor PTEN and induces epithelial-mesenchymal transition in human nasopharyngeal epithelial cells. J Clin Invest. 2009;119:3626-36.

125. Lukacs RU, Memarzadeh S, Wu H, Witte ON. Bmi-1 is a crucial regulator of prostate stem cell self-renewal and malignant transformation. Cell Stem Cell. 2010;7:682-93.

126. Bartel DP. MicroRNAs: target recognition and regulatory functions. Cell. 2009;136:215-33.

127. Poliseno L, Salmena L, Riccardi L, Fornari A, Song MS, Hobbs RM, et al. Identification of the miR-106b~25 microRNA cluster as a proto-oncogenic PTEN-targeting intron that cooperates with its host gene MCM7 in transformation. Sci Signal. 2010;3:ra29.

128. Poliseno L, Salmena L, Zhang J, Carver B, Haveman WJ, Pandolfi PP. A coding-independent function of gene and pseudogene mRNAs regulates tumour biology. Nature. 2010;465:1033-8.

129. Song MS, Salmena L, Pandolfi PP. The functions and regulation of the PTEN tumour suppressor. Nat Rev Mol Cell Biol. 2012;13:283-96.

130. Karreth FA, Tay Y, Perna D, Ala U, Tan SM, Rust AG, et al. In vivo identification of tumor- suppressive PTEN ceRNAs in an oncogenic BRAF-induced mouse model of melanoma. Cell. 2011;147:382-95.

131. Sumazin P, Yang X, Chiu HS, Chung WJ, Iyer A, Llobet-Navas D, et al. An extensive microRNA-mediated network of RNA-RNA interactions regulates established oncogenic pathways in glioblastoma. Cell. 2011;147:370-81.

132. Tay Y, Kats L, Salmena L, Weiss D, Tan SM, Ala U, et al. Coding-independent regulation of the tumor suppressor PTEN by competing endogenous mRNAs. Cell. 2011;147:344-57.

133. Torres J, Pulido R. The tumor suppressor PTEN is phosphorylated by the protein kinase CK2 at its C terminus. Implications for PTEN stability to proteasome-mediated degradation. J Biol Chem. 2001;276:993-8.

134. Georgescu MM, Kirsch KH, Akagi T, Shishido T, Hanafusa H. The tumor-suppressor activity of PTEN is regulated by its carboxyl-terminal region. Proc Natl Acad Sci U S A. 1999;96:10182-7.

135. Vazquez F, Grossman SR, Takahashi Y, Rokas MV, Nakamura N, Sellers WR. Phosphorylation of the PTEN tail acts as an inhibitory switch by preventing its recruitment into a protein complex. J Biol Chem. 2001;276:48627-30.

136. Das S, Dixon JE, Cho W. Membrane-binding and activation mechanism of PTEN. Proc Natl Acad Sci U S A. 2003;100:7491-6.

137. Miller SJ, Lou DY, Seldin DC, Lane WS, Neel BG. Direct identification of PTEN phosphorylation sites. FEBS Lett. 2002;528:145-53.

138. Rabinovsky R, Pochanard P, McNear C, Brachmann SM, Duke-Cohan JS, Garraway LA, et al. p85 Associates with unphosphorylated PTEN and the PTEN-associated complex. Mol Cell Biol. 2009;29:5377-88.

139. Odriozola L, Singh G, Hoang T, Chan AM. Regulation of PTEN activity by its carboxyl-terminal autoinhibitory domain. J Biol Chem. 2007;282:23306-15.

140. Leslie NR, Downes CP. PTEN function: how normal cells control it and tumour cells lose it. Biochem J. 2004;382:1-11.

141. Liang K, Esteva FJ, Albarracin C, Stemke-Hale K, Lu Y, Bianchini G, et al. Recombinant human erythropoietin antagonizes trastuzumab treatment of breast cancer cells via Jak2-mediated Src activation and PTEN inactivation. Cancer Cell. 2010;18:423-35.

142. Maccario H, Perera NM, Davidson L, Downes CP, Leslie NR. PTEN is destabilized by phosphorylation on Thr366. Biochem J. 2007;405:439-44.

143. Al-Khouri AM, Ma Y, Togo SH, Williams S, Mustelin T. Cooperative phosphorylation of the tumor suppressor phosphatase and tensin homologue (PTEN) by casein kinases and glycogen synthase kinase 3beta. J Biol Chem. 2005;280:35195-202.

144. Li Z, Dong X, Wang Z, Liu W, Deng N, Ding Y, et al. Regulation of PTEN by Rho small GTPases. Nat Cell Biol. 2005;7:399-404.

145. Sanchez T, Thangada S, Wu MT, Kontos CD, Wu D, Wu H, et al. PTEN as an effector in the signaling of antimigratory G protein-coupled receptor. Proc Natl Acad Sci U S A. 2005;102:4312-7.

146. Papakonstanti EA, Ridley AJ, Vanhaesebroeck B. The p110delta isoform of PI 3-kinase negatively controls RhoA and PTEN. EMBO J. 2007;26:3050-61.

147. Yim EK, Peng G, Dai H, Hu R, Li K, Lu Y, et al. Rak functions as a tumor suppressor by regulating PTEN protein stability and function. Cancer Cell. 2009;15:304-14.

148. Wang X, Trotman LC, Koppie T, Alimonti A, Chen Z, Gao Z, et al. NEDD4-1 is a proto-oncogenic ubiquitin ligase for PTEN. Cell. 2007;128:129-39.

149. Fouladkou F, Landry T, Kawabe H, Neeb A, Lu C, Brose N, et al. The ubiquitin ligase Nedd4-1 is dispensable for the regulation of PTEN stability and localization. Proc Natl Acad Sci U S A. 2008;105:8585-90.

150. Van Themsche C, Leblanc V, Parent S, Asselin E. X-linked inhibitor of apoptosis protein (XIAP) regulates PTEN ubiquitination, content, and compartmentalization. J Biol Chem. 2009;284:20462-6.

151. Maddika S, Kavela S, Rani N, Palicharla VR, Pokorny JL, Sarkaria JN, et al. WWP2 is an E3 ubiquitin ligase for PTEN. Nat Cell Biol. 2011;13:728-33.

152. Leslie NR, Batty IH, Maccario H, Davidson L, Downes CP. Understanding PTEN regulation: PIP2, polarity and protein stability. Oncogene. 2008;27:5464-76.

153. Lee SR, Yang KS, Kwon J, Lee C, Jeong W, Rhee SG. Reversible inactivation of the tumor suppressor PTEN by H2O2. J Biol Chem. 2002;277:20336-42.

154. Silva A, Yunes JA, Cardoso BA, Martins LR, Jotta PY, Abecasis M, et al. PTEN posttranslational inactivation and hyperactivation of the PI3K/Akt pathway sustain primary T cell leukemia viability. J Clin Invest. 2008;118:3762-74.

155. Okumura K, Mendoza M, Bachoo RM, DePinho RA, Cavenee WK, Furnari FB. PCAF modulates PTEN activity. J Biol Chem. 2006;281:26562-8.

156. Yu CX, Li S, Whorton AR. Redox regulation of PTEN by S-nitrosothiols. Mol Pharmacol. 2005;68:847-54.

157. Wu X, Hepner K, Castelino-Prabhu S, Do D, Kaye MB, Yuan XJ, et al. Evidence for regulation of the PTEN tumor suppressor by a membrane-localized multi-PDZ domain containing scaffold protein MAGI-2. Proc Natl Acad Sci U S A. 2000;97:4233-8.

158. Takahashi Y, Morales FC, Kreimann EL, Georgescu MM. PTEN tumor suppressor associates with NHERF proteins to attenuate PDGF receptor signaling. EMBO J. 2006;25:910-20.

159. Valiente M, Andres-Pons A, Gomar B, Torres J, Gil A, Tapparel C, et al. Binding of PTEN to specific PDZ domains contributes to PTEN protein stability and phosphorylation by microtubule-associated serine/threonine kinases. J Biol Chem. 2005;280:28936-43.

160. Subauste MC, Nalbant P, Adamson ED, Hahn KM. Vinculin controls PTEN protein level by maintaining the interaction of the adherens junction protein beta-catenin with the scaffolding protein MAGI-2. J Biol Chem. 2005;280:5676-81.

161. Vazquez F, Ramaswamy S, Nakamura N, Sellers WR. Phosphorylation of the PTEN tail regulates protein stability and function. Mol Cell Biol. 2000;20:5010-8.

162. Mosessian S, Avliyakulov NK, Mulholland DJ, Boontheung P, Loo JA, Wu H. Analysis of PTEN complex assembly and identification of heterogeneous nuclear ribonucleoprotein C as a component of the PTEN-associated complex. J Biol Chem. 2009;284:30159-66.

163. Mosessian S, Wu H. PTEN-Associated Complexes: An Overview. Curr Top Biochem Res. 2010;12:37-42.

164. Okahara F, Ikawa H, Kanaho Y, Maehama T. Regulation of PTEN phosphorylation and stability by a tumor suppressor candidate protein. J Biol Chem. 2004;279:45300-3.

165. Lima-Fernandes E, Enslen H, Camand E, Kotelevets L, Boularan C, Achour L, et al. Distinct functional outputs of PTEN signalling are controlled by dynamic association with beta-arrestins. EMBO J. 2011;30:2557-68.

166. Chagpar RB, Links PH, Pastor MC, Furber LA, Hawrysh AD, Chamberlain MD, et al. Direct positive regulation of PTEN by the p85 subunit of phosphatidylinositol 3-kinase. Proc Natl Acad Sci U S A. 2010;107:5471-6.

167. Kim YC, Kitaura H, Taira T, Iguchi-Ariga SM, Ariga H. Oxidation of DJ-1-dependent cell transformation through direct binding of DJ-1 to PTEN. Int J Oncol. 2009;35:1331-41.

168. Kim RH, Peters M, Jang Y, Shi W, Pintilie M, Fletcher GC, et al. DJ-1, a novel regulator of the tumor suppressor PTEN. Cancer Cell. 2005;7:263-73.

169. Fine B, Hodakoski C, Koujak S, Su T, Saal LH, Maurer M, et al. Activation of the PI3K pathway in cancer through inhibition of PTEN by exchange factor P-REX2a. Science. 2009;325:1261-5.

170. He L, Ingram A, Rybak AP, Tang D. Shank-interacting protein-like 1 promotes tumorigenesis via PTEN inhibition in human tumor cells. J Clin Invest. 2010;120:2094-108.

171. He L, Fan C, Kapoor A, Ingram AJ, Rybak AP, Austin RC, et al. alpha-Mannosidase 2C1 attenuates PTEN function in prostate cancer cells. Nat Commun. 2011;2:307.

172. Yeung T, Grinstein S. Lipid signaling and the modulation of surface charge during phagocytosis. Immunol Rev. 2007;219:17-36.

173. Vazquez F, Matsuoka S, Sellers WR, Yanagida T, Ueda M, Devreotes PN. Tumor suppressor PTEN acts through dynamic interaction with the plasma membrane. Proc Natl Acad Sci U S A. 2006;103:3633-8.

174. Yu Z, Fotouhi-Ardakani N, Wu L, Maoui M, Wang S, Banville D, et al. PTEN associates with the vault particles in HeLa cells. J Biol Chem. 2002;277:40247-52.

175. Sumitomo M, Iwase A, Zheng R, Navarro D, Kaminetzky D, Shen R, et al. Synergy in tumor suppression by direct interaction of neutral endopeptidase with PTEN. Cancer Cell. 2004;5:67-78.

176. van Diepen MT, Parsons M, Downes CP, Leslie NR, Hindges R, Eickholt BJ. MyosinV controls PTEN function and neuronal cell size. Nat Cell Biol. 2009;11:1191-6.

177. Liu F, Wagner S, Campbell RB, Nickerson JA, Schiffer CA, Ross AH. PTEN enters the nucleus by diffusion. J Cell Biochem. 2005;96:221-34.

178. Denning G, Jean-Joseph B, Prince C, Durden DL, Vogt PK. A short N-terminal sequence of PTEN controls cytoplasmic localization and is required for suppression of cell growth. Oncogene. 2007;26:3930-40.

179. Gil A, Andres-Pons A, Fernandez E, Valiente M, Torres J, Cervera J, et al. Nuclear localization of PTEN by a Ran-dependent mechanism enhances apoptosis: Involvement of an N-terminal nuclear localization domain and multiple nuclear exclusion motifs. Mol Biol Cell. 2006;17:4002-13.

180. Song MS, Salmena L, Carracedo A, Egia A, Lo-Coco F, Teruya-Feldstein J, et al. The deubiquitinylation and localization of PTEN are regulated by a HAUSP-PML network. Nature. 2008;455:813-7.

181. Yoshimoto M, Cutz JC, Nuin PA, Joshua AM, Bayani J, Evans AJ, et al. Interphase FISH analysis of PTEN in histologic sections shows genomic deletions in 68% of primary prostate cancer and 23% of high-grade prostatic intra-epithelial neoplasias. Cancer Genet Cytogenet. 2006;169:128-37.

182. Han B, Mehra R, Lonigro RJ, Wang L, Suleman K, Menon A, et al. Fluorescence in situ hybridization study shows association of PTEN deletion with ERG rearrangement during prostate cancer progression. Modern Pathology. 2009;22:1083-93.

183. Suzuki H, Freije D, Nusskern DR, Okami K, Cairns P, Sidransky D, et al. Interfocal heterogeneity of PTEN/MMAC1 gene alterations in multiple metastatic prostate cancer tissues. Cancer Res. 1998;58:204-9.

184. Wang SI, Parsons R, Ittmann M. Homozygous deletion of the PTEN tumor suppressor gene in a subset of prostate adenocarcinomas. Clin Cancer Res. 1998;4:811-5.

185. McMenamin ME, Soung P, Perera S, Kaplan I, Loda M, Sellers WR. Loss of PTEN expression in paraffin-embedded primary prostate cancer correlates with high Gleason score and advanced stage. Cancer Res. 1999;59:4291-6.

186. Verhagen PCMS, van Duijn PW, Hermans KGL, Looljenga LHJ, van Gurp RJHLM, Stoop H, et al. The PTEN gene in locally progressive prostate cancer is preferentially inactivated by bi-allelic gene deletion. Journal of Pathology. 2006;208:699-707.

187. Yoshimoto M, Cunha IW, Coudry RA, Fonseca FP, Torres CH, Soares FA, et al. FISH analysis of 107 prostate cancers shows that PTEN genomic deletion is associated with poor clinical outcome. British Journal of Cancer. 2007;97:678-85.

188. Yoshimoto M, Joshua AM, Cunha IW, Coudry RA, Fonseca FP, Ludkovski O, et al. Absence of TMPRSS2:ERG fusions and PTEN losses in prostate cancer is associated with a favorable outcome. Mod Pathol. 2008;21:1451-60.

189. Reid AH, Attard G, Ambroisine L, Fisher G, Kovacs G, Brewer D, et al. Molecular characterisation of ERG, ETV1 and PTEN gene loci identifies patients at low and high risk of death from prostate cancer. Br J Cancer. 2010;102:678-84.

190. Sircar K, Yoshimoto M, Monzon FA, Koumakpayi IH, Katz RL, Khanna A, et al. PTEN genomic deletion is associated with p-Akt and AR signalling in poorer outcome, hormone refractory prostate cancer. J Pathol. 2009;218:505-13.

191. Lotan TL, Gurel B, Sutcliffe S, Esopi D, Liu W, Xu J, et al. PTEN protein loss by immunostaining: analytic validation and prognostic indicator for a high risk surgical cohort of prostate cancer patients. Clin Cancer Res. 2011;17:6563-73.

192. Dong JT, Sipe TW, Hyytinen ER, Li CL, Heise C, McClintock DE, et al. PTEN/MMAC1 is infrequently mutated in pT2 and pT3 carcinomas of the prostate. Oncogene. 1998;17:1979-82.

193. Reid AH, Attard G, Brewer D, Miranda S, Riisnaes R, Clark J, et al. Novel, gross chromosomal alterations involving PTEN cooperate with allelic loss in prostate cancer. Mod Pathol. 2012;25:902-10.

194. Di Cristofano A, Pandolfi PP. The multiple roles of PTEN in tumor suppression. Cell. 2000;100:387-90.

195. Abate-Shen C, Shen MM. Molecular genetics of prostate cancer. Genes Dev. 2000;14:2410-34.

196. Verhagen PC, van Duijn PW, Hermans KG, Looijenga LH, van Gurp RJ, Stoop H, et al. The PTEN gene in locally progressive prostate cancer is preferentially inactivated by bi-allelic gene deletion. J Pathol. 2006;208:699-707.

197. Schmitz M, Grignard G, Margue C, Dippel W, Capesius C, Mossong J, et al. Complete loss of PTEN expression as a possible early prognostic marker for prostate cancer metastasis. Int J Cancer. 2007;120:1284-92.

198. Mulholland DJ, Dedhar S, Wu H, Nelson CC. PTEN and GSK3beta: key regulators of progression to androgen-independent prostate cancer. Oncogene. 2006;25:329-37.

199. Zafarana G, Ishkanian AS, Malloff CA, Locke JA, Sykes J, Thoms J, et al. Copy number alterations of c-MYC and PTEN are prognostic factors for relapse after prostate cancer radiotherapy. Cancer. 2012.

200. Antonarakis ES, Keizman D, Zhang Z, Gurel B, Lotan TL, Hicks JL, et al. An immunohistochemical signature comprising PTEN, MYC, and Ki67 predicts progression in prostate cancer patients receiving adjuvant docetaxel after prostatectomy. Cancer. 2012.

201. Tran LM, Chang CJ, Plaisier S, Wu S, Dang J, Mischel PS, et al. Determining PTEN functional status by network component deduced transcription factor activities. PLoS One. 2012;7:e31053.

202. De Velasco MA, Uemura H. Preclinical Remodeling of Human Prostate Cancer through the PTEN/AKT Pathway. Adv Urol. 2012;2012:419348.

203. Jeet V, Russell PJ, Khatri A. Modeling prostate cancer: a perspective on transgenic mouse models. Cancer Metastasis Rev. 2010;29:123-42.

204. van Weerden WM, Bangma C, de Wit R. Human xenograft models as useful tools to assess the potential of novel therapeutics in prostate cancer. Br J Cancer. 2009;100:13-8.

205. van Weerden WM, Romijn JC. Use of nude mouse xenograft models in prostate cancer research. Prostate. 2000;43:263-71.

206. Greenberg NM, DeMayo F, Finegold MJ, Medina D, Tilley WD, Aspinall JO, et al. Prostate cancer in a transgenic mouse. Proc Natl Acad Sci U S A. 1995;92:3439-43.

207. Mimeault M, Batra SK. Animal models relevant to human prostate carcinogenesis underlining the critical implication of prostatic stem/progenitor cells. Biochim Biophys Acta. 2011;1816:25-37.

208. Di Cristofano A, De Acetis M, Koff A, Cordon-Cardo C, Pandolfi PP. Pten and p27KIP1 cooperate in prostate cancer tumor suppression in the mouse. Nat Genet. 2001;27:222-4.

209. Di Cristofano A, Pesce B, Cordon-Cardo C, Pandolfi PP. Pten is essential for embryonic development and tumour suppression. Nat Genet. 1998;19:348-55.

210. Podsypanina K, Ellenson LH, Nemes A, Gu J, Tamura M, Yamada KM, et al. Mutation of Pten/Mmac1 in mice causes neoplasia in multiple organ systems. Proc Natl Acad Sci U S A. 1999;96:1563-8.

211. Trotman LC, Niki M, Dotan ZA, Koutcher JA, Di Cristofano A, Xiao A, et al. Pten dose dictates cancer progression in the prostate. PLoS Biol. 2003;1:E59.

212. Wang S, Gao J, Lei Q, Rozengurt N, Pritchard C, Jiao J, et al. Prostate-specific deletion of the murine Pten tumor suppressor gene leads to metastatic prostate cancer. Cancer Cell. 2003;4:209-21.

213. Freeman D, Lesche R, Kertesz N, Wang S, Li G, Gao J, et al. Genetic background controls tumor development in PTEN-deficient mice. Cancer Res. 2006;66:6492-6.

214. Alimonti A, Carracedo A, Clohessy JG, Trotman LC, Nardella C, Egia A, et al. Subtle variations in Pten dose determine cancer susceptibility. Nat Genet. 2010;42:454-8.

215. Knudson AG, Jr. Mutation and cancer: statistical study of retinoblastoma. Proc Natl Acad Sci U S A. 1971;68:820-3.

216. Wang S, Garcia AJ, Wu M, Lawson DA, Witte ON, Wu H. Pten deletion leads to the expansion of a prostatic stem/progenitor cell subpopulation and tumor initiation. Proc Natl Acad Sci U S A. 2006;103:1480-5.

217. Luchman HA, Benediktsson H, Villemaire ML, Peterson AC, Jirik FR. The pace of prostatic intraepithelial neoplasia development is determined by the timing of Pten tumor suppressor gene excision. PLoS One. 2008;3:e3940.

218. Blando J, Portis M, Benavides F, Alexander A, Mills G, Dave B, et al. PTEN deficiency is fully penetrant for prostate adenocarcinoma in C57BL/6 mice via mTOR-dependent growth. Am J Pathol. 2009;174:1869-79.

219. Elgavish A, Wood PA, Pinkert CA, Eltoum IE, Cartee T, Wilbanks J, et al. Transgenic mouse with human mutant p53 expression in the prostate epithelium. Prostate. 2004;61:26-34.

220. Maddison LA, Sutherland BW, Barrios RJ, Greenberg NM. Conditional deletion of Rb causes early stage prostate cancer. Cancer Res. 2004;64:6018-25.

221. Abdulkadir SA, Magee JA, Peters TJ, Kaleem Z, Naughton CK, Humphrey PA, et al. Conditional loss of Nkx3.1 in adult mice induces prostatic intraepithelial neoplasia. Mol Cell Biol. 2002;22:1495-503.

222. Ma X, Ziel-van der Made AC, Autar B, van der Korput HA, Vermeij M, van Duijn P, et al. Targeted biallelic inactivation of Pten in the mouse prostate leads to prostate cancer accompanied by increased epithelial cell proliferation but not by reduced apoptosis. Cancer Res. 2005;65:5730-9.

223. Backman SA, Ghazarian D, So K, Sanchez O, Wagner KU, Hennighausen L, et al. Early onset of neoplasia in the prostate and skin of mice with tissue-specific deletion of Pten. Proc Natl Acad Sci U S A. 2004;101:1725-30.

224. Ratnacaram CK, Teletin M, Jiang M, Meng X, Chambon P, Metzger D. Temporally controlled ablation of PTEN in adult mouse prostate epithelium generates a model of invasive prostatic adenocarcinoma. Proc Natl Acad Sci U S A. 2008;105:2521-6.

225. Wang X, Kruithof-de Julio M, Economides KD, Walker D, Yu H, Halili MV, et al. A luminal epithelial stem cell that is a cell of origin for prostate cancer. Nature. 2009;461:495-500.

226. Song H, Zhang B, Watson MA, Humphrey PA, Lim H, Milbrandt J. Loss of Nkx3.1 leads to the activation of discrete downstream target genes during prostate tumorigenesis. Oncogene. 2009;28:3307-19.

227. Kim MJ, Cardiff RD, Desai N, Banach-Petrosky WA, Parsons R, Shen MM, et al. Cooperativity of Nkx3.1 and Pten loss of function in a mouse model of prostate carcinogenesis. Proc Natl Acad Sci U S A. 2002;99:2884-9.

228. Gao H, Ouyang X, Banach-Petrosky W, Borowsky AD, Lin Y, Kim M, et al. A critical role for p27kip1 gene dosage in a mouse model of prostate carcinogenesis. Proc Natl Acad Sci U S A. 2004;101:17204-9.

229. Bhatia-Gaur R, Donjacour AA, Sciavolino PJ, Kim M, Desai N, Young P, et al. Roles for Nkx3.1 in prostate development and cancer. Genes Dev. 1999;13:966-77.

230. Cordon-Cardo C, Koff A, Drobnjak M, Capodieci P, Osman I, Millard SS, et al. Distinct altered patterns of p27KIP1 gene expression in benign prostatic hyperplasia and prostatic carcinoma. J Natl Cancer Inst. 1998;90:1284-91.

231. Guo Y, Sklar GN, Borkowski A, Kyprianou N. Loss of the cyclin-dependent kinase inhibitor p27(Kip1) protein in human prostate cancer correlates with tumor grade. Clin Cancer Res. 1997;3:2269-74.

232. Bowen C, Bubendorf L, Voeller HJ, Slack R, Willi N, Sauter G, et al. Loss of NKX3.1 expression in human prostate cancers correlates with tumor progression. Cancer Res. 2000;60:6111-5.

233. Abate-Shen C, Banach-Petrosky WA, Sun X, Economides KD, Desai N, Gregg JP, et al. Nkx3.1; Pten mutant mice develop invasive prostate adenocarcinoma and lymph node metastases. Cancer Res. 2003;63:3886-90.

234. Kwabi-Addo B, Giri D, Schmidt K, Podsypanina K, Parsons R, Greenberg N, et al. Haploinsufficiency of the Pten tumor suppressor gene promotes prostate cancer progression. Proc Natl Acad Sci U S A. 2001;98:11563-8.

235. Martin P, Liu YN, Pierce R, Abou-Kheir W, Casey O, Seng V, et al. Prostate epithelial Pten/TP53 loss leads to transformation of multipotential progenitors and epithelial to mesenchymal transition. Am J Pathol. 2011;179:422-35.

236. Ding Z, Wu CJ, Chu GC, Xiao Y, Ho D, Zhang J, et al. SMAD4-dependent barrier constrains prostate cancer growth and metastatic progression. Nature. 2011;470:269-73.

237. Ding Z, Wu CJ, Jaskelioff M, Ivanova E, Kost-Alimova M, Protopopov A, et al. Telomerase reactivation following telomere dysfunction yields murine prostate tumors with bone metastases. Cell. 2012;148:896-907.

238. Tomlins SA, Rhodes DR, Perner S, Dhanasekaran SM, Mehra R, Sun XW, et al. Recurrent fusion of TMPRSS2 and ETS transcription factor genes in prostate cancer. Science. 2005;310:644-8.

239. Tomlins SA, Laxman B, Varambally S, Cao X, Yu J, Helgeson BE, et al. Role of the TMPRSS2-ERG gene fusion in prostate cancer. Neoplasia. 2008;10:177-88.

240. FitzGerald LM, Agalliu I, Johnson K, Miller MA, Kwon EM, Hurtado-Coll A, et al. Association of TMPRSS2-ERG gene fusion with clinical characteristics and outcomes: results from a population-based study of prostate cancer. BMC Cancer. 2008;8:230.

241. Carver BS, Tran J, Gopalan A, Chen Z, Shaikh S, Carracedo A, et al. Aberrant ERG expression cooperates with loss of PTEN to promote cancer progression in the prostate. Nat Genet. 2009;41:619-24.

242. Zhong C, Saribekyan G, Liao CP, Cohen MB, Roy-Burman P. Cooperation between FGF8b overexpression and PTEN deficiency in prostate tumorigenesis. Cancer Res. 2006;66:2188-94.

243. Jenkins RB, Qian J, Lieber MM, Bostwick DG. Detection of c-myc oncogene amplification and chromosomal anomalies in metastatic prostatic carcinoma by fluorescence in situ hybridization. Cancer Res. 1997;57:524-31.

244. Ellwood-Yen K, Graeber TG, Wongvipat J, Iruela-Arispe ML, Zhang J, Matusik R, et al. Myc-driven murine prostate cancer shares molecular features with human prostate tumors. Cancer Cell. 2003;4:223-38.

245. Kim J, Eltoum IE, Roh M, Wang J, Abdulkadir SA. Interactions between cells with distinct mutations in c-MYC and Pten in prostate cancer. PLoS Genet. 2009;5:e1000542.

246. Haverkamp J, Charbonneau B, Ratliff TL. Prostate inflammation and its potential impact on prostate cancer: a current review. J Cell Biochem. 2008;103:1344-53.

247. Bardia A, Platz EA, Yegnasubramanian S, De Marzo AM, Nelson WG. Anti-inflammatory drugs, antioxidants, and prostate cancer prevention. Curr Opin Pharmacol. 2009;9:419-26.

248. De Marzo AM, Platz EA, Sutcliffe S, Xu J, Gronberg H, Drake CG, et al. Inflammation in prostate carcinogenesis. Nat Rev Cancer. 2007;7:256-69.

249. Blum DL, Koyama T, M'Koma AE, Iturregui JM, Martinez-Ferrer M, Uwamariya C, et al. Chemokine markers predict biochemical recurrence of prostate cancer following prostatectomy. Clin Cancer Res. 2008;14:7790-7.

250. Tassidis H, Culig Z, Wingren AG, Harkonen P. Role of the protein tyrosine phosphatase SHP-1 in Interleukin-6 regulation of prostate cancer cells. Prostate. 2010;70:1491-500.

251. Shariat SF, Andrews B, Kattan MW, Kim J, Wheeler TM, Slawin KM. Plasma levels of interleukin-6 and its soluble receptor are associated with prostate cancer progression and metastasis. Urology. 2001;58:1008-15.

252. Chung TD, Yu JJ, Kong TA, Spiotto MT, Lin JM. Interleukin-6 activates phosphatidylinositol-3 kinase, which inhibits apoptosis in human prostate cancer cell lines. Prostate. 2000;42:1-7.

253. Wen Z, Zhong Z, Darnell JE, Jr. Maximal activation of transcription by Stat1 and Stat3 requires both tyrosine and serine phosphorylation. Cell. 1995;82:241-50.

254. Abdulghani J, Gu L, Dagvadorj A, Lutz J, Leiby B, Bonuccelli G, et al. Stat3 promotes metastatic progression of prostate cancer. Am J Pathol. 2008;172:1717-28.

255. Blando JM, Carbajal S, Abel E, Beltran L, Conti C, Fischer S, et al. Cooperation between Stat3 and Akt signaling leads to prostate tumor development in transgenic mice. Neoplasia. 2011;13:254-65.

256. Schmid JA, Birbach A. IkappaB kinase beta (IKKbeta/IKK2/IKBKB)--a key molecule in signaling to the transcription factor NF-kappaB. Cytokine Growth Factor Rev. 2008;19:157-65.

257. Shukla S, MacLennan GT, Fu P, Patel J, Marengo SR, Resnick MI, et al. Nuclear factor-kappaB/p65 (Rel A) is constitutively activated in human prostate adenocarcinoma and correlates with disease progression. Neoplasia. 2004;6:390-400.

258. Kong D, Li Y, Wang Z, Banerjee S, Sarkar FH. Inhibition of angiogenesis and invasion by 3,3'-diindolylmethane is mediated by the nuclear factor-kappaB downstream target genes MMP-9 and uPA that regulated bioavailability of vascular endothelial growth factor in prostate cancer. Cancer Res. 2007;67:3310-9.

259. Birbach A, Eisenbarth D, Kozakowski N, Ladenhauf E, Schmidt-Supprian M, Schmid JA. Persistent inflammation leads to proliferative neoplasia and loss of smooth muscle cells in a prostate tumor model. Neoplasia. 2011;13:692-703.

260. Parent CA, Blacklock BJ, Froehlich WM, Murphy DB, Devreotes PN. G protein signaling events are activated at the leading edge of chemotactic cells. Cell. 1998;95:81-91.

261. Meili R, Ellsworth C, Lee S, Reddy TB, Ma H, Firtel RA. Chemoattractant-mediated transient activation and membrane localization of Akt/PKB is required for efficient chemotaxis to cAMP in Dictyostelium. EMBO J. 1999;18:2092-105.

262. Funamoto S, Meili R, Lee S, Parry L, Firtel RA. Spatial and temporal regulation of 3-phosphoinositides by PI 3-kinase and PTEN mediates chemotaxis. Cell. 2002;109:611-23.

263. Iijima M, Devreotes P. Tumor suppressor PTEN mediates sensing of chemoattractant gradients. Cell. 2002;109:599-610.

264. Servant G, Weiner OD, Herzmark P, Balla T, Sedat JW, Bourne HR. Polarization of chemoattractant receptor signaling during neutrophil chemotaxis. Science. 2000;287:1037-40.

265. Li Z, Hannigan M, Mo Z, Liu B, Lu W, Wu Y, et al. Directional sensing requires G beta gamma-mediated PAK1 and PIX alpha-dependent activation of Cdc42. Cell. 2003;114:215-27.

266. Liliental J, Moon SY, Lesche R, Mamillapalli R, Li D, Zheng Y, et al. Genetic deletion of the Pten tumor suppressor gene promotes cell motility by activation of Rac1 and Cdc42 GTPases. Curr Biol. 2000;10:401-4.

267. Kotelevets L, van Hengel J, Bruyneel E, Mareel M, van Roy F, Chastre E. The lipid phosphatase activity of PTEN is critical for stabilizing intercellular junctions and reverting invasiveness. J Cell Biol. 2001;155:1129-35.

268. Martin-Belmonte F, Gassama A, Datta A, Yu W, Rescher U, Gerke V, et al. PTEN-mediated apical segregation of phosphoinositides controls epithelial morphogenesis through Cdc42. Cell. 2007;128:383-97.

269. Gumerlock PH, Poonamallee UR, Meyers FJ, deVere White RW. Activated ras alleles in human carcinoma of the prostate are rare. Cancer Res. 1991;51:1632-7.

270. Cho NY, Choi M, Kim BH, Cho YM, Moon KC, Kang GH. BRAF and KRAS mutations in prostatic adenocarcinoma. Int J Cancer. 2006;119:1858-62.

271. Carter BS, Epstein JI, Isaacs WB. ras gene mutations in human prostate cancer. Cancer Res. 1990;50:6830-2.

272. Wang XS, Shankar S, Dhanasekaran SM, Ateeq B, Sasaki AT, Jing X, et al. Characterization of KRAS rearrangements in metastatic prostate cancer. Cancer Discov. 2011;1:35-43.

273. Wang J, Kobayashi T, Floc'h N, Kinkade CW, Aytes A, Dankort D, et al. Braf activation cooperates with Pten loss to regulate c-Myc activation in advanced prostate cancer. Cancer Res. 2012.

274. Maestro R, Dei Tos AP, Hamamori Y, Krasnokutsky S, Sartorelli V, Kedes L, et al. Twist is a potential oncogene that inhibits apoptosis. Genes Dev. 1999;13:2207-17.

275. Attard G, de Bono JS. Translating scientific advancement into clinical benefit for castration-resistant prostate cancer patients. Clin Cancer Res. 2011;17:3867-75.

276. de Bono JS, Logothetis CJ, Molina A, Fizazi K, North S, Chu L, et al. Abiraterone and increased survival in metastatic prostate cancer. N Engl J Med. 2011;364:1995-2005.

277. Scher HI, Beer TM, Higano CS, Anand A, Taplin ME, Efstathiou E, et al. Antitumour activity of MDV3100 in castration-resistant prostate cancer: a phase 1-2 study. Lancet. 2010;375:1437-46.

278. Attard G, Swennenhuis JF, Olmos D, Reid AH, Vickers E, A'Hern R, et al. Characterization of ERG, AR and PTEN gene status in circulating tumor cells from patients with castration-resistant prostate cancer. Cancer Res. 2009;69:2912-8.

279. Montgomery RB, Mostaghel EA, Vessella R, Hess DL, Kalhorn TF, Higano CS, et al. Maintenance of intratumoral androgens in metastatic prostate cancer: a mechanism for castration-resistant tumor growth. Cancer Res. 2008;68:4447-54.

280. Jiao J, Wang S, Qiao R, Vivanco I, Watson PA, Sawyers CL, et al. Murine cell lines derived from Pten null prostate cancer show the critical role of PTEN in hormone refractory prostate cancer development. Cancer Res. 2007;67:6083-91.

281. Ha S, Ruoff R, Kahoud N, Franke TF, Logan SK. Androgen receptor levels are upregulated by Akt in prostate cancer. Endocr Relat Cancer. 2011;18:245-55.

282. Wen Y, Hu MC, Makino K, Spohn B, Bartholomeusz G, Yan DH, et al. HER-2/neu promotes androgen-independent survival and growth of prostate cancer cells through the Akt pathway. Cancer Res. 2000;60:6841-5.

283. Shen MM, Abate-Shen C. Pten inactivation and the emergence of androgen-independent prostate cancer. Cancer Res. 2007;67:6535-8.

284. Gao H, Ouyang X, Banach-Petrosky WA, Shen MM, Abate-Shen C. Emergence of androgen independence at early stages of prostate cancer progression in Nkx3.1; Pten mice. Cancer Res. 2006;66:7929-33.

285. Friedlander TW, Roy R, Tomlins SA, Ngo VT, Kobayashi Y, Azameera A, et al. Common structural and epigenetic changes in the genome of castration-resistant prostate cancer. Cancer Res. 2012;72:616-25.

286. Li P, Nicosia SV, Bai W. Antagonism between PTEN/MMAC1/TEP-1 and androgen receptor in growth and apoptosis of prostatic cancer cells. J Biol Chem. 2001;276:20444-50.

287. Nan B, Snabboon T, Unni E, Yuan XJ, Whang YE, Marcelli M. The PTEN tumor suppressor is a negative modulator of androgen receptor transcriptional activity. J Mol Endocrinol. 2003;31:169-83.

288. Wang Y, Mikhailova M, Bose S, Pan CX, deVere White RW, Ghosh PM. Regulation of androgen receptor transcriptional activity by rapamycin in prostate cancer cell proliferation and survival. Oncogene. 2008;27:7106-17.

289. Roudier MP, True LD, Higano CS, Vesselle H, Ellis W, Lange P, et al. Phenotypic heterogeneity of end-stage prostate carcinoma metastatic to bone. Hum Pathol. 2003;34:646-53.

290. Heinlein CA, Chang C. Androgen receptor in prostate cancer. Endocr Rev. 2004;25:276-308.

291. Shah RB, Mehra R, Chinnaiyan AM, Shen R, Ghosh D, Zhou M, et al. Androgen-independent prostate cancer is a heterogeneous group of diseases: lessons from a rapid autopsy program. Cancer Res. 2004;64:9209-16.

292. Bluemn EG, Nelson PS. The androgen/androgen receptor axis in prostate cancer. Curr Opin Oncol. 2012;24:251-7.

293. Mulholland DJ, Tran LM, Li Y, Cai H, Morim A, Wang S, et al. Cell autonomous role of PTEN in regulating castration-resistant prostate cancer growth. Cancer Cell. 2011;19:792-804.

294. Carver BS, Chapinski C, Wongvipat J, Hieronymus H, Chen Y, Chandarlapaty S, et al. Reciprocal feedback regulation of PI3K and androgen receptor signaling in PTEN-deficient prostate cancer. Cancer Cell. 2011;19:575-86.

295. Mellinghoff IK, Vivanco I, Kwon A, Tran C, Wongvipat J, Sawyers CL. HER2/neu kinase-dependent modulation of androgen receptor function through effects on DNA binding and stability. Cancer Cell. 2004;6:517-27.

296. Armstrong AJ, Netto GJ, Rudek MA, Halabi S, Wood DP, Creel PA, et al. A pharmacodynamic study of rapamycin in men with intermediate- to high-risk localized prostate cancer. Clin Cancer Res. 2010;16:3057-66.

297. Chee KG, Longmate J, Quinn DI, Chatta G, Pinski J, Twardowski P, et al. The AKT inhibitor perifosine in biochemically recurrent prostate cancer: a phase II California/Pittsburgh cancer consortium trial. Clin Genitourin Cancer. 2007;5:433-7.

298. English HF, Santen RJ, Isaacs JT. Response of glandular versus basal rat ventral prostatic epithelial cells to androgen withdrawal and replacement. Prostate. 1987;11:229-42.

299. Bonkhoff H, Remberger K. Differentiation pathways and histogenetic aspects of normal and abnormal prostatic growth: a stem cell model. Prostate. 1996;28:98-106.

300. Tsujimura A, Koikawa Y, Salm S, Takao T, Coetzee S, Moscatelli D, et al. Proximal location of mouse prostate epithelial stem cells: a model of prostatic homeostasis. J Cell Biol. 2002;157:1257-65.

301. Richardson GD, Robson CN, Lang SH, Neal DE, Maitland NJ, Collins AT. CD133, a novel marker for human prostatic epithelial stem cells. J Cell Sci. 2004;117:3539-45.

302. Chaffer CL, Weinberg RA. A perspective on cancer cell metastasis. Science. 2011;331:1559-64.

303. Lawson DA, Xin L, Lukacs RU, Cheng D, Witte ON. Isolation and functional characterization of murine prostate stem cells. Proc Natl Acad Sci U S A. 2007;104:181-6.

304. Visvader JE, Lindeman GJ. Cancer stem cells in solid tumours: accumulating evidence and unresolved questions. Nat Rev Cancer. 2008;8:755-68.

305. Xin L, Lukacs RU, Lawson DA, Cheng D, Witte ON. Self-renewal and multilineage differentiation in vitro from murine prostate stem cells. Stem Cells. 2007;25:2760-9.

306. Lukacs RU, Lawson DA, Xin L, Zong Y, Garraway I, Goldstein AS, et al. Epithelial stem cells of the prostate and their role in cancer progression. Cold Spring Harb Symp Quant Biol. 2008;73:491-502.

307. Cunha GR, Lung B. The possible influence of temporal factors in androgenic responsiveness of urogenital tissue recombinants from wild-type and androgen-insensitive (Tfm) mice. J Exp Zool. 1978;205:181-93.

308. Xin L, Ide H, Kim Y, Dubey P, Witte ON. In vivo regeneration of murine prostate from dissociated cell populations of postnatal epithelia and urogenital sinus mesenchyme. Proc Natl Acad Sci U S A. 2003;100 Suppl 1:11896-903.

309. Zhang J, Grindley JC, Yin T, Jayasinghe S, He XC, Ross JT, et al. PTEN maintains haematopoietic stem cells and acts in lineage choice and leukaemia prevention. Nature. 2006;441:518-22.

310. Yilmaz OH, Valdez R, Theisen BK, Guo W, Ferguson DO, Wu H, et al. Pten dependence distinguishes haematopoietic stem cells from leukaemia-initiating cells. Nature. 2006;441:475-82.

311. Groszer M, Erickson R, Scripture-Adams DD, Dougherty JD, Le Belle J, Zack JA, et al. PTEN negatively regulates neural stem cell self-renewal by modulating G0-G1 cell cycle entry. Proc Natl Acad Sci U S A. 2006;103:111-6.

312. Leong KG, Wang BE, Johnson L, Gao WQ. Generation of a prostate from a single adult stem cell. Nature. 2008;456:804-8.

313. Xin L, Lawson DA, Witte ON. The Sca-1 cell surface marker enriches for a prostate-regenerating cell subpopulation that can initiate prostate tumorigenesis. Proc Natl Acad Sci U S A. 2005;102:6942-7.

314. Patrawala L, Calhoun T, Schneider-Broussard R, Li H, Bhatia B, Tang S, et al. Highly purified CD44+ prostate cancer cells from xenograft human tumors are enriched in tumorigenic and metastatic progenitor cells. Oncogene. 2006;25:1696-708.

315. Goldstein AS, Lawson DA, Cheng D, Sun W, Garraway IP, Witte ON. Trop2 identifies a subpopulation of murine and human prostate basal cells with stem cell characteristics. Proc Natl Acad Sci U S A. 2008;105:20882-7.

316. Signoretti S, Waltregny D, Dilks J, Isaac B, Lin D, Garraway L, et al. p63 is a prostate basal cell marker and is required for prostate development. Am J Pathol. 2000;157:1769-75.

317. Jiao J, Hindoyan A, Wang S, Tran LM, Goldstein AS, Lawson D, et al. Identification of CD166 as a Surface Marker for Enriching Prostate Stem/Progenitor and Cancer Initiating Cells. PLoS One. 2012;7:e42564.

318. Dubrovska A, Kim S, Salamone RJ, Walker JR, Maira SM, Garcia-Echeverria C, et al. The role of PTEN/Akt/PI3K signaling in the maintenance and viability of prostate cancer stem-like cell populations. Proc Natl Acad Sci U S A. 2009;106:268-73.

319. Maira SM, Stauffer F, Brueggen J, Furet P, Schnell C, Fritsch C, et al. Identification and characterization of NVP-BEZ235, a new orally available dual phosphatidylinositol 3-kinase/mammalian target of rapamycin inhibitor with potent in vivo antitumor activity. Mol Cancer Ther. 2008;7:1851-63.

320. van Leenders GJ, Dukers D, Hessels D, van den Kieboom SW, Hulsbergen CA, Witjes JA, et al. Polycomb-group oncogenes EZH2, BMI1, and RING1 are overexpressed in prostate cancer with adverse pathologic and clinical features. Eur Urol. 2007;52:455-63.

321. Glinsky GV, Berezovska O, Glinskii AB. Microarray analysis identifies a death-from-cancer signature predicting therapy failure in patients with multiple types of cancer. J Clin Invest. 2005;115:1503-21.

322. Nacerddine K, Beaudry JB, Ginjala V, Westerman B, Mattiroli F, Song JY, et al. Akt-mediated phosphorylation of Bmi1 modulates its oncogenic potential, E3 ligase activity, and DNA damage repair activity in mouse prostate cancer. J Clin Invest. 2012;122:1920-32.

323. Fan C, He L, Kapoor A, Rybak AP, De Melo J, Cutz JC, et al. PTEN inhibits BMI1 function independently of its phosphatase activity. Mol Cancer. 2009;8:98.

324. Goldstein AS, Huang J, Guo C, Garraway IP, Witte ON. Identification of a cell of origin for human prostate cancer. Science. 2010;329:568-71.

325. Lawson DA, Zong Y, Memarzadeh S, Xin L, Huang J, Witte ON. Basal epithelial stem cells are efficient targets for prostate cancer initiation. Proc Natl Acad Sci U S A. 2010;107:2610-5.

326. Tran CP, Lin C, Yamashiro J, Reiter RE. Prostate stem cell antigen is a marker of late intermediate prostate epithelial cells. Molecular cancer research : MCR. 2002;1:113-21.

327. Dubey P, Wu H, Reiter RE, Witte ON. Alternative pathways to prostate carcinoma activate prostate stem cell antigen expression. Cancer Res. 2001;61:3256-61.

328. Mulholland DJ, Xin L, Morim A, Lawson D, Witte O, Wu H. Lin-Sca-1+CD49fhigh stem/progenitors are tumor-initiating cells in the Pten-null prostate cancer model. Cancer Res. 2009;69:8555-62.

329. Korsten H, Ziel-van der Made A, Ma X, van der Kwast T, Trapman J. Accumulating progenitor cells in the luminal epithelial cell layer are candidate tumor initiating cells in a Pten knockout mouse prostate cancer model. PLoS One. 2009;4:e5662.

330. Choi N, Zhang B, Zhang L, Ittmann M, Xin L. Adult murine prostate basal and luminal cells are self-sustained lineages that can both serve as targets for prostate cancer initiation. Cancer Cell. 2012;21:253-65.

331. Kasper S, Cookson MS. Mechanisms leading to the development of hormone-resistant prostate cancer. Urol Clin North Am. 2006;33:201-10, vii.

332. Rini BI, Small EJ. Hormone-refractory Prostate Cancer. Curr Treat Options Oncol. 2002;3:437-46.

333. Singh P, Yam M, Russell PJ, Khatri A. Molecular and traditional chemotherapy: a united front against prostate cancer. Cancer Lett. 2010;293:1-14.

334. Petrylak DP, Tangen CM, Hussain MH, Lara PN, Jr., Jones JA, Taplin ME, et al. Docetaxel and estramustine compared with mitoxantrone and prednisone for advanced refractory prostate cancer. N Engl J Med. 2004;351:1513-20.

335. Tannock IF, de Wit R, Berry WR, Horti J, Pluzanska A, Chi KN, et al. Docetaxel plus prednisone or mitoxantrone plus prednisone for advanced prostate cancer. N Engl J Med. 2004;351:1502-12.

336. Higano CS, Schellhammer PF, Small EJ, Burch PA, Nemunaitis J, Yuh L, et al. Integrated data from 2 randomized, double-blind, placebo-controlled, phase 3 trials of active cellular immunotherapy with sipuleucel-T in advanced prostate cancer. Cancer. 2009;115:3670-9.

337. Kantoff PW, Higano CS, Shore ND, Berger ER, Small EJ, Penson DF, et al. Sipuleucel-T immunotherapy for castration-resistant prostate cancer. N Engl J Med. 2010;363:411-22.

338. Kwitkowski VE, Prowell TM, Ibrahim A, Farrell AT, Justice R, Mitchell SS, et al. FDA approval summary: temsirolimus as treatment for advanced renal cell carcinoma. Oncologist. 2010;15:428-35.

339. Bukowski RM, Yasothan U, Kirkpatrick P. Pazopanib. Nat Rev Drug Discov. 2010;9:17-8.

340. Joensuu H, DeMatteo RP. The management of gastrointestinal stromal tumors: a model for targeted and multidisciplinary therapy of malignancy. Annu Rev Med. 2012;63:247-58.

341. Tkaczuk KH. Review of the contemporary cytotoxic and biologic combinations available for the treatment of metastatic breast cancer. Clin Ther. 2009;31 Pt 2:2273-89.

342. Burris H, 3rd, Rocha-Lima C. New therapeutic directions for advanced pancreatic cancer: targeting the epidermal growth factor and vascular endothelial growth factor pathways. Oncologist. 2008;13:289-98.

343. Eng C. The evolving role of monoclonal antibodies in colorectal cancer: early presumptions and impact on clinical trial development. Oncologist. 2010;15:73-84.

344. Cataldo VD, Gibbons DL, Perez-Soler R, Quintas-Cardama A. Treatment of non-small-cell lung cancer with erlotinib or gefitinib. N Engl J Med. 2011;364:947-55.

345. Wee S, Wiederschain D, Maira SM, Loo A, Miller C, deBeaumont R, et al. PTEN-deficient cancers depend on PIK3CB. Proc Natl Acad Sci U S A. 2008;105:13057-62.

346. Lin J, Adam RM, Santiestevan E, Freeman MR. The phosphatidylinositol 3'-kinase pathway is a dominant growth factor-activated cell survival pathway in LNCaP human prostate carcinoma cells. Cancer Res. 1999;59:2891-7.

347. Gupta AK, Cerniglia GJ, Mick R, Ahmed MS, Bakanauskas VJ, Muschel RJ, et al. Radiation sensitization of human cancer cells in vivo by inhibiting the activity of PI3K using LY294002. Int J Radiat Oncol Biol Phys. 2003;56:846-53.

348. Brunn GJ, Williams J, Sabers C, Wiederrecht G, Lawrence JC, Jr., Abraham RT. Direct inhibition of the signaling functions of the mammalian target of rapamycin by the phosphoinositide 3-kinase inhibitors, wortmannin and LY294002. EMBO J. 1996;15:5256-67.

349. Stein RC. Prospects for phosphoinositide 3-kinase inhibition as a cancer treatment. Endocr Relat Cancer. 2001;8:237-48.

350. El-Kholy W, Macdonald PE, Lin JH, Wang J, Fox JM, Light PE, et al. The phosphatidylinositol 3-kinase inhibitor LY294002 potently blocks K(V) currents via a direct mechanism. FASEB J. 2003;17:720-2.

351. Pasapera Limon AM, Herrera-Munoz J, Gutierrez-Sagal R, Ulloa-Aguirre A. The phosphatidylinositol 3-kinase inhibitor LY294002 binds the estrogen receptor and inhibits 17beta-estradiol-induced transcriptional activity of an estrogen sensitive reporter gene. Mol Cell Endocrinol. 2003;200:199-202.

352. Knight ZA, Shokat KM. Chemically targeting the PI3K family. Biochem Soc Trans. 2007;35:245-9.

353. Knight ZA, Gonzalez B, Feldman ME, Zunder ER, Goldenberg DD, Williams O, et al. A pharmacological map of the PI3-K family defines a role for p110alpha in insulin signaling. Cell. 2006;125:733-47.

354. Ihle NT, Lemos R, Jr., Wipf P, Yacoub A, Mitchell C, Siwak D, et al. Mutations in the phosphatidylinositol-3-kinase pathway predict for antitumor activity of the inhibitor PX-866 whereas oncogenic Ras is a dominant predictor for resistance. Cancer Res. 2009;69:143-50.

355. Le Page C, Koumakpayi IH, Alam-Fahmy M, Mes-Masson AM, Saad F. Expression and localisation of Akt-1, Akt-2 and Akt-3 correlate with clinical outcome of prostate cancer patients. Br J Cancer. 2006;94:1906-12.

356. Floryk D, Thompson TC. Perifosine induces differentiation and cell death in prostate cancer cells. Cancer Lett. 2008;266:216-26.

357. Marsh Rde W, Rocha Lima CM, Levy DE, Mitchell EP, Rowland KM, Jr., Benson AB, 3rd. A phase II trial of perifosine in locally advanced, unresectable, or metastatic pancreatic adenocarcinoma. Am J Clin Oncol. 2007;30:26-31.

358. Hillman GG, Wang Y, Kucuk O, Che M, Doerge DR, Yudelev M, et al. Genistein potentiates inhibition of tumor growth by radiation in a prostate cancer orthotopic model. Mol Cancer Ther. 2004;3:1271-9.

359. Li Y, Sarkar FH. Inhibition of nuclear factor kappaB activation in PC3 cells by genistein is mediated via Akt signaling pathway. Clin Cancer Res. 2002;8:2369-77.

360. Lakshman M, Xu L, Ananthanarayanan V, Cooper J, Takimoto CH, Helenowski I, et al. Dietary genistein inhibits metastasis of human prostate cancer in mice. Cancer Res. 2008;68:2024-32.

361. Li Y, Kucuk O, Hussain M, Abrams J, Cher ML, Sarkar FH. Antitumor and antimetastatic activities of docetaxel are enhanced by genistein through regulation of osteoprotegerin/receptor activator of nuclear factor-kappaB (RANK)/RANK ligand/MMP-9 signaling in prostate cancer. Cancer Res. 2006;66:4816-25.

362. Rhodes N, Heerding DA, Duckett DR, Eberwein DJ, Knick VB, Lansing TJ, et al. Characterization of an Akt kinase inhibitor with potent pharmacodynamic and antitumor activity. Cancer Res. 2008;68:2366-74.

363. Chandarlapaty S, Sawai A, Scaltriti M, Rodrik-Outmezguine V, Grbovic-Huezo O, Serra V, et al. AKT inhibition relieves feedback suppression of receptor tyrosine kinase expression and activity. Cancer Cell. 2011;19:58-71.

364. Sun SY, Rosenberg LM, Wang X, Zhou Z, Yue P, Fu H, et al. Activation of Akt and eIF4E survival pathways by rapamycin-mediated mammalian target of rapamycin inhibition. Cancer Res. 2005;65:7052-8.

365. Gao N, Zhang Z, Jiang BH, Shi X. Role of PI3K/AKT/mTOR signaling in the cell cycle progression of human prostate cancer. Biochem Biophys Res Commun. 2003;310:1124-32.

366. Peffley DM, Sharma C, Hentosh P, Buechler RD. Perillyl alcohol and genistein differentially regulate PKB/Akt and 4E-BP1 phosphorylation as well as eIF4E/eIF4G interactions in human tumor cells. Arch Biochem Biophys. 2007;465:266-73.

367. MacManus CF, Pettigrew J, Seaton A, Wilson C, Maxwell PJ, Berlingeri S, et al. Interleukin-8 signaling promotes translational regulation of cyclin D in androgen-independent prostate cancer cells. Mol Cancer Res. 2007;5:737-48.

368. Gera JF, Mellinghoff IK, Shi Y, Rettig MB, Tran C, Hsu JH, et al. AKT activity determines sensitivity to mammalian target of rapamycin (mTOR) inhibitors by regulating cyclin D1 and c-myc expression. J Biol Chem. 2004;279:2737-46.

369. Podsypanina K, Lee RT, Politis C, Hennessy I, Crane A, Puc J, et al. An inhibitor of mTOR reduces neoplasia and normalizes p70/S6 kinase activity in Pten+/- mice. Proc Natl Acad Sci U S A. 2001;98:10320-5.

370. Wu L, Birle DC, Tannock IF. Effects of the mammalian target of rapamycin inhibitor CCI-779 used alone or with chemotherapy on human prostate cancer cells and xenografts. Cancer Res. 2005;65:2825-31.

371. Cao C, Subhawong T, Albert JM, Kim KW, Geng L, Sekhar KR, et al. Inhibition of mammalian target of rapamycin or apoptotic pathway induces autophagy and radiosensitizes PTEN null prostate cancer cells. Cancer Res. 2006;66:10040-7.

372. Masiello D, Mohi MG, McKnight NC, Smith B, Neel BG, Balk SP, et al. Combining an mTOR antagonist and receptor tyrosine kinase inhibitors for the treatment of prostate cancer. Cancer Biol Ther. 2007;6:195-201.

373. Majumder PK, Febbo PG, Bikoff R, Berger R, Xue Q, McMahon LM, et al. mTOR inhibition reverses Akt-dependent prostate intraepithelial neoplasia through regulation of apoptotic and HIF-1-dependent pathways. Nat Med. 2004;10:594-601.

374. Amato RJ, Jac J, Mohammad T, Saxena S. Pilot study of rapamycin in patients with hormone-refractory prostate cancer. Clin Genitourin Cancer. 2008;6:97-102.

375. Sarker D, Reid AH, Yap TA, de Bono JS. Targeting the PI3K/AKT pathway for the treatment of prostate cancer. Clin Cancer Res. 2009;15:4799-805.

376. Park S, Zhao D, Hatanpaa KJ, Mickey BE, Saha D, Boothman DA, et al. RIP1 activates PI3K-Akt via a dual mechanism involving NF-kappaB-mediated inhibition of the mTOR-S6K-IRS1 negative feedback loop and down-regulation of PTEN. Cancer Res. 2009;69:4107-11.

377. O'Reilly KE, Rojo F, She QB, Solit D, Mills GB, Smith D, et al. mTOR inhibition induces upstream receptor tyrosine kinase signaling and activates Akt. Cancer Res. 2006;66:1500-8.

378. Wan X, Harkavy B, Shen N, Grohar P, Helman LJ. Rapamycin induces feedback activation of Akt signaling through an IGF-1R-dependent mechanism. Oncogene. 2007;26:1932-40.

379. Serra V, Markman B, Scaltriti M, Eichhorn PJ, Valero V, Guzman M, et al. NVP-BEZ235, a dual PI3K/mTOR inhibitor, prevents PI3K signaling and inhibits the growth of cancer cells with activating PI3K mutations. Cancer Res. 2008;68:8022-30.

380. Feldman ME, Apsel B, Uotila A, Loewith R, Knight ZA, Ruggero D, et al. Active-site inhibitors of mTOR target rapamycin-resistant outputs of mTORC1 and mTORC2. PLoS Biol. 2009;7:e38.

381. Thoreen CC, Kang SA, Chang JW, Liu Q, Zhang J, Gao Y, et al. An ATP-competitive mammalian target of rapamycin inhibitor reveals rapamycin-resistant functions of mTORC1. J Biol Chem. 2009;284:8023-32.

382. Hsieh AC, Liu Y, Edlind MP, Ingolia NT, Janes MR, Sher A, et al. The translational landscape of mTOR signalling steers cancer initiation and metastasis. Nature. 2012;485:55-61.

383. Schnell CR, Stauffer F, Allegrini PR, O'Reilly T, McSheehy PM, Dartois C, et al. Effects of the dual phosphatidylinositol 3-kinase/mammalian target of rapamycin inhibitor NVP-BEZ235 on the tumor vasculature: implications for clinical imaging. Cancer Res. 2008;68:6598-607.

384. Garlich JR, De P, Dey N, Su JD, Peng X, Miller A, et al. A vascular targeted pan phosphoinositide 3-kinase inhibitor prodrug, SF1126, with antitumor and antiangiogenic activity. Cancer Res. 2008;68:206-15.

385. Mallon R, Feldberg LR, Lucas J, Chaudhary I, Dehnhardt C, Santos ED, et al. Antitumor efficacy of PKI-587, a highly potent dual PI3K/mTOR kinase inhibitor. Clin Cancer Res. 2011;17:3193-203.

386. Raynaud FI, Eccles S, Clarke PA, Hayes A, Nutley B, Alix S, et al. Pharmacologic characterization of a potent inhibitor of class I phosphatidylinositide 3-kinases. Cancer Res. 2007;67:5840-50.

387. Dan S, Yoshimi H, Okamura M, Mukai Y, Yamori T. Inhibition of PI3K by ZSTK474 suppressed tumor growth not via apoptosis but G0/G1 arrest. Biochem Biophys Res Commun. 2009;379:104-9.

388. Fan QW, Cheng CK, Nicolaides TP, Hackett CS, Knight ZA, Shokat KM, et al. A dual phosphoinositide-3-kinase alpha/mTOR inhibitor cooperates with blockade of epidermal growth factor receptor in PTEN-mutant glioma. Cancer Res. 2007;67:7960-5.

389. Carracedo A, Ma L, Teruya-Feldstein J, Rojo F, Salmena L, Alimonti A, et al. Inhibition of mTORC1 leads to MAPK pathway activation through a PI3K-dependent feedback loop in human cancer. J Clin Invest. 2008;118:3065-74.

390. Kinkade CW, Castillo-Martin M, Puzio-Kuter A, Yan J, Foster TH, Gao H, et al. Targeting AKT/mTOR and ERK MAPK signaling inhibits hormone-refractory prostate cancer in a preclinical mouse model. J Clin Invest. 2008;118:3051-64.

391. Engelman JA, Chen L, Tan X, Crosby K, Guimaraes AR, Upadhyay R, et al. Effective use of PI3K and MEK inhibitors to treat mutant Kras G12D and PIK3CA H1047R murine lung cancers. Nat Med. 2008;14:1351-6.

392. Tanaka H, Kono E, Tran CP, Miyazaki H, Yamashiro J, Shimomura T, et al. Monoclonal antibody targeting of N-cadherin inhibits prostate cancer growth, metastasis and castration resistance. Nat Med. 2010;16:1414-20.

393. Weber MJ, Gioeli D. Ras signaling in prostate cancer progression. J Cell Biochem. 2004;91:13-25.

394. Gao H, Ouyang X, Banach-Petrosky WA, Gerald WL, Shen MM, Abate-Shen C. Combinatorial activities of Akt and B-Raf/Erk signaling in a mouse model of androgen-independent prostate cancer. Proc Natl Acad Sci U S A. 2006;103:14477-82.

395. Floc'h N, Kinkade CW, Kobayashi T, Aytes A, Lefebvre C, Mitrofanova A, et al. Dual targeting of the Akt/mTOR signaling pathway inhibits castration-resistant prostate cancer in a genetically engineered mouse model. Cancer Res. 2012.

396. Zhang W, Zhu J, Efferson CL, Ware C, Tammam J, Angagaw M, et al. Inhibition of tumor growth progression by antiandrogens and mTOR inhibitor in a Pten-deficient mouse model of prostate cancer. Cancer Res. 2009;69:7466-72.

Chapter 2:

Pten null prostate epithelium promotes localized myeloid-derived suppressor cell expansion and immune suppression during prostate cancer initiation and progression

Pten Null Prostate Epithelium Promotes Localized Myeloid-Derived Suppressor Cell Expansion and Immune Suppression during Tumor Initiation and Progression

Alejandro J. Garcia,[a,b] Marcus Ruscetti,[a,b,e] Teresita L. Arenzana,[c] Linh M. Tran,[a,b] Daniella Bianci-Frias,[d] Elysia Sybert,[a,b] Saul J. Priceman,[a,b] Lily Wu,[a,b] Peter S. Nelson,[d] Stephen T. Smale,[c] Hong Wu[a,b,f]

Department of Molecular and Medical Pharmacology,[a] Institute for Molecular Medicine,[b] and Department of Microbiology, Immunology and Molecular Genetics,[c] David Geffen School of Medicine at UCLA, Los Angeles, California, USA; Divisions of Human Biology and Clinical Research, Fred Hutchinson Cancer Research Center, Seattle, Washington, USA[d]; Molecular Biology Institute, University of California, Los Angeles, Los Angeles, California, USA[e]; School of Life Sciences, PKU-Tsinghua Center for Life Sciences, Peking University, Beijing, China[f]

Chronic inflammation is known to be associated with prostate cancer development, but how epithelium-associated cancer-initiating events cross talk to inflammatory cells during prostate cancer initiation and progression is largely unknown. Using the *Pten* null murine prostate cancer model, we show an expansion of Gr-1$^+$ CD11b$^+$ myeloid-derived suppressor cells (MDSCs) occurring intraprostatically immediately following epithelium-specific *Pten* deletion without expansion in hematopoietic tissues. This MDSC expansion is accompanied by sustained immune suppression. Prostatic Gr-1$^+$ CD11b$^+$ cells, but not those isolated from the spleen of the same tumor-bearing mice, suppress T cell proliferation and express high levels of *Arginase 1* and *iNOS*. Mechanistically, the loss of PTEN in the epithelium leads to a significant upregulation of genes within the inflammatory response and cytokine-cytokine receptor interaction pathways, including *Csf1* and *Il1b*, two genes known to induce MDSC expansion and immunosuppressive activities. Treatment of *Pten* null mice with the selective CSF-1 receptor inhibitor GW2580 decreases MDSC infiltration and relieves the associated immunosuppressive phenotype. Our study indicates that epithelium-associated tumor-initiating events trigger the secretion of inflammatory cytokines and promote localized MDSC expansion and immune suppression, thereby promoting tumor progression.

Recent studies suggest that tumor-infiltrating myeloid cells, and in particular myeloid-derived suppressor cells (MDSCs), are important mediators of a tumor-permissive microenvironment that contributes to tumor growth and, moreover, could account for the limited success of immunotherapeutic strategies (1, 2).

MDSCs are a heterogeneous population of cells that are precursors of dendritic cells (DCs), macrophages, and granulocytes. They are characterized in mice by the dual expression of the cell surface molecules Gr-1 (Ly6C and Ly6G) and CD11b, although other markers, such as CD80, CD115, and F4/80, have been used to characterize subtypes of MDSCs in different tumors (3). MDSCs suppress innate immunity by secreting cytokines and suppressing DC and macrophage maturation (4–6). MDSCs can also suppress adaptive immunity by blocking T cell activation (7), inducing T_{reg} accumulation (8), and inhibiting natural killer (NK) cell cytotoxicity against tumor cells (9).

Although the association between MDSCs and immune suppression has been demonstrated in various animal models and in human cancers, the causes of MDSC expansion, especially during tumor initiation and progression, are largely unknown. Since prostate cancer is known to be associated with chronic inflammation (10, 11), we sought to investigate how MDSCs are involved in prostate cancer initiation and progression. Using the endogenous *Pten* null prostate cancer model that recapitulates the major genetic alterations and disease hallmarks seen in human prostate cancers (12), we found that proinflammatory cytokines produced by *Pten* null prostate epithelial cells are the major causes of intraprostatic MDSC expansion and the establishment of a tumor-permissive microenvironment.

MATERIALS AND METHODS

Mouse strains. The generation of *Pb-Cre*$^+$; *Pten*$^{lox/lox}$ mice was described previously by our group (12). All animal experiments were approved by the UCLA Animal Research Committee and conducted according to relevant regulatory standards.

Histology and immunohistochemistry. Immunohistochemical analysis was performed on formalin-fixed, paraffin-embedded tissue sections. Antigen retrieval was performed by heating the slides to 95°C in citrate buffer (pH 6.0) for 30 min before staining. The following primary antibodies were used: rat anti-CD45 (1:100; BD Biosciences), rabbit anti-E-cadherin (anti-E-cad) (1:500; BD Biosciences), mouse anti-α-smooth muscle actin (anti-α-SMA) (1:1,000; Sigma-Aldrich), rabbit anti-Ki67 (1:500; Vector Laboratories), rabbit anti-phospho-colony-stimulating factor 1 receptor (anti-p-CSF-1R) (1:100; Santa Cruz), and rat antibromodeoxyuridine (anti-BrdU) (1:500; BD Biosciences).

Tissue dissociation and single-cell suspension. Single-cell suspensions were prepared from prostates, draining lymph nodes, spleen, bone marrow (BM), and liver of age- and genetic background-matched wild-type (WT) and *Pb-Cre*$^+$; *Pten*$^{lox/lox}$ mice at the indicated time points. For prostates, ventral and dorsolateral prostate lobes of individual mice were separated from the remainder of the prostate. All tissues were minced in

Received 17 January 2014 Returned for modification 26 January 2014
Accepted 14 March 2014
Published ahead of print 24 March 2014
Address correspondence to Hong Wu, hwu@mednet.ucla.edu.
A.J.G. and M.R. contributed equally to this work.

doi:10.1128/MCB.00090-14

sterile tissue culture dishes and subjected to collagenase A (1 mg/ml; Roche) and DNase I (0.1 mg/ml; Roche) digestion for 1 h at 37°C with constant agitation. Undigested tissue was passed through a 70-μm filter to facilitate dissociation, followed by washes in phosphate-buffered saline (PBS) and resuspension in Hanks' balanced salt solution. Live cells were quantified by trypan blue exclusion. Spleens and livers were subjected to a red blood cell lysis step using ammonium-chloride-potassium (ACK) lysing buffer (Quality Biological, Inc.) after digestion, followed by passage through a 70-μm filter. All cells were resuspended in Hanks' balanced salt solution plus 2% fetal bovine serum (FBS).

Fluorescence-activated cell sorting (FACS) analysis and cell sorting. Single-cell suspensions were stained with directly conjugated antibodies against CD45, Gr-1, CD11b, CD4, CD8, CD69, B220 (BD Biosciences), F4/80, CD19, CD11c, major histocompatibility complex class II (MHCII) (eBioscience), and Ly6C (BioLegend), according to the manufacturers' instructions. Flow cytometric analysis was performed on a FACSCanto II instrument (BD Biosciences), and data were analyzed by using BDFACS Diva software (BD Biosciences). For isolation of MDSCs, single-cell suspensions were stained with directly conjugated antibodies against CD45, Gr-1, and CD11b, sorted on a FACSAria instrument (BD Biosciences) as $CD45^+$ $GR\text{-}1^+$ $CD11b^+$ fractions, and collected in Dulbecco's modified Eagle medium plus 50% fetal bovine serum. For isolation of prostate epithelial cells, single-cell suspensions were stained with directly conjugated antibodies against CD45 (BD Biosciences), CD31, Ter119, and Epcam (Biolegend) and sorted on a FACSAria instrument (BD Biosciences) as $CD45^-$ $CD31^-$ $Ter119^-$ $Epcam^+$ fractions. Cells were collected in Dulbecco's modified Eagle medium plus 50% fetal bovine serum.

BrdU pulse labeling. Mice were injected intraperitoneally with a single dose of BrdU (dissolved in PBS to a final concentration of 10 mg/ml) at 100 mg/kg of body weight. Prostates, spleens, and bone marrow were harvested 24 h after injection.

Quantitative RT-PCR. RNA was extracted and purified from FACS-sorted cell populations by using RNeasy Mini and RNeasy Micro columns (Qiagen) according to the manufacturer's protocols. Purified total RNA was reverse transcribed to cDNA by the High-Prostate Cancecity cDNA Archive kit (Applied Biosystems, Foster City, CA, USA) with random primers and MultiScribe reverse transcriptase (RT). The relative gene expression levels were measured by real-time RT-PCR using gene-specific primers and iQ SYBR green Supermix (Bio-Rad) and normalized to the β-actin RNA quantity for each cDNA sample as an endogenous control. The primers used are as follows: forward (F) primer AAGAAAAGGCCG ATTCACCT and reverse (R) primer CACCTCCTCTGCTGTCTTCC for *Arg1*, F primer CAGCTGGCCAATGAGGTACT and R primer GTGCCA GAAGCTGGAACTCT for *iNOS*, F primer ACAACACCCCCAATGC TAAC and R primer GCTGTTGTTGCAGTTCTTGG for *Csf1*, F primer GCCCATCCTCTGTGACTCAT and R primer AGGCCACAGGTATTTT GTCG for *Il1b*, F primer ATCGATTTCTCCCCTGTGAA and R primer GCTCTGTCTAGGTCCTGGAGTC for *Il10*, F primer GGGGGCTTTAT CATCCTCAC and R primer CCAAGACCTCAGGCAACAGT for *Il1ra*, and F primer TCTCAGTCTCAACGCTGTGG and R primer GGCCCTT TGGGTGATAAACT for *Csf1r*.

Cell culture and T cell suppression assays. FACS-sorted MDSCs were spun down, counted, and plated into 96-well plates at an MDSC/T cell ratio of 1:1, 1:2, 1:5, or 1:10. A total of 3.0×10^5 to 5.0×10^5 MDSCs were used for the 1:1 ratio. T cells were harvested from naive, wild-type littermate animals by mashing whole spleen through a 40-μm filter, followed by red blood cell lysis using ACK buffer. FACS-sorted $CD8^+$ or $CD4^+$ T cells were then washed, counted, and stained with carboxyfluorescein diacetate succinimidyl ester (CFSE) (Invitrogen, Carlsbad, CA) according to the manufacturer's instructions. Labeled T cells were plated onto 96-well plates in the presence or absence of anti-CD3 antibody (1 μg/ml), with and without MDSCs, and allowed to proliferate for 5 days. Proliferation rates were measured as a function of CFSE dilution and reported as a percentage of cells with diluted CFSE. Values were then normalized to the proliferation rate at an MDSC/T cell ratio of 0:1.

Data analysis and statistics. All experiments were conducted in a minimum of three independent sets. Graphpad Prism software (Graphpad, La Jolla, CA) was used to calculate means and standard deviations (SD). A Student *t* test was used to determine statistical evaluations. Data are presented as means ± SD.

Laser capture and microarray analysis. Freshly dissected prostates from age- and genetic background-matched WT and $Pb\text{-}Cre^+$; $Pten^{lox/lox}$ mice ($n = 3$; 28 to 30 weeks) were snap-frozen in OCT. Consecutive frozen sections were used for hematoxylin and eosin (H&E) and PTEN immunohistochemical staining to confirm pathological lesions and PTEN loss before laser capture microdissection (approximately 5,000 cells per sample) (13). RNA isolation, amplification, and quantification were performed as previously described (13). To provide a reference standard RNA for use on two-color cDNA microarrays, we used pooled total RNA from normal adult male Swiss-Webster mice (10% prostate and 30% each testis, liver, and kidney). For *Pten* null prostate cancer cell lines (PTEN-CaP2 and -CaP8), cells were cultured according to our previously reported methods and harvested for RNA extraction (14). Total RNA was also extracted from microdissected benign mouse prostate epithelial cells as the wild-type control against cell lines. A total of 825 ng of amplified mRNA from each sample was labeled with Cy3 fluorescent dye, and the reference standard was labeled with Cy5. Samples were then hybridized to Agilent 44K whole-mouse genome expression oligonucleotide microarray slides (Agilent Technologies, Inc.) according to the manufacturer's suggested protocols. Fluorescence array images were collected for Cy3 and Cy5 by using the Agilent DNA G2565BA microarray scanner, and Agilent Feature Extraction software was used to grid, extract, and normalize data.

Bioinformatics analysis. Before bioinformatics analysis, we first filtered out the probes that were determined by Agilent software to be of poor quality ($P > 0.05$). For those genes detected by multiple probes, the intensities of probes were first averaged before the analysis. *In vivo* and *in vitro* samples were analyzed separately before being combined for clustering analysis (Cluster 3.0). For pathway and molecular signature analysis (15) as well as Gene Ontology analysis (http://www.geneontology.org/), we used Fisher's exact test to determine the pathways or biological processes enriched in the *Pten* null samples, based on genes that are significantly altered (fold change, ≥2) in *Pten* null samples compared to the WT. *P* values were calculated by using the Benjamini-Hochberg method (16) for multiple-hypothesis testing. The statistically significant altered pathways (adjusted *P* value of <0.05) were then reanalyzed by using gene set enrichment analysis (GSEA) to assess the direction of deregulation in the *Pten* null samples.

GW2580 treatment. Male $Pb\text{-}Cre^+$; $Pten^{lox/lox}$ mice were treated with either vehicle (0.5% carboxymethyl cellulose in distilled H_2O) or GW2580 (160 mg/kg GW2580) daily for 3 weeks by oral gavage, beginning at 6 weeks of age. Mice were sacrificed, and the prostate, spleen, and lymph nodes were harvested for FACS and immunohistochemical analyses.

Microarray data accession number. Raw microarray data have been deposited in the NCBI Gene Expression Omnibus under accession no. GSE56470.

RESULTS

***Pten* null murine prostate cancer initiation and progression are associated with chronic immune cell infiltration.** To determine if PTEN loss in the prostate epithelium is associated with localized inflammatory responses, we took an unbiased approach to characterize the nature and extent of immune cell infiltration by using quantitative fluorescence-activated cell sorting (FACS), semiquantitative immunohistochemistry (IHC), and double-immunofluorescent (IF) analyses. Single-cell suspensions were prepared from dorsolateral and ventral lobes of individual prostates of $Pb\text{-}Cre^+$; $Pten^{lox/lox}$ male mice (mutant [MT]) at the prostatic intraepithelial neoplasia (mPIN) and invasive adenocarcinoma stages (Fig. 1A). Cre-negative ($Pb\text{-}Cre^-$; $Pten^{lox/lox}$) littermates were used

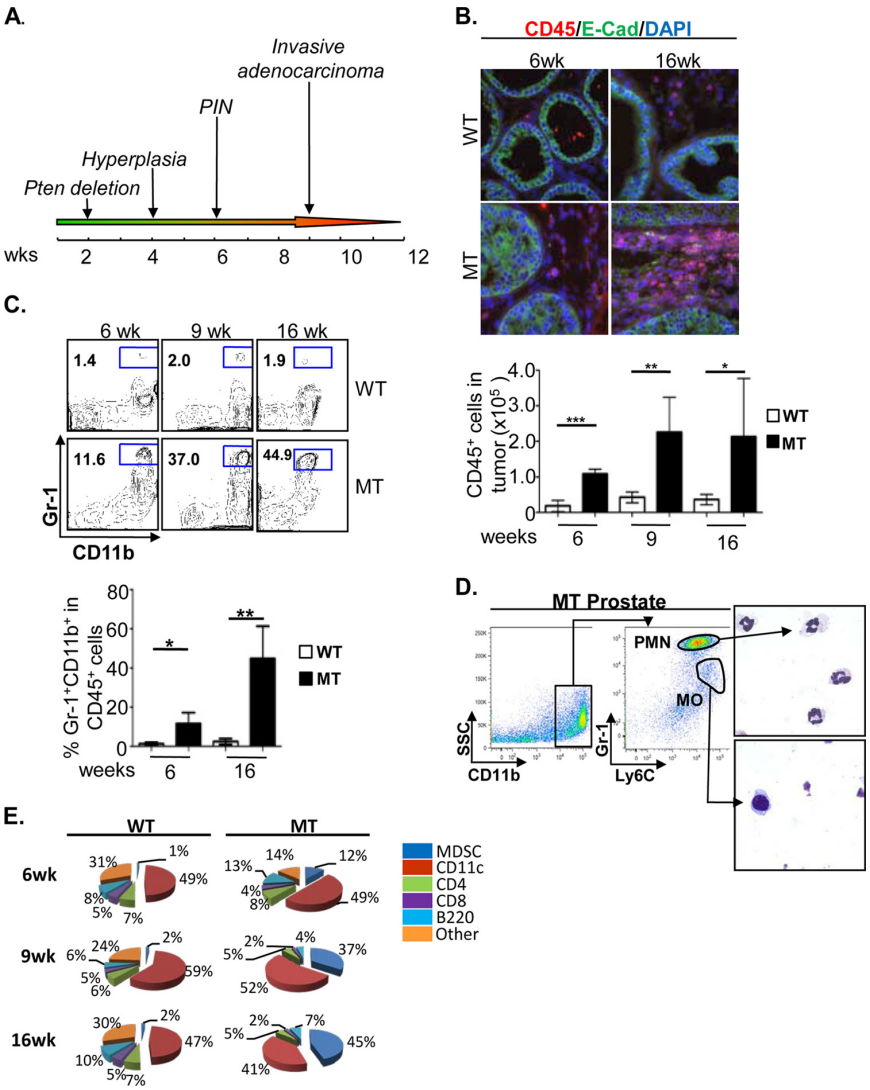

FIG 1 *Pten* null murine prostate cancer initiation and progression are marked by persistent immune cell infiltration. (A) Kinetics of prostate cancer initiation and progression in the *Pten* null murine prostate cancer model. (B, top) Representative immunofluorescence images showing significant $CD45^+$ (red) immune cell infiltration surrounding E-cadherin (E-Cad) (green)-positive luminal epithelial cells at the early mPIN (6 weeks) and late adenocarcinoma (16 weeks) stages in mutant (MT) mice compared to wild-type (WT) littermates. (Bottom) FACS analysis demonstrating that levels of $CD45^+$ immune cell infiltrates remain elevated throughout all stages of disease progression. (C) Immune cell infiltrates are made up of predominantly Gr-1^+ $CD11b^+$ cells and reach nearly 50% of all $CD45^+$ cells by the adenocarcinoma stage. (D, left) The majority of prostate-infiltrating Gr-1^+ $CD11b^+$ cells display a Gr-1^{Hi} $Ly6C^{Lo}$ polymorphonuclear (PMN) cell phenotype. (Right) Representative images of cytospun and Giemsa-stained PMN and mononuclear (MO) cell populations. (E) Percentages of various immune cell populations within the $CD45^+$ infiltrate in WT and MT mice. Panels B to D show means ± standard errors of the means from a minimum of 5 animals per age/genotype. *, $P < 0.05$; **, $P < 0.01$; ***, $P < 0.001$.

as controls (WT). Significant immune cell infiltration, marked by the pan-leukocyte antibody CD45, can be found within the prostate surrounding E-cadherin (E-cad)-positive (green) epithelial cells in both precancerous (mPIN) (6 weeks) and cancer (16 weeks) lesions (Fig. 1B). In MT prostates, $CD45^+$ immune cell infiltrates made up 12% of all cells at the mPIN stage, while approximately 5% of cells in WT prostates were reactive to antibodies against CD45 ($P < 0.05$) (data not shown). Following disease progression and significant prostatic epithelial cell expansion, both the total number and percentage of $CD45^+$ cells remained elevated compared to those of their age- and genetic background-matched WT littermates (Fig. 1B, bottom).

To better understand the nature of the immune cell infiltrate, we labeled cells with antibodies against common myeloid and lymphoid cell surface antigens. Comparing MT prostates with those of their WT littermates, we observed a significant increase in the number of Gr-1^+ $CD11b^+$ cells within the infiltrating $CD45^+$ population, particularly at the invasive adenocarcinoma stage

(Fig. 1C, top and bottom). Gr-1$^+$ CD11b$^+$ cells comprised approximately 12% of all CD45$^+$ cells at the mPIN stage ($P < 0.05$) while reaching over 40% of all infiltrating leukocytes at late invasive stages ($P < 0.01$) (Fig. 1C). Of the CD11b$^+$ cells, the vast majority was comprised of Gr-1^{Hi} Ly6C^{Lo} polymorphonuclear (PMN) cells (Fig. 1D). The remaining CD45$^+$ cells were mainly CD11c$^+$ cells and T and B cells (Fig. 1E). Levels of B220$^+$ B cells did not increase significantly in MT prostate tissue during cancer initiation and progression (Fig. 1E). This study suggests that prostate cancer initiation and progression caused by PTEN loss in epithelial cells are associated with marked chronic and extensive Gr-1$^+$ CD11b$^+$ immune cell infiltration.

Gr-1$^+$ CD11b$^+$ cell expansion does not occur in lymph nodes, bone marrow, spleen, or liver of tumor-bearing animals during tumor initiation. It has been well established, particularly in xenograft models, that Gr-1$^+$ CD11b$^+$ MDSCs are recruited from hematopoietic organs, and their expansion and suppressive capacity can be detected in both tumors and hematopoietic and nonhematopoietic organs such as the blood, spleen, liver, bone marrow, and lymph nodes (17). Therefore, we set out to determine whether Gr-1$^+$ CD11b$^+$ cell expansion occurs in hematopoietic and nonhematopoietic organs with kinetics similar to those at the tumor site. In sharp contrast to previous reports (17–19), we did not observe a significant increase in the number of Gr-1$^+$ CD11b$^+$ cells in the lymph nodes, spleen, bone marrow, or liver of the tumor-bearing mice (Fig. 2A to D).

To further investigate the mechanisms underlying the localized prostatic expansion of Gr-1$^+$ CD11b$^+$ cells during prostate cancer initiation and progression, 6- to 8-week-old WT and MT mice were pulse labeled with BrdU for 24 h. Gr-1$^+$ CD11b$^+$ cells were FACS sorted from the prostate, spleen, and bone marrow and analyzed for anti-BrdU reactivity. While there were no significant differences in the percentages of BrdU-positive (BrdU$^+$) Gr-1$^+$ CD11b$^+$ cells between the spleen and bone marrow of WT and MT mice, we found a substantial increase in the percentage of cycling BrdU$^+$ Gr-1$^+$ CD11b$^+$ cells in the MT prostates ($P < 0.001$) (Fig. 2E), suggesting that in an endogenous prostate cancer model, oncogenic *Pten* deletion in prostatic epithelial cells may trigger the localized expansion of Gr-1$^+$ CD11b$^+$ cells during tumor initiation.

PTEN loss in epithelial cells leads to upregulated inflammatory and cytokine-cytokine receptor signaling pathways. In order to better understand how epithelial cell-associated tumor-initiating events cross talk with inflammatory cells to potentiate prostate cancer initiation and progression, we performed laser capture microdissection of epithelial cells from age- and genetic background-matched WT and MT prostates ($n = 3$) and conducted gene expression analysis (see Materials and Methods). Pathway analysis and gene set enrichment analysis (GSEA) (15) demonstrated that the inflammatory response, the immune response, chemotaxis, the extracellular matrix (ECM)-receptor interaction, and cytokine-cytokine receptor interaction pathways are among the major pathways enriched in the MT epithelial cells (Fig. 3A and data not shown). Importantly, the upregulated genes in these pathways were also found to be significantly upregulated in human prostate cancer samples ($P < 0.05$ by Fisher's exact test) (Fig. 3B) (20).

Since laser-captured epithelial cells may be contaminated by nonepithelial cells, including inflammatory components, gene expression analysis was also performed on *Pten* null epithelial cell lines (PTEN-CaP2 and PTEN-CaP8) (14). As illustrated by a Venn diagram, many genes associated with inflammatory responses and cytokine-cytokine receptor interaction pathways are indeed upregulated in PTEN null epithelial cells in the absence of any potential leukocyte contamination (Fig. 3B). These studies further support the thought that PTEN loss in prostate epithelial cells triggers a localized immune response and recruits inflammatory cells to the tumor microenvironment.

To investigate the mechanisms underlying the localized Gr-1$^+$ CD11b$^+$ cell expansion and proliferation, we next sought to determine which paracrine factors may be secreted from MT prostate epithelial cells. Epcam$^+$ epithelial cells from 6- to 8-week-old MT and WT mice were FACS sorted to avoid possible contamination from leukocytes and stromal cells. CSF-1 (21–23) was previously implicated in the localization and expansion of MDSCs at the tumor site in a number of murine carcinoma models, including spontaneous and xenograft mammary tumor models (24, 25). Indeed, when FACS-sorted Epcam$^+$ epithelial cells from MT and WT mice were compared, there was a 2-fold induction of *Csf1* mRNA expression ($n = 5$; $P < 0.01$) (Fig. 3C, left). Similarly, epithelial cell lines generated from MT mice also showed upregu-

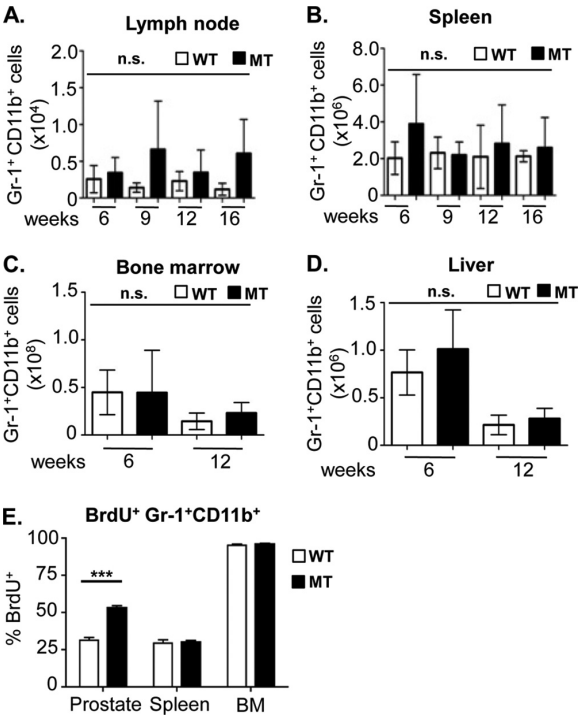

FIG 2 Gr-1$^+$ CD11b$^+$ cell expansion does not occur in lymph nodes, bone marrow, spleen, or liver of tumor-bearing animals. (A to D) Absolute numbers of Gr-1$^+$ CD11b$^+$ cells in the draining lymph nodes (A), spleen (B), bone marrow (C), and liver (D) of WT and MT mice throughout disease progression (means ± standard errors of the means from a minimum of 3 animals per age/genotype). (E) The percentage of prostatic BrdU$^+$ Gr-1$^+$ CD11b$^+$ cells is significantly higher in MT animals than in WT littermates. The percentage of spleen and bone marrow BrdU$^+$ Gr-1$^+$ CD11b$^+$ cells remained unchanged between MT and WT littermate tissues (***, $P < 0.001$). Ten high-power microscopic fields were counted for each organ and genotype (minimum of 3 animals per genotype). n.s., not significant.

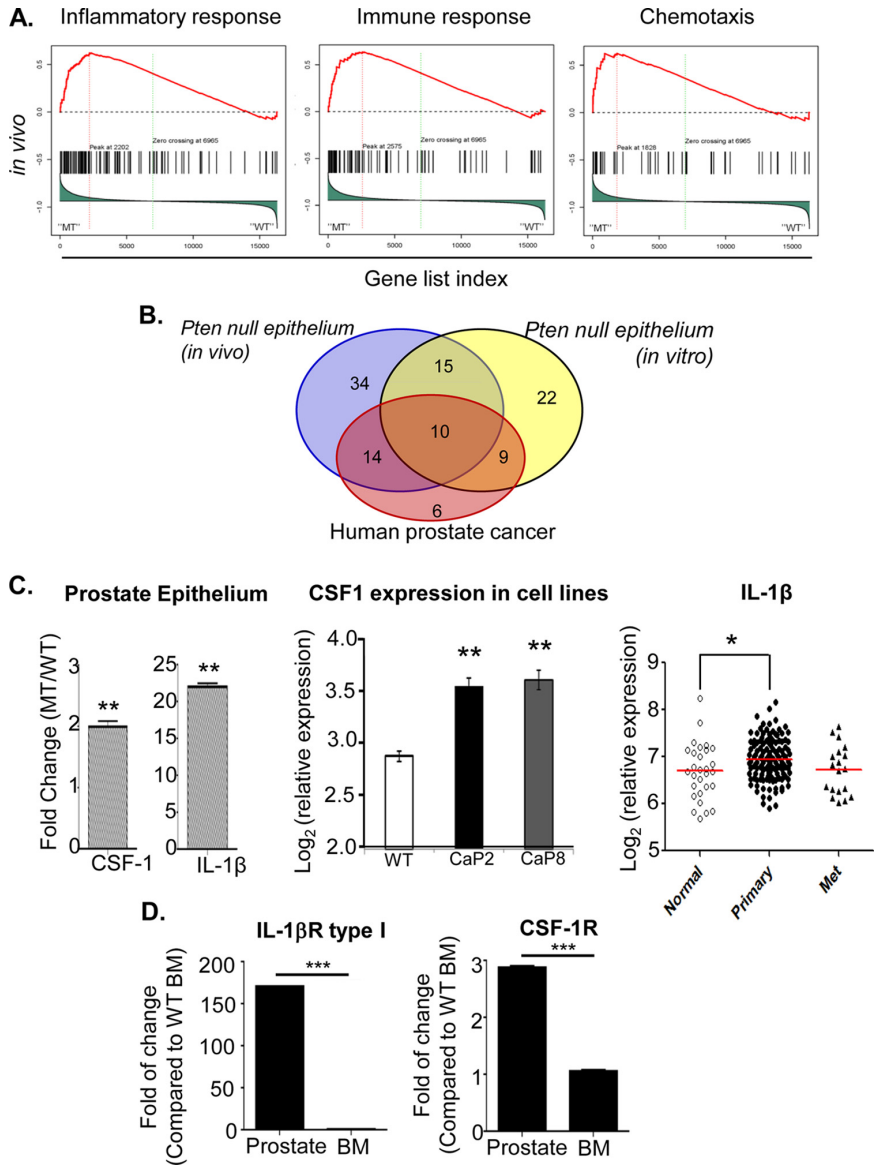

FIG 3 PTEN loss in epithelial cells leads to upregulated inflammatory and cytokine-cytokine receptor signaling pathways. (A) GSEA shows enhanced activation of inflammatory response and cytokine-cytokine receptor interaction pathways *in vivo* in *Pten* null (MT) prostate epithelial cells. (B) Inflammatory genes upregulated in PTEN null murine prostate epithelial cells significantly overlap those in human prostate cancer samples ($P < 0.05$). (C, left) Epcam$^+$ epithelial cells sorted from MT mice at the mPIN stage express higher levels of *Csf1* and *Il1b* mRNA. Relative gene expression was normalized to levels in sorted WT prostate epithelial cells. (Middle) *Csf1* expression is upregulated in two independent PTEN null prostate epithelial cells lines. (Right) *IL1b* expression is significantly upregulated in human prostate cancer specimens compared to normal prostate tissue ($P < 0.05$ by two-tailed test). (D) *Il1ra* (left) and *Csf1r* (right) gene expression levels are increased in sorted Gr-1$^+$ CD11b$^+$ cells from prostates of 6- to 8-week-old MT mice. The relative gene expression level was normalized to levels in WT BM (minimum 5 animals per age/genotype for panels C and D). *, $P < 0.05$; **, $P < 0.01$; ***, $P < 0.001$.

lated *Csf1* mRNA expression ($n = 3$; $P < 0.005$) (Fig. 3C, middle). Interleukin-1β (IL-1β), which has been demonstrated to both induce MDSC migration toward tumor lesions and lead to MDSC-mediated inhibition of T cell activity through the induction of *Arg1* and *iNOS* mRNA expression (26–29), was shown to have 22-fold-higher levels of mRNA expression in sorted Epcam$^+$ MT prostate epithelial cells than in WT epithelial cells ($n = 5$; $P < 0.01$) (Fig. 3C, left). Similarly, using a human expression data set available in GEO (accession number GSE21034), we confirmed that IL-1β mRNA expression was also significantly upregulated ($P < 0.05$ by two-tailed *t* test) in human primary tumors compared to normal prostate tissue (Fig. 3C, right) (20).

Finally, to uncover whether CSF-1 and IL-1β may act directly on prostatic Gr-1$^+$ CD11b$^+$ MDSCs, we analyzed the expression of CSF-1R and IL-1β receptor (IL-1βR) type I, respectively, on Gr-1$^+$ CD11b$^+$ cells isolated from the prostate

and BM of mutant mice. Indeed, Gr-1$^+$ CD11b$^+$ cells isolated from the prostate had significantly higher *Csf1r* and *Il1ra* mRNA expression levels than Gr-1$^+$ CD11b$^+$ cells isolated from the BM of the same mice ($n = 5$; $P < 0.001$) (Fig. 3D). As PTEN loss in prostate epithelial cells leads to upregulated inflammatory responses and enhanced production of paracrine and pleiotropic factors such as CSF-1 and IL-1β, these factors may further propagate the infiltration and homing of Gr-1$^+$ CD11b$^+$ MDSCs to the prostate and promote their local proliferation and expansion (Fig. 1C and 2E).

Gr-1$^+$ CD11b$^+$ cells from the prostate but not spleen of tumor-bearing mice can suppress T cell proliferation. MDSCs can suppress T cell function through the production of arginase (ARG) and inducible nitric oxide synthase (iNOS) enzymes, both of which metabolize and deplete arginine, an essential nutrient for T cell proliferation (30). iNOS activity can also lead to T cell unresponsiveness through the nitration of T cell receptors (TCRs) and subsequent inhibition of TCR-MHC-peptide interactions (31). Moreover, increased ARG activity has been shown for a variety of human malignancies, including prostate cancer (32). To test whether prostate-associated Gr-1$^+$ CD11b$^+$ cells have typical immune-suppressive activities, we analyzed gene expression by quantitative PCR (qPCR) using Gr-1$^+$ CD11b$^+$ cells isolated from the prostate, spleen, and bone marrow of WT and MT mice. Gr-1$^+$ CD11b$^+$ cells isolated from spleen and bone marrow samples have low to undetectable levels of *Arg1* and *iNOS* mRNA in either WT or MT mice (Fig. 4A, right, and data not shown). In contrast, Gr-1$^+$ CD11b$^+$ cells isolated from MT prostates had significantly higher *Arg1* ($P < 0.0001$) and *iNOS* ($P < 0.05$) mRNA expression levels than did those sorted from age-matched WT controls (Fig. 4A, left). It is worth noting that *Arg1* and *iNOS* mRNA expression levels in Gr-1$^+$ CD11b$^+$ cells isolated from WT prostate tissue are elevated relative to the levels in their spleen and bone marrow counterparts (Fig. 4A, left). These findings suggest that the prostate microenvironment itself may be relatively immunosuppressive and that the loss of *Pten* and the formation of precancerous PIN lesions further exacerbate this condition.

The induction of immunosuppressive gene expression in Gr-1$^+$ CD11b$^+$ cells isolated from the prostate of MT mice prompted us to functionally test their immunosuppressive properties. Naive CD4$^+$ or CD8$^+$ T cells isolated from the spleens of WT animals were preloaded with carboxyfluorescein succinimidyl ester (CFSE) and cocultured with sorted Gr-1$^+$ CD11b$^+$ cells from MT prostates at various ratios in the presence of activating anti-CD3 antibody. T cell proliferation was measured according to the intensity of CFSE staining and presented as the percent change without Gr-1$^+$ CD11b$^+$ cell coculturing. CD4$^+$ T cell proliferation was effectively inhibited by prostate cancer-associated Gr-1$^+$ CD11b$^+$ cells by 5-fold ($P < 0.0001$) at a 1:1 ratio and nearly 2.5-fold ($P < 0.05$) at a 1:2 ratio (Fig. 4B, left). Similarly, CD8$^+$ T cell proliferation was suppressed by >2.5-fold ($P < 0.01$) at a 1:1 ratio (Fig. 4B, right). Because Gr-1$^+$ CD11b$^+$ cells are rare in WT prostate, we sorted Gr-1$^+$ CD11b$^+$ cells from the spleens of WT and MT mice and performed identical assays to determine if the immune-suppressive activity of Gr-1$^+$ CD11b$^+$ cells is specific to tumor-infiltrating MDSCs. As predicted from our gene expression analysis, splenic Gr-1$^+$ CD11b$^+$ cells from neither MT nor WT mice could suppress T cell proliferation at any dilution (Fig. 4C and data not shown). These results suggest that only Gr-1$^+$ CD11b$^+$ cells associated with prostate cancer initiation and progression have immune-suppressive activity, although we cannot rule out the possible

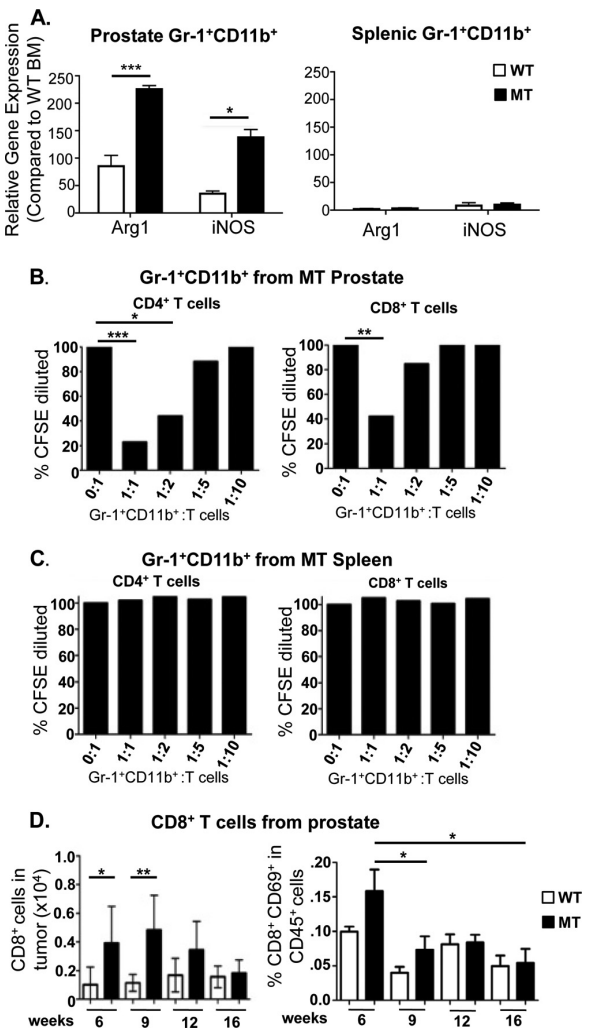

FIG 4 Gr-1$^+$ CD11b$^+$ cells from the prostate but not spleen of tumor-bearing mice can suppress T cell function. (A, left) Gr-1$^+$ CD11b$^+$ cells sorted from MT prostates have higher expression levels of *Arg1* and *iNOS* than do Gr-1$^+$ CD11b$^+$ cells from WT prostates. (Right) Gr-1$^+$ CD11b$^+$ cells sorted from spleens of MT and WT littermate animals revealed no difference in and low levels of *Arg1* and *iNOS* expression. The relative gene expression level for each sample was normalized to levels in WT BM (minimum of 5 animals per genotype). (B) Sorted Gr-1$^+$ CD11b$^+$ cells from mutant prostates were cocultured with naive CFSE-loaded CD4$^+$ or CD8$^+$ cells from spleens of wild-type animals at the indicated ratios. CD4$^+$ (left) and CD8$^+$ (right) T cell proliferations were suppressed by infiltrating Gr-1$^+$ CD11b$^+$ cells. (C) Identical assays using Gr-1$^+$ CD11b$^+$ cells from spleens of tumor-bearing mice show an inability to suppress T cell proliferation (means of 3 independent experiments for panels B and C). (D, left) FACS analysis demonstrates increased levels of CD8$^+$ immune cell infiltrates as the disease initiates, which then decrease as the disease progresses. (Right) Levels of activated CD8$^+$ CD69$^+$ T cells decrease during disease progression. *, $P < 0.05$; **, $P < 0.01$; ***, $P < 0.001$.

immune-suppressive potential of prostatic Gr-1$^+$ CD11b$^+$ cells isolated from WT prostate because of their rarity. Consistent with these findings, we found that CD8$^+$ T cell numbers were transiently increased in precancer mPIN lesions but were reduced during cancer progression, inversely following the curve of MDSC expansion *in vivo*

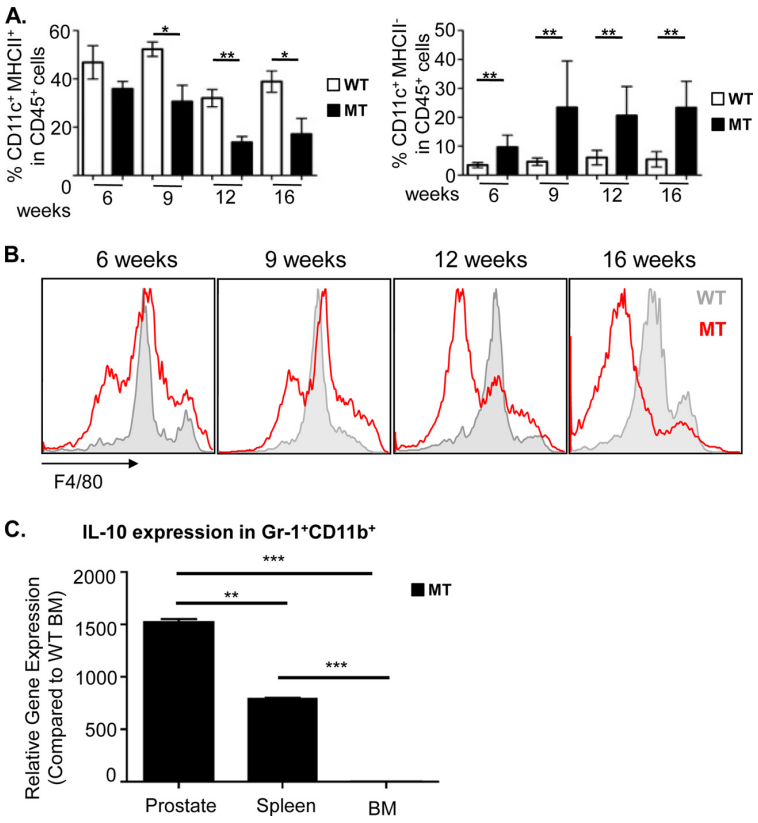

FIG 5 Prostate-specific Gr-1$^+$ CD11b$^+$ cell expansion is associated with suppression of dendritic cell and macrophage maturation. (A, left) Mature CD11c$^+$ MHCII$^+$ dendritic cells are present in both wild-type and mutant prostates, but their levels decrease precipitously in mutant animals as the disease progresses. (Right) Levels of immature CD11c$^+$ MHCII$^-$ DCs increase in mutant prostates as the disease progresses. (B) Macrophage F4/80 expression shifts away from a mature F4/80$^{int/high}$ phenotype to an immature F4/80^{low} phenotype as the disease progresses. (For panels A and B, data are means ± standard errors of the means from a minimum of 4 animals per age/genotype.) (C) The *IL10* gene expression level increased in sorted Gr-1$^+$ CD11b$^+$ cells from the prostate, compared to levels in cells from the spleen and BM of MT mice. The relative gene expression level for each sample was normalized to the values for WT BM ($n = 5$). *, $P < 0.05$; **, $P < 0.01$; ***, $P < 0.001$.

in MT prostates (Fig. 4D, left). Levels of T cell activation, as measured by the percentage of CD8$^+$ CD69$^+$ cells within the CD45$^+$ population, spiked at the mPIN lesion stage but subsequently decreased as the disease progressed and MDSC numbers and suppressive activity increased (Fig. 4D, right).

Prostate-specific MDSC expansion is associated with suppression of dendritic cell and macrophage maturation. In addition to suppressing T cell proliferation, MDSCs also produce cytokines known to suppress DC and macrophage maturation (4, 5, 33). Therefore, we evaluated the maturation status of both infiltrating DCs and macrophages in the MT prostate as a function of disease progression. Although mature CD11c$^+$ MHCII$^+$ DCs were present throughout all stages of disease, their relative percentages in the CD45$^+$ population decreased precipitously during disease progression (36% ± 3.0% in mPIN lesions versus 17% ± 6.5% at the cancer stage) (Fig. 5A, left). This reduction in the number of mature DCs was accompanied by a relative increase in the number of immature CD11c$^+$ MHCII$^-$ cells during the same progression period (9.7% ± 1.7% versus 23.4% ± 4.6%) (Fig. 5A, right), suggesting that the maturation of antigen-presenting cells (APCs) may be suppressed by the expansion and/or local cytokine production of MDSCs in the prostate. Similarly, macrophage F4/80 expression shifted away from a mature F4/80$^{int/high}$ phenotype to an immature F4/80^{low} phenotype as the disease progressed (Fig. 5B). In order to understand how prostatic MDSCs may suppress DC and macrophage maturation, we looked at the expression of IL-10, which has been demonstrated to not only polarize F4/80^{hi} M1 macrophages to an F4/80^{lo} M2 phenotype (4) but also reduce DC maturation and DC-mediated activation of T cells through various mechanisms (6, 34, 35). Indeed, the *Il10* mRNA expression level was significantly elevated in prostatic Gr-1$^+$ CD11b$^+$ cells isolated from MT mice compared to the levels in cells isolated from spleen ($P < 0.01$) and BM ($P < 0.001$) of the same tumor-bearing animals (Fig. 5C). Not surprisingly, MHCII expression on DCs has also been shown to be inhibited by CSF-1 (36), which may further contribute to an immune-suppressive tumor microenvironment that prevents proper T cell activation. Therefore, the suppression of innate immune cell maturation by MDSC-derived IL-10 and tumor prostatic epithelial cell-derived CSF-1 is yet another mechanism by which prostate tumor-specific MDSCs may inhibit T cell functions.

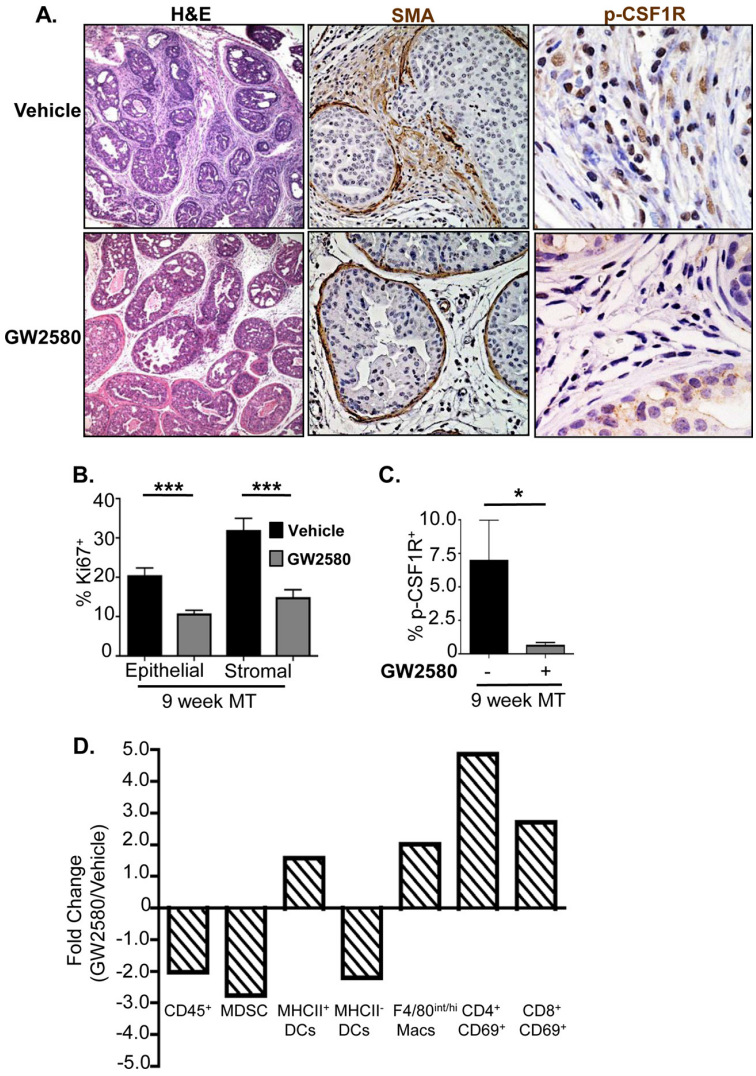

FIG 6 The selective CSF-1 receptor inhibitor GW2580 reduces Gr-1$^+$ CD11b$^+$ cell infiltration and reverses the immune-suppressive phenotype. (A, left) Stromal reactivity and the desmoplastic response are reduced in the prostates of GW2580-treated animals. (Middle) Invasive adenocarcinoma, as measured by SMA breakdown, is diminished in the prostates of GW2580-treated animals. (Right) Numbers of p-CSFR-1$^+$ cells are greatly reduced in the stroma of GW2580-treated prostates. (B) Epithelial and stromal cell Ki67 proliferation indices are reduced following GW2580 treatment. (C) Quantification of stromal p-CSF-1R$^+$ cells demonstrates a significant decrease in the percentage of p-CSF-1R$^+$ cells following GW2580 treatment. (D) GW2580 treatment alleviates immune-suppressive phenotypes associated with MDSC expansion. Values are represented as fold changes between GW2580- and vehicle-treated MT mice. For panels B to D, there were 6 animals per treatment group; for panels B and C, there were a minimum of 10 high-power microscopic fields/animal. *, $P < 0.05$; **, $P < 0.01$; ***, $P < 0.001$. Macs, macrophages.

The selective CSF-1 receptor inhibitor GW2580 reduces MDSC infiltration and reverses the immune-suppressive phenotype. *Csf1* mRNA is overexpressed in the prostate epithelium of *Pten* null mice as well as in epithelial cell lines derived from the *Pten* null prostate cancer model (Fig. 3C, left and middle) (14). In order to determine whether CSF-1 indeed plays an essential role in MDSC infiltration and prostate cancer development, we treated a cohort of MT animals with the selective CSF-1 receptor antagonist GW2580 (22, 37, 38) daily for 3 weeks, starting at 6 weeks of age. Prostate, draining lymph nodes, and spleen were collected at the end of treatment and processed for analysis. Histopathological examination revealed significant differences between vehicle- and GW2580-treated cohorts ($n = 6$) within the stromal and epithelial compartments. Stromal reactivity and the desmoplastic response were noticeably reduced in the tumors of GW2580-treated animals compared to age-matched vehicle-treated MT animals (Fig. 6A, left). GW2580 treatment significantly reduced basement membrane degradation and local invasion, as evidenced by strong α-SMA-positive staining (Fig. 6A, middle). In addition, the Ki67 proliferation indices of the epithelial and stromal compartments

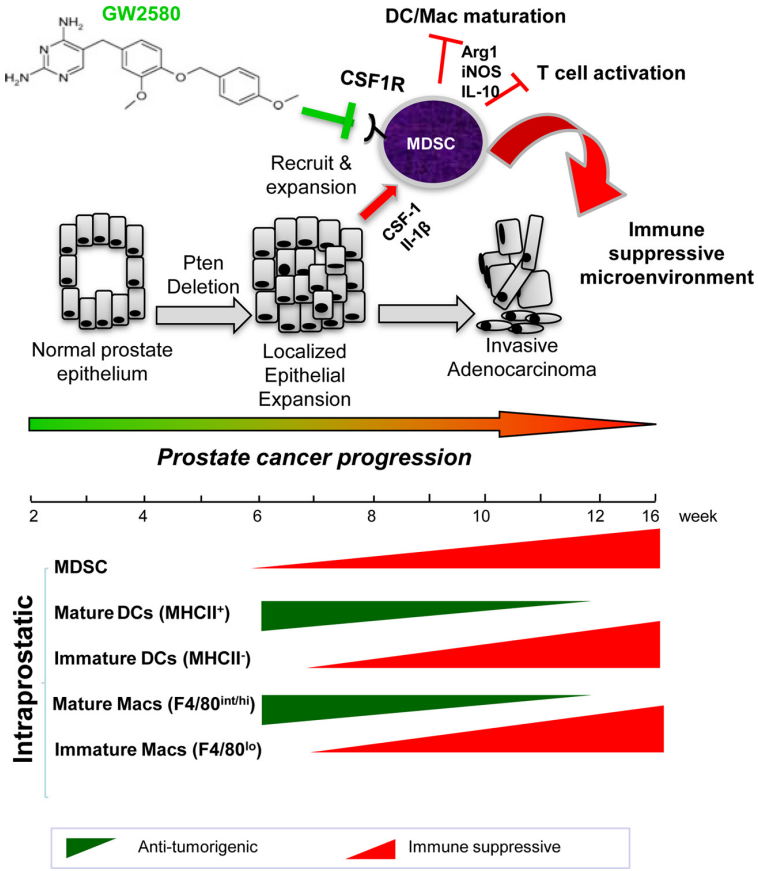

FIG 7 Cross talk between epithelial cell-associated tumor-initiating events and inflammatory cells facilitates prostate cancer progression. Epithelial cell *Pten* loss leads to the upregulation of genes associated with inflammatory response and cytokine-cytokine receptor interaction pathways. Increased cytokine production by *Pten* null epithelial cells, including CSF-1 and IL-1β production, leads to the recruitment and expansion of MDSCs, which in turn facilitate an immune-suppressive environment and promote tumor progression through the secretion of Arg1, iNOS, and IL-10. Inhibiting immune-responsive pathways, through the use of compounds like GW2580, can decrease immune cell recruitment, alleviate the immune-suppressive environment, delay tumor progression, and potentiate immunotherapeutic modalities. Mac, macrophage.

were significantly reduced by 2- and 3-fold, respectively, in GW2580-treated animals (Fig. 6B). This was accompanied by a significant reduction in p-CSF-1R$^+$ cells in the stromal compartment (Fig. 6A, right, and C), verifying that the drug indeed modulated its target.

Quantitative FACS analysis of prostate tissue demonstrated a significant reduction in the number of tumor-infiltrating CD45$^+$ cells as well as an almost 3-fold reduction in the number of Gr-1$^+$ CD11b$^+$ MDSCs in GW2580-treated mice (Fig. 6D). Consistent with our previous results showing that localized MDSC expansion leads to an immune-suppressive state, inhibition of CSF-1R signaling led to an increase in the number of mature MHCII$^+$ DCs, as well as mature F4/80$^{int/high}$ macrophages, within the prostate of treated animals (Fig. 6D). Activated CD4$^+$ and CD8$^+$ T cell numbers also increased after GW2580 treatment (Fig. 6D). These results suggest that GW2580 can inhibit epithelial cell-associated CSF-1 signaling, reduce MDSC expansion, and alleviate the immune-suppressive microenvironment.

DISCUSSION

Similar to human prostate cancer development, the *Pten* null murine prostate cancer model progresses through distinct stages of disease, including mPIN and localized invasive adenocarcinoma, providing unique and advantageous windows to investigate early events associated with prostate cancer initiation and progression. Using this model, we sought to study how epithelial cell-associated tumor initiation events cross talk with inflammatory cells and orchestrate prostate cancer development. Our work shows that in addition to increased cell proliferation, survival, and motility imposed by the loss of PTEN in prostate epithelial cells (12), the changes in inflammatory gene expression as a result of PTEN loss profoundly influence immune cell infiltration and immune-suppressive activities, which in turn promote cancer progression (Fig. 7).

We found that concomitant with mPIN formation, there was a significant expansion of Gr-1$^+$ CD11b$^+$ MDSCs in the prostate, accompanied by decreased DC and macrophage mat-

uration (Fig. 7). In contrast to the majority of reports, which used xenograft and allograft models (19, 39, 40), our endogenous model indicates that MDSC expansion occurs solely in the prostate during disease initiation and progression. There is no significant expansion of Gr-1$^+$ CD11b$^+$ cells in the lymph nodes, spleen, liver, or bone marrow of these same tumor-bearing mice. Gr-1$^+$ CD11b$^+$ cells from these hematopoietic organs do not show T cell-suppressive activities and MDSC gene expression signatures, such as increased expression levels of arginase 1 and iNOS. These results suggest that MDSC infiltration and expansion in the prostate following the initial oncogenic insult are likely triggered by localized stimuli from the epithelium. Indeed, analysis of gene expression alterations demonstrated the upregulation of inflammatory response genes and cytokine-cytokine receptor interaction pathways in *Pten* null epithelial cells. This localized cytokine release, including CSF-1 production by *Pten* null epithelial cells, likely contributes to the recruitment and maintenance of infiltrating myeloid cells, as was similarly observed for other epithelial cell cancers (6, 41–43). A concomitant increase in the level of *Csf1r* mRNA in infiltrating Gr-1$^+$ CD11b$^+$ MDSCs suggests an autocrine pathway for the propagation of immunosuppressive signals. Similarly, increased IL-1β production likely promotes the immunosuppressive activities of tumor-associated MDSCs through stimulating their Arg1, iNOS, and IL-10 production. The resultant increase in the *Il1ra* mRNA expression level, again, in infiltrating Gr-1$^+$ CD11b$^+$ MDSCs further supports the notion that immunosuppressive inflammatory signals are self-propagating and confirms previous observations of similar bidirectional cross talk between MDSCs and tumor cells within the microenvironment (5). Our results are also consistent with recent work by Haverkamp and colleagues, who demonstrated an immediate and enhanced immune-suppressive ability of MDSCs in local inflammatory sites compared to Gr-1$^+$ CD11b$^+$ cells present at peripheral tissues (44). It can now be appreciated, through our work and the work of Haverkamp et al. and others, that there are important functional differences between Gr-1$^+$ CD11b$^+$ MDSCs that infiltrate tumors and the Gr-1$^+$ CD11b$^+$ cells in the peripheral tissues.

The localized immune-suppressive conditions also suggest a difference between inflammatory conditions induced by spontaneous cancer models and those incited by subcutaneous or orthotopic xenograft models with established cancer cell lines. Although expansion of MDSCs in peripheral organs was largely absent from our studies, possibly due to the spontaneous nature of the initial insult and the early stage of cancer development, work by other groups has shown the expansion and immune-suppressive activities of MDSCs isolated from hematopoietic and nonhematopoietic organs of xenograft models (17, 45). Since most transplanted tumor models are of an aggressive nature with fast kinetics, the expansion and activation of MDSCs at hematopoietic and nonhematopoietic sites in these models may more closely resemble late stages of human disease.

The recent U.S. Food and Drug Administration approval of sipuleucel-T, a first-of-its-kind cancer vaccine for antigen-specific immunotherapy, uses a patient's own immature monocytes that have been exogenously stimulated and matured in order to mount an antitumor response. Although phase III clinical trial results showed improved survival when comparing sipuleucel-T and conventional therapy, disease-free progression was not changed significantly (46, 47). Our study suggests that immune-suppressive mechanisms mediated by MDSCs within the local tumor environment are directly influenced by epithelial cell-associated tumor-initiating events. Therefore, cotargeting of tumor-associated MDSCs and epithelial cell-mediated paracrine pathways may alleviate the immune-suppressive environment and benefit prostate cancer immunotherapy. Treatment of prostate-tumor-bearing mice with the selective CSF-1 receptor inhibitor GW2580 demonstrated that interrupting an epithelial cell-associated signaling cascade that drives MDSC infiltration to the tumor site can have ameliorative effects not only on tumor growth kinetics but also on the immune-suppressive status of the microenvironment. Our preclinical study clearly demonstrates the potential benefits of using this and similar therapies to alleviate the immunosuppressive and tumor-tolerant environments imposed by infiltrating MDSCs.

ACKNOWLEDGMENTS

We thank colleagues in our laboratories for suggestions and comments. We thank Dapei Li for microdissection assistance and Ilsa Coleman for assistance with the analysis of microarray data.

A.J.G. was supported by an NIH minority supplement award (R01 CA107166S); M.R. and L.M.T. were supported by NIH grant T32 CA009056. This work has been supported in part by awards from the Prostate Cancer Foundation (to H.W. and P.S.N.), a DOD idea development award (to H.W.), and grants from the NIH (R01 CA107166 and RO1 CA121110 to H.W., UO1 CA164188 to H.W. and P.S.N., R01 CA165573 P.S.N., and P50CA097186 to P.S.N.).

We have no conflicting interests to disclose.

REFERENCES

1. **Qian BZ, Pollard JW.** 2010. Macrophage diversity enhances tumor progression and metastasis. Cell **141:**39–51. http://dx.doi.org/10.1016/j.cell.2010.03.014.
2. **Grivennikov SI, Greten FR, Karin M.** 2010. Immunity, inflammation, and cancer. Cell **140:**883–899. http://dx.doi.org/10.1016/j.cell.2010.01.025.
3. **Chow A, Brown BD, Merad M.** 2011. Studying the mononuclear phagocyte system in the molecular age. Nat. Rev. Immunol. **11:**788–798. http://dx.doi.org/10.1038/nri3087.
4. **Sinha P, Clements VK, Bunt SK, Albelda SM, Ostrand-Rosenberg S.** 2007. Cross-talk between myeloid-derived suppressor cells and macrophages subverts tumor immunity toward a type 2 response. J. Immunol. **179:**977–983. http://www.jimmunol.org/content/179/2/977.long.
5. **Ostrand-Rosenberg S, Sinha P, Beury DW, Clements VK.** 2012. Cross-talk between myeloid-derived suppressor cells (MDSC), macrophages, and dendritic cells enhances tumor-induced immune suppression. Semin. Cancer Biol. **22:**275–281. http://dx.doi.org/10.1016/j.semcancer.2012.01.011.
6. **Mantovani M, Allavena P, Sica A, Balkwill F.** 2008. Cancer-related inflammation. Nature **454:**436–444. http://dx.doi.org/10.1038/nature07205.
7. **Almand B, Clark JI, Nikitina E, van Beynen J, English NR, Knight SC, Carbone DP, Gabrilovich DI.** 2001. Increased production of immature myeloid cells in cancer patients: a mechanism of immunosuppression in cancer. J. Immunol. **166:**678–689. http://www.jimmunol.org/content/166/1/678.long.
8. **Serafini P, Mgebroff S, Noonan K, Borrello I.** 2008. Myeloid-derived suppressor cells promote cross-tolerance in B-cell lymphoma by expanding regulatory T cells. Cancer Res. **68:**5439–5449. http://dx.doi.org/10.1158/0008-5472.CAN-07-6621.
9. **Li H, Han Y, Guo Q, Zhang M, Cao X.** 2009. Cancer-expanded myeloid-derived suppressor cells induce anergy of NK cells through membrane-bound TGF-beta 1. J. Immunol. **182:**240–249. http://www.jimmunol.org/content/182/1/240.long.
10. **Sfanos KS, De Marzo AM.** 2012. Prostate cancer and inflammation: the evidence. Histopathology **60:**199–215. http://dx.doi.org/10.1111/j.1365-2559.2011.04033.x.

11. **Nelson WG, De Marzo AM, DeWeese TL, Isaacs WB.** 2004. The role of inflammation in the pathogenesis of prostate cancer. J. Urol. **172:**S6–S11; discussion S11–S12. http://dx.doi.org/10.1097/01.ju.0000142058.99614.ff.
12. **Wang S, Gao J, Lei Q, Rozengurt N, Pritchard C, Jiao J, Thomas GV, Li G, Roy-Burman P, Nelson PS, Liu C, Wu H.** 2003. Prostate-specific deletion of the murine Pten tumor suppressor gene leads to metastatic prostate cancer. Cancer Cell **4:**209–221. http://dx.doi.org/10.1016/S1535-6108(03)00215-0.
13. **Bianchi-Frias D, Vakar-Lopez F, Coleman IM, Plymate SR, Reed MJ, Nelson PS.** 2010. The effects of aging on the molecular and cellular composition of the prostate microenvironment. PLoS One **5:**e12501. http://dx.doi.org/10.1371/journal.pone.0012501.
14. **Jiao J, Wang S, Qiao R, Vivanco I, Watson PA, Sawyers CL, Wu H.** 2007. Murine cell lines derived from Pten null prostate cancer show the critical role of PTEN in hormone refractory prostate cancer development. Cancer Res. **67:**6083–6091. http://dx.doi.org/10.1158/0008-5472.CAN-06-4202.
15. **Subramanian A, Tamayo P, Mootha VK, Mukherjee S, Ebert BL, Gillette MA, Paulovich A, Pomeroy SL, Golub TR, Lander ES, Mesirov JP.** 2005. Gene set enrichment analysis: a knowledge-based approach for interpreting genome-wide expression profiles. Proc. Natl. Acad. Sci. U. S. A. **102:**15545–15550. http://dx.doi.org/10.1073/pnas.0506580102.
16. **Benjamini Y, Hochberg Y.** 1995. Controlling the false discovery rate: a practical and powerful approach to multiple testing. J. R. Stat. Soc. B **57:**289–300.
17. **Ilkovitch D, Lopez DM.** 2009. The liver is a site for tumor-induced myeloid-derived suppressor cell accumulation and immunosuppression. Cancer Res. **69:**5514–5521. http://dx.doi.org/10.1158/0008-5472.CAN-08-4625.
18. **Sfanos KS, Bruno TC, Maris CH, Xu L, Thoburn CJ, DeMarzo AM, Meeker AK, Isaacs WB, Drake CG.** 2008. Phenotypic analysis of prostate-infiltrating lymphocytes reveals TH17 and Treg skewing. Clin. Cancer Res. **14:**3254–3261. http://dx.doi.org/10.1158/1078-0432.CCR-07-5164.
19. **Youn JI, Nagaraj S, Collazo M, Gabrilovich DI.** 2008. Subsets of myeloid-derived suppressor cells in tumor-bearing mice. J. Immunol. **181:**5791–5802. http://www.jimmunol.org/content/181/8/5791.long.
20. **Taylor BS, Schultz N, Hieronymus H, Gopalan A, Xiao Y, Carver BS, Arora VK, Kaushik P, Cerami E, Reva B, Antipin Y, Mitsiades N, Landers T, Dolgalev I, Major JE, Wilson M, Socci ND, Lash AE, Heguy A, Eastham JA, Scher HI, Reuter VE, Scardino PT, Sander C, Sawyers CL, Gerald WL.** 2010. Integrative genomic profiling of human prostate cancer. Cancer Cell **18:**11–22. http://dx.doi.org/10.1016/j.ccr.2010.05.026.
21. **Kusmartsev S, Cheng F, Yu B, Nefedova Y, Sotomayor E, Lush R, Gabrilovich D.** 2003. All-trans-retinoic acid eliminates immature myeloid cells from tumor-bearing mice and improves the effect of vaccination. Cancer Res. **63:**4441–4449. http://cancerres.aacrjournals.org/content/63/15/4441.long.
22. **Priceman SJ, Sung JL, Shaposhnik Z, Burton JB, Torres-Collado AX, Moughon DL, Johnson M, Lusis AJ, Cohen DA, Iruela-Arispe ML, Wu L.** 2010. Targeting distinct tumor-infiltrating myeloid cells by inhibiting CSF-1 receptor: combating tumor evasion of antiangiogenic therapy. Blood **115:**1461–1471. http://dx.doi.org/10.1182/blood-2009-08-237412.
23. **Menetrier-Caux C, Montmain G, Dieu MC, Bain C, Favrot MC, Caux C, Blay JY.** 1998. Inhibition of the differentiation of dendritic cells from CD34(+) progenitors by tumor cells: role of interleukin-6 and macrophage colony-stimulating factor. Blood **92:**4778–4791.
24. **Aharinejad S, Paulus P, Sioud M, Hofmann M, Zins K, Schafer R, Stanley ER, Abraham D.** 2004. Colony-stimulating factor-1 blockade by antisense oligonucleotides and small interfering RNAs suppresses growth of human mammary tumor xenografts in mice. Cancer Res. **64:**5378–5384. http://dx.doi.org/10.1158/0008-5472.CAN-04-0961.
25. **Lin EY, Nguyen AV, Russell RG, Pollard JW.** 2001. Colony-stimulating factor 1 promotes progression of mammary tumors to malignancy. J. Exp. Med. **193:**727–740. http://dx.doi.org/10.1084/jem.193.6.727.
26. **Elkabets M, Ribeiro VS, Dinarello CA, Ostrand-Rosenberg S, Di Santo JP, Apte RN, Vosshenrich CA.** 2010. IL-1beta regulates a novel myeloid-derived suppressor cell subset that impairs NK cell development and function. Eur. J. Immunol. **40:**3347–3357. http://dx.doi.org/10.1002/eji.201041037.
27. **Tu S, Bhagat G, Cui G, Takaishi S, Kurt-Jones EA, Rickman B, Betz KS, Penz-Oesterreicher M, Bjorkdahl O, Fox JG, Wang TC.** 2008. Overexpression of interleukin-1beta induces gastric inflammation and cancer and mobilizes myeloid-derived suppressor cells in mice. Cancer Cell **14:**408–419. http://dx.doi.org/10.1016/j.ccr.2008.10.011.
28. **Song X, Krelin Y, Dvorkin T, Bjorkdahl O, Segal S, Dinarello CA, Voronov E, Apte RN.** 2005. CD11b+/Gr-1+ immature myeloid cells mediate suppression of T cells in mice bearing tumors of IL-1beta-secreting cells. J. Immunol. **175:**8200–8208. http://www.jimmunol.org/content/175/12/8200.long.
29. **Condamine T, Gabrilovich DI.** 2011. Molecular mechanisms regulating myeloid-derived suppressor cell differentiation and function. Trends Immunol. **32:**19–25. http://dx.doi.org/10.1016/j.it.2010.10.002.
30. **Bronte V, Serafini P, De Santo C, Marigo I, Tosello V, Mazzoni A, Segal DM, Staib C, Lowel M, Sutter G, Colombo MP, Zanovello P.** 2003. IL-4-induced arginase 1 suppresses alloreactive T cells in tumor-bearing mice. J. Immunol. **170:**270–278. http://www.jimmunol.org/content/170/1/270.long.
31. **Gabrilovich DI, Ostrand-Rosenberg S, Bronte V.** 2012. Coordinated regulation of myeloid cells by tumours. Nat. Rev. Immunol. **12:**253–268. http://dx.doi.org/10.1038/nri3175.
32. **Cederbaum SD, Yu H, Grody WW, Kern RM, Yoo P, Iyer RK.** 2004. Arginases I and II: do their functions overlap? Mol. Genet. Metab. **81**(Suppl 1)**:**S38–S44. http://dx.doi.org/10.1016/j.ymgme.2003.10.012.
33. **Chen DS, Mellman I.** 2013. Oncology meets immunology: the cancer-immunity cycle. Immunity **39:**1–10. http://dx.doi.org/10.1016/j.immuni.2013.07.012.
34. **Hu CE, Gan J, Zhang RD, Cheng YR, Huang GJ.** 2011. Up-regulated myeloid-derived suppressor cell contributes to hepatocellular carcinoma development by impairing dendritic cell function. Scand. J. Gastroenterol. **46:**156–164. http://dx.doi.org/10.3109/00365521.2010.516450.
35. **Vicari AP, Chiodoni C, Vaure C, Ait-Yahia S, Dercamp C, Matsos F, Reynard O, Taverne C, Merle P, Colombo MP, O'Garra A, Trinchieri G, Caux C.** 2002. Reversal of tumor-induced dendritic cell paralysis by CpG immunostimulatory oligonucleotide and anti-interleukin 10 receptor antibody. J. Exp. Med. **196:**541–549. http://dx.doi.org/10.1084/jem.20020732.
36. **Tagliani E, Shi C, Nancy P, Tay CS, Pamer EG, Erlebacher A.** 2011. Coordinate regulation of tissue macrophage and dendritic cell population dynamics by CSF-1. J. Exp. Med. **208:**1901–1916. http://dx.doi.org/10.1084/jem.20110866.
37. **Conway JG, McDonald B, Parham J, Keith B, Rusnak DW, Shaw E, Jansen M, Lin P, Payne A, Crosby RM, Johnson JH, Frick L, Lin MH, Depee S, Tadepalli S, Votta B, James I, Fuller K, Chambers TJ, Kull FC, Chamberlain SD, Hutchins JT.** 2005. Inhibition of colony-stimulating-factor-1 signaling in vivo with the orally bioavailable cFMS kinase inhibitor GW2580. Proc. Natl. Acad. Sci. U. S. A. **102:**16078–16083. http://dx.doi.org/10.1073/pnas.0502000102.
38. **Karaman MW, Herrgard S, Treiber DK, Gallant P, Atteridge CE, Campbell BT, Chan KW, Ciceri P, Davis MI, Edeen PT, Faraoni R, Floyd M, Hunt JP, Lockhart DJ, Milanov ZV, Morrison MJ, Pallares G, Patel HK, Pritchard S, Wodicka LM, Zarrinkar PP.** 2008. A quantitative analysis of kinase inhibitor selectivity. Nat. Biotechnol. **26:**127–132. http://dx.doi.org/10.1038/nbt1358.
39. **Abe F, Dafferner AJ, Donkor M, Westphal SN, Scholar EM, Solheim JC, Singh RK, Hoke TA, Talmadge JE.** 2010. Myeloid-derived suppressor cells in mammary tumor progression in FVB Neu transgenic mice. Cancer Immunol. Immunother. **59:**47–62. http://dx.doi.org/10.1007/s00262-009-0719-2.
40. **Donkor MK, Lahue E, Hoke TA, Shafer LR, Coskun U, Solheim JC, Gulen D, Bishay J, Talmadge JE.** 2009. Mammary tumor heterogeneity in the expansion of myeloid-derived suppressor cells. Int. Immunopharmacol. **9:**937–948. http://dx.doi.org/10.1016/j.intimp.2009.03.021.
41. **Patsialou A, Wyckoff J, Wang Y, Goswami S, Stanley ER, Condeelis JS.** 2009. Invasion of human breast cancer cells in vivo requires both paracrine and autocrine loops involving the colony-stimulating factor-1 receptor. Cancer Res. **69:**9498–9506. http://dx.doi.org/10.1158/0008-5472.CAN-09-1868.
42. **Denardo DG, Brennan DJ, Rexhepaj E, Ruffell B, Shiao SL, Madden SF, Gallagher WM, Wadhwani N, Keil SD, Junaid SA, Rugo HS, Hwang ES, Jirstrom K, West BL, Coussens LM.** 2011. Leukocyte complexity predicts breast cancer survival and functionally regulates response to chemotherapy. Cancer Discov. **1:**54–67. http://dx.doi.org/10.1158/2159-8274.CD-10-0028.
43. **Balkwill F, Mantovani A.** 2001. Inflammation and cancer: back to Virchow? Lancet **357:**539–545. http://dx.doi.org/10.1016/S0140-6736(00)04046-0.
44. **Haverkamp JM, Charbonneau B, Crist SA, Meyerholz DK, Cohen MB, Snyder PW, Svensson RU, Henry MD, Wang HH, Ratliff TL.** 2011. An

inducible model of abacterial prostatitis induces antigen specific inflammatory and proliferative changes in the murine prostate. Prostate **71:** 1139–1150. http://dx.doi.org/10.1002/pros.21327.

45. **Kusmartsev SA, Li Y, Chen SH.** 2000. Gr-1+ myeloid cells derived from tumor-bearing mice inhibit primary T cell activation induced through CD3/CD28 costimulation. J. Immunol. **165:**779–785. http://www.jimmunol.org/content/165/2/779.long.
46. **Small EJ, Schellhammer PF, Higano CS, Redfern CH, Nemunaitis JJ, Valone FH, Verjee SS, Jones LA, Hershberg RM.** 2006. Placebo-controlled phase III trial of immunologic therapy with sipuleucel-T (APC8015) in patients with metastatic, asymptomatic hormone refractory prostate cancer. J. Clin. Oncol. **24:**3089–3094. http://dx.doi.org/10.1200/JCO.2005.04.5252.
47. **Higano CS, Schellhammer PF, Small EJ, Burch PA, Nemunaitis J, Yuh L, Provost N, Frohlich MW.** 2009. Integrated data from 2 randomized, double-blind, placebo-controlled, phase 3 trials of active cellular immunotherapy with sipuleucel-T in advanced prostate cancer. Cancer **115:** 3670–3679. http://dx.doi.org/10.1002/cncr.24429.

Chapter 3:

Pten loss and RAS/MAPK activation cooperate to promote EMT and metastasis initiated from prostate cancer stem/progenitor cells

Pten Loss and RAS/MAPK Activation Cooperate to Promote EMT and Metastasis Initiated from Prostate Cancer Stem/Progenitor Cells

David J. Mulholland[1], Naoko Kobayashi[1], Marcus Ruscetti[1], Allen Zhi[1], Linh M. Tran[1], Jiaoti Huang[2], Martin Gleave[4], and Hong Wu[1,3]

Abstract

PTEN loss or PI3K/AKT signaling pathway activation correlates with human prostate cancer progression and metastasis. However, in preclinical murine models, deletion of *Pten* alone fails to mimic the significant metastatic burden that frequently accompanies the end stage of human disease. To identify additional pathway alterations that cooperate with PTEN loss in prostate cancer progression, we surveyed human prostate cancer tissue microarrays and found that the RAS/MAPK pathway is significantly elevated in both primary and metastatic lesions. In an attempt to model this event, we crossed conditional activatable *K-ras*$^{G12D/WT}$ mice with the prostate conditional *Pten* deletion model. Although RAS activation alone cannot initiate prostate cancer development, it significantly accelerated progression caused by PTEN loss, accompanied by epithelial-to-mesenchymal transition (EMT) and macrometastasis with 100% penetrance. A novel stem/progenitor subpopulation with mesenchymal characteristics was isolated from the compound mutant prostates, which was highly metastatic upon orthotopic transplantation. Importantly, inhibition of RAS/MAPK signaling by PD325901, a mitogen–activated protein (MAP)–extracellular signal–regulated (ER) kinase (MEK) inhibitor, significantly reduced the metastatic progression initiated from transplanted stem/progenitor cells. Collectively, our findings indicate that activation of RAS/MAPK signaling serves as a potentiating second hit to alteration of the PTEN/PI3K/AKT axis, and cotargeting both the pathways is highly effective in preventing the development of metastatic prostate cancers. *Cancer Res; 72(7); 1878–89. ©2012 AACR.*

Introduction

Prostate cancer is the most common male malignancy and a frequent cause of mortality in Western countries (1). During late-stage disease, oncogenic signaling pathways act collaboratively to promote metastasis and castration-resistant prostate cancer (CRPC) development. Alteration of the PTEN/PI3K/AKT pathway is well correlated with prostate cancer development with about 70% of late-stage samples showing PTEN loss or phosphoinositide 3-kinase (PI3K) activation (2). The *Pten*-null prostate cancer model mimics human disease, including hyperplasia, pancreatic intraepithelial neoplasia, and invasive carcinoma, with defined kinetics (3). However, inactivation of *Pten* alone (3–5) or in combination with homozygous deletion of p53 (6, 7) or Nkx3.1 (8) fails to recapitulate the critical aspect of end-stage human prostate cancer, that is, significant metastatic burden. Thus, identification of signaling mechanisms that collaborate with alteration of the PI3K pathway in promoting prostate cancer metastasis is critical for modeling late stage of human disease and for testing therapeutic strategies.

Despite the low frequencies of RAS mutations (9–12) and RAS fusion events (13), compelling evidence suggests that RAS/MAPK pathway activation plays a significant role in human prostate cancer progression, particularly, in metastasis and CRPC development. Enhanced *RAS* signaling can reduce dependency for androgens in the LNCaP prostate cancer cell line (14), whereas inhibition of RAS can restore hormone dependence in C42 cells, a line that is otherwise hormone independent (14, 15). Furthermore, patients who have failed hormone ablation therapy display augmentation of p-mitogen–activated protein kinase (MAPK) levels, a downstream target of RAS signaling (16). Finally, RAS activation in the DU145 human prostate cancer cell line can promote metastasis to the brain and bone (17). Despite these *in vitro* observations, it is unclear that (i) whether activation of the RAS/MAPK pathway is sufficient to initiate the full spectrum of prostate cancer development and (ii) whether the RAS/MAPK pathway

Authors' Affiliations: [1]Department of Molecular and Medical Pharmacology and Institute for Molecular Medicine, [2]Department of Pathology and Laboratory Medicine, David Geffen School of Medicine; [3]Eli and Edythe Broad Center of Regenerative Medicine and Stem Cell Research, University of California, Los Angeles, California; and [4]The Vancouver Prostate Centre and University of British Columbia, Vancouver, British Columbia, Canada

Note: Supplementary data for this article are available at Cancer Research Online (http://cancerres.aacrjournals.org/).

Corresponding Author: Hong Wu, UCLA School of Medicine, Howard Hughes Medical Institute, CHS 33-131E, 650 Charles E Young Drive S. Los Angeles, CA 90095. Phone: 310-825-5160; Fax: 310-267-0242; E-mail: hwu@mednet.ucla.edu

doi: 10.1158/0008-5472.CAN-11-3132

can collaborate with the PTEN/PI3K pathway in promoting metastasis and CRPC development.

We hypothesized that activating the RAS/MAPK pathway in conjunction with reduced *Pten* dosage may promote metastasis. To test this hypothesis, we incorporated the activating *K-ras*$^{G12D/WT}$ allele (18), as a means to activate the RAS/MAPK axis, to the *Pten*-null prostate cancer model that we generated previously (3). We report here the important collaborative effects of RAS/MAPK and PTEN/PI3K pathways in promoting prostate cancer metastasis and potential molecular mechanisms underlying such collaboration. Collectively, our results suggest that RAS/MAPK pathway activation may serve as a critical "second hit" to PTEN/PI3K/AKT pathway alterations to androgen-dependent prostate cancer and CRPC.

Methods

Human tissue microarray and bone metastasis samples

Human prostate cancer tissue microarrays (TMA) are composed of 194 patients and 388 cores (19). Histopathologic composition of the array is outlined in Supplementary Fig. S1. All bone metastasis are from patients with prostate cancer with abnormal bone scans.

Mouse strains, tissue collection and reconstitution

Mutant mice with prostate-specific deletion of *Pten* were generated as previously described under a mixed background (3). To generate the *Pb-Cre*$^{+}$*;Pten*$^{L/L}$*;K-ras*$^{G12D/W}$ or *Pb-Cre*$^{+}$*;Pten*$^{L/W}$*;K-ras*$^{G12D/W}$ mice, *Pb-Cre*$^{+}$*;Pten*$^{L/W}$ male mice were bred with female *Cre*$^{-}$*;Pten*$^{L/L}$*;K-ras*$^{G12D/W}$ mice (20). To generate *Pb-Cre*$^{+}$*;Pten*$^{L/L}$*;K-ras*$^{G12D/W}$*;LSL-Rosa26-LacZ* or *Pb-Cre*$^{+}$*;Pten*$^{L/L}$*;K-ras*$^{G12D/W}$*;LSL-Rosa26-Luc* mice, *Cre*$^{+}$*;Pten*$^{L/L}$*;K-ras*$^{G12D/W}$ male mice were bred with female, *Cre*$^{-}$*;Pten*$^{L/L}$*;LSL-Rosa26-LacZ* (21) or *Cre*$^{-}$*;Pten*$^{L/L}$*;LSL-Rosa26-Luc* (*LSL-Rosa26-Luc* was obtained from National Cancer Institute eMICE Strain 01XAC). All animal housing, breeding, and surgical procedures were conducted under the regulation of the Division of Laboratory Animal Medicine at the University of California at Los Angeles (UCLA; Los Angeles, CA).

mRNA extraction and microarray hybridization

RNA was extracted from pooled lobes resected from mutant prostates. Microarrays were conducted in the UCLA Clinical Microarray Facility using Affymetrix mouse 430 2 arrays. In brief, total RNA was extracted using the miRNeasy Mini Kit (Qiagen). Array hybridization, washing, and scanning were carried out as per the manufacturer's instructions. For genes represented by multiple probes, its expression was represented by the average of its probe expressions. Microarray data are available at the National Center for Biotechnology Information Gene Expression Omnibus (GSE34839).

Rank–rank analysis

In rank–rank geometric overlap analysis (RRHO), genes in human data sets derived from the studies of Lapointe and colleagues (22) and Taylor and colleagues (2) were ranked on the basis of their log-transformed *P* values of *t* test comparing between 2 subgroups/genotypes as previously described (23, 24).

Immunohistochemistry and LacZ detection

To detect LacZ^{+} cells, frozen sections were fixed in methanol, followed by X-gal staining (25) for 6 to 12 hours, and then counterstained with Fast Red. Immunohistochemistry was carried out as previously described (3, 26) using the following antibodies: PTEN (Cell Signaling Technology; 9559), p-MAPK (Cell Signaling Technology; 4376), androgen receptor (AR; Santa Cruz; sc-816), pan-cytokeratin (Sigma; C1801), E-cadherin (Cell Signaling Technology; 610181), vimentin (Abcam; ab39376), p-AKT (Cell Signaling Technology; 3787), Ki67 (Vector; VP-RM04), and p63 (BD Transduction; 559952).

FACS analysis and cell sorting

Cell isolation was carried out as previously described (26) using the following fluorescence-activated cell-sorting (FACS) antibodies: Sca1-PE (BD Pharm; 553336), CD49f-APC (Biolegend; 313610), EpCAM-APC/Cy7 (Biolegend; 118218), and CD24-PE/Cy7 (Biolegend; 101822).

Real time PCR

Total RNA was extracted from the mouse prostate or from the sorted cells using TRIzol reagent (Invitrogen) and purified using an RNeasy Mini column (Qiagen) according to the manufacturers' protocols. One microgram of purified total RNA was reverse transcribed to cDNA by the High-Capacity cDNA Reverse Transcription Kit (Applied Biosystems) with the random primers and MultiScribe Reverse Transcriptase. The relative gene expressions were measured by real-time PCR using the gene-specific primers and iQ SYBR Green Supermix (Bio-Rad) compared with the RPL13a RNA quantity for each cDNA sample as an endogenous control. Primers used for cell lineage marker expression were used as previously described (27) and epithelial-to-mesenchymal transition (EMT) markers as follows: *Cdh1:* F, CAGGTCTCCTCATGGCTTTGC, R, CTTCCGAAAAGAAGGCTGTCC; *Fn*: F, AGCAGTGGGAACGGACCTAC, R, ACGTAGGACGTCCCAGCAGC; *Foxc2:* F, AAGATCACTCTGAACGGCATC, R: CACTTTCACGAAGCACTCATTG; *Mmp2*: F, CACCTACACCAAGAACTTCC, R, GAACACAGCCTTCTCCTCCT; *N-cad*: F, CAGGTCTCCTCATGGCTTTGC, R, CTTCCGAAAAGAAGGCTGTCC; *RPL13a*: F, TACGCTGTGAAGGCATCAAC, R, ATCCCATCCAACACCTTGAG; *Snail*: F, AAGATGCACATCCGAAGC, R, ATCTCTTCACATCCGAGTGG; Twist: F, CGGGTCATGGCTAACGTG, R, CAGCTTGCCATCTTGGAGTC; *Vim*: F, CGGCTGCGAGAGAAATTGC, R, CCACTTTCCGTTCAAGGTCAAG; *Zeb1*: F, CATGTGACCTGTGTGACAAG, R, GCGGTGATTCATGTGTTGAG; and *Zeb2*: F, TAGCCGGTCCAGAAGAAATG, R, GGCCATCTCTTTCCTCCAGT.

Cell line

The *Pten*$^{-/-}$*;K-ras*^{G12D} cell line was isolated from a 10-week *C*$^{+}$*;Pten*$^{L/L}$*;K-ras*$^{L/W}$ mutant prostate through FACS sorting of Lin^{-}EpCAM^{high}CD24^{high} cells. Cells were passaged in culture at least 10 times and PCR authenticated for *Pten* deletion and the presence of the *K-ras*^{G12D} activating allele. *Pten*$^{-/-}$*;K-ras*^{G12D} cells were infected with lenti-GFP virus for detection by immunohistochemistry.

Orthotopic injections, bioluminescence imaging, and measurement of lung lesions

Prostate sphere cells or subpopulations of primary cancer cells were isolated from C^{+};$Pten^{L/L}$;$K\text{-}ras^{L/W}$;*LSL-Luc* mutant prostates. Prostate orthotopic injections were carried out using approximately 2,000 cells in 50% Matrigel/media using a 10 μL Hamilton syringe (Microliter #701). Tumor development was then monitored using bioluminescence detection (Xenogen IVIS, Caliper Life Sciences). For measurement of lung lesions, accumulated lesion area per mouse was measured and then calculated as a percentage of total lung section area. Tibial, orthotopic injections to *NOD;SCID;IL2rγ*-null recipients were carried out using a 10 μL Hamilton syringe (Microliter #701) to deliver no more than 1,000 $Pten^{-/-}$;$K\text{-}ras^{G12D}$ cells injected in 10 μL volume of 50% Matrigel/media.

Drug treatment

NOD;SCID;IL2rγ-null mice with various orthotopic transplantations were treated with rapamycin (4 mg/kg/d, intraperitoneally) and/or PD325901 (5 mg/kg/d, *per os*) daily for 14 days.

Results

RAS/MAPK pathway is activated in human primary and metastatic prostate cancer lesions

Of several well-known pathway alterations found in human prostate cancers is the RAS/RAF/MAPK pathway, showing frequencies of 43% and 90% alteration in primary and metastatic lesions, respectively (2). To investigate the potential collaboration between the PTEN/PI3K and RAS/MAPK pathways, we assessed the correlation between PTEN loss and MAPK activation using (i) a human prostate cancer TMA composed of 194 patients and 388 cores (Fig. 1A and Supplementary Fig. S1) and (ii) 30 human prostate cancer bone metastasis specimens obtained from 4 U.S. medical institutions (Fig. 1B). While p-MAPK levels were not significantly elevated in untreated specimens, levels were significantly increased in neoadjuvant-treated (neoadjuvant hormone therapy) and recurrent patients with CRPC as compared with benign prostatic hyperplasia specimens, coinciding with at least a 1-fold reduction in PTEN expression (Fig. 1A, *, $P < 0.05$; **, $P < 0.005$). In metastatic bone lesions, we observed elevated p-MAPK staining in 80% (24 of 30) of samples (Fig. 1B), a finding similar to what was reported previously for lymph node metastasis (28). In nearly all bone lesions, PTEN expression was low or negative (Fig. 1B, right). Interestingly, prominent p-MAPK expression was found near the basal compartment, corresponding to the potential transient amplifying stem/progenitor cell populations in human bone metastatic lesions (Fig. 1B, arrow). Collectively, these data indicate that the RAS/MAPK signaling pathway is highly active in human prostate cancer specifically in patients who have received anti-androgen therapy. These data also suggest that there may be selection for coinciding activation of PI3K/AKT and RAS/MAPK signaling in patients with late-stage disease.

PTEN loss and RAS activation cooperate in accelerating primary and metastatic prostate cancer progression

To assess the role of RAS pathway activation in promoting prostate cancer development and metastasis, we conditionally activated *K-ras* in the prostatic epithelium by crossing the $K\text{-}ras^{G12D/W}$ ($K\text{-}ras^{L/W}$; ref. 29) allele to the *Pb-Cre* line (C^{+}; ref. 30). While RAS activation was sufficient to enhance p-MAPK levels, it failed to promote significant cell proliferation, AKT activation, and prostate cancer development (Supplementary Fig. S2). Therefore, activation of the RAS pathway alone is not sufficient to induce prostate cancer. To assess RAS/MAPK activation as an additional hit to PTEN/PI3K/AKT pathway alteration in promoting prostate cancer progression, we crossed *Pb-Cre*$^{+}$;$Pten^{L/L}$ mice (C^{+};$Pten^{L/L}$) with $K\text{-}ras^{L/W}$ mice to generate C^{+};$Pten^{L/L}$;$K\text{-}ras^{L/W}$ mutants. In comparison to C^{+};$Pten^{L/L}$ mutants, simultaneously deleting *Pten* and activating *K-ras* led to early lethality (Fig. 2A, comparing red and green lines) with enhanced progression at both gross (Fig. 2B; arrows, anterior lobes; solid black arrowheads, dorsolateral lobes) and histologic levels (Fig. 2C). While pathology in C^{+};$Pten^{L/L}$ mutants was predominantly adenocarcinoma localized to the dorsolateral lobes, C^{+};$Pten^{L/L}$;$K\text{-}ras^{L/W}$ mutants showed invasive carcinoma both in the dorsolateral and anterior lobes as early as 4 weeks with poorly differentiated carcinoma occurring by 10 weeks (Fig. 2B and C).

Because partially reduced PTEN expression occurs frequently during human prostate cancer progression (Fig. 1B; refs. 31, 32), we then considered whether loss of a single *Pten* allele could also cooperate with RAS activation. While under the genetic background we studied, neither C^{+};$Pten^{L/WT}$ (3, 26, 24) nor C^{+};$K\text{-}ras^{L/WT}$ mutants showed little evidence of cancer when older than 1 year (data not shown and Supplementary Fig. S2), C^{+};$Pten^{L/W}$;$K\text{-}ras^{L/W}$ mice developed focal neoplastic expansions by 10 weeks, invasive carcinoma by 20 weeks (Supplementary Fig. S4A and S4B), and lethality around 40 weeks (Fig. 2A, orange line) accompanied by PTEN loss and p-AKT-S473 activation (Supplementary Fig. S4C).

Importantly, in contrast to micrometastasis seen in 15% to 30% of age- and genetic background–matched C^{+};$Pten^{L/L}$ mice (3), both C^{+};$Pten^{L/L}$;$K\text{-}ras^{L/W}$ and C^{+};$Pten^{L/W}$;$K\text{-}ras^{L/W}$ mutants developed macrometastatic lesions in the lung and liver with 100% penetrance (Fig. 3A). Lesions were largely pan-cytokeratin positive (Fig. 3A) with activated MAPK and PTEN loss (Fig. 3B). Interestingly, AR expression was highly heterogeneous in lung lesions (Fig. 3A) and primary tumor samples from C^{+};$Pten^{L/W}$;$K\text{-}ras^{L/W}$ mutants (Supplementary Fig. S3A). Moreover, gene set enrichment analysis (GSEA) showed that C^{+};$Pten^{L/L}$;$K\text{-}ras^{L/W}$ mutant prostates have reduced expression of AR target genes (Supplementary Fig. S3C), in comparison to C^{+};$Pten^{L/L}$ mutants, including *Mme*, *Msmb*, and *Nkx3.1* (Supplementary Fig. S3C).

Importantly, cells with genotype of Cre^{+}, *Pten* deletion and activated *K-ras* were detected in 4 of 6 bone marrow flushes of C^{+};$Pten^{L/L}$;$K\text{-}ras^{L/W}$ or C^{+};$Pten^{L/W}$;$K\text{-}ras^{L/W}$ mutants (Fig. 3C). However, because of early lethality of these animals, we did not observe overt metastasis in the bone at the histologic level or by bone imaging (data not shown). Collectively, our results indicate that the cooperation between PTEN loss and RAS

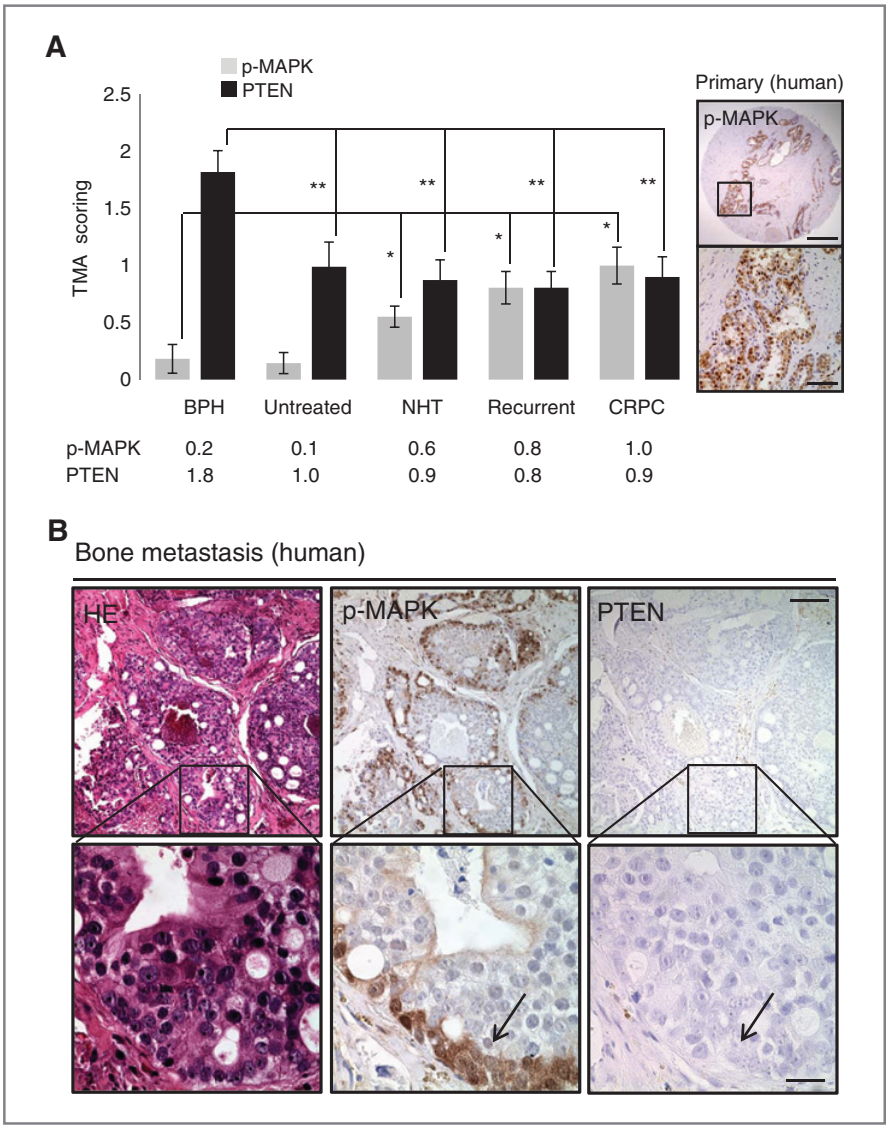

Figure 1. RAS/MAPK signaling is enriched in human prostate cancer. A, PTEN and p-MAPK expression in human TMAs (patient samples = 194, cores = 388; left) and p-MAPK expression in recurrent prostate cancer (right). *, $P < 0.05$; **, $P < 0.005$; low magnification bar, 1 mm; high magnification bar, 100 μm. BPH, benign prostatic hyperplasia; NHT, neoadjuvant hormone therapy. B, expression of PTEN and p-MAPK in human bone metastasis. Low magnification bar, 250 μm; high magnification bar, 50 μm. HE, hematoxylin and eosin.

activation yields significantly enhanced metastatic prostate cancer progression in these new murine models.

RAS activation promotes *Pten*-null epithelial cells to undergo EMT and acquisition of a human prostate cancer signature

A striking feature found in C^{+};$Pten^{L/L}$;$K\text{-}ras^{L/W}$ and C^{+};$Pten^{L/W}$;$K\text{-}ras^{L/W}$ prostates was the mesenchymal morphology associated with the aggressive behavior of cancer cells, similar to poorly differentiated human cancers (Supplementary Fig. S5). Similar to human prostate cancer, we observed a loss of p63 expression in the basal compartment of cancerous acini of C^{+};$Pten^{L/L}$;$K\text{-}ras^{L/W}$ mutants (Supplementary Fig. S5A). We also observed further reduction of p53 and p27 in C^{+};$Pten^{L/L}$;$K\text{-}ras^{L/W}$ mutants compared with those with *Pten* single deletion (Supplementary Fig. S5B). Consistent with EMT phenotype, we observed enhanced N-cadherin expression in transition regions, especially in poorly differentiated cancer, indicating that many of these cells displayed neuroendocrine expansion. Interestingly, synaptophysin-positive cells were generally rare in this new model (Supplementary Fig. S5C).

To assess the role of Ras activation in promoting EMT in *Pten*-null epithelium, we examined regions with morphologic transition using the epithelial (E-cadherin) and mesenchymal markers (vimentin; Fig. 4A). While adenocarcinoma and mesenchymal cancer regions showed distinct marker expression, transition regions showed coexpression of both epithelial and mesenchymal markers (Fig. 4A, yellow in overlay).

To ascertain that the observed mesenchymal pathology occurred as a result of a true EMT, and not expansion of the native stromal compartment, we crossed a Cre-activatable *LacZ* reporter line (*LSL-Rosa26-LacZ*; ref. 25) onto the

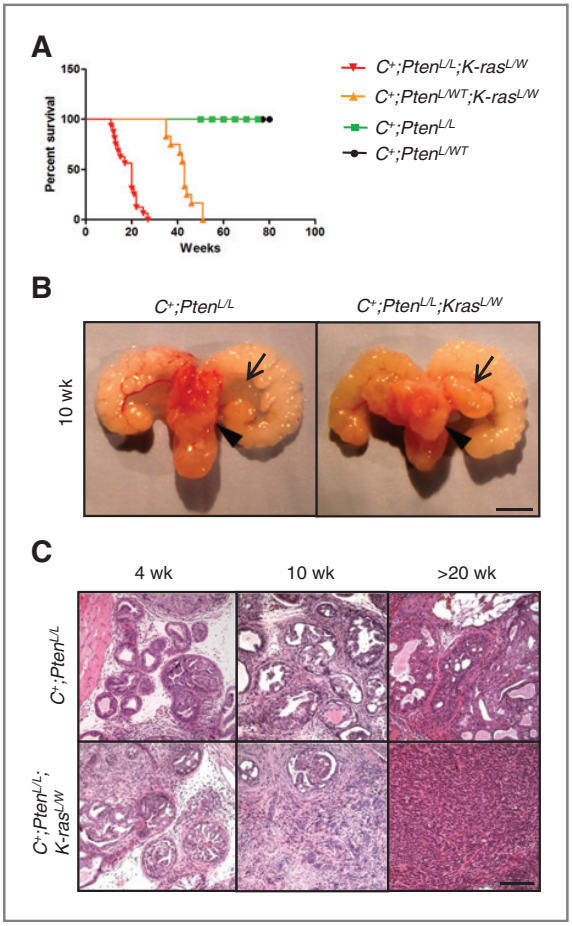

Figure 2. *Pten* loss and Ras activation cooperate to enhance murine prostate cancer progression. A, Kaplan–Meier survival curve of *Pten* and *Pten;K-ras* mutants. B, gross structure of intact $C^+;Pten^{L/L}$ and $C^+;Pten^{L/L};K\text{-}ras^{L/W}$ mutant prostates at 10 weeks (arrowhead, lateral lobe; arrow, anterior lobe). Bar, 4 mm. C, histology of intact $C^+;Pten^{L/L}$ and $C^+;Pten^{L/L};K\text{-}ras^{L/W}$ mutant prostates at 4, 10, and >20 weeks. Bar, 250 μm.

compound mutant line. Because *LacZ* expression is activated by the same Cre recombinase, $LacZ^+$ cells could be used for lineage tracing for those *Pten*-null and *Ras*-activated epithelial cells. Analysis of $C^+;Pten^{L/L};LSL\text{-}Rosa26\text{-}LacZ$ mutant prostates showed LacZ-positive regions to be restricted to prostate epithelium (data not shown); however, $C^+;Pten^{L/L};K\text{-}ras^{L/W};LSL\text{-}Rosa26\text{-}LacZ$ prostates showed expansion of *LacZ*-positive cells from epithelial acini (Fig. 4B, arrows) to regions with mesenchymal morphology (Fig. 4B, arrowheads in middle). These data indicate that RAS activation facilitates EMT of *Pten*-null epithelial cells.

We then conducted unbiased microarray analysis on age- and genetic background–matched $C^+;Pten^{L/L};K\text{-}ras^{L/W}$ and $C^+;Pten^{L/L}$ prostates ($n = 3$; 10 weeks) and found that 370 and 336 genes were significantly up- and downregulated for more than 3-fold, respectively, due to RAS activation. Among those upregulated genes, 11 were EMT-associated genes ($P = 1.7e\text{-}13$, Fisher's exact test; Fig. 4C). We further validated the array analysis by real-time PCR using independent prostate samples from $C^+;K\text{-}ras^{L/W}$, $C^+;Pten^{L/L}$, and $C^+;Pten^{L/L};K\text{-}ras^{L/W}$ mutants at 10 weeks of age. Prostates from $C^+;Pten^{L/L};K\text{-}ras^{L/W}$ mutants showed significantly enhanced expression of EMT markers including Snail (*Snail*), vimentin (*Vim*), Fibronectin (*Fn1*), MMP2 (*Mmp2*), Twist (*Twist1*), Zeb1 (*Zeb1*), and Foxc2 (*Foxc2*; Fig. 4D). Thus, at the gene expression level, $C^+;Pten^{L/L};K\text{-}ras^{L/W}$ mutants display an EMT signature.

Because of the association of PTEN/PI3K/AKT and RAS/RAF/MAPK pathway alterations in human prostate cancer progression, we hypothesized that murine prostate cancer with concomitant PTEN and RAS pathway alterations may closely resemble gene signatures of end-stage human prostate cancers. To test this hypothesis, we used RRHO analysis to compare the overlap of differentially expressed genes in human primary versus metastatic tumors from either the data sets in the study of Lapointe and colleagues (22) or Taylor and colleagues (2) with either $Pb\text{-}C^+;Pten^{L/L}$ or $Pb\text{-}C^+;Pten^{L/L};K\text{-}ras^{L/W}$ mutants. The heatmap signals on the bottom left (blue circle) and top right (red circle) corners indicate that primary human tumors shared the greatest overlap with $Pb\text{-}C^+;Pten^{L/L}$ primary tumors whereas the human metastatic data set overlapped more with the signature derived from $Pb\text{-}C^+;Pten^{L/L};K\text{-}ras^{L/W}$ mutants (Supplementary Fig. S6A).

On the basis of previously published RAS signature gene sets (33), several gene sets were noted to be altered to a greater extent in *Pten;K-ras* metastatic lesions, similar to that of human disease, as exemplified by the downregulation of fibroblast growth factor receptor 2 (*FGFR2*) expression and enhanced *UBE2C* expression, a ubiquitin-conjugating enzyme known to be overexpressed in human prostate cancer (Supplementary Fig. S6B; ref. 34). Together, these analyses provide strong support of our hypothesis that the *Pten;K-ras* model closely mimics the biology of human prostate cancer, especially metastatic disease.

Pten loss and Ras activation cooperate to enhance stem/progenitor activity

Recent studies suggest that EMT is associated with the formation of breast cancer stem cells (35) and the progression of prostate cancer (19, 36). To test whether RAS activation induces EMT in *Pten*-null prostatic stem/progenitor cells and consequently promotes prostate cancer progression and metastasis, we characterized prostatic stem/progenitor cells *in vitro* sphere-forming analysis. Our previous study indicates that LSC^{high} ($Lin^-Sca1^+CD49f^{high}$) stem/progenitor cells have high sphere-forming activity and are both necessary and sufficient for initiating *Pten*-null prostate cancers (26). Similar to *Pten*-null prostates, the compound *Pten;K-ras* prostates showed significant expansion of the leukemia stem cell $(LSC)^{high}$ subpopulation (Fig. 5A, left; **, $P < 0.01$, $n = 4$) and further enhanced sphere-forming activity (Fig. 5A, right, **, $P < 0.01$). However, different from *Pten*-null prostates, the LSC^{low} ($Lin^-Sca1^+CD49f^{low}$) subpopulation isolated from the compound mutants had significantly enhanced sphere-forming activity in free-floating conditions (Fig. 5A, right; *, $P <$

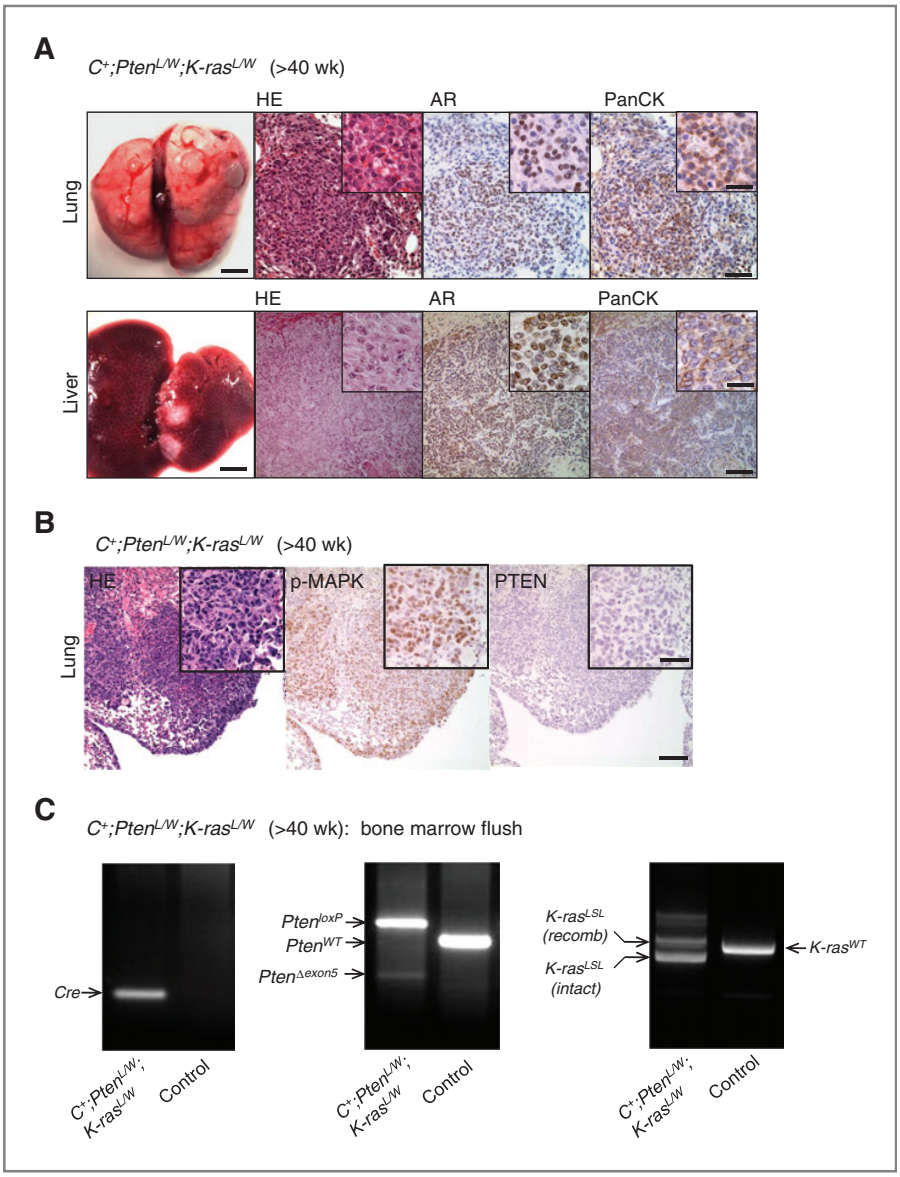

Figure 3. *Pten* loss and Ras activation cooperate to significantly enhance metastatic burden. A, gross lung and liver structure showing the presence of macrometastasis and corresponding stains for hematoxylin and eosin (HE), AR, and pan-cytokeratin (PanCK) in $C^{+};Pten^{L/WT};K\text{-}ras^{L/W}$ mutants (>40 weeks). Low magnification bar, 150 μm; high magnification bar, 50 μm. B, lung lesions from $C^{+};Pten^{L/W};K\text{-}ras^{L/W}$ mutants showing p-MAPK and PTEN expression. Low magnification bar, 150 μm; high magnification bar, 50 μm. C, bone marrow flush and PCR genotyping for excised *Pten* (Δexon5) and recombined *LSL-K-Ras* in $C^{+};Pten^{L/W};K\text{-}ras^{L/WT}$ and control (WT, wild-type) mice.

0.05). To assess whether certain epithelial stem/progenitor cells have acquired mesenchymal characteristics and, therefore, reduced epithelial marker expression on the cell surface, we isolated $Lin^{-}EpCAM^{low}CD24^{low}$ cells from the above mutants and found that only $Lin^{-}EpCAM^{low}CD24^{low}$ cells (Fig. 5B, right FACS plot) from $C^{+};Pten^{L/L};K\text{-}ras^{L/W}$ mutants had significant sphere-forming activity ($P < 0.001$; Fig. 5A, right). Using real-time PCR analysis, we affirmed that LSC^{high} and LSC^{low} subpopulations corresponded to the basal (*Ck5*, *p63*, *Ck14*), and luminal cell populations (*Ar*, *Ck8*, *Ck18*, *E-cdh*, and *Psca*), respectively, whereas the $EpCAM^{low}/CD24^{low}$ subpopulation corresponded to mesenchymal cells on the basis of the heightened gene expression of *Ar*, *Mmp2*, *N-cadherin*, *Snail*, *Twist*, *vimentin*, and *Zeb2* (Fig. 5B, $n = 4$). Therefore, *Pten* loss and *Ras* activation collaborate in stem/progenitor expansion and Ras activation promotes EMT in *Pten*-null sphere-forming cells.

Stem/progenitor cells with *Pten* loss and Ras activation can reconstitute EMT and macrometastatic prostate cancer

Our previous study showed that the LSC^{high} subpopulation or its derived sphere cells isolated from *Pten*-null primary cancers could reconstitute adenocarcinoma when subject to the prostate regeneration assay (26). Because primary $C^{+};Pten^{L/L};K\text{-}ras^{L/W}$ mutants develop macrometastasis, we then considered whether sphere cells derived from these mutants could also initiate a metastatic phenotype via orthotopic

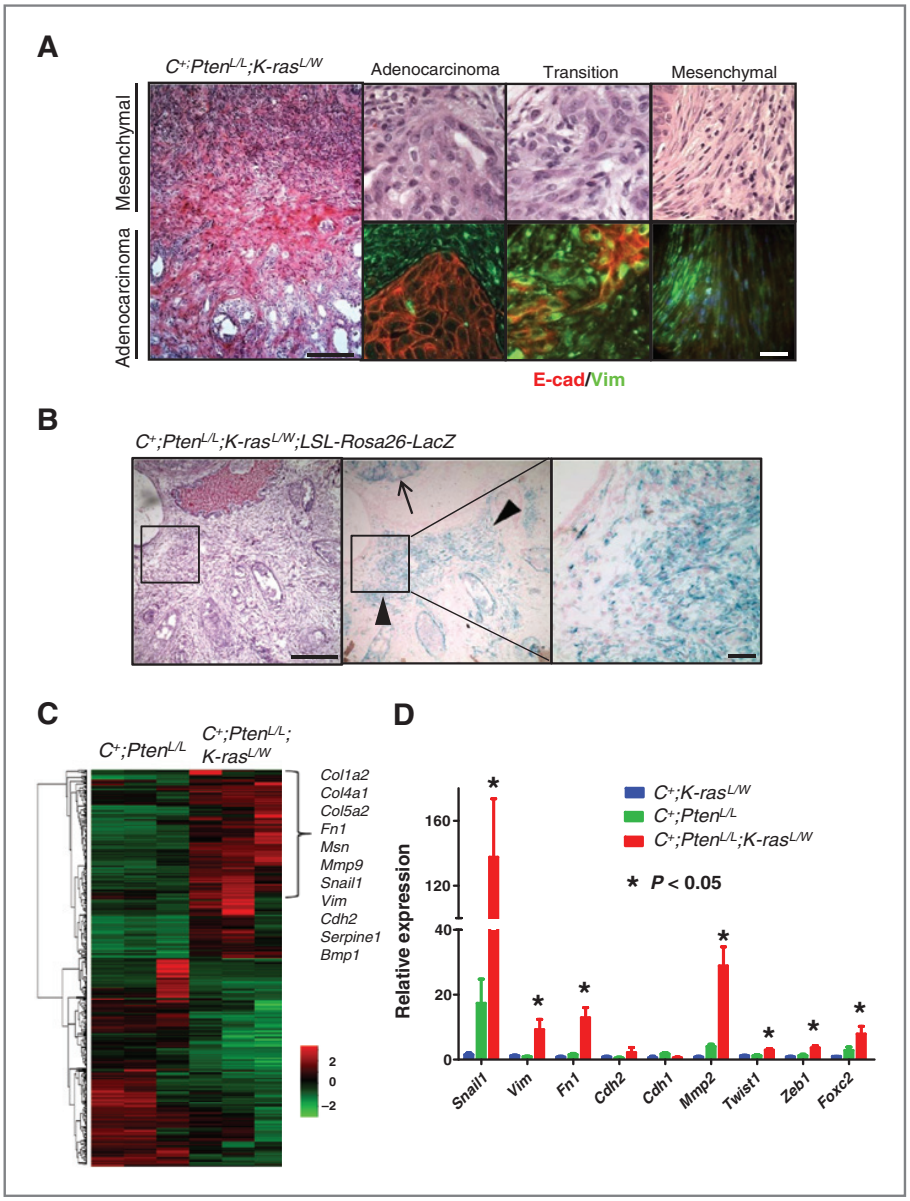

Figure 4. *Pten* loss and Ras pathway activation propagate an EMT signature. A, histology (left, top) and immunostains [E-cadherin (E-cad), vimentin (Vim); bottom] showing regions of transition between epithelial and mesenchymal phenotypes. Low magnification bar, 500 μm; high magnification bar, 100 μm. B, lineage tracing using β-gal staining and the *LSL-Rosa26-LacZ* reporter in conjunction with the epithelial specific probasin promoter in C^{+};$Pten^{L/L}$;$K\text{-}ras^{L/W}$ mutants (10 weeks). Low magnification bar, 500 μm; high magnification bar, 200 μm. C, gene microarray analysis showing EMT pathway gene activity in between C^{+};$Pten^{L/L}$;$K\text{-}ras^{L/W}$ and C^{+};$Pten^{L/L}$ mutants. D, RT-PCR confirmation of EMT gene alterations in C^{+};$Pten^{L/L}$;$K\text{-}ras^{L/W}$ mutant prostates (*, $P < 0.05$).

transplantations, an assay thought to closely mimic the natural metastatic process (37). To test this, we dissociated passage 3 sphere cells from C^{+};$K\text{-}ras^{L/W}$, C^{+};$Pten^{L/L}$, and C^{+};$Pten^{L/L}$;$K\text{-}ras^{L/W}$ mice followed by orthotopic injection of approximately 2×10^{3} cells to the proximal region of the anterior lobe of *NOD;SCID;IL2rg*-null mice. Genotypes of sphere cells were confirmed by PCR analysis, before transplantation, on individual P3 spheres (Supplementary Fig. S7A and data not shown).

Although C^{+};$Pten^{L/L}$ (data not shown) and C^{+};$Pten^{L/L}$;$K\text{-}ras^{L/W}$ sphere cells could initiate primary engraftments after 3 to 4 weeks, only recipient mice with C^{+};$Pten^{L/L}$;$K\text{-}ras^{L/W}$ sphere cells appeared morbid with poorly differentiated carcinoma (Fig. 6A, left). Extensive micro- and macrometastases was observed in the lymph nodes, lung, and liver of mice that received C^{+};$Pten^{L/L}$;$K\text{-}ras^{L/W}$ sphere cells. The metastatic lesions maintained morphology similar to the primary cancers (data not shown). Importantly, recipients of either C^{+};$K\text{-}ras^{L/W}$ or C^{+};$Pten^{L/L}$ sphere cell transplants revealed no detectable macrometastasis or morbidity by 10 weeks posttransplantation (data not shown), suggesting that concomitant alteration of both PTEN/PI3K and RAS/MAPK pathways in stem/progenitor cells is required for the metastasis development in the orthotopic transplantation models.

To further support our hypothesis that stem/progenitor cells can reconstitute both EMT and metastatic phenotypes, we FACS sorted the LSC^{high}, LSC^{low} and EpCAM^{low}/CD24^{low} mesenchymal subpopulations from *C^{+};K-ras$^{L/W}$*, *C^{+};Pten$^{L/L}$*, and *C^{+};Pten$^{L/L}$;K-ras$^{L/W}$* mutant prostates at 8 to 10 weeks of age (Supplementary Fig. S7B and data not shown), followed by orthotopic transplantation. Consistent with our previous studies, transplantation of *Pten*-null LSC^{high} cells could form adenocarcinoma (ref. 26; Fig. 6A, right) but without detectable metastasis. However, in the recipients of *C^{+};Pten$^{L/L}$;K-ras$^{L/W}$* LSC^{high} cells and EpCAM^{low}/CD24^{low} mesenchymal cells, we observed similar EMT and metastatic phenotypes (Fig. 6B). PCR genotyping of resected metastatic lesions validated the presence of *C^{+};Pten$^{-/-}$;K-ras$^{G12D/W}$* cancer cells (Supplementary Fig. S7C). Therefore, both LSC^{high} and EpCAM^{low}/CD24^{low} stem/progenitor cells isolated from *C^{+};Pten$^{L/L}$;K-ras$^{L/W}$* mutant mice have enhanced prostate capacity to reconstitute EMT and drive distant metastasis compared with stem/progenitor cells with either PI3K activation or RAS/MAPK activation alone.

Pharmacologic targeting of RAS/MAPK signaling inhibits metastatic disease initiated from stem/progenitor cells

Because transplantation of stem/progenitor cells isolated from *C^{+};Pten$^{L/L}$;K-ras$^{L/W}$* mutants yielded metastatic disease with reliable kinetics, we investigated whether targeting of the PI3K/AKT and RAS/MAPK signaling pathways could inhibit such a phenotype. To noninvasively monitor metastasis *in vivo*, we crossed the *Rosa26-Luc* reporter line onto the compound mutant mice so both primary and metastatic lesions can be easily monitored via bioluminescence imaging (BLI; Fig. 7A and data not shown). We first tested the ability of mTOR inhibitor rapamycin (4 mg/kg/d, intraperitoneally) and MEK inhibitor PD325901 (5 mg/kg/d, *per os*) to effectively inhibit the PI3K and RAS pathways *in vivo*, using *C^{+};Pten$^{L/L}$;K-ras$^{L/W}$* mutant mice. As shown in Fig. 7B, left, these small-molecule inhibitors could hit their respective pathways *in vivo*, indicated by the reduction of their downstream surrogate markers p-S6 and p-MAPK staining. Coinciding with efficient reduction of phospho-targets, we observed marked reduction of Ki67^{+} cells

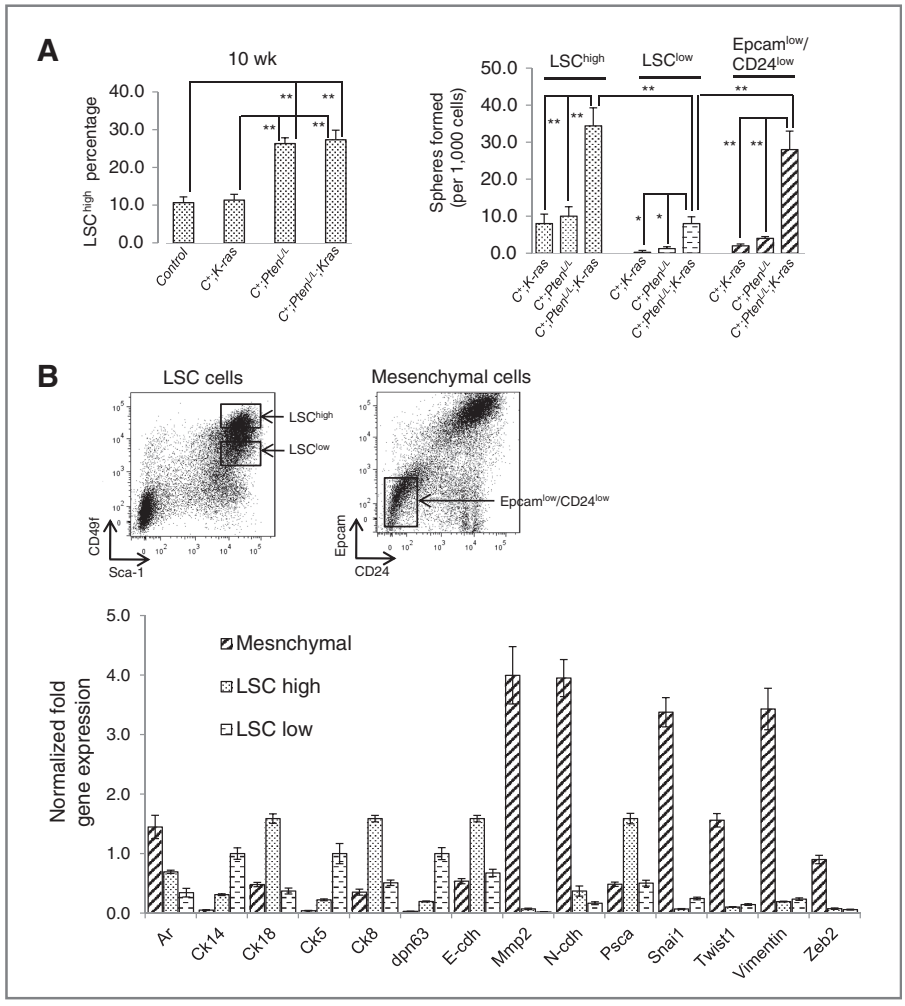

Figure 5. *C^{+};Pten$^{L/L}$;K-ras$^{L/W}$* mutant LSC^{high} and mesenchymal cells show high stem/progenitor activity. A, comparison of percentage of LSC^{high} subpopulation in control, *C^{+};K-ras$^{L/W}$*, *C^{+};Pten$^{L/L}$*, and *C^{+};Pten$^{L/L}$;K-ras$^{L/W}$* mutant prostates (10 weeks; left). Comparison of sphere-plating efficiency between LSC^{high}, LSC^{low}, and mesenchymal cells isolated from *C^{+};Pten$^{L/L}$* and *C^{+};Pten$^{L/L}$;K-ras$^{L/W}$* mutant prostates (10 weeks; *, $P < 0.05$; **, $P < 0.01$; right). B, isolation of LSC^{high} (Lin^{-}Sca1^{+}CD49f^{high}), LSC^{low} (Lin^{-}Sca1^{+}CD49f^{low}), and mesenchymal cells from *C^{+};Pten$^{L/L}$;K-ras$^{L/W}$* mutants (10 weeks) with RT-PCR analysis (bottom).

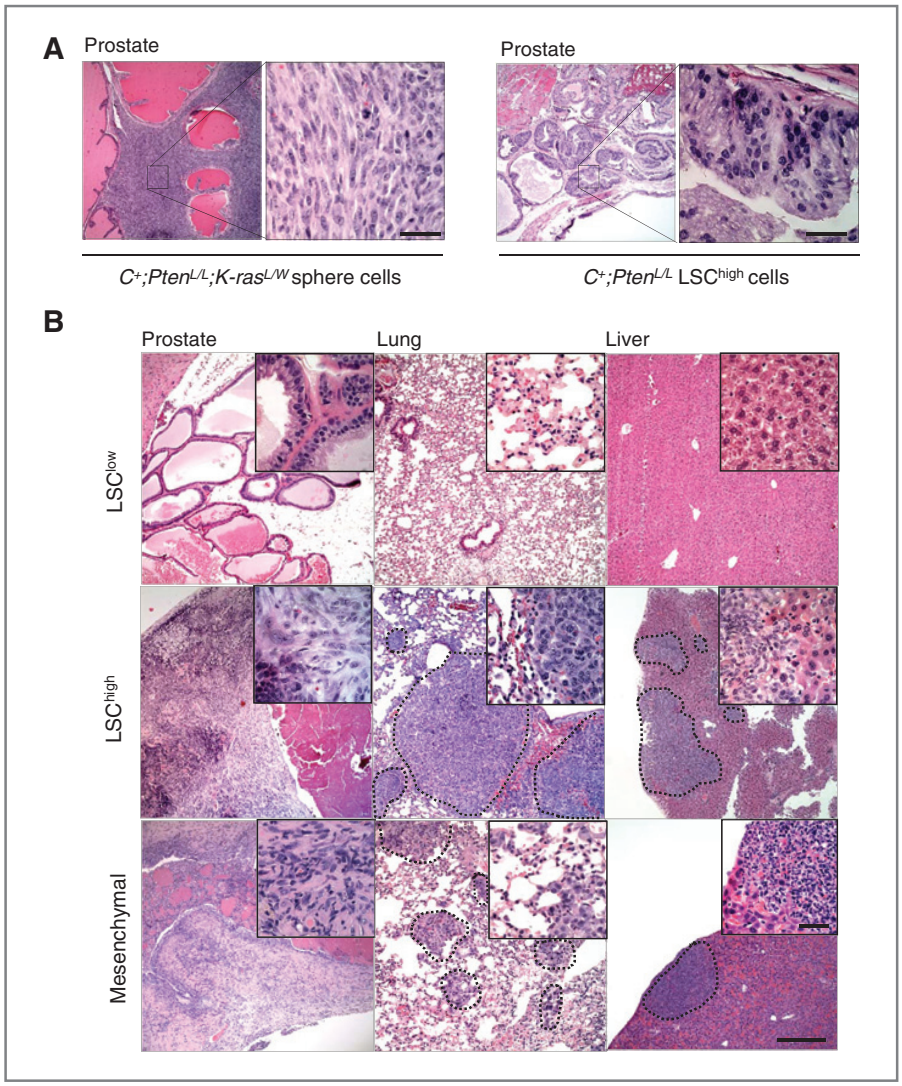

Figure 6. Transplantation of C^+;$Pten^{L/L}$;$K\text{-}ras^{L/W}$ stem/progenitor cells are sufficient to initiate EMT and metastasis. A, orthotopic transplantation of C^+;$Pten^{L/L}$;$K\text{-}ras^{L/W}$ spheres cells (left) and C^+;$Pten^{L/L}$ LSC^{high} cells (right) to *NOD;SCID;IL2rγ*-null recipients and resulting pathology (left). B, transplantation of LSC^{low}, LSC^{high}, and mesenchymal cells isolated from primary C^+;$Pten^{L/L}$;$K\text{-}ras^{L/W}$ mutant cells and resulting pathology observed in *NOD;SCID;IL2rγ*-null recipients. Low magnification bar, 500 μm; high magnification bar, 100 μm.

in C^+;$Pten^{L/L}$;$K\text{-}ras^{L/W}$ mutants treated with rapamycin and PD325901 (Fig. 7B, middle).

NOD;SCID;IL2rγ-null male mice were then orthotopically transplanted with approximately 2×10^3 sphere cells derived from C^+;$Pten^{L/L}$;$K\text{-}ras^{L/W}$;*Rosa26-luc* mice. Two days postinjection, mice were treated daily with placebo, rapamycin, and/or PD325901, and tumor growth and metastasis were monitored weekly *in vivo* by BLI. While placebo-treated mice showed rapid primary disease and progression to lung metastasis, as indicated by BLI signals (Fig. 7C, left, $n = 10$), mice receiving combination treatment showed both reduced primary tumor burden and little detectable signal in the thoracic region (Fig. 7C, left and quantified in middle, $n = 10$). Histologic analysis revealed that combination treatment significantly abolished enhanced cell proliferation and EMT phenotype seen in placebo cohort of sphere transplantation recipients (Fig. 7B, middle and right) and the metastatic potential of the C^+;$Pten^{L/L}$;$K\text{-}ras^{L/W}$;*Rosa26-luc* sphere cells to the lung (Fig. 7C, right). To further test our hypothesis that RAS/MAPK pathway activation is critical for the promotion of metastatic disease, we treated transplantation recipients with only the MEK inhibitor. After 3 to 4 weeks of daily treatment with PD325901, we observed a similar reduction in metastasis (Fig. 7C, $n = 10$), although the effect on primary cancers were less significant compared with the combination treatment. Together these data suggest that the RAS/MAPK pathway activation, in collaboration with PTEN loss or PI3K pathway activation, indeed, plays an essential role in the development of metastatic prostate cancers and that cotargeting both the pathways may be effective in preventing metastasis or slowing down tumor progression.

Discussion

The study of molecular mechanisms underlying late-stage metastatic prostate cancer has been challenging partly as a result of the paucity of prostate cancer models that recapitulate the multistep process of the metastasis. While alterations in the

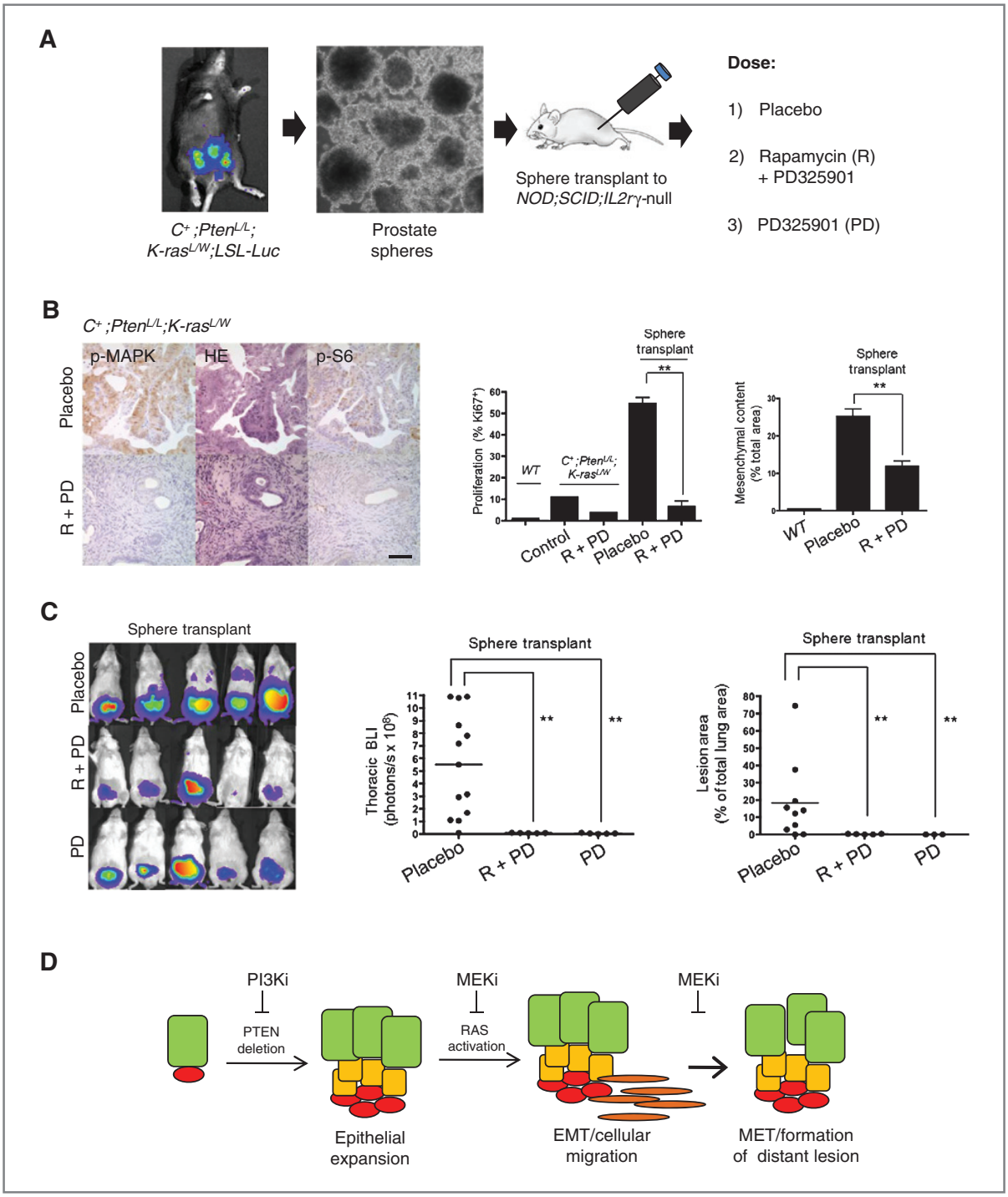

Figure 7. Pharmacologic targeting of RAS/MAPK signaling inhibits metastatic disease initiated from $C^{+};Pten^{L/L};K\text{-}ras^{L/W}$ mutant stem/progenitor cells. A, isolation of prostate sphere cells from $C^{+};Pten^{L/L};K\text{-}ras^{L/W};LSL\text{-}Luc$ mutants and orthotopic injection to *NOD;SCID;IL2rγ*-null mice. Recipients were then treated with placebo, rapamycin (R) + PD325901 (PD), or PD325901 alone. B, effect of rapamycin/PD325901 treatment on p-MAPK and p-S6 levels (left), cell proliferation ($Ki67^{+}$ index; middle), and mesenchymal content (right). HE, hematoxylin and eosin; WT, wild-type. **, $P < 0.005$. C, effect of rapamycin/PD325901 or PD325901 on thoracic region BLI (left, middle) and metastatic lung lesion content (right). **, $P < 0.005$. D, model showing that Pten-null LSC^{high} cells can initiate prostate cancer and with RAS/MAPK activation lead to EMT, metastatic disease, and formation of macrometastatic lesions. MEKi, MEK inhibitor; MET, mesenchymal-to-epithelial transition. PI3Ki, PI3K inhibitor.

PTEN/PI3K/AKT signaling axis occur frequently in human disease, such pathway alterations are not sufficient to manifest a significant metastatic phenotype in preclinical animal models (3–5, 38). In this study, we identified significant enhancement of RAS signaling in both recurrent primary tumors and bone metastasis. In consideration of these findings, we evaluated the possibility that RAS/MAPK activation could serve as a critical, additional hit to alteration of PTEN/PI3K/AKT signaling in promoting prostate cancer progression and metastasis (Fig. 7D). Through coordinate *Pten* deletion and *K-ras*$^{G12D/W}$ activation, we observed markedly enhanced tumor progression compared with *Pten* deletion alone. Striking features of *C*$^{+}$*;Pten*$^{L/L}$*;K-ras*$^{L/W}$ and *C*$^{+}$*;Pten*$^{L/W}$*;K-ras*$^{L/W}$ mutants included the presence of EMT and significant metastatic burden. Importantly, our study also showed that both LSC^{high} epithelial and EpCAM^{low}/CD24^{low} mesenchymal stem/progenitor cells have sphere-forming activity *in vitro* and could reconstitute both local invasive and distance metastatic disease *in vivo*.

EMT has been postulated to play a critical role in the process of metastasis (39–41). Expression of EMT markers is correlated with human prostate cancer progression as exemplified by the enhanced levels of the Twist (36) and N-cadherin (19) in late-stage primary and metastatic diseases. Moreover, monoclonal antibody targeting of N-cadherin significantly delays progression in prostate cancer xenograft models (19). However, as few preclinical prostate cancer models progress from invasive carcinoma to EMT and metastasis, the functional significance and the pathways involved with EMT have been difficult to study. Using the *Pten*;p53 prostate cancer model (6), a recent study derived lineage-specific cell lines which could metastasize upon orthotopic injection into immunocompromised hosts (7). However, the interpretation of these findings is confounded by the fact that primary *Pten*;p53 mutant tumors rarely show extensive metastasis and that derived cell lines may undergo *in vitro* adaptation or acquire additional mutations. Therefore, the new *Pten*-null;*K-ras* activated model provides a unique opportunity for studying the significant impact of EMT in prostate cancer progression *in vivo* and the pathway that regulates the EMT biology in the context of PTEN loss. Because both K-ras and B-raf alterations occur in primary and metastatic prostate cancer (2), it will be important to model these alterations and determine whether these genetic changes have distinct or overlapping roles in prostate cancer development.

Cells with qualities of stemness and invasiveness have also been postulated to confer greater therapeutic resistance, particularly, in recurrent disease (42). If true, then such a hypothesis would explain the relatively poor response that therapies have toward metastatic cancers in comparison with differentiated primary tumors. Recent studies using breast cancer cell lines treated with paclitaxel or 5-fluorouracil, showed a 5-fold increase in CD44^{+}/CD24^{low} cells (43) whereas primary breast cancer samples isolated from chemotherapy-treated patients showed a 7-fold increase in the same cell population (44). That the CD44^{+}/CD24^{low} cells share a stem cell signature and mesenchymal characteristics suggests that EMT may be involved in the formation of cancer stem cells and therapeutic resistance. In prostate cancer, such studies are far fewer in number; however, the CD44^{+}CD24^{low} subpopulation isolated from prostate cancer cell lines has been attributed to both stemness and invasiveness mediated by EMT (45) and correlated with poor clinical outcome in patients with prostate cancer (46). In our study, we have identified significant expansion of EpCAM^{low}/CD24^{low} mesenchymal cells that have sphere-forming activity and can lead to the regeneration of primary and metastatic lesions upon orthotopic transplantation. It will be interesting to test whether this is the population responsible for therapeutic resistance.

Because our model is based on the coordinate loss of *Pten* and Ras activation, we tested the effectiveness of combined mTOR and MEK inhibition on stem/progenitor cell–mediated transplantations. We observed near complete inhibition of metastatic lung lesions in treatment cohorts. Previous studies have shown that combined pharmacologic targeting of mTOR and MEK may lead to reduced primary tumor progression (31). Thus, to further test that RAS/MAPK signaling serves as a critical step in the metastatic process, we also treated animals with MEK inhibitor alone. Remarkably, using only PD325901, we also observed near-complete abolishment of metastasis, possibly as a result of impeding Ras-dependent EMT (Fig. 7D). Collectively, our observations indicate that in *Pten*-null;Ras activated prostate cancer, the RAS/MAPK pathway plays a significant role in metastasis.

Disclosure of Potential Conflicts of Interest

No potential conflicts of interest were disclosed.

Acknowledgments

The authors thank Drs. Liang Cheng (Indiana University, Bloomington, IN), Adeboye Osunkoya (Emory University, Atlanta, GA), Steven Shen (the Methodist Hospital, Houston, TX), and Jorge Yao (University of Rochester, Rochester, NY) for providing deidentified pathologic material of bony metastasis.

Grant Support

D.J. Mulholland is supported by NIH F32 CA112988-01 and CIRM TG2-01169 grants and L.M. Tran is supported by NIH T32 CA009056 grant. This work has been supported, in part, by awards from the Prostate Cancer Foundation (to H. Wu and J. Huang), DOD Idea Development Award (to J. Huang), and a grant from NIH (R01 CA107166 and RO1 CA121110 to H. Wu).

The costs of publication of this article were defrayed in part by the payment of page charges. This article must therefore be hereby marked *advertisement* in accordance with 18 U.S.C. Section 1734 solely to indicate this fact.

Received September 19, 2011; revised January 9, 2012; accepted January 30, 2012; published OnlineFirst February 20, 2012.

References

1. American Cancer Society. Cancer facts & figures 2010. Atlanta, GA: American Cancer Society; 2010.
2. Taylor BS, Schultz N, Hieronymus H, Gopalan A, Xiao Y, Carver BS, et al. Integrative genomic profiling of human prostate cancer. Cancer Cell 2010;18:11–22.
3. Wang S, Gao J, Lei Q, Rozengurt N, Pritchard C, Jiao J, et al. Prostate-specific deletion of the murine Pten tumor suppressor gene leads to metastatic prostate cancer. Cancer Cell 2003;4:209–21.
4. Svensson RU, Haverkamp JM, Thedens DR, Cohen MB, Ratliff TL, Henry MD. Slow disease progression in a C57BL/6 pten-deficient

mouse model of prostate cancer. Am J Pathol 2011;179: 502–12.
5. Ma X, Ziel-van der Made AC, Autar B, van der Korput HA, Vermeij M, van Duijn P, et al. Targeted biallelic inactivation of Pten in the mouse prostate leads to prostate cancer accompanied by increased epithelial cell proliferation but not by reduced apoptosis. Cancer Res 2005;65:5730–9.
6. Chen Z, Trotman LC, Shaffer D, Lin HK, Dotan ZA, Niki M, et al. Crucial role of p53-dependent cellular senescence in suppression of Pten-deficient tumorigenesis. Nature 2005;436:725–30.
7. Martin P, Liu YN, Pierce R, Abou-Kheir W, Casey O, Seng V, et al. Prostate epithelial Pten/TP53 loss leads to transformation of multipotential progenitors and epithelial to mesenchymal transition. Am J Pathol 2011;179:422–35.
8. Kim MJ, Cardiff RD, Desai N, Banach-Petrosky WA, Parsons R, Shen MM, et al. Cooperativity of Nkx3.1 and Pten loss of function in a mouse model of prostate carcinogenesis. Proc Natl Acad Sci U S A 2002;99:2884–9.
9. Gumerlock PH, Poonamallee UR, Meyers FJ, deVere White RW. Activated ras alleles in human carcinoma of the prostate are rare. Cancer Res 1991;51:1632–7.
10. Cho NY, Choi M, Kim BH, Cho YM, Moon KC, Kang GH. BRAF and KRAS mutations in prostatic adenocarcinoma. Int J Cancer 2006;119:1858–62.
11. Carter BS, Epstein JI, Isaacs WB. ras gene mutations in human prostate cancer. Cancer Res 1990;50:6830–2.
12. Silan F, Gultekin Y, Atik S, Kilinc D, Alan C, Yildiz F, et al. Combined point mutations in codon 12 and 13 of KRAS oncogene in prostate carcinomas. Mol Biol Rep 2012;39:1595–9.
13. Edgren H, Kangaspeska S, Kallioniemi O. KRas oncogene rearrangements and gene fusions: unexpected rare encounters in late-stage prostate cancers. Cancer Discovery 2011;1:35–43.
14. Bakin RE, Gioeli D, Bissonette EA, Weber MJ. Attenuation of Ras signaling restores androgen sensitivity to hormone-refractory C4-2 prostate cancer cells. Cancer Res 2003;63:1975–80.
15. Erlich S, Tal-Or P, Liebling R, Blum R, Karunagaran D, Kloog Y, et al. Ras inhibition results in growth arrest and death of androgen-dependent and androgen-independent prostate cancer cells. Biochem Pharmacol 2006;72:427–36.
16. Suzuki A, Nakano T, Mak TW, Sasaki T. Portrait of PTEN: messages from mutant mice. Cancer science 2008;99:209–13.
17. Yin J, Pollock C, Tracy K, Chock M, Martin P, Oberst M, et al. Activation of the RalGEF/Ral pathway promotes prostate cancer metastasis to bone. Mol Cell Biol 2007;27:7538–50.
18. Jackson EL, Willis N, Mercer K, Bronson RT, Crowley D, Montoya R, et al. Analysis of lung tumor initiation and progression using conditional expression of oncogenic K-ras. Genes Dev 2001;15:3243–8.
19. Tanaka H, Kono E, Tran CP, Miyazaki H, Yamashiro J, Shimomura T, et al. Monoclonal antibody targeting of N-cadherin inhibits prostate cancer growth, metastasis and castration resistance. Nat Med 2010;16:1414–20.
20. Gregorian C, Nakashima J, Dry SM, Nghiemphu PL, Smith KB, Ao Y, et al. PTEN dosage is essential for neurofibroma development and malignant transformation. Proc Natl Acad Sci U S A 2009;106:19479–84.
21. Guo W, Lasky JL, Chang CJ, Mosessian S, Lewis X, Xiao Y, et al. Multi-genetic events collaboratively contribute to Pten-null leukaemia stem-cell formation. Nature 2008;453:529–33.
22. Lapointe J, Li C, Higgins JP, van de Rijn M, Bair E, Montgomery K, et al. Gene expression profiling identifies clinically relevant subtypes of prostate cancer. Proc Natl Acad Sci U S A 2004;101:811–6.
23. Plaisier SB, Taschereau R, Wong JA, Graeber TG. Rank-rank hypergeometric overlap: identification of statistically significant overlap between gene-expression signatures. Nucleic Acids Res 2010;38:e169.
24. Mulholland DJ, Tran LM, Li Y, Cai H, Morim A, Wang S, et al. Cell autonomous role of PTEN in regulating castration-resistant prostate cancer growth. Cancer Cell 2011;19:792–804.
25. Soriano P. Generalized lacZ expression with the ROSA26 Cre reporter strain. Nat Genet 1999;21:70–1.
26. Mulholland DJ, Xin L, Morim A, Lawson D, Witte O, Wu H. Lin-Sca-1+CD49fhigh stem/progenitors are tumor-initiating cells in the Pten-null prostate cancer model. Cancer Res 2009;69:8555–62.
27. Jiao J, Wang S, Qiao R, Vivanco I, Watson PA, Sawyers CL, et al. Murine cell lines derived from Pten null prostate cancer show the critical role of PTEN in hormone refractory prostate cancer development. Cancer Res 2007;67:6083–91.
28. Gioeli D, Mandell JW, Petroni GR, Frierson HF Jr, Weber MJ. Activation of mitogen-activated protein kinase associated with prostate cancer progression. Cancer Res 1999;59:279–84.
29. Jackson EL. Analysis of lung tumor initiation and progression using conditional expression of oncogenic K-ras. Genes Dev 2001;15: 3243–8.
30. Wu X, Wu J, Huang J, Powell WC, Zhang J, Matusik RJ, et al. Generation of a prostate epithelial cell-specific Cre transgenic mouse model for tissue-specific gene ablation. Mech Dev 2001;101:61–9.
31. Kinkade CW, Castillo-Martin M, Puzio-Kuter A, Yan J, Foster TH, Gao H, et al. Targeting AKT/mTOR and ERK MAPK signaling inhibits hormone-refractory prostate cancer in a preclinical mouse model. J Clin Invest 2008;118:3051–64.
32. Gioeli D, Wunderlich W, Sebolt-Leopold J, Bekiranov S, Wulfkuhle JD, Petricoin EF, et al. Compensatory pathways induced by MEK inhibition are effective drug targets for combination therapy against castration-resistant prostate cancer. Mol Cancer Ther 2011;10:1581–90.
33. Bild AH, Yao G, Chang JT, Wang Q, Potti A, Chasse D, et al. Oncogenic pathway signatures in human cancers as a guide to targeted therapies. Nature 2006;439:353–7.
34. Chen Z, Zhang C, Wu D, Chen H, Rorick A, Zhang X, et al. Phospho-MED1-enhanced UBE2C locus looping drives castration-resistant prostate cancer growth. EMBO J 2011;30:2405–19.
35. Mani SA, Guo W, Liao MJ, Eaton EN, Ayyanan A, Zhou AY, et al. The epithelial-mesenchymal transition generates cells with properties of stem cells. Cell 2008;133:704–15.
36. Kwok WK, Ling MT, Lee TW, Lau TC, Zhou C, Zhang X, et al. Up-regulation of TWIST in prostate cancer and its implication as a therapeutic target. Cancer Res 2005;65:5153–62.
37. Bastide C, Bagnis C, Mannoni P, Hassoun J, Bladou F. A Nod Scid mouse model to study human prostate cancer. Prostate Cancer Prostatic Dis 2002;5:311–5.
38. Majumder PK, Yeh JJ, George DJ, Febbo PG, Kum J, Xue Q, et al. Prostate intraepithelial neoplasia induced by prostate restricted Akt activation: the MPAKT model. Proc Natl Acad Sci U S A 2003;100:7841–6.
39. Maestro R, Dei Tos AP, Hamamori Y, Krasnokutsky S, Sartorelli V, Kedes L, et al. Twist is a potential oncogene that inhibits apoptosis. Genes Dev 1999;13:2207–17.
40. Vega S, Morales AV, Ocana OH, Valdes F, Fabregat I, Nieto MA. Snail blocks the cell cycle and confers resistance to cell death. Genes Dev 2004;18:1131–43.
41. Yang J, Mani SA, Donaher JL, Ramaswamy S, Itzykson RA, Come C, et al. Twist, a master regulator of morphogenesis, plays an essential role in tumor metastasis. Cell 2004;117:927–39.
42. Pardal R, Clarke MF, Morrison SJ. Applying the principles of stem-cell biology to cancer. Nat Rev Cancer 2003;3:895–902.
43. Fillmore CM, Kuperwasser C. Human breast cancer cell lines contain stem-like cells that self-renew, give rise to phenotypically diverse progeny and survive chemotherapy. Breast Cancer Res 2008;10:R25.
44. Yu F, Yao H, Zhu P, Zhang X, Pan Q, Gong C, et al. let-7 regulates self renewal and tumorigenicity of breast cancer cells. Cell 2007;131:1109–23.
45. Klarmann GJ, Hurt EM, Mathews LA, Zhang X, Duhagon MA, Mistree T, et al. Invasive prostate cancer cells are tumor initiating cells that have a stem cell-like genomic signature. Clin Exp Metastasis 2009;26:433–46.
46. Hurt EM, Kawasaki BT, Klarmann GJ, Thomas SB, Farrar WL. CD44+ CD24(-) prostate cells are early cancer progenitor/stem cells that provide a model for patients with poor prognosis. Br J Cancer 2008;98:756–65.

Supplemental Figure Legends

Supplemental Figure 1. Composition of human tissue microarray (TMA).

Supplemental Figure 2. *K-ras* activation is sufficient to drive the RAS/MAPK pathway but is not sufficient to initiate cancer. *A*, Control (*WT*) and *C^{+};K-ras$^{L/W}$* prostates showing P-MAPK and P-AKT expression. Low mag bar = 150 μm, high mag bar = 50 μm. B, *Pten$^{-/-}$;Kras^{G12D}* cells were isolated from *C^{+};Pten$^{L/L}$;K-ras$^{L/W}$* mutant prostates, infected with GFP-lenti virus and injected to the tibia of *NOD;SCID;IL2rγ*-null recipients.

Supplemental Figure 3. AR signaling is repressed in *C^{+};Pten$^{L/L}$;K-ras$^{L/W}$* mutants. *A,* AR expression in control (*WT*), *C^{+};K-ras$^{L/W}$*, *C^{+};Pten$^{L/L}$* and *C^{+};Pten$^{L/L}$;K-ras$^{L/W}$* (primary and lung metastasis), low mag bar = 150 μm, high mag bar = 50 μm. *B*, Effect of K-ras activation on AR gene expression as evaluated by Gene Set Enrichment Analysis (GSEA) comparing *C^{+};Pten$^{L/L}$* and *C^{+};Pten$^{L/L}$;K-ras$^{L/W}$* mutants, as exemplified in, *C*, by the reduction of the AR target genes *Mme*, *Msmb* and *Nkx3.1* in *C^{+};Pten$^{L/L}$;K-ras$^{L/W}$* mutants..

Supplemental Figure 4. *C^{+};Pten$^{L/WT}$;K-ras$^{L/W}$* mutants progress to invasive and poorly differentiated carcinoma correlating with PTEN loss. *A*, Histology of *C^{+};Pten$^{L/WT}$;K-ras$^{L/W}$* mutant prostates at 10, 20 and 30 wks. *B,* P-AKT and Ki67 expression in *C^{+};Pten$^{L/WT}$;K-ras$^{L/W}$* mutants at 10 wks and *C*, PTEN loss and P-AKT expression in *C^{+};Pten$^{L/L}$* and *C^{+};Pten$^{L/WT}$;K-ras$^{L/W}$* mutants (40 wks). Low mag bar = 150 μm, high mag bar = 50 μm.

Supplemental Figure 5. *A*, p63 expression in human and murine (*C^{+};Pten$^{L/L}$;K-ras$^{L/W}$*) prostate cancer progression, bar = 50 μm. *B*, p53 and p27 expression in *C^{+};Pten$^{L/L}$* and *C^{+};Pten$^{L/L}$;K-ras$^{L/W}$* mutants (10 wks), low mag bar = 150 μm, high mag bar = 50 μm. *C*, N-cadherin and synaptophysin expression in *C^{+};Pten$^{L/L}$;K-ras$^{L/W}$* mutants (10 wks), bar = 50 μm.

Supplemental Figure 6. *A,* Heat maps comparing the overlap of differentially expressed genes in human metastatic tumors (metastasis – primary; y-axis) and in murine *Pb-Cre^{+};Pten$^{L/L}$;K-ras$^{L/W}$* mutants (*Pten;Kras* – *Pten* null; x-axis) based on rank-rank hypergeometric overlap (RRHO) analysis used to measure and visualize the degree of statistically significant overlap between two expression signatures. The color bar indicates the transformed $\log_{10}$ hypergeometric enrichment p-value between two signature gene sets. The high heat areas on

bottom left and top right corners indicate the significant overlap between differentially expressed genes in *Pb-Cre^{+};Pten$^{L/L}$;K-ras$^{L/W}$* mutants and human metastatic tumors. *B*, corresponding examples of repressed and elevated genes (lower panel).

Supplemental Figure 7. Genotyping of isolated stem/progenitor cells and resulting metastatic lesions. *A*, Genotyping of passage 3 spheres derived from *C^{+};Pten$^{L/L}$;K-ras$^{L/W}$* mutants. *B*, Genotyping of FACS sorted primary cells from *C^{+};Pten$^{L/L}$;K-ras$^{L/W}$* mutants. *C*, Genotyping of metastatic lesions resulting from transplantation of primary, FACS sorted cells from *C^{+};Pten$^{L/L}$;K-ras$^{L/W}$* mutants.

Gleason Graded TMA-2009

Pathology	# Patients	# Cores	Treatment
BPH/PIN	23	46	None
Gleason 6-7	35	70	None
Gleason 7-8	24	48	None
Gleason 9-10	6	12	None
Total	88	176	

NHT TMA-2009

Pathology	# Patients	# Cores	Treatment
G3	7	14	None
G4	3	6	None
G5	4	8	None
TR Pattern	5	10	1 M
TR Pattern	3	6	1.5 M
TR Pattern	3	6	2 M
TR Pattern	5	10	3 M
TR Pattern	8	16	5-6 M
TR Pattern	18	36	7-8 M
TR Pattern	16	32	9-12 M
TR Pattern	16	32	CRPC
Total	88	176	

CRPC/TURP-2009

Pathology	# Patients	# Cores	Treatment
CRPC	12	24	N/A
Benign	3	2	N/A
Cancer		2	N/A
Naïve		6	N/A
Total	18	36	N/A

Total # of Patients: 194
Total # of Cores: 388

S2.

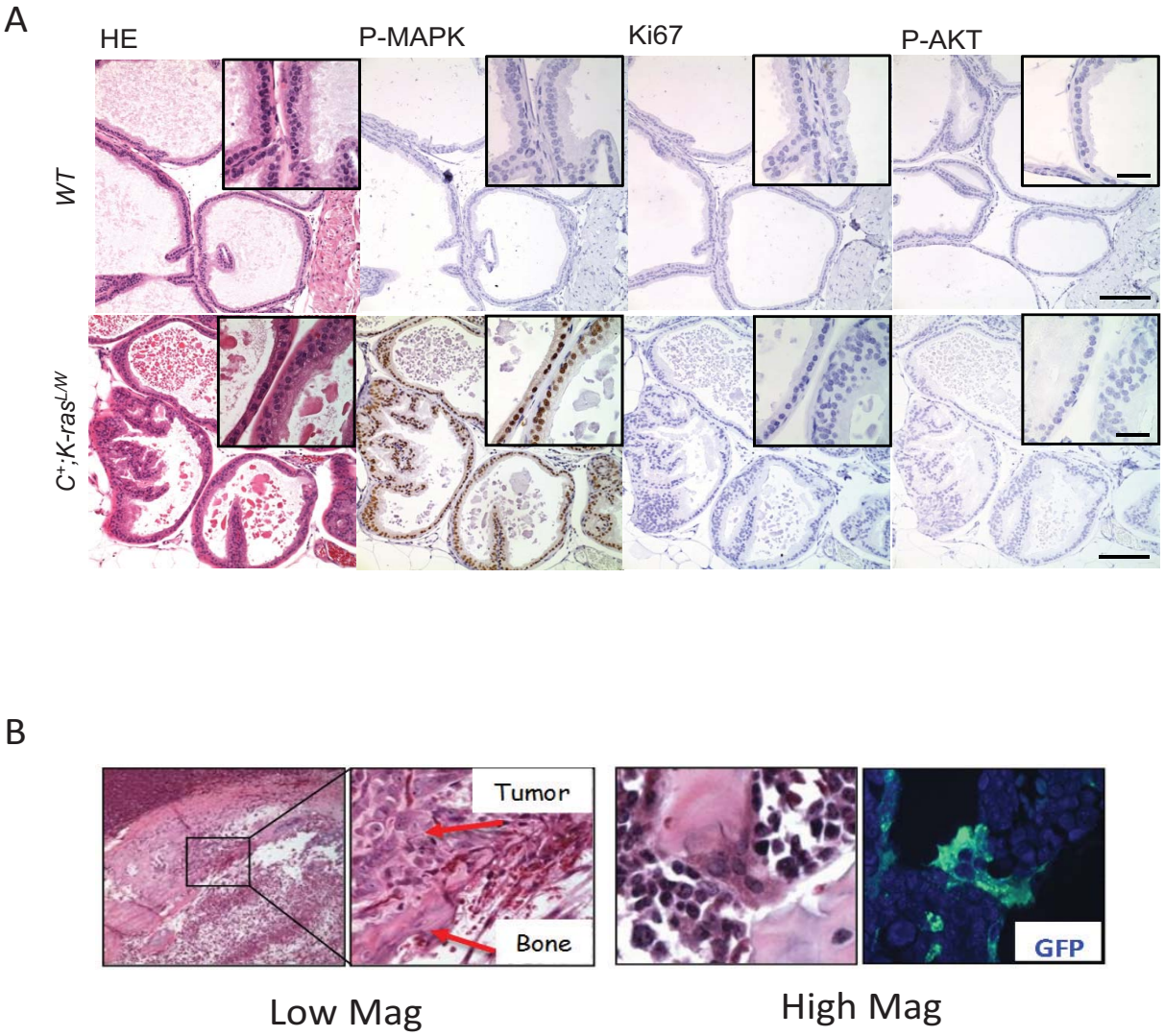
A
HE
P-MAPK
Ki67
P-AKT
WT
C+;K-rasLW
B
Tumor
Bone
GFP
Low Mag
High Mag

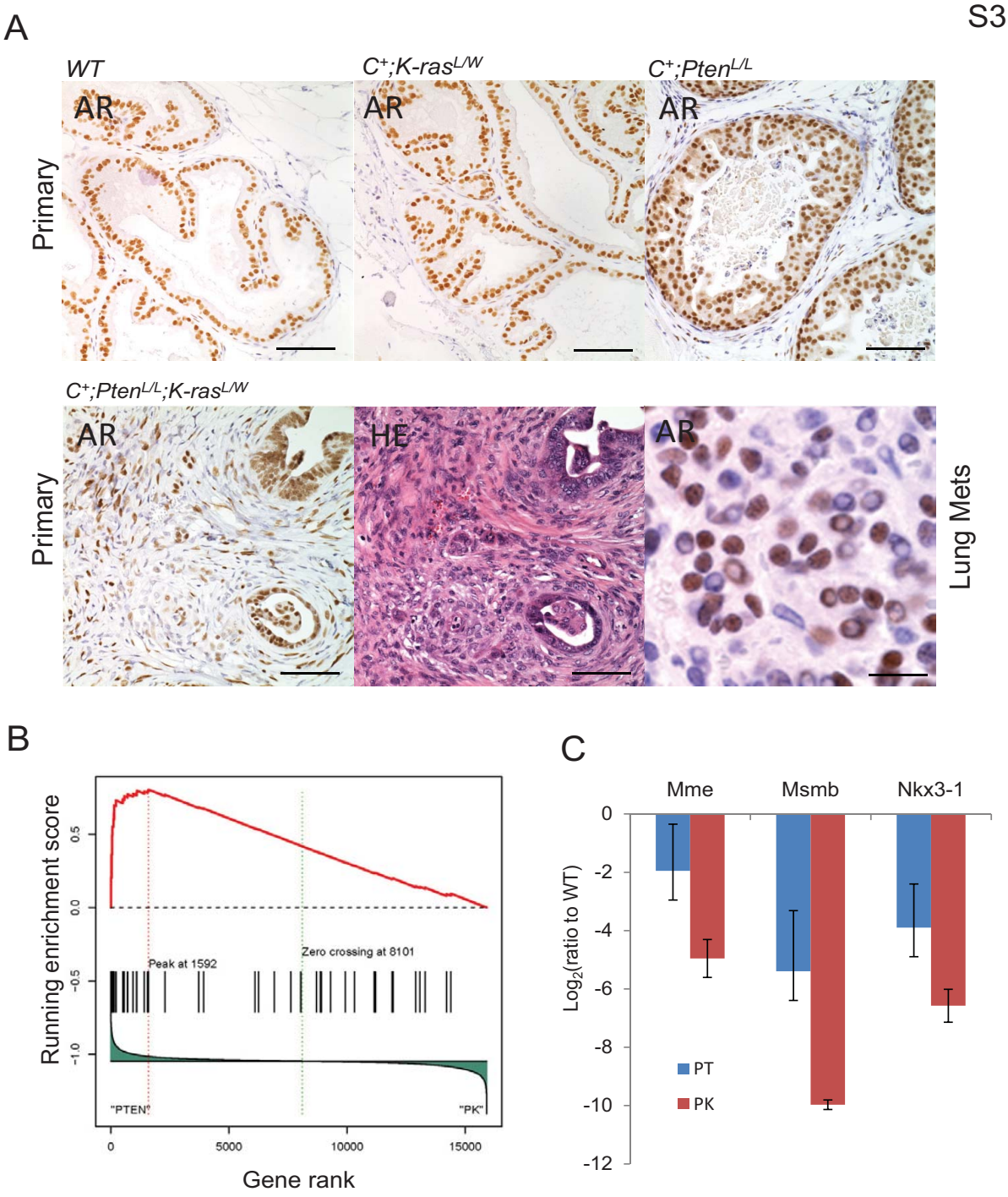
A
WT
C+;K-rasL/W
C+;PtenL/L
AR
AR
AR
Primary
C+;PtenL/L;K-rasL/W
AR
HE
AR
Primary
Lung Mets
B
Running enrichment score
0.5
0.0
-0.5
-1.0
Peak at 1592
Zero crossing at 8101
"PTEN"
"PK"
0
5000
10000
15000
Gene rank
C
Mme
Msmb
Nkx3-1
0
-2
-4
-6
-8
-10
-12
Log2(ratio to WT)
PT
PK

A $C^{+};Pten^{L/W};K\text{-}ras^{L/W}$

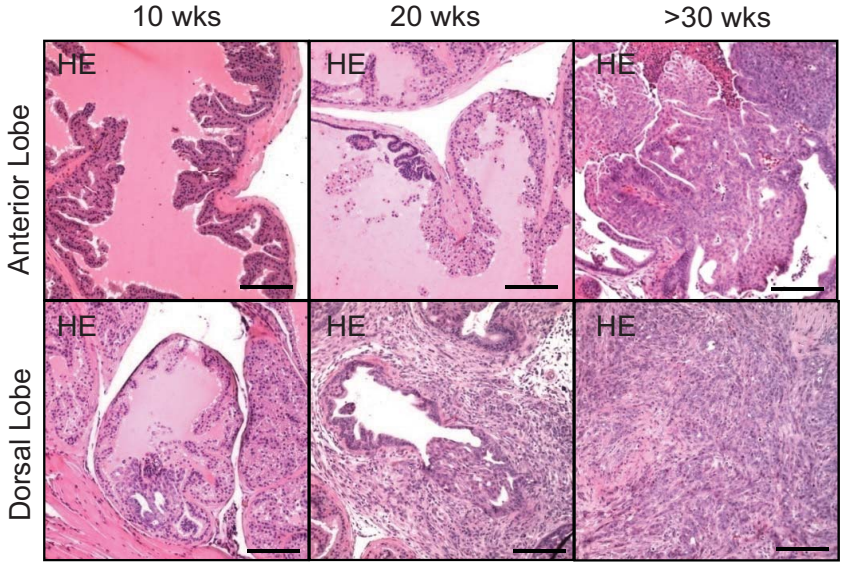

B $C^{+};Pten^{L/W};K\text{-}ras^{L/W}$ (10 wks)

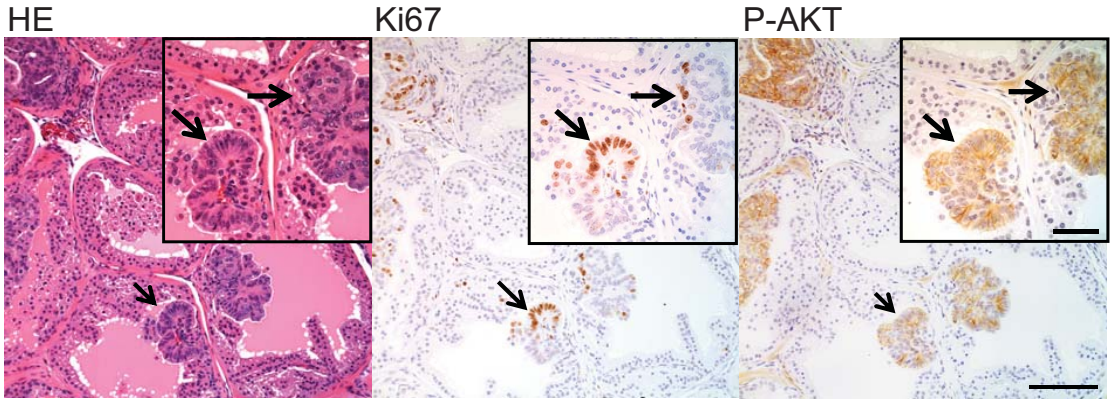

C $C^{+};Pten^{L/L}$ (40 wks)

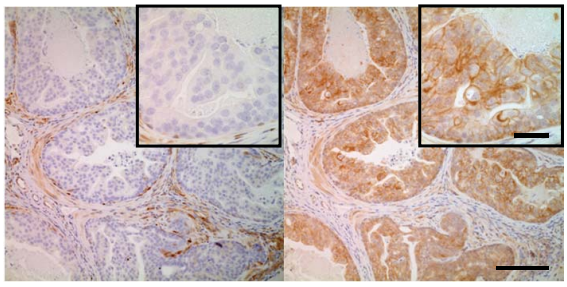

$C^{+};Pten^{L/W};K\text{-}ras^{L/W}$ (40 wks)

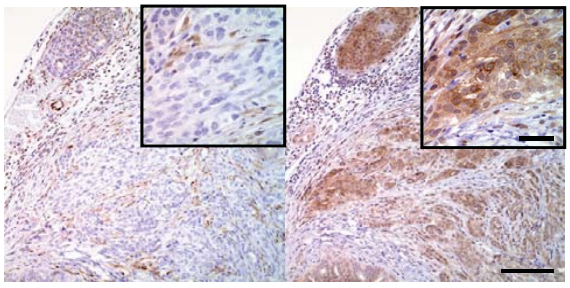

S5.

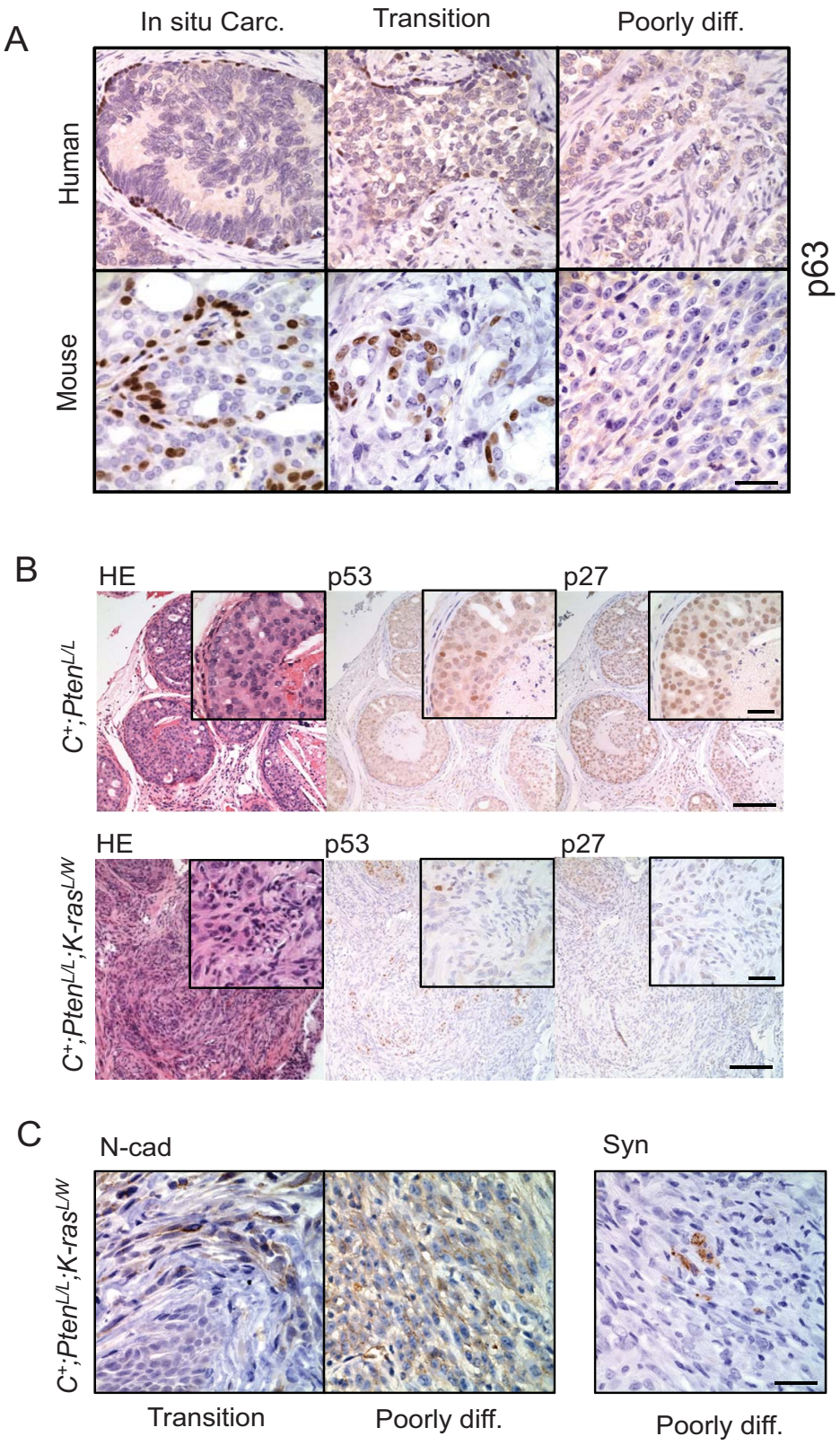
A
In situ Carc.
Transition
Poorly diff.
Human
Mouse
p63
B
HE
p53
p27
C+;PtenL/L
HE
p53
p27
C+;PtenL/L;K-rasL/W
C
N-cad
Syn
C+;PtenL/L;K-rasL/W
Transition
Poorly diff.
Poorly diff.

A

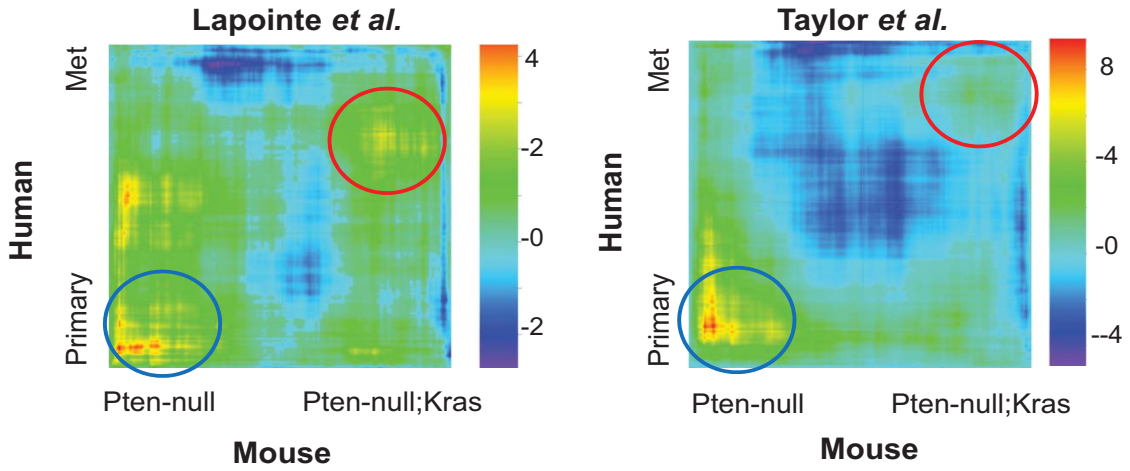
Lapointe *et al.*
Taylor *et al.*
Human
Met
Primary
Pten-null
Pten-null;Kras
Mouse
4
-2
-0
-2
8
-4
-0
--4

B

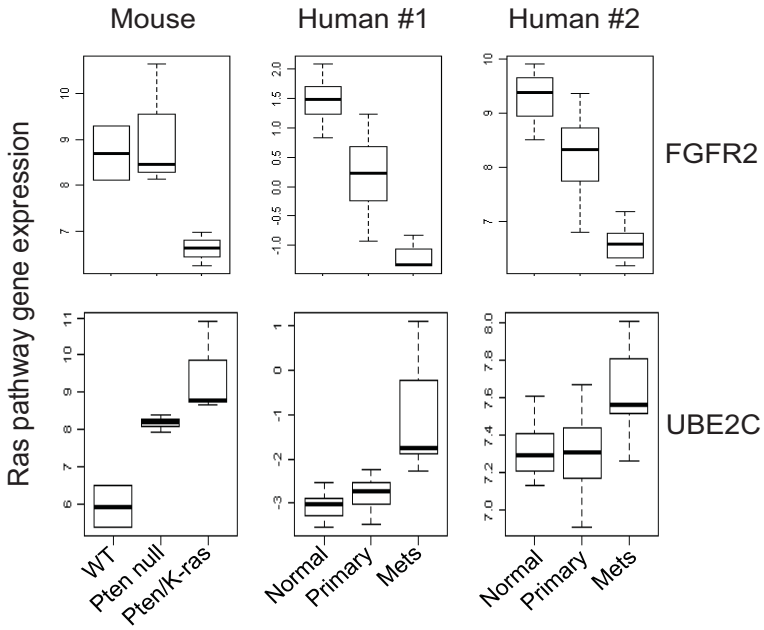
Mouse
Human #1
Human #2
Ras pathway gene expression
FGFR2
UBE2C
WT
Pten null
Pten/K-ras
Normal
Primary
Mets

A

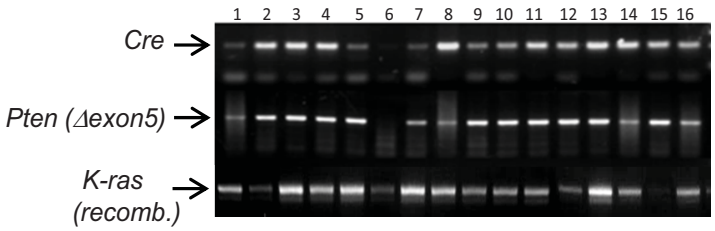
1 2 3 4 5 6 7 8 9 10 11 12 13 14 15 16
Cre
Pten (Δexon5)
K-ras
(recomb.)

B

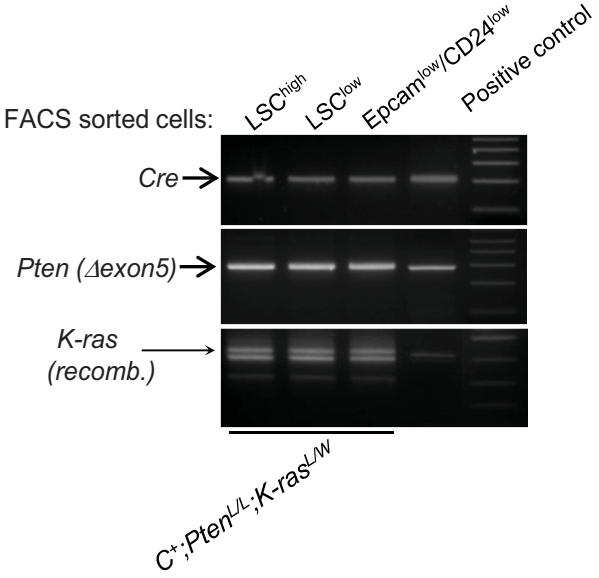
FACS sorted cells:
LSC^high
LSC^low
Epcam^low/CD24^low
Positive control
Cre
Pten (Δexon5)
K-ras
(recomb.)
C+;PtenL/L;K-rasL/W

C

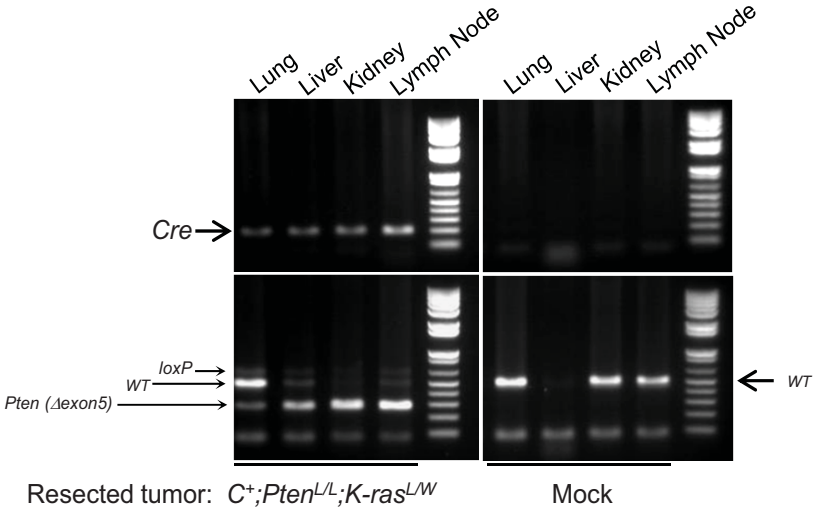
Lung
Liver
Kidney
Lymph Node
Lung
Liver
Kidney
Lymph Node
Cre
loxP
WT
Pten (Δexon5)
WT
Resected tumor: C+;PtenL/L;K-rasL/W
Mock

Chapter 4:

The PI3K and MAPK pathways promote prostate cancer metastasis by inducing SNAIL-mediated epithelial-mesenchymal transition (EMT)

Introduction

Although the new generation of anti-androgen and androgen receptor therapies have begun to improve outcomes in the management of advanced prostate cancer (PCa), there is currently not an effective treatment for metastatic disease (1-3). We and others have found that PI3K and MAPK co-activation is associated with human PCa metastasis, and that resistance to androgen deprivation therapy (ADT) coincides with increased MAPK activation and N-cadherin expression, two markers associated with the epithelial-to-mesenchymal transition (EMT) program (5-8). An integrated genomic analysis of human PCa also identified alterations in the PTEN/PI3K/AKT and RAS/MAPK pathways as common events in human metastatic PCa, with 100% and 90% of metastatic specimens showing activation of the PTEN/PI3K/AKT pathway and the RAS/MAPK pathway, respectively (6). Therefore, in order to combat the lethal disease, it is crucial to mechanistically identify the consequences of co-activation of these two pathways.

Based on the above-mentioned clinical findings, we concomitantly activated both the PI3K/AKT and RAS/MAPK pathways genetically in the murine system to model human metastatic PCa. Deletion of the *Pten* tumor suppressor, which antagonizes the PI3K pathway, and conditional activation of the *Kras* oncogene, which mimics RAS/MAPK activation, in the prostate epithelium in the *Pb-Cre*$^{+/-}$*;Pten*$^{L/L}$*;Kras*$^{G12D/W}$ mice (*CPK,* hereafter) leads to significantly earlier lethality, more aggressive adenocarcinoma, and increased distant macrometastasis to lung and liver, compared to PI3K/AKT or RAS/MAPK pathway activation alone (*Pb-Cre*$^{+/-}$*;Pten*$^{L/L}$, *CP* hereafter*; Pb-Cre*$^{+/-}$*;Kras*$^{G12D/W}$) (7). Comprehensive gene expression analysis showed that murine PCa with combined *Pten* deletion and *Kras* activation is more similar to metastatic human PCa, while murine PCa with *Pten* deletion alone more closely resembles localized primary human PCa (7). An important signature associated with the *CPK*

murine model is increased EMT-associated gene expression, similar to late stage metastatic castration-resistant human PCa (6-10).

EMT plays an essential role during embryogenesis and is regulated by distinct transcription factors, including Snail, Slug, Twist1, Twist2, Goosecoid, FOXC2, ZEB1 and ZEB2 (11). EMT is also accompanied by expression of mesenchymal markers such as N-cadherin, Vimentin and Fibronectin, as well as decreased expression of epithelial markers such as cytokeratins and E-cadherin, indicative of a loss in cell adhesion and cell-cell interactions that are essential for epithelial morphology (11). Epithelial cells are naturally non-motile, noninvasive, and susceptible to apoptosis upon loss of cell-cell or cell-basement membrane attachment. EMT has been postulated as a prerequisite step for cancer cells to invade, migrate, survive in the circulation, and establish metastasis in distant organs (12). However, the evidence for EMT in PCa is largely based on manipulation of cultured cells or the expression of EMT-associated marker genes in human cancer samples and circulating tumor cells in patients (13, 14). Although our genetic model links PI3K/AKT and RAS/MAPK pathway co-activation with EMT and PCa metastasis, a causal relationship between EMT and metastasis needs to be established.

In this study, we set out to understand the mechanisms underlying EMT program activation by PI3K/AKT and RAS/MAPK pathway collaboration, and whether EMT is essential for PCa progression and metastasis.

Materials and Methods

Cell lines, transfection, transduction and reagents

The generation *of* $Pten^{-/-}$ and $Pten^{+/-}$ cell lines was previously described in Jiao J. *et al.* (15) (referred to as PTEN-CaP8 and PTEN-P8 therein.) A constitutively activated form of *Kras,* $Kras^{G12D}$, was cloned into the retroviral MSCV-GFP vector and introduced into $Pten^{-/-}$ cells in the presence of 5 ug/ml polybrene to generate the $Pten^{-/-};Kras^{G12D}$ cell line. The empty vector without the $Kras^{G12D}$ insert (MSCV-GFP) was used to generate the $Pten^{-/-}$*-MSCV and* $Pten^{+/-}$*-MSCV* cell lines. Transduced cells were selected for by sorting for high GFP expression by FACS (Fluorescence-Activated Cell Sorting). The *PTK* ($Cre^{+};Pten^{-/-};Kras^{G12D/W}$) cell line was derived from $Pb\text{-}Cre^{+/-};Pten^{L/L};Kras^{G12D/W}$ mutant prostates as previously described (7). Growth conditions for $Pten^{-/-}$, $Pten^{+/-}$, $Pten^{-/-};Kras^{G12D}$, and *PTK* cells were as described previously (15). ARCaP cells are obtained from Novicure. Growth conditions for ARCaP cells were as described in Zhau HE *et al.* (16).

To generate *PKS* ($Pten^{-/-};Kras^{G12D/W};Snail^{-/-}$) cells, prostates from $Cre^{-/-}$; $Pten^{L/L};Kras^{G12D/W};Snail^{L/L}$ mice were dissociated into single cells (17) and transduced with a lenti-Cre-RFP-virus (Cre-FUCRW) (18). $RFP^{high};EpCam^{high}$ cells were sorted by the BD FACSAria II cell sorter. *PKS* cells were grown in DMEM media with 10% FBS, 1% PenStrep, 4 mM L-glutamate, 10mM Hepes, 25 μg /mL bovine pituitary extract, 5 μg /mL bovine insulin, and 6 ng/mL recombinant human EGF initially, and subsequently in DMEM (10% FBS, 1% PenStrep, 4 mM L-glutamate). Five independent *PKS* cell lines were isolated from a single cell by limiting dilution. The presence of *Snail* and *Pten* deletion and the recombined $Kras^{G12D}$ allele in *PKS* cells were confirmed by PCR (Fig. S6A).

To generate *PKS*-Snail-ER (*PKS*-iS), *PKS* cells were transduced with a Snail-ER retrovirus (Addgene No. 18798: pWZL-Blast-Snail-ER) and selected with Blasticidin at 2 ug/ml for 10 days. The ER has a G525R point mutation which abrogates its binding to 17β-estradiol but binds to the synthetic ligand 4-Hydroxytamoxifen. 4-Hydroxytamoxifen was purchased from Sigma-Aldrich and dissolved at 10 mg/ml in ethanol and diluted in media at final concentration 100 nM.

For the *Snail* knockdown, cells were seeded at $2x10^5$, $1x10^5$ and $5x10^4$ cells per 6-well, 12-well, and 24-well tissue culture plates, respectively, and transfected with 5nM siRNA using Qiagen Hiperfect transfection reagent. siRNAs targeting mouse *Snail* (SASI_Mm01_00097354 and SASI_Mm01_00097355), human *SNAIL* (SASI_Hs01_00039785 and SASI_Hs01_00039786), and the MISSION siRNA universal negative control (SIC001) were purchased from Sigma. The Trp53 Smartpool siRNA was purchased from Dharmacon (M-040642-2). Snail silencing by siSnail was assessed 3 days after transfection by quantitative RT-PCR and immunoblotting. Casp3/7 activity was measured using Caspase-Glo 3/7 reagents according to the manufacturer's protocol (Promega).

TGF-β (TGF-β1; R & D systems) was reconstituted at 1mg/ml in BSA and diluted to a final concentration of 4 or 5 ng/ml in the growth media as indicated. IPA-3 was purchased from Calbiochem. LY294001, rapamycin, and PD035901 were purchased from Reagent Direct. Vehicle (DMSO) was added to the control experiments at a concentration which did not exceed 0.1% of the total volume.

Immunoblots

Protein extracts were prepared by lysing cells in buffer containing 50mM Tris-HCl (pH 8), 150 mM NaCl, 1% NP-40, 0.2 % SDS, 1 mM EDTA, 0.5 % sodium deoxycholate, phosphatase inhibitor cocktails 2 and 3 (Sigma Aldrich), 1 mM of PMSF, and complete protease inhibitors (Roche), followed by brief sonication and 10 min centrifugation at 20,000xg at 4^{o} C. 30 mg of cleared lysate was subjected to SDS-PAGE followed by Western blot analysis using the ECL Plus Western Blotting Detection Reagents (GE Healthcare Amersham). Nuclear and cytoplasmic protein extracts were prepared using the NE-PER Nuclear and Cytoplasmic Extraction Kit from Pierce according to the manufacturer's protocol. The primary antibodies used are as follows: AR (Santa Cruz; SC-816), Cleaved Caspase-3 (Cell Signaling; 9664), E-Cadherin (Cell Signaling; 3195), Fibronectin (BD Biosciences; 610077), PAK1 (Cell Signaling; 2604), Phospho-AKT (Ser473) (Cell Signaling; 4060), Phospho-GSK3αβ (Ser21/9) (Cell Signaling; 9331), Phospho-PAK1/(Thr423) / PAK2(Thr402) (Cell Signaling; 2601), Phospho-SMAD2 (Ser465/467) (Cell Signaling; 3108), Phospho-SNAIL (Ser246) (Abcam; ab63568), SNAIL (Cell Signaling; 3895), AKT (Cell Signaling; 3895), P53 (CalBiochem; OPO3), TWIST (Cell Signaling; 4119), β-ACTIN (Sigma; A5441), Cleaved PARP (Cell Signaling; 9544), PTEN (Cell Signaling; 9559), GSK3β (Cell Signaling; 9315), P-S6 (Ser 240/244) (Cell Signaling; 2215), P-ERK 1/2 (Thr202/Try204) (Cell Signaling; 4376), MAPK (p44/p42) (Cell Signaling; 9102), and P-4EBP1 (Thr37/46) (Cell Signaling; 2855). The band densities were quantified using ImageJ.

Gene expression analysis

Total RNA from mouse prostates and tissue culture cells was isolated using Trizol reagent (Invitrogen) according to the manufacturer's protocol, purified on RNeasy mini columns (Qiagen), and used for reverse transcription with the High Capacity cDNA reverse Transcription

kit (Invitrogen). Transcript levels were assessed with quantitative real-time PCR with mouse gene specific RT-PCR primers and iQ™ SYBR® Green Supermix (Bio-Rad) using the CFX Real-Time PCR detection System (Bio-Rad) and normalized against the RLP13a RNA loading control. The relative expression levels were derived from the delta-delta Ct values using the CFX software (Bio-Rad). The primer sequences are as listed in (7). Additional primers: *Cldn3*: F, ACCAACTGCGTACAAGACGAG, R, CAGAGCCGCCAACAGGAAA. *Bim*: F, TCCCGGTCCTCCAGTGGGTA, R, CGTATGGAAGCCATTGCACTGAGA .

Mouse strains

Mutant mice *Pb-Cre*$^{+/-}$;*Pten*$^{L/L}$;*Kras*$^{G12D/W}$ (*CPK*) and *Pb-Cre*$^{+/-}$;*Pten*$^{L/L}$ (*CP*) were generated as previously described (7). *Pb-Cre*$^{+/-}$;*Pten*$^{L/L}$;*Snai1*$^{L/L}$ (*CPS*) *mutants* were generated by crossing *CP* mice with *Snai1*$^{flox/flox}$ mice (19). To generate *Pb-Cre*$^{+/-}$;*Pten*$^{L/L}$;*Kras*$^{G12D/W}$;*Snai1*$^{L/L}$ (*CPKS*) mutants, female *Pb-Cre*$^{-/-}$;*Pten*$^{L/L}$;*Kras*$^{G12D/W}$;*Snai1*$^{L/L}$ or female *Pb-Cre*$^{-/-}$;*Pten*$^{L/L}$;*Kras*$^{G12D/W}$;*Snai1*$^{L/W}$ mice were bred with male *Pb-Cre*$^{+/-}$;*Pten*$^{L/L}$;*Snai1*$^{L/L}$ or male *Pb-Cre*$^{+/-}$;*Pten*$^{L/L}$;*Snai1*$^{L/W}$ mice. The strains have been maintained on a mixed strain background. All studies with animals were performed under the regulation of the division of Laboratory Animal Medicine at the University of California at Los Angeles (UCLA).

Histology and immunohistochemistry (IHC)

Mutant mice were subjected to a full necropsy. Macrometasteses were scored by gross histopathological analyses of the lungs, liver, and lumbar lymph nodes under a dissecting microscope, as well as by examining Hematoxylin and Eosin stained sections from paraffin-embedded tissues. IHC was performed on 4μm sections of formalin-fixed, paraffin-embedded

tissues. Sections were deparaffinized in xylene and graded alcohol. Antigen retrieval was performed by boiling the sections in pH6 citrate buffer in a pressure cooker or in a vegetable steamer for 30 min. After incubation with blocking solution (5% normal donkey serum) for 60 min, sections were incubated with a primary antibody overnight, a biotinylated secondary antibody for 60 min, and then with streptavidin horseradish peroxidase (ABC kit; Vector lab) for 30 min. The antibody was visualized with diaminobenzidine (DAB) chromogen, and sections were counterstained with hematoxylin. Primary antibodies used in this study are as follows: AR (Santa Cruz; SC-816), E-Cadherin (BD; 610181), Ki67 (Vector Laboratories; VP-RM04), Pan-Cytokeratin (Sigma; C1801), SMA (Sigma; A2547), SNAIL (Cell Signaling; 3895), Vimentin (Abcam; ab39376), and F4/80 (AbD Serotec; MCA497R). TUNEL staining was performed using the ApopTag® Plus Peroxidase *In Situ* Apoptosis Kit (Millipore) according to the manufacturer's protocol. TUNEL and Ki67-positive prostate ductal epithelial cells were scored using the Metamorph System and calculated as the percentage of positive cells relative to total epithelial cells.

For immunofluorescence staining, cells were grown in chamber slides, fixed with 3.7% paraformaldehyde, permeabilized with 0.5% Triton X-100, blocked in 5% normal donkey serum in PBS with 0.1% Tween-20, and incubated with primary antibodies. The slides were treated with a fluorescent-labeled secondary antibody (1/1000 dilution, Invitrogen), counterstained with DAPI (ProlongGold Antifade with DAPI, Invitrogen), and visualized under a fluorescent microscopy.

Orthotopic injections and quantification of lung metastasis

PCa stem cells were isolated from *Pb-Cre*$^{+/-}$;*Pten*$^{L/L}$;*Kras*$^{G12D/W}$;*LSL-Luc* mutant prostates and orthotopically injected into male *NSG* mice as previously described (7). The presence of lung macrometastases was assessed by bioluminescence imaging (Xenogen IVIS, Caliper Life Sciences) of *Pb-Cre*$^{+/-}$;*Pten*$^{L/L}$;*Kras*$^{L/W}$;*LSL-Luc*$^{+}$ cells in the thoracic area of orthotopically transplanted mice, as well as by gross examination of formalin-fixed lung samples under a dissecting microscope. Aperio Imagescope 11.1 software was used to measure the diameter of lung metastases from paraffin-embedded lung tissue samples.

Drug treatment

CPK mice were treated with rapamycin (4 mg/kg/day, I.P.) and PD0325901 (5 mg/kg/day, P.O) starting at 6 weeks of age for 28 days. Orthotopically transplanted *NOD;SCID;IL2γ-null* mice were treated with rapamycin and/or PD0325901 for 21 days beginning 2 days post-transplantation. Rapamycin was reconstituted in 100% ethanol and diluted at 1:100 in vehicle (5.2% Tween-80 and 5.2% PEG400 in PBS). PD0325901 was first reconstituted in DMSO and then freshly diluted in vehicle (0.2 % Tween-80 and 0.5% hydroxypropyl methylcellulose).

Statistical analysis

Student's *t*-test was used to calculate the statistical significance between the two groups of data. $P<0.05$ is considered significant.

Accession codes

Gene expression datasets used in this study are available at Gene Expression Omnibus (GEO). The human PCa dataset is under accession number GSE35988 (20), and the murine PCa datasets are under accession number GSE34839 (7).

Expression microarray analyses of human prostate cancer

The human expression data used in this study was from a published dataset (20). We first removed probes frequently absent in more than 70% of samples, and then centered expression of each probe by its median prior to further analyses. For each probe, expression was then transformed to a z-score based on those in normal samples to determine if it was significantly altered in a sample of interest.

For each sample, the deregulation of a pathway was justified from the sum of absolute expression-based z-scores of the involved genes. In this study, the reference gene sets for PI3K/AKT and RAS/MAPK pathways were ones identified as frequently altered in PCa (6). Student's t-test was used to determine if the observed alterations in each pathway between two patient cohorts were statistically significant.

Gene set enrichment analysis (GSEA) of murine prostate cancer models

Affymetrix mouse 430 2 arrays (accession GSE34839) were used to investigate gene expression in murine *CP* (n=3) and *CPK* (n=3) prostate tumors. For genes represented by multiple probes, its expression was represented by the average of its probe expressions before GSEA (21) to determine if pathways of interest were deregulated in *CPK* samples as compared to *CP samples*. The reference genesets for the PAK1 transcriptionally regulated genes were from Table S1 in reference (22) listing significantly altered genes in *Pak1* deleted murine embryonic fibroblasts as

compared to WT fibroblasts. Besides these gene sets, we also included gene sets involving other signaling pathways available from the Molecular Signature Database. For GSEA, we ranked genes based on their expression ratios, instead of signal-to-noise values, because of the small sample size (n=3 for each group).

Results

SNAIL is upregulated in human metastatic PCa with PI3K/AKT and RAS/MAPK pathway co-activation and correlates with poor prognosis

To understand how PI3K/AKT and RAS/MAPK pathway co-activation promotes human PCa metastasis, we analyzed the gene expression database of PCa samples from the rapid autopsy program reported by Grasso *et al*. (20) and found that the activity of both the PI3K/AKT and RAS/MAPK pathways is much higher in the metastatic tumors compared to benign and localized disease (Fig. 1A). We then searched for those genes associated with higher levels of PI3K/AKT and RAS/MAPK pathway activities and found that the expression of the EMT transcription factor *SNAIL* is significantly higher in metastatic disease compared to benign and localized PCa (Fig. 1A). Importantly, among patients with metastatic PCa, those with higher *SNAIL* expression have a significantly poorer overall survival (Fig. 1B), suggesting that PI3K/AKT and RAS/MAPK pathway co-activation may lead to up-regulated *SNAIL* expression and promote PCa metastasis.

We then studied a pair of epithelial and mesenchymal-like human PCa cell lines to examine if there were inherent differences in PI3K/AKT and RAS/MAPK pathway activation and Snail expression between these contrasting cell states. $ARCaP_E$ cells have typical epithelial cell morphology and exhibit only limited tumorigenic potential (23), while $ARCaP_M$ cells have mesenchymal features and are able to produce bone metastasis with 100% penetrance *in vivo* (16). Compared to $ARCaP_E$ cells, $ARCaP_M$ cells showed higher PI3K/AKT and MAPK pathway activities as indicated by the increased levels of phospho-AKT (S473), phospho-4E-BP1

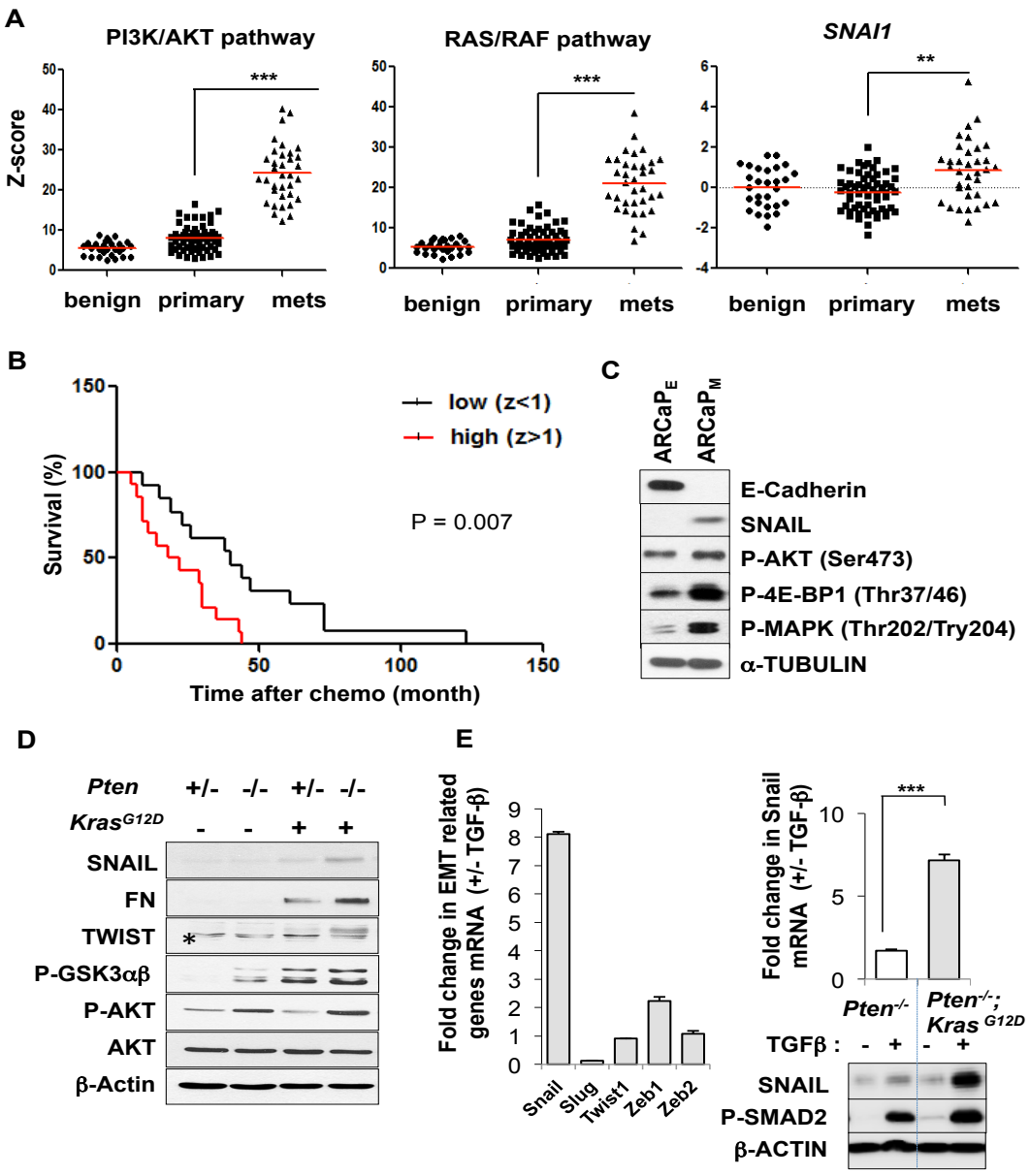

Figure 1. ***Snail*** **induction is characteristic of prostate cancer with PI3K/AKT and RAS/MAPK pathway co-activation and indicates poor prognosis in human metastatic disease.** (A) Activation of PI3K/AKT and RAS/RAF pathways in human metastases was analyzed for the genes frequently deregulated in metastatic tumors based on Taylor et. al. Sum of z-scores of these genes based on benign prostates indicates the activities of the PI3K/AKT (left panel) and RAS/RAF (middle panel) pathways are highest in metastatic tumors. *SNAIL* expression was significantly upregulated in metastatic tumors as compared to primary tumors (right panel). (B) Kaplan-Meier survival curves of patients with high and low *SNAIL* expression in metastatic tumors which had both pathways deregulated. (C) ARCaP$_M$ cells have elevated PI3K/AKT and Ras/MAPK pathway activity compared to ARCaP$_E$.cells (D) Mouse prostate epithelial cells with *Pten* heterozygous (+/-) or homozygous (-/-) deletions transduced with *Kras*^{G12D} retrovirus (+) or with the parental vector without *Kras*^{G12D} (-) were analyzed for pathway-specific activation of EMT proteins by immunoblotting; *non-specific cross-reacting protein. (E) The mRNA levels of TGF-β induced EMT-associated transcription factors in *Pten*$^{-/-}$;*Kras*^{G12D} cells were determined by qRT-PCR (left panel). TGF-β induction of *Snail* in *Pten*$^{-/-}$ and *Pten*$^{-/-}$;*Kras*^{G12D} cells (right) and the immunoblots of the protein extract from *Pten*$^{-/-}$ and *Pten*$^{-/-}$;*Kras*^{G12D} cells with and without TGF-β treatment (bottom) are shown. The bar graph represents means ± SEM; *, p<0.05. **, p<0.01. ***, p<0.001.

(Thr37/46), and phospho-MEK (Try202/204) (Fig. 1C). In contrast to $ARCaP_E$ cells, which express high levels of E-cadherin and low levels of SNAIL, $ARCaP_M$ cells displayed low levels of E-cadherin and high levels of SNAIL (Fig. 1C). These results point out that PI3K/AKT and RAS/MAPK pathway co-activation and SNAIL upregulation co-exist in human metastatic PCa, and are associated with the acquisition of EMT characteristics.

Snail is preferentially activated by PI3K/AKT and RAS/MAPK pathway co-activation

To understand the mechanisms by which the PI3K/AKT and RAS/MAPK pathways regulate the EMT program, we analyzed isogenic prostatic epithelial lines with heterozygous and homozygous *Pten* deletion ($Pten^{+/-}$ and $Pten^{-/-}$, respectively) (15). Loss of one or both alleles of *Pten* resulted in activation of the PI3K/AKT pathway, as evidenced by increased P-AKT levels (Fig. 1D). However, activation of the PI3K/AKT pathway alone was not sufficient to induce the expression of the EMT markers SNAIL, TWIST1 (*, background signal) and FIBRONECTIN (FN), for which the additional activation of the RAS/MAPK pathway was required (Fig. 1D).

EMT is modulated by several key transcription factors that are controlled by the TGF-β pathway (11, 12, 24, 25). We next investigated the EMT-associated transcription factors in prostate epithelium that are regulated by TGF-β by using the *PTK* ($Cre^{+};Pten^{-/-};Kras^{G12D}$) cell line derived from the *CPK* mouse model (7). In comparison to other EMT-associated transcription factors, *Snail* was preferentially activated by TGF-β stimulation in the *PTK* cells (Fig. 1E, left panel). *Zeb1*, whose transcription is directly regulated by SNAIL (26), was also increased significantly (Fig. 1E, left panel).

TGF-β treatment of *PTK* cells resulted in a 7.2-fold and 23-fold induction of *Snail* mRNA and protein levels respectively, whereas $Pten^{-/-}$ cells showed only a modest increase (1.7-fold and

3-fold, respectively) (Fig. 1E, right panel). The RAS signaling pathway has been shown to facilitate SMAD activation (27-29), which is required for TGF-β induction of *SNAIL* mRNA (30). Consistently, TGF-β treatment induced phospho-SMAD2 expression in *PTK* cells more robustly than in *Pten*$^{-/-}$ cells (2-fold difference) (Fig. 1E, bottom panel). Taken together, PCa cells with PI3K/AKT and RAS/MAPK pathway co-activation are more sensitive to TGF-β-induced upregulation of the SNAIL transcription factor than cells in which only the PI3K/AKT pathway is activated.

PI3K/AKT and RAS/MAPK pathway co-activation leads to PAK1/2 activation and increased nuclear SNAIL protein half-life

Using unbiased phosphoproteomic analysis, we recently identified hyper-phosphorylation of PAK1 (Thr423)/PAK2(Thr402) in PTEN-null ES cells compared to the wild type ES cells (unpublished results). PAK GTPases are downstream of RAC and CDC42, which control cytoskeletal organization, motility, and cell proliferation (31, 32). We found significantly higher levels of phospho-PAK1 (Thr423)/ PAK2(Thr402) in *Pten*$^{-/-}$;*Kras*^{G12D} cells as compared to *Pten*$^{-/-}$ and *Pten*$^{+/-}$ cells (Fig. 2A; Fig. S1A), suggesting that PAK1/2 activities are modulated by PI3K and MAPK pathway co-activation. A PAK1-regulated gene signature (22) is also significantly upregulated in *CPK* murine prostates as compared to the *CP* murine prostates as measured by Gene Set Enrichment Analysis (GSEA) (22) (Fig. 2A, lower panel).

PAK1 phosphorylates SNAIL at Ser246 and promotes SNAIL nuclear localization (33). Thus, we hypothesized that PAK1 activation, resulting from PI3K/AKT and RAS/MAPK pathway co-activation, may enhance SNAIL nuclear localization and protein stability, promoting the EMT program in *Pten*$^{-/-}$;*Kras*^{G12D} cells. Indeed, there was significantly increased

phosphorylation of SNAIL (6-fold) at the PAK target site Ser246 in *Pten*$^{-/-}$;*Kras*^{G12D} cells compared to *Pten*$^{-/-}$ cells (Fig. 2A; Fig. S1A). The half-life of SNAIL in *Pten*$^{-/-}$;*Kras*^{G12D} cells was significantly longer (28 min) compared to that in *Pten*$^{-/-}$ cells (12 min) (Fig. 2B). Treatment with the pan-PAK1/2 inhibitor IPA-3 substantially diminished nuclear SNAIL levels in *Pten*$^{-/-}$;*Kras*^{G12D} cells (Fig. 2B; Fig. S1B). IPA-3 did not affect SNAIL levels in the presence of proteasome-inhibitor MG132 (Fig. 2C), suggesting that PAK1/2 controls SNAIL protein levels through inhibition of SNAIL degradation. PAK inhibition with IPA-3 reduced SNAIL protein expression both at basal and at TGF-β-stimulated expression levels (Fig. 2C, lower panel). Importantly, IPA-3 inhibition did not change the phosphorylation status of GSK3β, a previously reported modulator of SNAIL degradation (4), which suggests that PAK1-regulated SNAIL nuclear translocation and protein stability may be independent of GSK3β-regulated SNAIL degradation (Fig. 2C). SNAIL expression is required for the maintenance of the EMT phenotype in *PTK* cells, as knocking down endogenous *Snail* expression with a short interfering RNA (siRNA) increased expression of epithelial markers and E-cadherin protein levels, reduced expression of MMP2, and caused a significant morphological change in *PTK* cells from a spindle-shaped mesenchymal morphology to a cobblestone-like appearance typical for epithelial cells (Fig. 2D). Taken together, PI3K/AKT and RAS/MAPK pathway co-activation regulates the EMT program and SNAIL activity by at least two mechanisms: 1) sensitizing prostatic epithelial cells to TGF-β stimulation, which leads to preferential *Snail* overexpression, and 2) synergistically activating PAK1/2, which promotes SNAIL nuclear localization and protein stability.

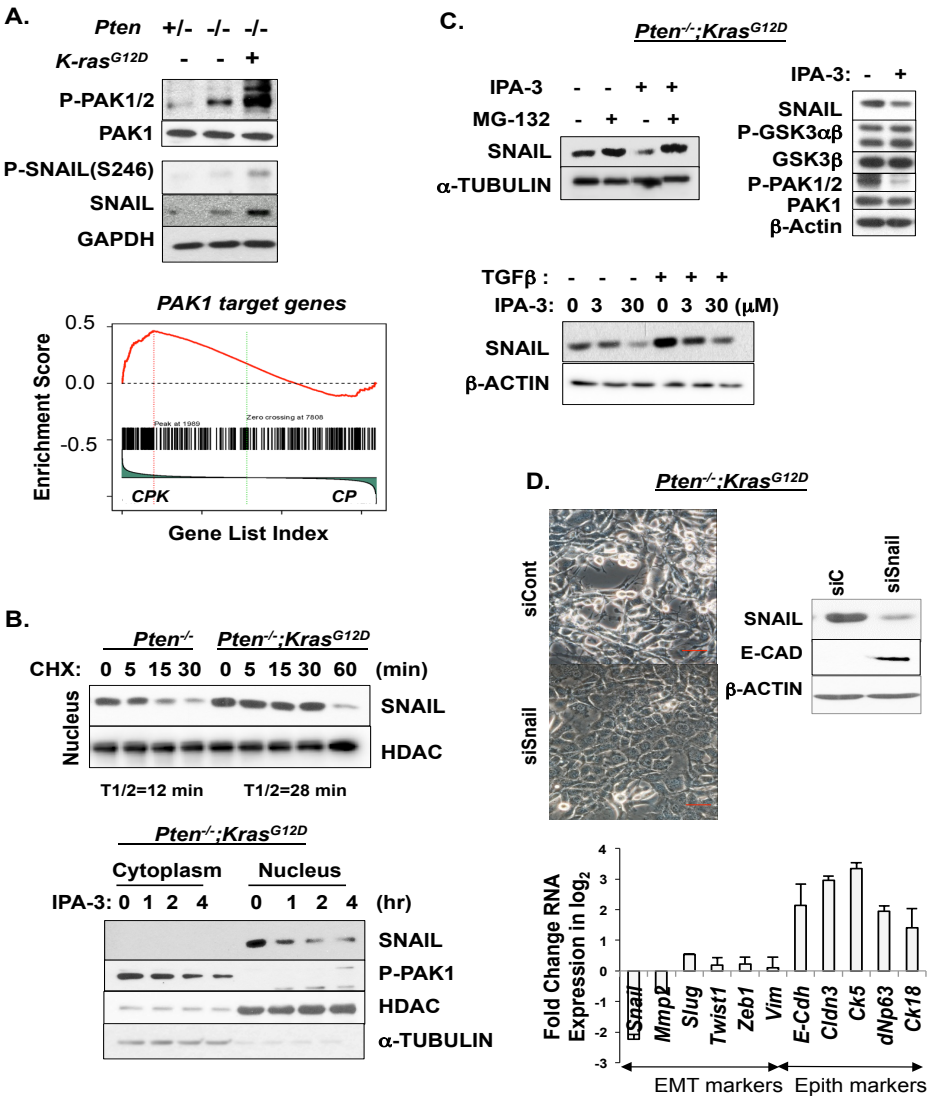

Figure 2. PI3K/AKT and RAS/MAPK pathway co-activation leads to PAK1/2 activation, increased nuclear SNAIL protein half-life, and suppression of the epithelial state. (A) *Pten* deletion and *Kras* activation resulted in elevated phospho-PAK1/2 (P-PAK1/2) (Try423/402) and phospho-Snail (P-SNAIL) (Ser246) levels. Bottom, Gene Set Enrichment analysis (GSEA) was used to look at enrichment of PAK1 target genes in the gene expression profiles of *CPK* compared to *CP* murine prostates. (B) *Pten*$^{-/-}$ *and Pten*$^{-/-}$*;Kras*^{G12D} cells were treated with 20 mM cycloheximide for indicated lengths of time, harvested, and nuclear lysates were prepared. HDAC band intensities were used for a loading control. SNAIL band intensities were normalized to the HDAC bands and used to determine the SNAIL protein half-life (T1/2). Bottom panel, Phospho-PAK1 and nuclear SNAIL protein levels were rapidly diminished by IPA-3 treatment in *Pten*$^{-/-}$*;Kras*^{G12D} cells. HDAC and α-tublin were used as nuclear and cytoplasmic loading controls, respectively. (C) *Pten*$^{-/-}$*;Kras*^{G12D} cells were treated with IPA-3 (+) or with vehicle (-) in the absence (-) or presence of MG-132 (+). The effects on SNAIL expression (left) and P-GSK3αβ (Ser21/9) and P-PAK1/2 (Try423/402) levels (right) were assessed by immunoblotting. Bottom, *Pten*$^{-/-}$*;Kras*^{G12D} cells were treated with vehicle or with IPA-3 in the absence or presence of TGF-β, and cell lysates were immunoblotted for SNAIL. (D) Phase-contrast images show changes in cell morphology as a result of Snail knockdown (siSnail) compared to control (siCont) cells. The effect of Snail knockdown in *Pten*$^{-/-}$*;Kras*^{G12D} cells on SNAIL and E-Cadherin (E-CAD) expression was analyzed by immunoblotting. siSnail, Snail siRNA; siCont, scrambled siRNA. The fold-change in EMT marker and epithelium-associated gene expression by Snail knockdown in *Pten*$^{-/-}$*;Kras*^{G12D} cells was determined by qRT-PCR. The values are represented as mean ± SEM.

Genetic deletion of *Snail* in *CPK* mice prevents EMT and prolongs animal survival

To investigate the causal relationship between *Snail* upregulation and PCa progression and metastasis *in vivo* in the context of PI3K/AKT and RAS/MAPK pathway co-activation, we crossed *CPK* mice with *Snail*-conditional knockout mice (19) to generate the *Pb-Cre*$^{+/-}$;*Pten*$^{L/L}$;*Kras*$^{G12D/W}$;*Snail*$^{L/L}$ mouse model (*CPKS,* hereafter). Compared to the age-matched *CPK* mice, *CPKS* mutants had significantly prolonged survival (Fig. S3A; p=0.0001), matching the finding that metastatic prostate cancer patients with lower *SNAIL* expression have a better overall survival compared to patients with high *SNAIL* expression (Fig. 1B).

To assess the effect of *Snail* deletion on EMT signature gene expression, we performed quantitative RT-PCR analysis. Prostates from *CPKS* mice showed significantly reduced levels of *Snail* mRNA as compared to *CPK* mutants (Fig. 3A). As a consequence of *Snail* deletion, the expression of other EMT markers, such as *Mmp2*, *Vimentin*, and *Fibronectin*, was also significantly lower than the expression levels found in *CPK* mutants, while *E-Cadherin* mRNA expression significantly increased in *CPKS* prostates (Fig. 3A).

The prostates of 10-13 weeks old *CPKS* mice were significantly smaller (Fig. 3B), especially in cancerous lesions of the anterior lobes, as compared to *CPK* mutants (Fig. 3B, arrows; Fig. S2B, traced outlines). Comparing the matched regions in the anterior lobes of *CPK* and *CPKS* mice, we noted that the *CPK* prostates displayed disseminated E-cad^{+} epithelial cells in the stroma (area marked as I in Fig. S3B) and in the lesions near the urethra where poorly differentiated carcinoma with sarcomatoid features had developed (area II in Fig. S2B). Many disseminated cancer cells were also positive for nuclear SNAIL staining (Fig. S2B, lower left two panels). By contrast, the majority of the anterior lobes in *CPKS* prostates contained prostatic

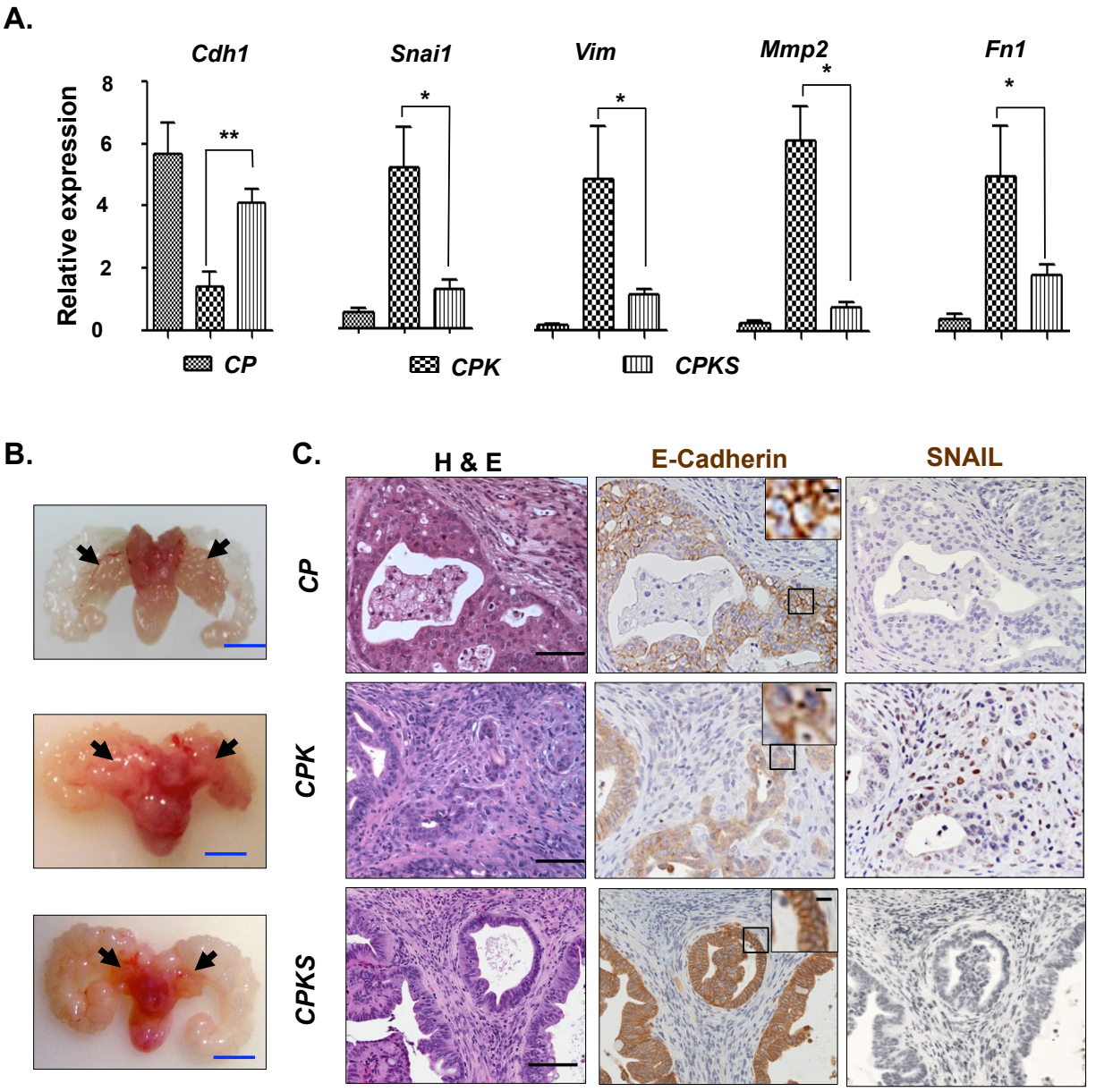

Figure 3. Genetic deletion of *Snail* in *CPK* mice restores epithelial gene expression, impedes prostate cancer progression, and prolongs survival. (A) qRT-PCR analysis of changes in the expression of E-cadherin and EMT genes in the prostates of *CP*, *CPK*, and *CPKS* mice. The values are represented as mean ± SEM; *, $p<0.05$; **, $p<0.001$; n=5-7. (B) Gross prostate structures of $C^{+};Pten^{L/L}$(*CP*), $C^{+};Pten^{L/L};Kras^{G12D/W}$(*CPK*), and $C^{+};Pten^{L/L};Kras^{G12D/W};Snai1^{L/L}$(*CPKS*) mice 10-13 weeks of age. Anterior prostate lobes are indicated by arrows. Scale bar, 4 mm. (C) A comparison of hematoxylin and eosin (H & E) and immunohistochemical staining for E-cadherin (E-cad) and SNAIL on consecutive sections of dorsolateral prostates of 10-week old *CP*, *CPK*, and *CPKS* mice. Higher magnification pictures of the boxed areas are presented for E-cadherin. Scale bar, 100 μm. Scale bar for higher magnification insets, 10 μm.

intraepithelial neoplasia (PIN) lesions with "cauliflower-like" morphology and E-cad$^+$ cells confined within the prostate glands (area III in Fig. S2B). Lesions in *CPKS* prostates were also less aggressive and invasive, as evidenced by intact and complete SMA staining around epithelial glandular structures (Fig. S2B). Interestingly, in the region proximal to urethra where poorly differentiated carcinomas were observed in age-matched *CPK* prostates (II), *CPKS* mice showed degenerated epithelial structures with abundant F4/80$^+$ macrophage infiltration, characteristic of an inflammatory response (area IV in Fig. S2B). Reduced tumor progression was also observed in the dorsolateral regions of *CPKS* prostates in which prostate epithelial glandular structures showed strong membrane staining for E-cadherin (Fig. 3C). Importantly, very few Snail$^+$ cells with EMT features could be detected in *CPKS* prostates (Fig. 3C; Fig. S2B). These results thereby suggest that deletion of *Snail* in the context of PI3K and RAS/MAPK pathway co-activation prevents EMT at the primary prostate tumor site and prolongs animal survival.

PCa cells with EMT features are hypersensitive to SNAIL loss-induced apoptosis in a p53-dependent manner

At 16 weeks of age and beyond, *CPK* mice developed aggressive solid tumors with obliterated seminal vesicles (arrowhead; Fig. 4A, left panels). Prostatic glands in *CPKS* mice were smaller in size and the anterior lobes frequently had a brown or dark red appearance (arrows in Fig. 4A, right panels). Histopathological analyses demonstrated that the solid tumors in the anterior lobes of *CPK* prostates were composed of sarcomatoid tumor cells with elongated, pleomorphic nuclei and prominent nucleoli. The tumor cells were highly proliferative with low E-cadherin expression and high Snail nuclear staining and Vimentin expression (Fig. 4A, left panels; Fig. S3A). In contrast, epithelial structures in the anterior lobes of *CPKS* prostate were E-cadherin

positive, and low for Ki67, Snail and Vimentin staining (Fig. 4A, right panels; Fig. S3A). Necrotic areas were often observed in the anterior lobes of *CPKS* prostates, with abundant neutrophils and degenerated epithelial cells within cystic structures (Fig. S3B, upper panels). In the dorsolateral lobes, degenerated glandular structures were surrounded by dense reactive stroma (Fig. S3B, lower panels). These results suggest that, in the absence of Snail and the Snail-regulated EMT program, cancer cells in *CPKS* prostates may not sustain the growth and pro-survival pathways driven by the activated PI3K/AKT and RAS/MAPK pathways, resulting in epithelial degeneration and subsequent neutrophil infiltration and a reactive stromal response.

Quantitative analysis of *CPKS* prostates revealed decreased cell proliferation and increased cell death in comparison to the *CPK* luminal epithelial regions, as measured by Ki67 and TUNEL immunohistochemical staining, respectively (Fig. 4B, left and middle panels; Fig. S4A). We compared p53 mRNA expression in *CPK* and *CPKS* prostates and observed increased expression of p53 (Fig. 4B, right panel) in the prostates of *CPKS* mice as compared to *CPK* mice. Snail suppresses p53 expression and confers resistance to cell death during embryogenesis and during tumor dissemination (34-37). Therefore, increased apoptosis observed in *CPKS* prostates may be caused by a p53-dependent mechanism in the prostate epithelium whereby suppression of p53 by Snail (38, 39) is impaired. To test this hypothesis, we knocked down *Snail* expression in *PTK* cells with siSnail (Fig. 4C, left panel; Fig. S4C), and found that downregulated *Snail* expression significantly increased p53 mRNA and protein levels, accompanied by elevated levels of cleaved-Caspase 3 (Fig. 4C; Fig. S4B). Caspase 3/7 activity induced by *Snail* knockdown was partially suppressed by concomitantly knocking down p53 (sip53), suggesting a p53-dependent mechanism for SNAIL loss-induced apoptosis (Fig. 4C, right panel).

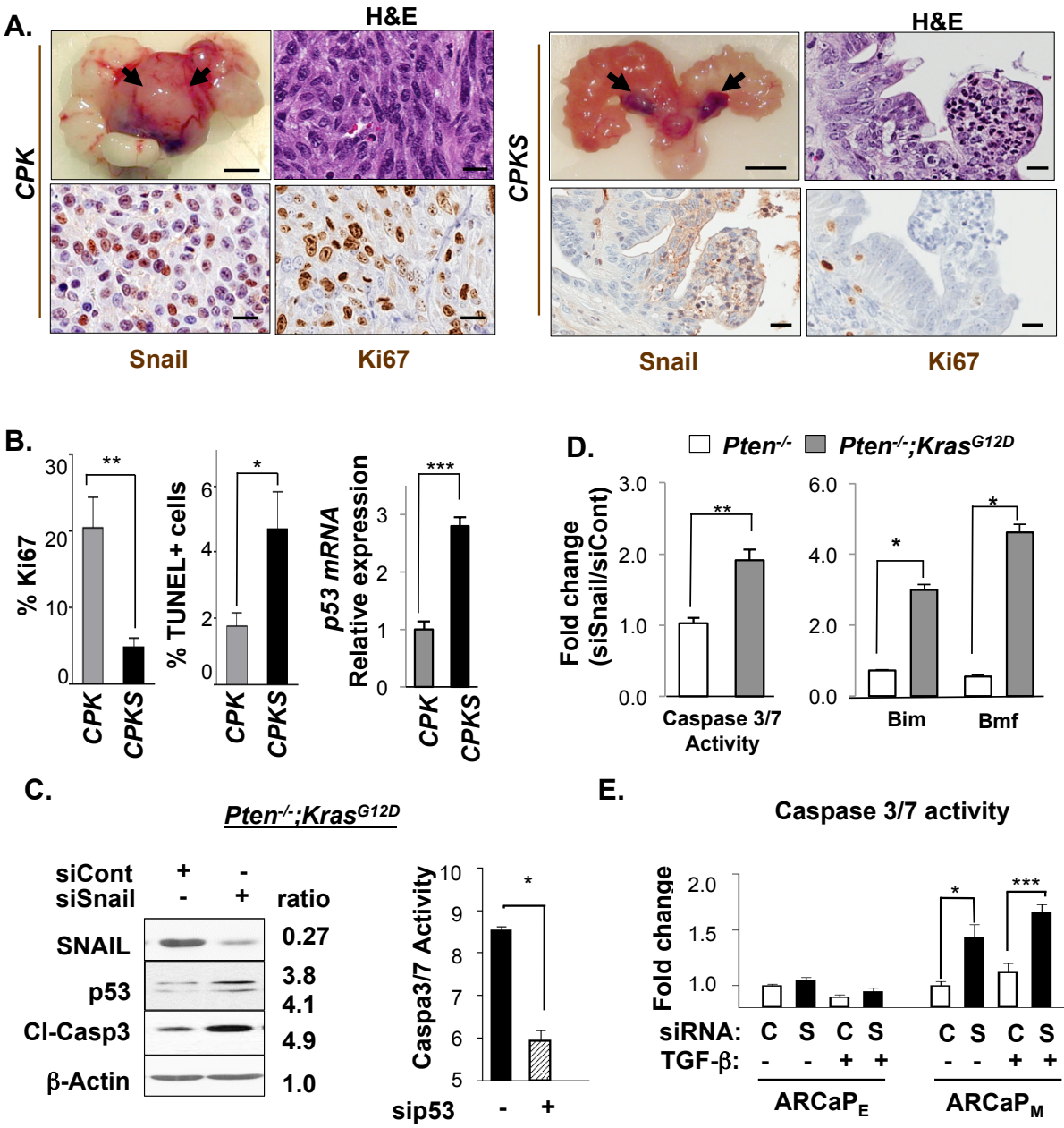

Figure 4. Prostate cancer cells with EMT features are more sensitive to *Snail* knockdown-induced cell death. (A) Gross prostate structure of a *CPK* and *CPKS* mouse (littermates) at 16 weeks of age. Arrow, anterior prostate lobes. The prostate sections were stained with H&E, Snail, and Ki67. Scale bar for gross prostates, 4 mm. Histology image scale bar, 10 μm. (B) Percentage of TUNEL and Ki67-positive cells in the prostate glandular structures in *CPK* and *CPKS* mice (left and middle). Right panel, the relative p53 mRNA expression levels for the *CPK* and *CPKS* mouse prostates as determined by qRT-PCR (n=5). (C) The effects of Snail knockdown in *Pten*$^{-/-}$*;Kras*^{G12D} cells on p53 and cleaved-Caspase 3 (Cl-Casp3) protein levels were assessed by Western blot. Cells were treated either with siRNA for Snail (siSnail) or with control siRNA (siCont). Right, Caspase3/7 activity was measured after Snail knockdown in the absence or presence of siRNA targeting p53. (D) Left, Caspase 3/7 activity was measured 3 days post-transfection and presented as the ratio of siSnail to siControl for indicated cell lines. Right, mRNA levels of the proapoptotic genes *Bim* and *Bmf* upon Snail knockdown. (E) Caspase3/7 activity in $ARCaP_E$ and $ARCaP_M$ cells after SNAIL knockdown with or without TGF-β treatment. Caspase3/7 activity was normalized to the control siRNA cells without TGF-β treatment. B-E are represented as mean ± SEM. *, $p<0.05$; **, $p<0.01$; ***; $p<0.005$.

Notably, *PTK* cells were much more sensitive to *Snail* knockdown-induced apoptosis than *Pten*$^{-/-}$ cells, as measured by increased Caspase 3/7 activity and expression of the pro-apoptotic genes *Bim* and *Bmf* (Fig. 4D), despite a similar level of Snail knockdown in both cell lines by (Fig. S4C). Of note, deletion of *Snail* in the *Pten* null PCa mouse model (*CPS*) did not result in any significant change in tumorigenesis or tumor cell survival (Fig. S4D), indicating that cells with PI3K/AKT pathway activation alone are not sensitive to Snail knockdown-induced apoptosis. Although *Pten*$^{-/-}$ cells were more resistant than *PTK* cells to *Snail* knockdown-induced apoptosis, they were similarly sensitive to Staurosporine-induced apoptosis (Fig. S4E), suggesting that increased sensitivity to apoptosis induced by *Snail* knockdown may be unique to *PTK* cells with EMT features. To test this hypothesis, we used $ARCaP_E$ and $ARCaP_M$ to examine their susceptibility to *Snail* knockdown-induced apoptosis. Similar to murine PCa cell lines, *SNAIL* knockdown resulted in increased apoptosis of $ARCaP_M$, but not $ARCaP_E$ cells, with or without TGF-β stimulation (Fig. 4E). Taken together, PCa cells with EMT features are more sensitive to *Snail* knockdown-induced apoptosis, which may explain the increased apoptosis, degeneration of the epithelial structures, and neutrophil infiltration observed in *CPKS* prostates *in vivo*.

Genetic deletion of *Snail* in *CPK* mice prevents distant macrometastasis to the liver and lungs

Strikingly, deletion of *Snail* in the prostate epithelium completely prevented macrometastasis to the lung and liver of the *CPKS* mice, providing genetic evidence that EMT is critical for the metastasis of PCa cells to distant organ sites (Fig. 5A; n=14). Figures 5B and 5C show a comparison of liver and lungs harvested from *CPK* and *CPKS* littermates.

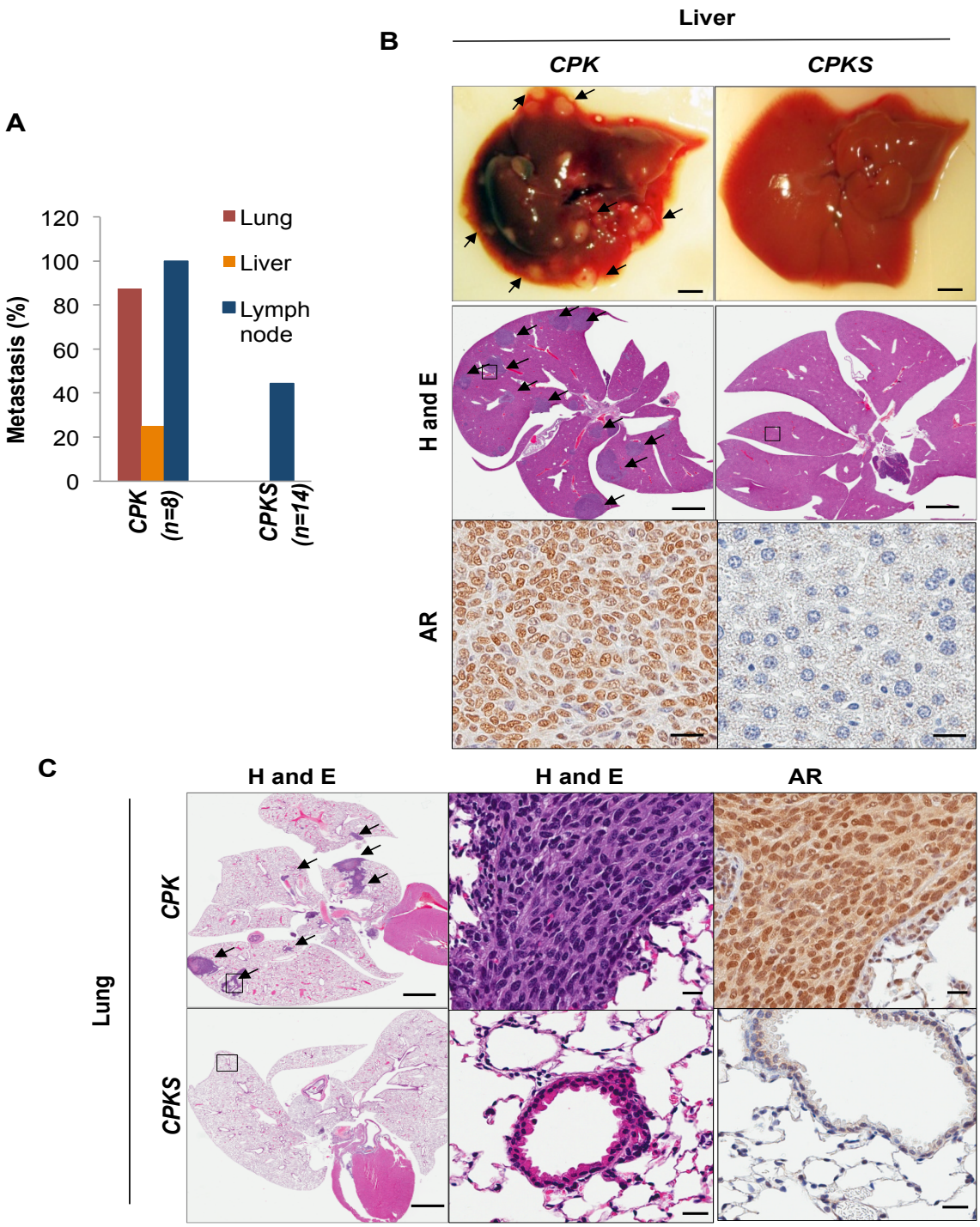

Figure 5. Genetic deletion of *Snail* in *CPK* mice prevents distant macrometastasis to the liver and lungs. (A) The percent occurrence of macrometastasis in the lungs, liver, and lymph nodes of mice with indicated genotypes. (B) Gross and H&E stained liver sections from 16 weeks old *CPK* and *CPKS* littermates. Arrows point to macrometastases; scale bar, 2 mm. AR immunohistochemical stains of the boxed area in the H&E panels are presented at high magnification. Scale bar, 20 μm. (C) H&E stained sections of lungs from 16-week old *CPK* and *CPKS* littermates. The arrows point to macrometastases; scale bar, 2 mm. Higher magnification views of the boxed area of the H&E and AR stained sections are presented. Scale bar, 20 μm.

Interestingly, Pan-Cytokeratin^{+}, AR^{+}, and Ki-67^{+} metastases were found in the draining lymph nodes of *CPKS* mice (Fig. 5A; Fig. S5) at a rate similar to what we previously reported in *CP* mice (40). This result suggests that metastasis through lymphatic vessels, which directly connect the primary cancer to the draining lymph nodes, may be less dependent on the acquisition of EMT properties by the cancer cells. Together, these observations indicate that *Snail* expression is necessary for PCa distant metastasis in the context of PI3K/AKT and RAS/MAPK pathway co-activation.

Induced Snail re-expression in *Pten*$^{-/-}$;*Kras*$^{G12D/+}$;*Snail*$^{-/-}$ (*PKS*) cells can restore the EMT program and metastasis *in vivo*

To further examine the function that Snail plays in PCa metastasis, an epithelial cell line, the *PKS* cell line, was generated by transducing Cre^{-};*Pten*$^{L/L}$;*Kras*$^{G12D/W}$;*Snai*$^{L/L}$ transgenic mouse prostate tissue with a Cre-FUCRW lentivirus (18) *in vitro*. *PKS* cells have genetic deletion of the *Snail* gene and remain in an epithelial state despite comparable activation of the PI3K/AKT and RAS/MAPK signaling pathways to that of *PTK* cells (Fig. S6A-C). In contrast to *PTK* cells, *PKS* cells grew as clusters with cobblestone-like morphology, had high expression of E-cadherin at cell-cell junctions, and did not express fibronectin (Fig. 6A; Fig. S6C). *PKS* cells also showed organized membrane staining at tight junctions with high expression of Zona Occluden 2 (ZO2), an adaptor protein for junction adhesion molecules (Fig. 6A).

We then introduced a retrovirus containing an inducible *Snail-ER* construct into the *PKS* line to generate an isogenic *PKS*-Snail-ER (*PKS*-iS hereafter) line. The expression of SNAIL in 4-Hydroxytamoxifen (Tam)-treated *PKS*-iS cells was exclusively localized in the nucleus (Fig. 6A). These cells had decreased levels of E-cadherin and increased Vimentin expression and were

loosely attached to each other with spindle-shaped morphology, as indicated by loss of ZO2 staining (Fig. 6A).

Next, we tested whether *PKS* and *PKS*-iS cells could form macrometastases *in vivo* by orthotopically transplanting them into the anterior lobes of *NOD/SCID/IL2Rγ-null* (*NSG*) mice. The *PKS* and *PKS*-iS cells were engineered to express Red Fluorescence Protein (RFP) as a result of the Cre-FUCRW lentivirus (18) used to generate the *PKS* cell line. Mice which were orthotopically transplanted with *PKS*-iS cells developed extensive RFP^+ lung metastases (Fig. 6B, arrows; Fig. S6D). However, the mice injected with *PKS* cells failed to form lung metastases (Fig. 6B), verifying that SNAIL is necessary for EMT and distant macrometastasis in PCa cells with PI3K/AKT and RAS/MAPK pathway co-activation.

Co-inhibition of the PI3K and MAPK pathways leads to downregulation of *Snail* and prevents PCa invasion and metastasis *in vivo*

Our *in vitro* and *in vivo* analyses make a compelling case for the essential role of SNAIL in regulating EMT and PCa progression and distant metastasis. However, as a transcription factor, SNAIL is difficult to directly target pharmacologically. One potential alternative approach may be to interfere with the upstream signaling pathways that regulate *Snail* expression in our model, namely the PI3K/AKT and RAS/MAPK pathways.

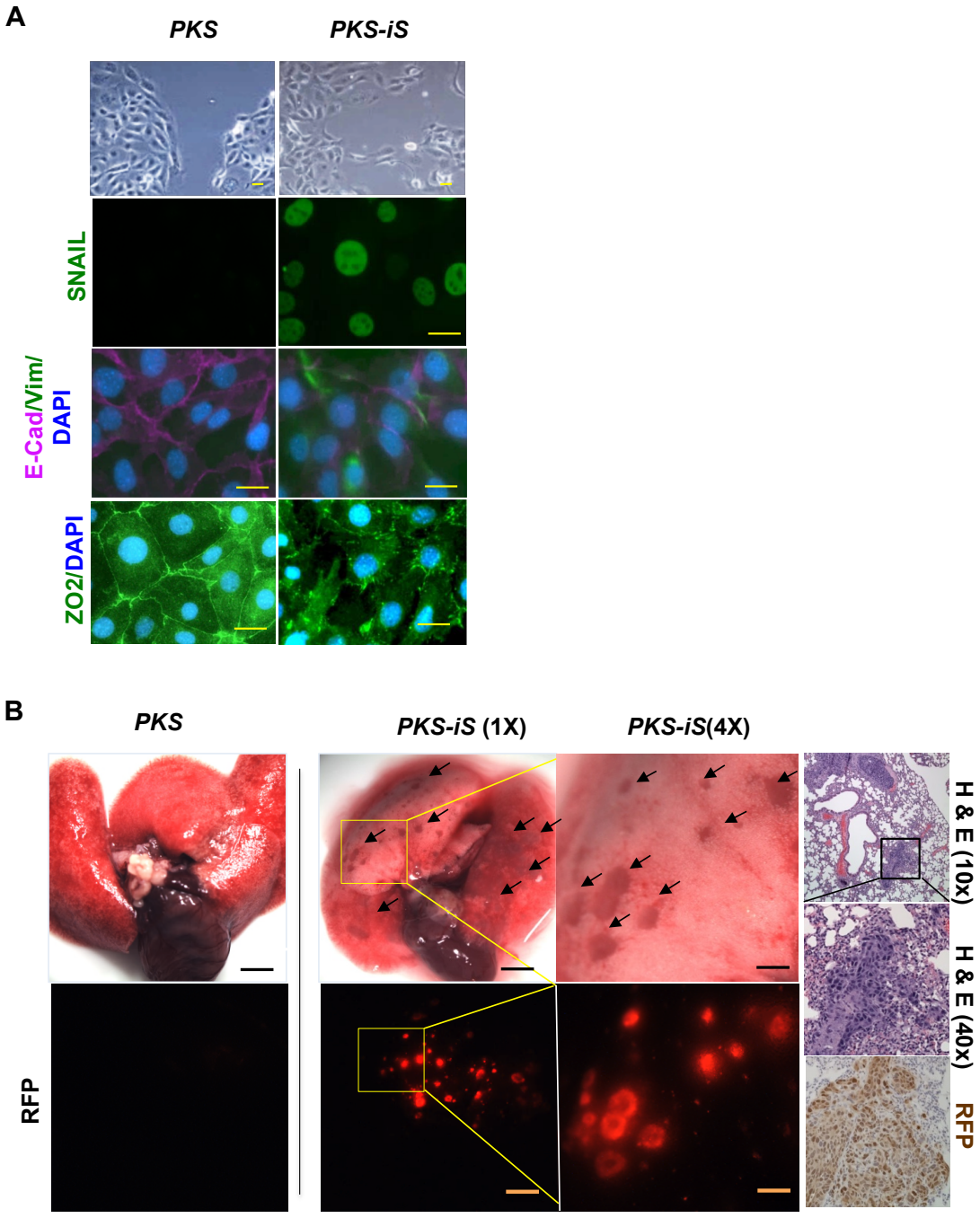

Fig. 6. *Snail* is required for formation of distant macrometastases by *Pten*$^{-/-}$;*Kras*^{G12D} cells. (A) Phase contrast and immunofluorescence images of *PKS* and *PKS*-iS cells. SNAIL (green) and Vimentin (Vim; green) are absent in *PKS* cells, but are expressed in *PKS*-iS cells. E-cadherin (E-Cad; magenta) and ZO-2 (green) mark epithelial cell tight junctions in *PKS* cells. Scale bars, 10 μm. (B) The metastatic seeding potential of *PKS* and *PKS*-iS cells was examined by orthotopic injection. 10,000 cells were grafted into each anterior prostate lobe of *NSG* mice, and lungs were harvested 5-7 weeks post-injection. Gross and fluorescence images of the representative lungs isolated from the mice that had been orthotopically grafted with *PKS* cells or *PKS*-iS cells are presented. RFP^{+} macrometastases were absent in the lungs of mice injected with *PKS* cells (n=5), but were visible in mice orthotopically injected with *PKS*-iS cells (n=5). Arrows point to macrometastases. Scale bar, 2 mm for (1x) and 500 μm for (4x).

While inhibition of the PI3K or MAPK pathway individually resulted in a decrease in *Snail* expression in *PTK* cells, dual treatment with either rapamycin (mTOR inhibitor) or LY294002 (PI3K inhibitor) and the MEK inhibitor PD0325901 acted synergistically to further diminish *Snail* mRNA levels by nearly 5-fold as compared to untreated control *PTK* cells (Fig. 7A). SNAIL has also been previously shown to confer tumors cells with increased motility and migratory capacity (11, 35). Since combination treatment with LY294002 and PD0325901 dramatically reduces *Snail* expression, a wound-healing assay was carried out to assess the effect of dual PI3K and MAPK pathway inhibition on cell migration. Indeed, combined LY294002 and PD0325901 treatment *in vitro* dramatically reduced the migration of *PTK* cells (Fig. 7B). Dual treatment of human $ARCaP_M$ cells with PD0325901 + LY294001 or PD0325901 + rapamycin was also able to down-regulate SNAIL expression more effectively compared to the treatment with a single inhibitor alone (Fig. S7A).

To assess the impact of dual PI3K and MAPK pathway inhibition on *Snail* expression, tumor cell dissemination, and disease progression *in vivo*, we treated *CPK* mice with rapamycin and PD0325901 starting at 6 weeks of age, when the onset of tumor cell dissemination and an EMT phenotype have been observed (7). After 4 weeks of treatment, prostates from untreated and Rapa+PD treated *CPK* mice were harvested for histopathological analysis. The PCa lesions of the *CPK* mice treated with rapamycin and PD0325901 were significantly smaller than those in the vehicle-treated *CPK* mice prostates (Fig. 7C). While untreated *CPK* mice displayed extensive invasion of E-cad^+ epithelial tumor cells into the stroma in the dorsolateral lobe, combination treatment with rapamycin and PD0325901 prevented tumor cell invasion in the same lobe, as evidenced by the well-defined E-cad^+ glandular structures and lack of invasive E-cad^+ cells in the nearby stroma (Fig. 7C, bottom panel). Tumor cell invasion in *CPK* mice was also marked by

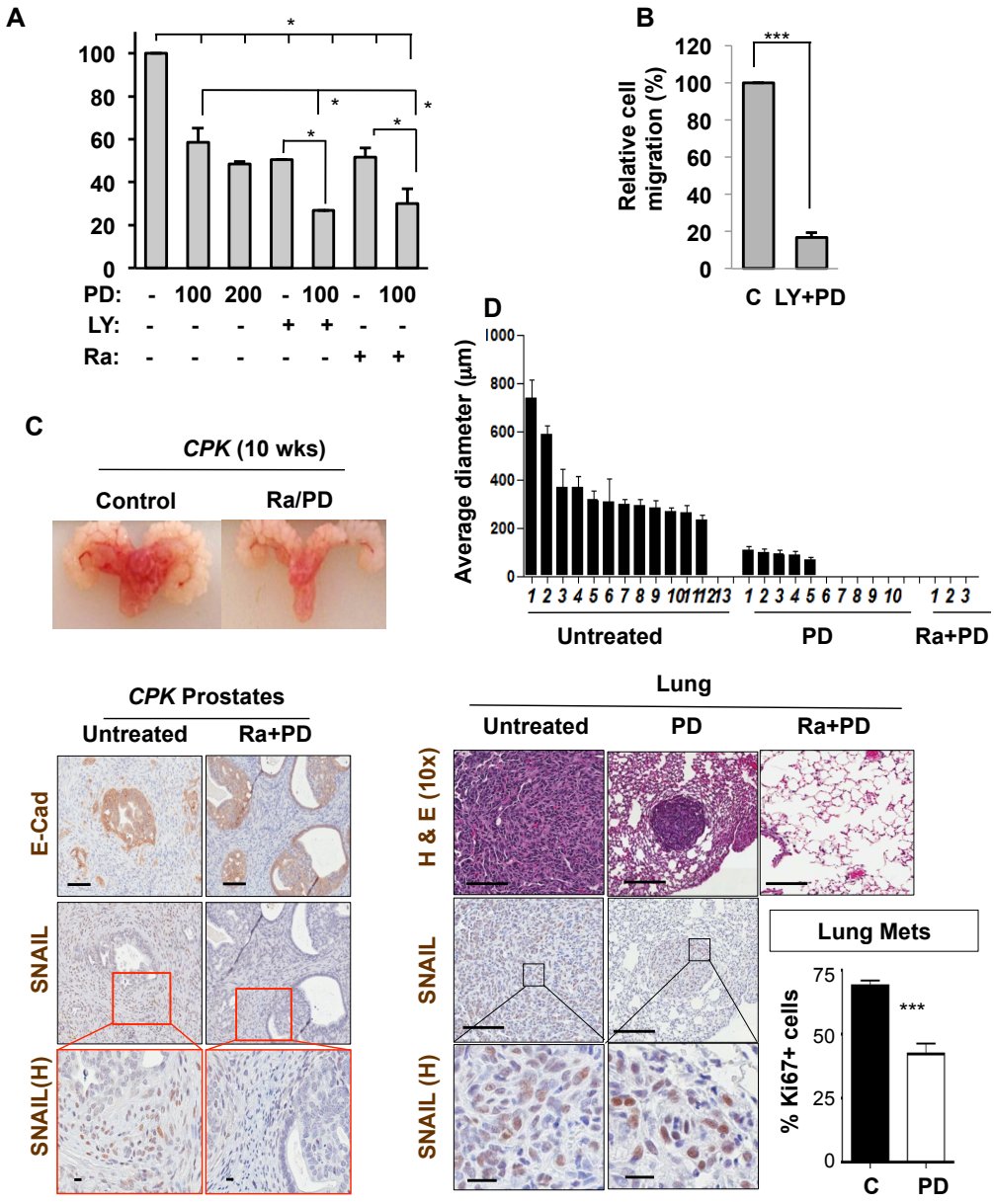

Figure 7. Co-inhibition of the PI3K and MAPK pathways leads to downregulation of *Snail* and prevents tumor cell invasion and distant macrometastasis. (A) Changes in Snail mRNA levels in *Pten*$^{-/-}$;*Kras*^{G12D} cells after treatment with PD0325901 (PD), LY294002 (LY), and/or rapamycin (Ra). Snail mRNA in vehicle-treated cells was normalized to 100%. (B) The effect of PD0325901 and LY294002 (PD+LY) treatment on cell migration as determined by scratch assay. Distances that *Pten*$^{-/-}$;*Kras*^{G12D} cells migrated is expressed as a percentage of the migration distances traveled by control (C) cells, which are normalized to 100%. (C) Gross prostate images from 10-week old *CPK* mice after 4-week treatment with rapamycin (Ra) and PD0325901 (PD). Bottom, E-cadherin (E-cad) and Snail immunohistochemical staining of prostates harvested from control or Ra+PD treated *CPK* prostates. Scale bars are 100 μm at low magnification and 10 μm at high magnification (H). (D) Average diameter of lung metastases, including micrometastases, in animals orthotopically injected with *Pten*$^{-/-}$;*Kras*^{G12D}–*Luc* prostate sphere cells with or without drug treatment (Top panel). Each number indicates an individual mouse. Bottom, representative low magnification images of H&E stained lung tissue from control, PD alone, and Ra+PD treated mice. Ra + PD dual treatment completely eliminated lung metastases. The boxed areas are presented as high magnification images of Snail staining (H) in the lowest panel. Low magnification scale bar, 200 μm; high magnification scale bar, 20 μm. Bottom right, the percentage of Ki67 positive cells in the lung metastases. Data in A, B, and D are represented as mean ± SEM. *, $p<0.05$; ***, $p<0.001$.

the induction of SNAIL protein expression in EMT cells that invaded into the stroma (Fig. 7C, bottom panel). In contrast, dual inhibition of the PI3K and MAPK pathways resulted in loss of SNAIL protein expression in the prostates of *CPK* mice (Fig. 7, bottom panel), mirroring the effects of combined rapamycin and PD0325901 treatment on *Snail* mRNA expression levels found *in vitro* (Fig. 7A). Similar to the degenerated epithelium seen in aged *CPKS* prostates, dual treatment with rapamycin and PD0325901 also resulted in degenerated epithelial structures (arrows, Fig. S7B) and scar-like tissue (arrowheads, Fig. S7B) in *CPK* prostates. These results suggest that dual inhibition of the PI3K and MAPK pathways in prostate tumors that have already acquired an EMT phenotype can effectively inhibit *Snail* expression, reverse EMT, and consequently prevent tumor cell invasion and cancer cell dissemination.

Our laboratory has previously shown that orthotopic transplantation of $Lin^{-}Sca1^{+}CD49f^{Hi}$ (LSC^{Hi}) PCa stem cells isolated from *CPK;Rosa26-Luc* mice into male *NSG* mice leads to metastatic disease to lungs with reliable kinetics (7). Utilizing this orthotopic model, we sought to investigate the effect of rapamycin and PD0325091 treatment alone or in combination on distant metastasis. While 12/13 untreated control mice developed large macrometastases to the lung by 3 weeks post-transplantation, we found that 2/5 rapamycin and 0/10 PD0325901 treated mice developed macrometastases over the same time period as judged by gross examination and bioluminescent imaging (Fig. 7D; Fig. S8). Interestingly, 5/10 PD0325901-treated mice contained between 1-5 micrometastases in the lung as determined by histological examination (Fig. 7D; Fig. S8A). Although these micrometastases were substantially smaller in size and less proliferative compared to the macrometastases of the untreated mice, nuclear SNAIL was prominent in these lesions (Fig. 7D), suggesting that single agent treatment with PD0325901 did

not completely inhibit Snail expression and failed to prevent the early stages of metastasis. Strikingly, combination treatment with rapamycin and PD0325901 completely inhibited the formation of macro- and micrometastases in the lungs. Together, these data indicate that combined PI3K and MAPK pathway inhibition is able to fully ablate distant metastasis, and that this effect may be partially mediated through inhibition of *Snail* expression.

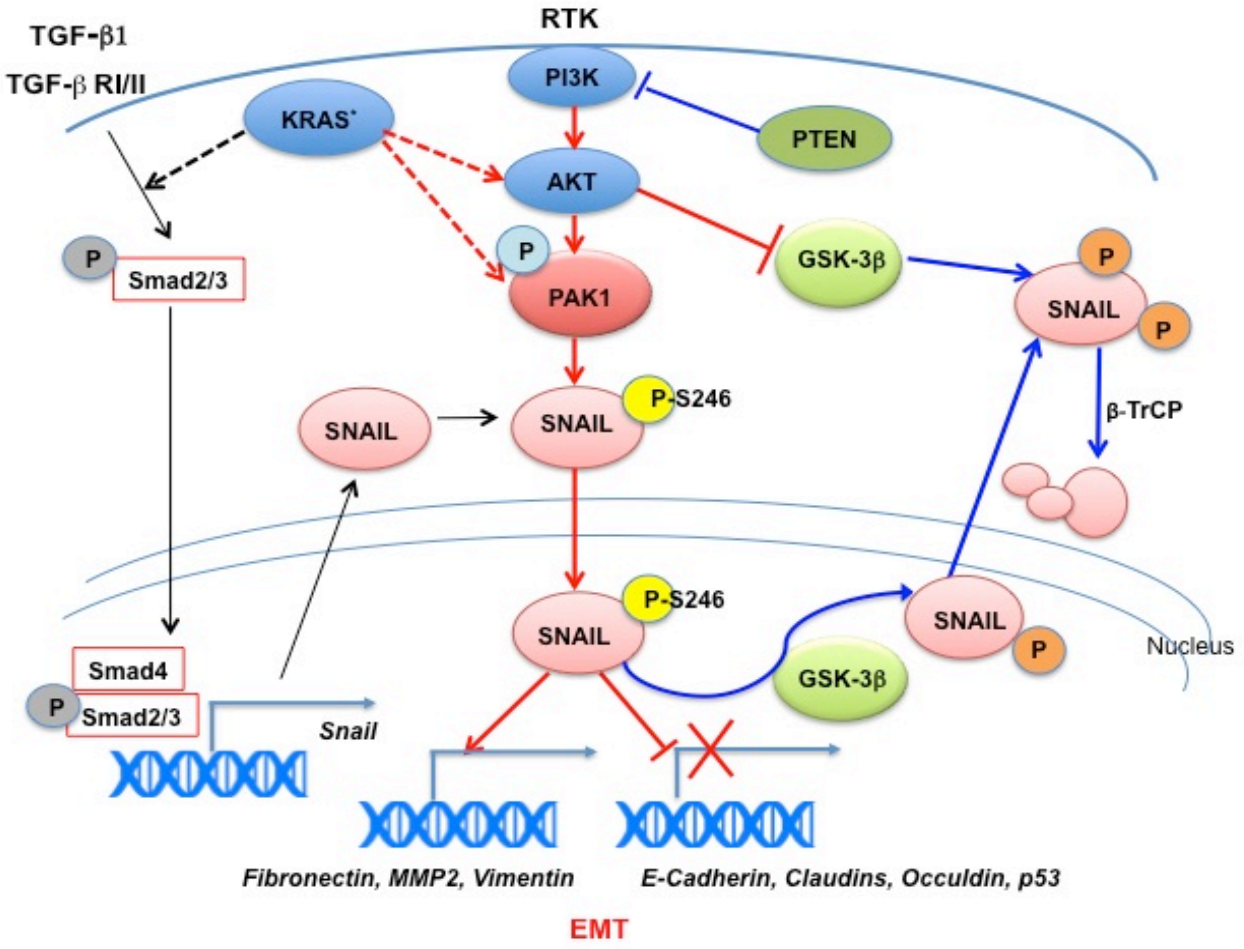

Figure 8. Mechanisms of Snail regulation by the PI3K/AKT and RAS/MAPK pathways. Prostate cancer cells with PI3K/AKT and RAS/MAPK pathway co-activation are hypersensitive to TGF-β-induced upregulation of *Snail* transcription. PAK1 is a target of both the PI3K/AKT and RAS/MAPK pathways, and synergistic activation of PAK1 promotes nuclear translocation of SNAIL via phosphorylation at Ser246. GSK3-β-mediated phosphorylation of SNAIL near the nuclear export sequence and at the β-TrCP destruction motif leads to the nuclear export and subsequent degradation of SNAIL by β-TrCP (4). When the PI3K/AKT and RAS/MAPK pathways are activated, GSK-3β is phosphorylated at Ser9, inactivating its kinase activity and leading to increased SNAIL protein stability. SNAIL represses epithelial genes such as E-Cadherin and Claudins, and activates survival pathways and mesenchymal genes like Zeb1, Vimentin, MMP2, and Fibronectin, leading to EMT, increased motility, and metastasis.

Discussion

Although EMT has been proposed to be an underlying mechanism for tumor cell dissemination and the metastatic process in many epithelial-derived tumors, direct *in vivo* evidence for the essential role of the EMT process in driving metastatic disease remains less clear. In this study, we found that genetic deletion of *Snail* was sufficient not only to reduce tumor cell invasion, but also to ablate distant macrometastases in the *CPK* mouse model of PCa. *Snail* deletion impedes the development of an EMT phenotype at the primary tumor site and causes prostate tumor cells with EMT features to become susceptible to p53-dependent apoptosis. Overall, this new genetic mouse model provides the first direct *in vivo* evidence that the EMT program regulated by SNAIL is required for PCa distant macrometastasis.

Our previous work and that of others have found that the activation of the PI3K/AKT and RAS/MAPK pathways is prevalent and critical for metastatic PCa (6, 7, 41). However, it has remained unclear how cross-talk between these two pathways promotes cancer metastasis. We showed in this study that activation of either pathway alone is not sufficient to induce an EMT, and that the co-activation of both the PI3K/AKT and RAS/MAPK pathways is indeed required for EMT. We found that prostatic epithelial tumor cells with *Pten* deletion and $Kras^{G12D}$ activation are more sensitive to TGF-β-induced upregulation of *Snail* expression. Tumor-derived TGF-β, as well as TGF-β from the tumor microenvironment, are known to cause EMT in advanced cancer cells (29). We demonstrated that the PI3K/AKT and RAS/MAPK pathways collaborate to enhance the activation of the TGF-β-SMAD pathway and sensitize cells to transcriptional upregulation of the *Snail* gene. This observation is consistent with earlier reports that transcriptional regulation of *Snail* is mediated through both the PI3K and RAS signaling pathways (42), and that TGF-β-activated SMAD proteins directly facilitate upregulation of Snail

transcription from its promoter (25, 29, 43, 44). In addition to transcriptional regulation of *Snail*, we found that PI3K/AKT and RAS/MAPK pathway co-activation resulted in PAK1 activation and increased Snail nuclear localization and protein half-life. This is the first study to show that the PI3K/AKT and RAS/MAPK pathways synergistically activate PAK1. GSK3β is also known to regulate SNAIL subcellular localization and protein half-life (4). In *PTK* cells with PI3K/AKT and RAS/MAPK pathways co-activation, GSK3β was highly phosphorylated at Ser9 and thus inactivated, preventing the inhibitory phosphorylation of SNAIL that is necessary for SNAIL nuclear export and b-TrCP-mediated degradation (4). Therefore, co-activation of PI3K/AKT and RAS/MAPK pathways upregulates SNAIL activity through multiple mechanisms, which include transcriptional activation, as well as post-transcriptional modifications that positively regulate PAK activity and negatively regulate GSK3β activity, leading to increased SNAIL nuclear localization and protein half-life (Fig. 8).

In spite of reports that SNAIL expression and SNAIL nuclear localization correlate with the advanced disease and metastasis in clinical PCa (45-49), the presence of SNAIL expression in human PCa specimens is still considered inconclusive. This may be due to the unstable nature of the Snail protein, as well as the fact that Snail may be expressed transiently during EMT. We found clinical relevance for *SNAIL* expression in human metastatic PCa with PI3K/AKT and RAS/MAPK pathway co-activation using a dataset obtained from a rapid autopsy program (20). We further found that *SNAIL* expression is associated with early lethality among patients who have been treated with chemotherapy. These findings indicate that *SNAIL* expression can be used to stratify human PCa patients that are likely to progress to metastatic disease and have a poor overall survival.

Significantly, *Snail* deletion or knockdown restored epithelial morphology and gene expression in the *PTK* cells, and prevented macrometastasis to distant organs in *CPK* mice. Furthermore, the studies with *PKS* and *PKS*-iS isogenic cells strongly support the conclusion that SNAIL is necessary for EMT and macrometastasis formation. However, this observation does not exclude the possibility that forced expression of other EMT transcription factors can also induce EMT and metastasis in the absence of SNAIL. It is noteworthy that TGF-β-induced EMT found in the *Pten*$^{-/-}$;*p53*$^{-/-}$ murine PCa model is driven by Slug, not Snail (50), suggesting that the regulation of EMT in cancer is complex and context-dependent. SNAIL is a pleiotropic factor with many functions, as it is not only a strong transcriptional repressor of E-cadherin, but also plays a role in cell survival, cell cycle regulation, stem cell self-renewal and multipotency, and in the development of therapeutic resistance (35-37, 51). Therefore, the biological effects of *Snail* deletion observed *in vivo* in *CPKS* mice may be attributed to the loss of one or more of the above SNAIL functions.

Directly targeting SNAIL and other EMT-associated transcription factors pharmacologically has been difficult. Recent studies suggest that the TGF-β pathway may collaborate with PTEN loss in promoting PCa invasion and metastasis, which may be in part due to its regulation of the EMT program (52-54). Although antagonists of the TGF-β signaling pathway have been developed (55, 56), the context-dependent opposing functions of the TGF-β pathway (29, 57-60) make these antagonists difficult to be considered as general cancer therapeutics. We therefore sought to inhibit the two cell intrinsic signaling pathways that are involved in *Snail* upregulation in our model: the PI3K/AKT and RAS/MAPK pathways. Using the *PTK* and ARCaPM cell lines and the *CPK* mouse model, we showed that dual treatment with rapamycin and PD0325901 was effective in (i) down-regulating SNAIL expression, (ii)

inhibiting cell migration, (iii) inhibiting EMT, and (iv) preventing lung macrometastasis. Snail has been shown to induce neuroendocrine transdifferentiation in LNCaP cells (61). It will be interesting to test if inhibition of Snail expression by inhibiting both the PI3K/AKT and RAS/MAPK pathways could halt neuroendocrine differentiation in clinical PCa. Additionally, inhibitors of PAK1 should be tested for their potential to treat metastatic disease given the role of PAK1 in regulating SNAIL protein stability and EMT as shown by this study and that of others (62). Taken together, interfering with the "oncogene addicted" state of EMT tumor cells by targeting the upstream inducers of the EMT program may be an effective therapeutic strategy for the treatment of metastatic PCa (49, 61).

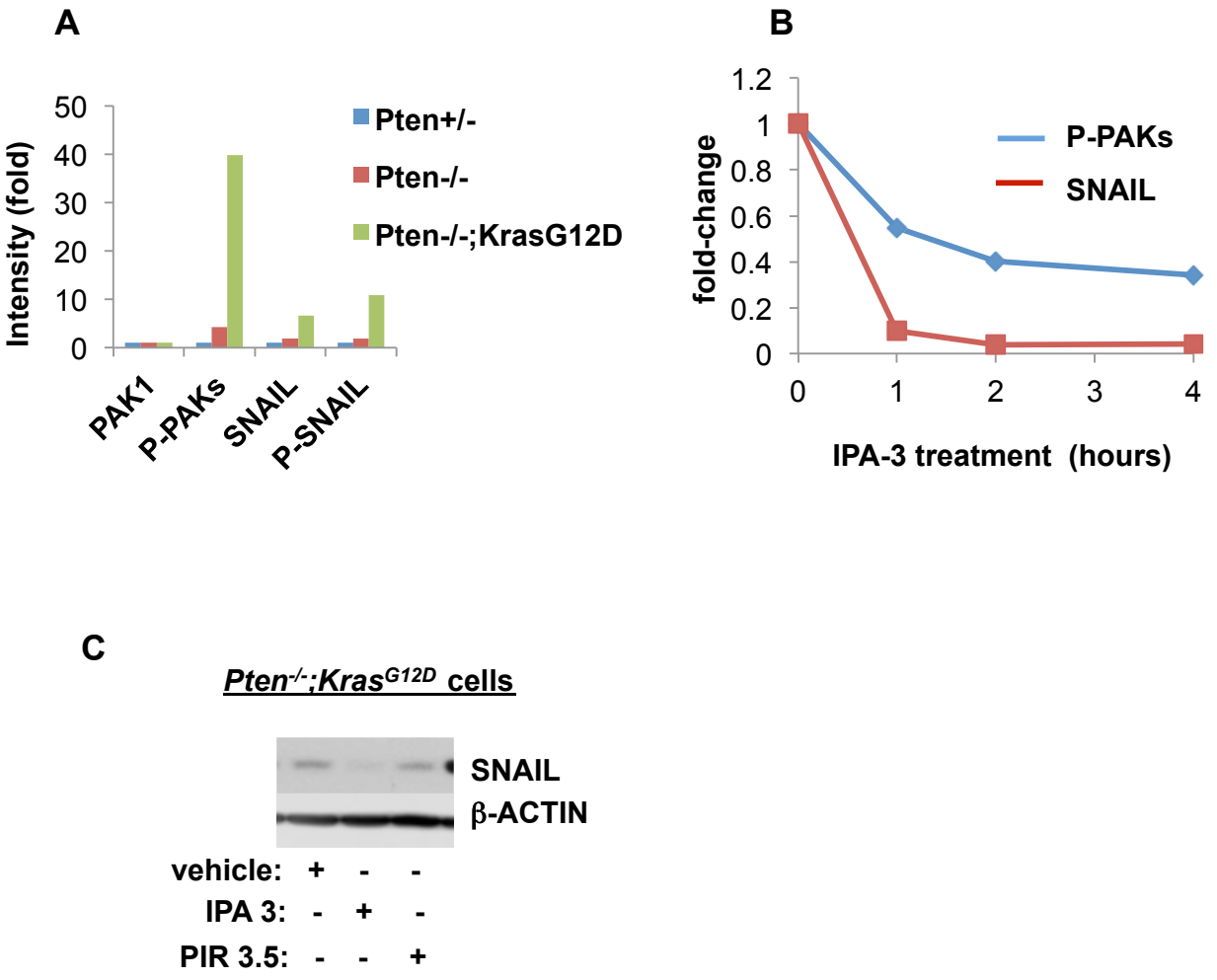

Figure S1. *Pten* deletion and *Kras*^{G12D} activation synergistically activate PAK1, which promotes the nuclear localization of SNAIL. (A) Immunoblots in Figure 2B were scanned and quantitated for PAK1, phospho-PAKs, phospho-SNAIL, and SNAIL levels. Values were normalized to the GAPDH loading control and expressed as fold changes compared to the expression in Pten$^{+/-}$ cells. (B) *PTK* cells were incubated with the PAK inhibitor IPA-3 for the lengths of time indicated. The nuclear and cytoplasmic fractions were analyzed for expression of SNAIL, P-PAK1, and total PAK1 by immunoblotting. HDAC and α-tubulin were used as nuclear and cytoplasmic protein loading controls, respectively. (C) SNAIL protein levels were examined by immunoblotting using protein lysates from *PTK* cells treated with vehicle (0.1% DMSO), IPA-3 (30 uM), or with PIR3.5 (30 mM) for 2 hrs. PIR3.5 is a PAK1 isomer with the same redox effects as IPA-3 but without inhibitory effects on PAK1 kinase activity. β-Actin was used as a loading control.

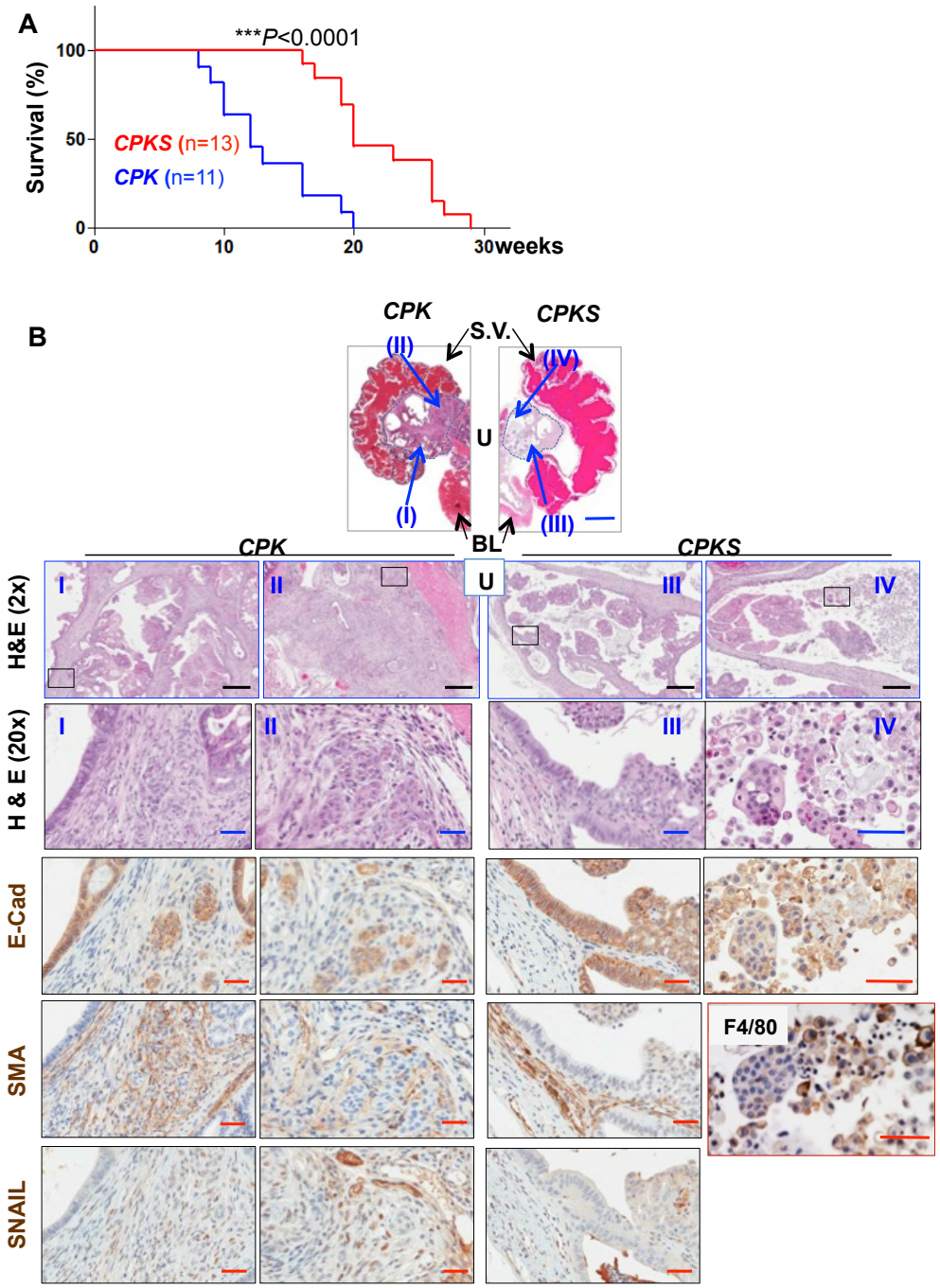

Figure S2. Effects of *Snail* deletion in *CPK* mice on survival and prostate cancer progression. (A) Kaplan-Meier survival curve of $C^{+};Pten^{L/L};Kras^{G12D/W}$ (*CPK*) and $C^{+};Pten^{L/L};Kras^{G12D/W};Snai1^{L/L}$ (*CPKS*) mutants. Median survival for *CPK* and *CPKS* mutants is 12 wks (n=11) and 20 wks (n=10), respectively. (B) *Snail* deletion leads to deterioration of prostate epithelial ductal structures in *CPK* mutants. Representative images of H&E-stained urogenital area of *CPK* (left) and *CPKS* (right) at 10 weeks. Dotted lines encompass anterior prostates. SV, Seminal vesicles, BL, Bladder. U, Urethra. The regions I to IV correspond to the magnified views (2x) of the H&E sections shown below. Consecutive sections were stained for E-cadherin (E-cad), smooth muscle actin (SMA), Snail, and (F4/80) (to identify macrophages). Boxed areas in the (2x) H&E sections are shown at higher magnification (20x). Blue scale bar, 2 mm; black bar, 200 μm; red bar, 50 μm.

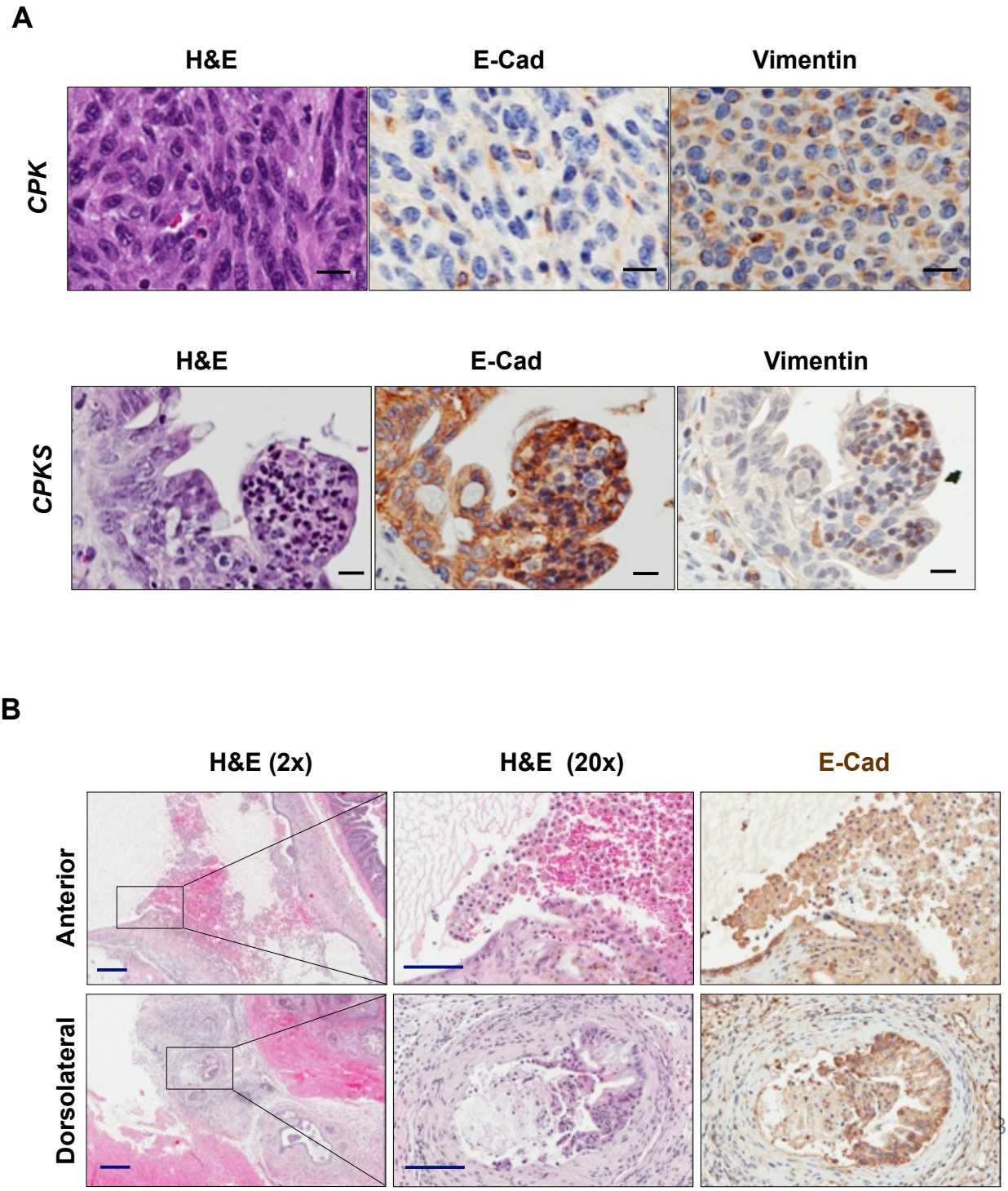

Figure S3. *Snail* deletion in *CPK* mice promotes a reversion to an epithelial morphology and induces cell death. (A) Prostate sections of 16-week old *CPK* and *CPKS* littermates were stained for E-Cadherin (E-Cad) and Vimentin by IHC. Anterior prostate morphology is shown. Scale bar, 10 μm. (B) Anterior and dorsolateral prostates lobes from a 26-week old *CPKS* mouse stained with H&E and E-Cad. Low magnification (2x) scale bar, 1 mm. High magnification (20x) scale bar, 100 μm.

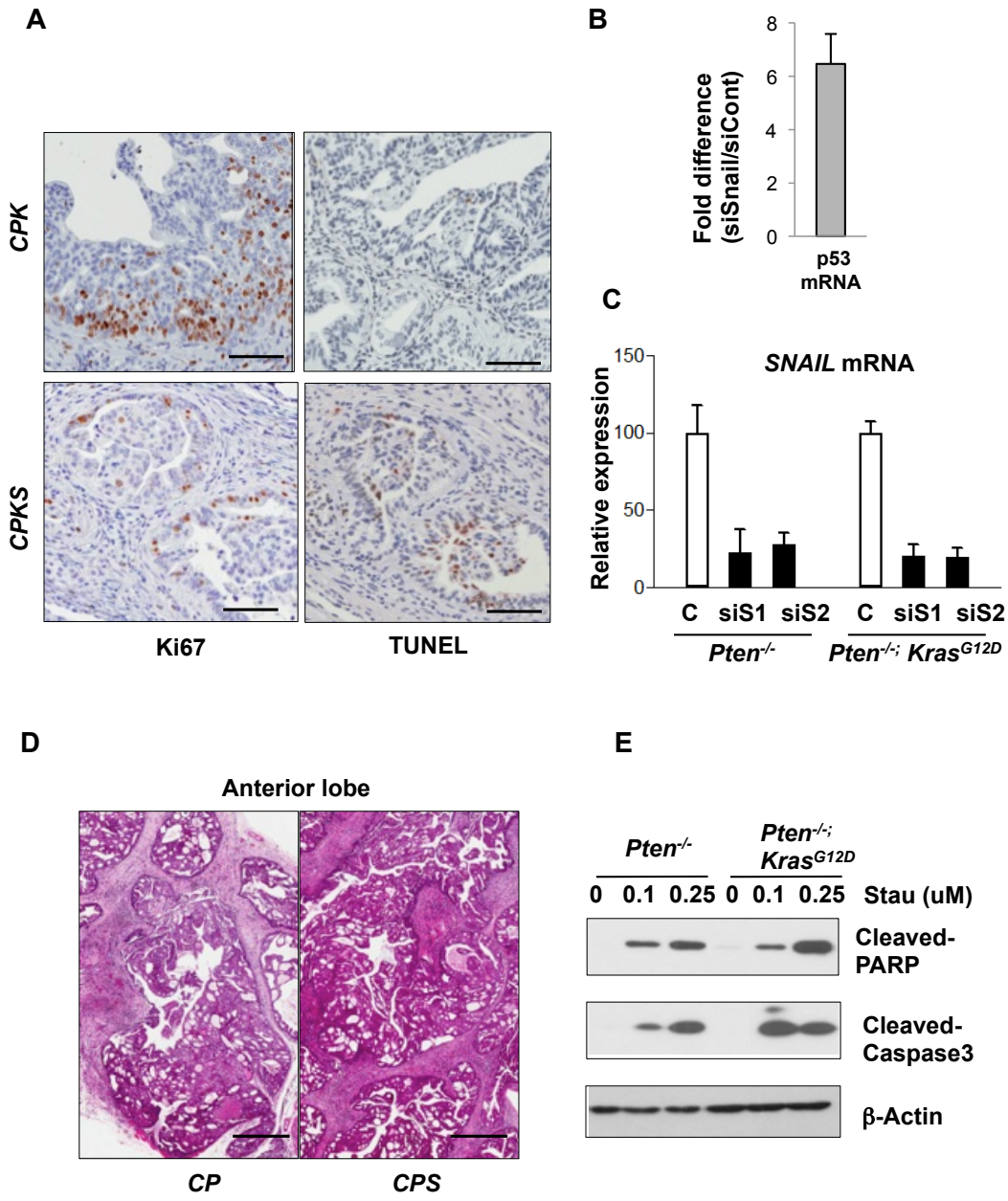

Figure S4. Effects of Snail knockdown in *CPK* mice and *Pten*$^{-/-}$;*Kras*^{G12D} cells. (A) Representative images of the Ki67 and TUNEL staining in 10 wk old *CPK* and *CPKS* prostates. Scale bar, 100 μm. (B) The effect of Snail knockdown in *Pten*$^{-/-}$;*Kras*^{G12D} cells on p53 mRNA expression was assessed by qRT-PCR. Cells were treated with either siRNA targeting Snail (siSnail) or with control siRNA (siCont) for 3 days. Expression is presented as the fold difference between p53 levels in siSnail compared to siCont treated cells. (C) *Snail* expression was knocked down by two independent siRNAs (siS1 and siS2) against Snail in both *Pten*$^{-/-}$ and *Pten*$^{-/-}$;*Kras*^{G12D} cells with a similar efficiency as measured by qRT-PCR. *Snail* expression is presented as the percentage of *Snail* expression relative to cells treated with scrambled siRNA control (C). (D) 16-week old *Pb-Cre*$^{+/-}$;*Pten*$^{L/L}$;*Snail*$^{L/L}$ (*CPS*) mutant prostates have glandular structures similar to age-matched *Pb-Cre*$^{+/-}$;*Pten*$^{L/L}$ (*CP*) prostates. The prostate sections were stained with H&E. Scale bar, 500 μm. (E) Staurosporin induced apoptosis in *Pten*$^{-/-}$ and *Pten*$^{-/-}$;*Kras*^{G12D} cells. *Pten*$^{-/-}$ and *Pten*$^{-/-}$;*Kras*^{G12D} cells treated with Staurosporin at indicated concentrations were analyzed by immunoblotting for cleaved Caspase3 and cleaved PARP. β-actin was used as a loading control.

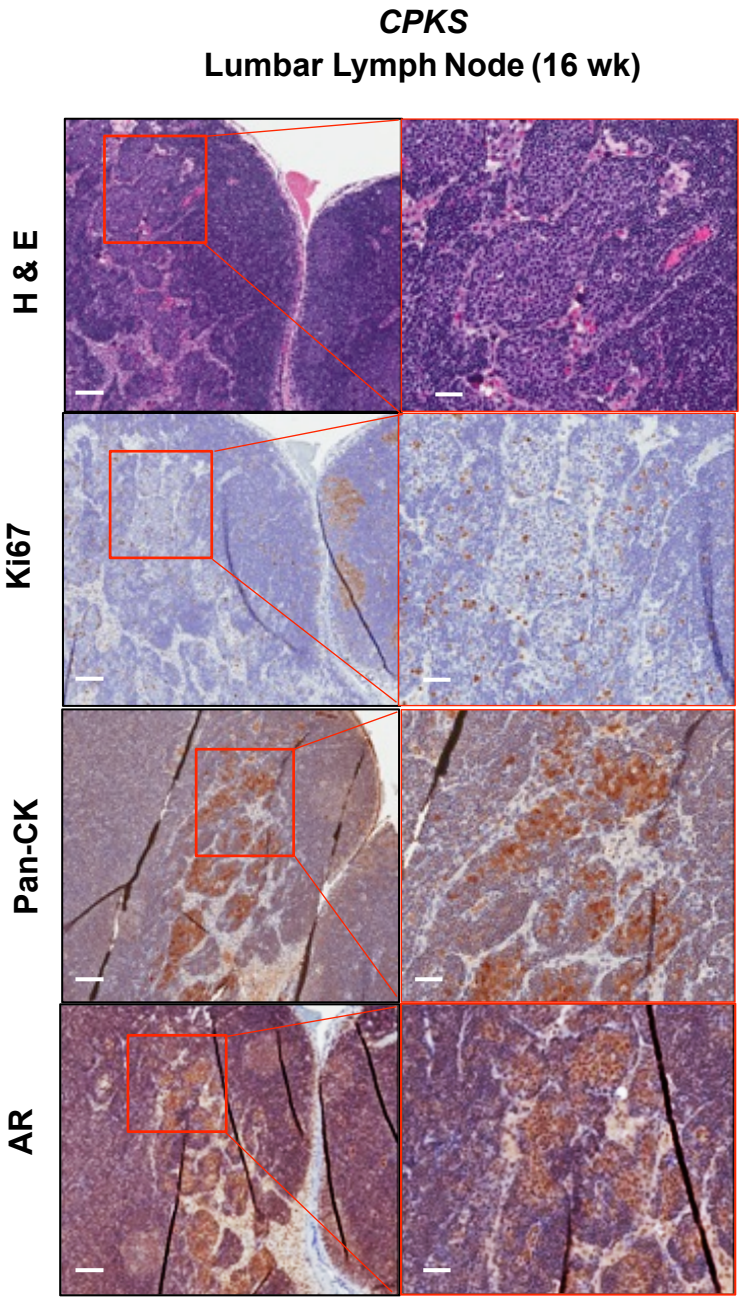

Figure S5. Lymph node metastases in *CPKS* mice. A representative lumbar lymph node from a 16-week old *CPKS* mutant stained with H&E and for Ki67, Pan-cytokeratin (Pan-CK), and AR by IHC. The higher magnification views are presented on the right panels. Low magnification scale bar, 100 μm; High magnification scale bar, 50 μm.

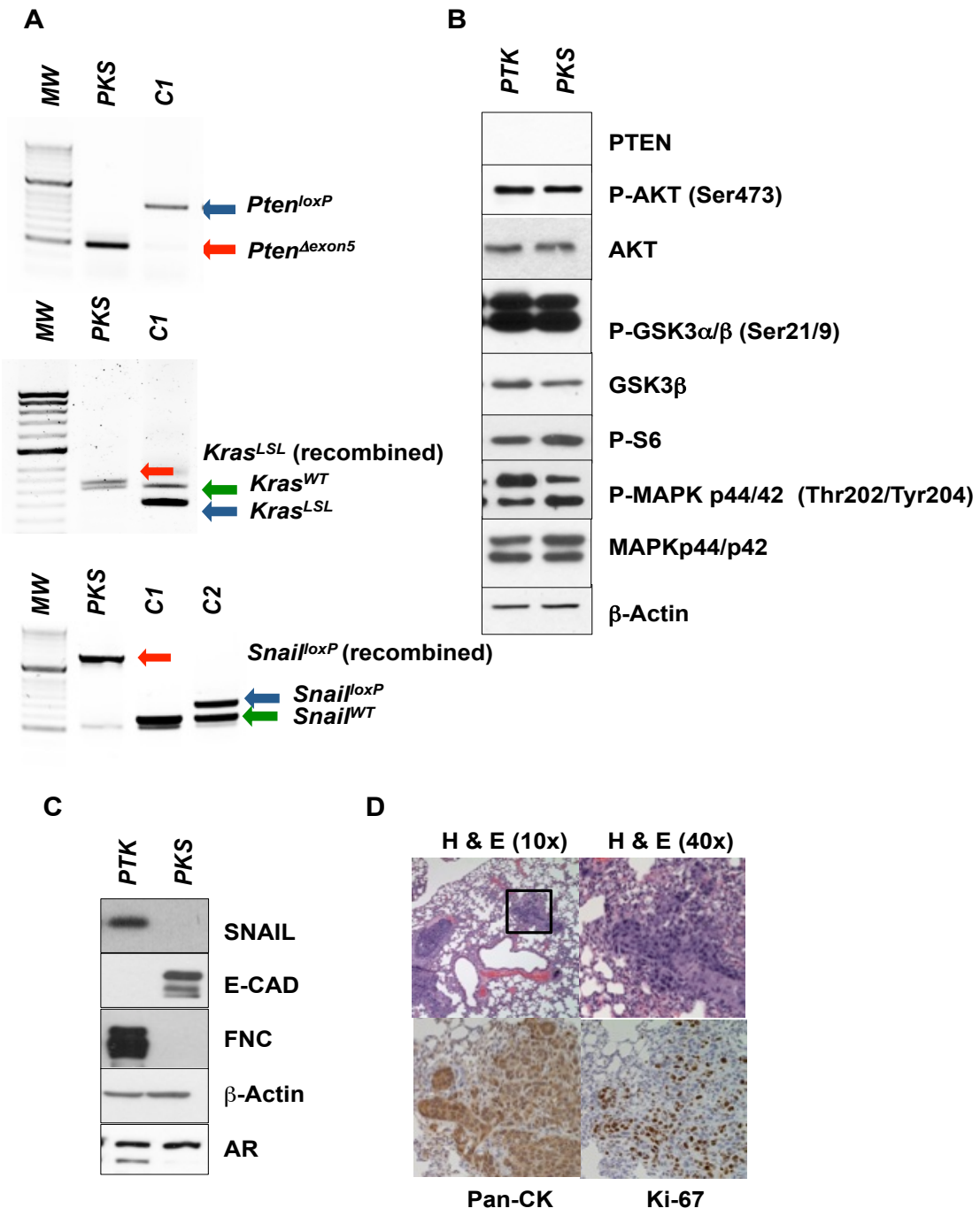

Figure S6. *PKS* cells are *Snail*-null, *Pten*-null, and have *Kras*^{G12D} activation and AR expression. (A) Genomic PCR analysis confirmed that *PKS* cells have *Pten* deletion, *Snail* deletion, and *Kras*^{G12D} activation induced by *in vitro* Cre recombination. Red arrows indicate the recombined allele. C1 (*Pten*$^{L/L}$;*Kras*$^{G12D/W}$;*Snai1*$^{L/L}$) and C2 (*Snai1*$^{L/+}$) are controls for the PCR products expected before Cre recombination. (B) Assessment of PI3K and MAPK pathway activation in *PTK* cells compared to *PKS* cells by immunoblot analysis. (C) Immunoblotting confirmed that *PKS* cells are devoid of SNAIL expression, have high E-cadherin expression, and do not express Fibronectin (FNC). The Androgen Receptor (AR) is expressed in both *PTK* and *PKS* cells. β-actin was used as a loading control. (D) A representative lung section from an *NSG* mouse transplanted orthotopically with *PKS-iS* cells. The metastatic lesion is stained with H&E, RFP, Pan-Cytokeratin (Pan-CK), and Ki67.

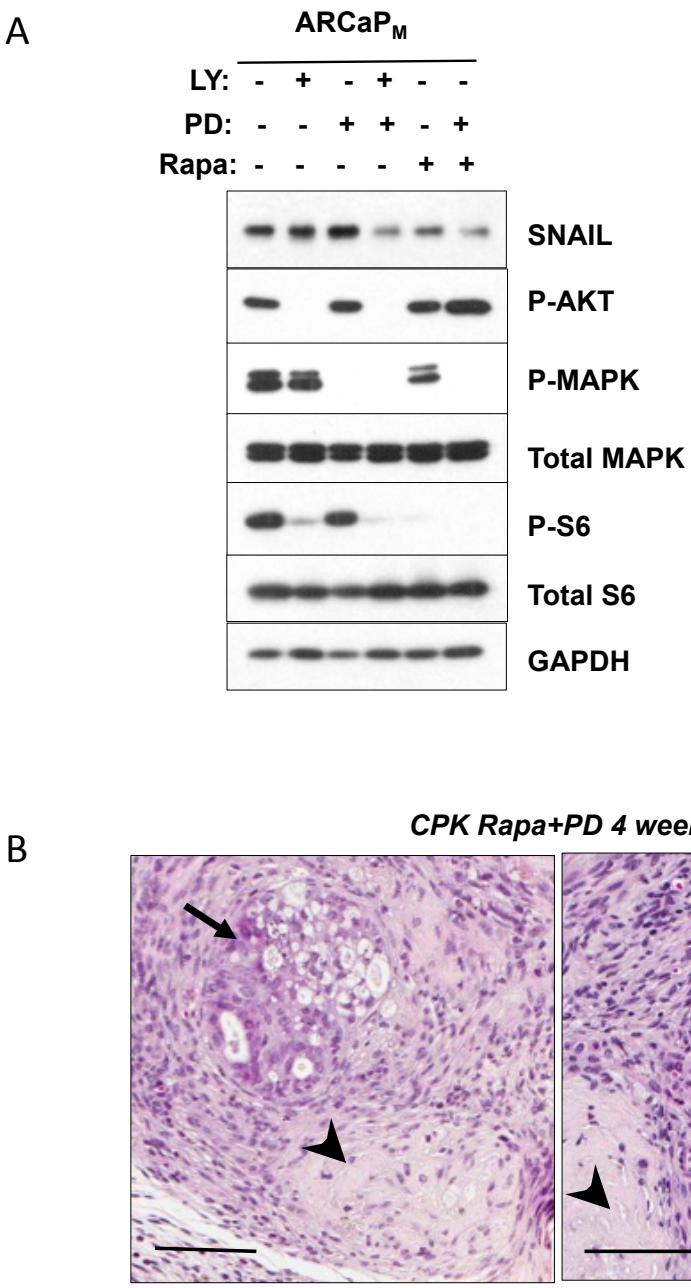

Figure S7. Combined PI3K and MAPK pathway inhibition reduces SNAIL expression and induces the degeneration of epithelial glandular structures. (A) ARCaPM cells were treated with LY294110 (40 uM), PD0325901 (100 nM), rapamycin (100 nM), or a combination of two inhibitors as indicated for 4 hours. Cell lysates were immunoblotted for SNAIL, phospho-AKT (Ser473), and phospho-Erk (Try204/202). GAPDH was used as a loading control. (B) H&E stained prostate from a *CPK* mouse after 4 weeks of dual treatment with rapamycin and PD0325901. Arrows, degenerated epithelial structures. Arrowheads, scar-like degenerated loci. Scale bar, 100 μm.

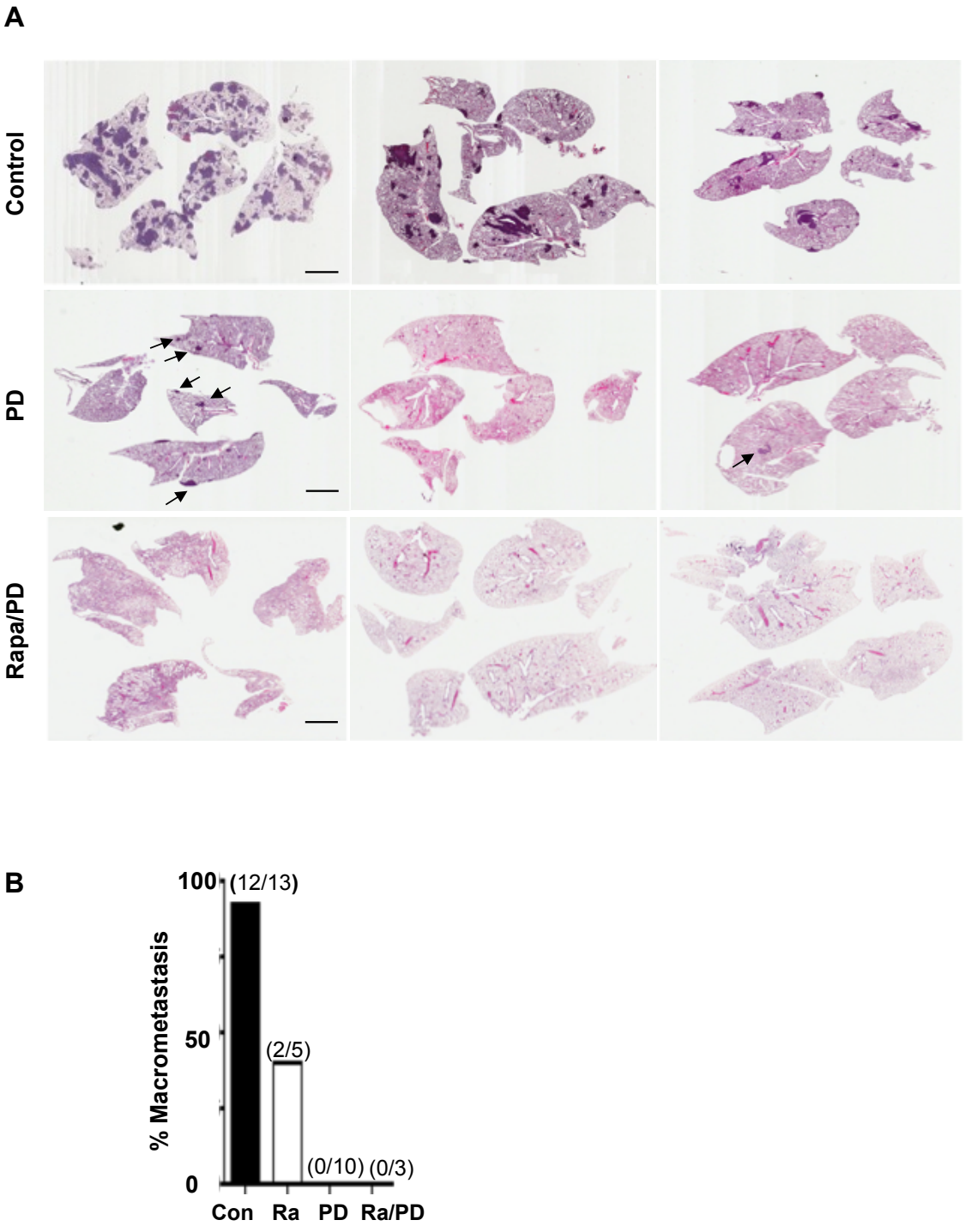

Figure S8. PD0325901 treatment prevents the formation of lung macrometastases. (A) H&E stained images of lung sections from vehicle (Control), PD0325901 (PD) alone, and rapamycin and PD0325901 treated (Rapa/PD) *NSG* mice orthotopically transplanted with *Pten*$^{-/-}$;*Kras*^{G12D}–*Luc* prostate sphere cells. Arrows in the PD-treated cohort point to micrometastases. Scale bar, 3mm. (B) The percent occurrence of lung macrometastasis, as detected by Bioluminescent Imaging (BLI) and gross histology, in animals orthotopically injected with *Pten*$^{-/-}$;*Kras*^{G12D}–Luc prostate sphere cells with or without drug treatment as indicated. Drug treatment was initiated 2 days after transplantation and administered daily for 3 weeks.

References

1. Wang D, Tindall DJ. Androgen action during prostate carcinogenesis. Methods Mol Biol. 2011;776:25-44.

2. Courtney KD, Taplin ME. The evolving paradigm of second-line hormonal therapy options for castration-resistant prostate cancer. Curr Opin Oncol. 2012;24:272-7.

3. Nelson PS. Molecular states underlying androgen receptor activation: a framework for therapeutics targeting androgen signaling in prostate cancer. J Clin Oncol. 2012;30:644-6.

4. Zhou BP, Deng J, Xia W, Xu J, Li YM, Gunduz M, et al. Dual regulation of Snail by GSK-3beta-mediated phosphorylation in control of epithelial-mesenchymal transition. Nature cell biology. 2004;6:931-40.

5. Tanaka H, Kono E, Tran CP, Miyazaki H, Yamashiro J, Shimomura T, et al. Monoclonal antibody targeting of N-cadherin inhibits prostate cancer growth, metastasis and castration resistance. Nat Med. 2010;16:1414-20.

6. Taylor BS, Schultz N, Hieronymus H, Gopalan A, Xiao Y, Carver BS, et al. Integrative genomic profiling of human prostate cancer. Cancer cell. 2010;18:11-22.

7. Mulholland DJ, Kobayashi N, Ruscetti M, Zhi A, Tran LM, Huang J, et al. Pten loss and RAS/MAPK activation cooperate to promote EMT and metastasis initiated from prostate cancer stem/progenitor cells. Cancer Res. 2012;72:1878-89.

8. Sun Y, Wang BE, Leong KG, Yue P, Li L, Jhunjhunwala S, et al. Androgen deprivation causes epithelial-mesenchymal transition in the prostate: implications for androgen-deprivation therapy. Cancer Res. 2012;72:527-36.

9. Lapointe J, Li C, Higgins JP, van de Rijn M, Bair E, Montgomery K, et al. Gene expression profiling identifies clinically relevant subtypes of prostate cancer. Proc Natl Acad Sci U S A. 2004;101:811-6.

10. De Craene B, Berx G. Regulatory networks defining EMT during cancer initiation and progression. Nat Rev Cancer. 2013;13:97-110.

11. Thiery JP, Acloque H, Huang RY, Nieto MA. Epithelial-mesenchymal transitions in development and disease. Cell. 2009;139:871-90.

12. Valastyan S, Weinberg RA. Tumor metastasis: molecular insights and evolving paradigms. Cell. 2011;147:275-92.

13. Nauseef JT, Henry MD. Epithelial-to-mesenchymal transition in prostate cancer: paradigm or puzzle? Nature reviews Urology. 2011;8:428-39.

14. Armstrong AJ, Marengo MS, Oltean S, Kemeny G, Bitting RL, Turnbull JD, et al. Circulating tumor cells from patients with advanced prostate and breast cancer display both epithelial and mesenchymal markers. Mol Cancer Res. 2011;9:997-1007.

15. Jiao J, Wang S, Qiao R, Vivanco I, Watson PA, Sawyers CL, et al. Murine cell lines derived from Pten null prostate cancer show the critical role of PTEN in hormone refractory prostate cancer development. Cancer Res. 2007;67:6083-91.

16. Zhau HE, Odero-Marah V, Lue HW, Nomura T, Wang R, Chu G, et al. Epithelial to mesenchymal transition (EMT) in human prostate cancer: lessons learned from ARCaP model. Clin Exp Metastasis. 2008;25:601-10.

17. Lukacs RU, Goldstein AS, Lawson DA, Cheng D, Witte ON. Isolation, cultivation and characterization of adult murine prostate stem cells. Nat Protoc. 2010;5:702-13.

18. Mulholland DJ, Tran LM, Li Y, Cai H, Morim A, Wang S, et al. Cell autonomous role of PTEN in regulating castration-resistant prostate cancer growth. Cancer cell. 2011;19:792-804.

19. Murray SA, Carver EA, Gridley T. Generation of a Snail1 (Snai1) conditional null allele. Genesis. 2006;44:7-11.

20. Grasso CS, Wu YM, Robinson DR, Cao X, Dhanasekaran SM, Khan AP, et al. The mutational landscape of lethal castration-resistant prostate cancer. Nature. 2012;487:239-43.

21. Subramanian A, Tamayo P, Mootha VK, Mukherjee S, Ebert BL, Gillette MA, et al. Gene set enrichment analysis: a knowledge-based approach for interpreting genome-wide expression profiles. Proc Natl Acad Sci U S A. 2005;102:15545-50.

22. Motwani M, Li DQ, Horvath A, Kumar R. Identification of novel gene targets and functions of p21-activated kinase 1 during DNA damage by gene expression profiling. PloS one. 2013;8:e66585.

23. Xu J, Wang R, Xie ZH, Odero-Marah V, Pathak S, Multani A, et al. Prostate cancer metastasis: role of the host microenvironment in promoting epithelial to mesenchymal transition and increased bone and adrenal gland metastasis. Prostate. 2006;66:1664-73.

24. Peinado H, Olmeda D, Cano A. Snail, Zeb and bHLH factors in tumour progression: an alliance against the epithelial phenotype? Nat Rev Cancer. 2007;7:415-28.

25. Heldin CH, Vanlandewijck M, Moustakas A. Regulation of EMT by TGFbeta in cancer. FEBS letters. 2012;586:1959-70.

26. Guaita S, Puig I, Franci C, Garrido M, Dominguez D, Batlle E, et al. Snail induction of epithelial to mesenchymal transition in tumor cells is accompanied by MUC1 repression and ZEB1 expression. J Biol Chem. 2002;277:39209-16.

27. Horiguchi K, Shirakihara T, Nakano A, Imamura T, Miyazono K, Saitoh M. Role of Ras signaling in the induction of snail by transforming growth factor-beta. J Biol Chem. 2009;284:245-53.

28. Matsuzaki K. Smad phosphoisoform signaling specificity: the right place at the right time. Carcinogenesis. 2011;32:1578-88.

29. Massague J. TGFbeta signalling in context. Nature reviews Molecular cell biology. 2012;13:616-30.

30. Brandl M, Seidler B, Haller F, Adamski J, Schmid RM, Saur D, et al. IKK(alpha) controls canonical TGF(ss)-SMAD signaling to regulate genes expressing SNAIL and SLUG during EMT in panc1 cells. J Cell Sci. 2010;123:4231-9.

31. Dummler B, Ohshiro K, Kumar R, Field J. Pak protein kinases and their role in cancer. Cancer Metastasis Rev. 2009;28:51-63.

32. Molli PR, Li DQ, Murray BW, Rayala SK, Kumar R. PAK signaling in oncogenesis. Oncogene. 2009;28:2545-55.

33. Yang Z, Rayala S, Nguyen D, Vadlamudi RK, Chen S, Kumar R. Pak1 phosphorylation of snail, a master regulator of epithelial-to-mesenchyme transition, modulates snail's subcellular localization and functions. Cancer Res. 2005;65:3179-84.

34. Vega S, Morales AV, Ocana OH, Valdes F, Fabregat I, Nieto MA. Snail blocks the cell cycle and confers resistance to cell death. Genes & development. 2004;18:1131-43.

35. Barrallo-Gimeno A, Nieto MA. The Snail genes as inducers of cell movement and survival: implications in development and cancer. Development. 2005;132:3151-61.

36. Kurrey NK, Jalgaonkar SP, Joglekar AV, Ghanate AD, Chaskar PD, Doiphode RY, et al. Snail and slug mediate radioresistance and chemoresistance by antagonizing p53-mediated apoptosis and acquiring a stem-like phenotype in ovarian cancer cells. Stem cells. 2009;27:2059-68.

37. Franco DL, Mainez J, Vega S, Sancho P, Murillo MM, de Frutos CA, et al. Snail1 suppresses TGF-beta-induced apoptosis and is sufficient to trigger EMT in hepatocytes. Journal of cell science. 2010;123:3467-77.

38. Kajita M, McClinic KN, Wade PA. Aberrant expression of the transcription factors snail and slug alters the response to genotoxic stress. Molecular and cellular biology. 2004;24:7559-66.

39. Dhasarathy A, Phadke D, Mav D, Shah RR, Wade PA. The transcription factors Snail and Slug activate the transforming growth factor-beta signaling pathway in breast cancer. PloS one. 2011;6:e26514.

40. Wang S, Gao J, Lei Q, Rozengurt N, Pritchard C, Jiao J, et al. Prostate-specific deletion of the murine Pten tumor suppressor gene leads to metastatic prostate cancer. Cancer cell. 2003;4:209-21.

41. Wang J, Kobayashi T, Floc'h N, Kinkade CW, Aytes A, Dankort D, et al. B-Raf activation cooperates with PTEN loss to drive c-Myc expression in advanced prostate cancer. Cancer research. 2012;72:4765-76.

42. Peinado H, Quintanilla M, Cano A. Transforming growth factor beta-1 induces snail transcription factor in epithelial cell lines: mechanisms for epithelial mesenchymal transitions. J Biol Chem. 2003;278:21113-23.

43. Zhang L, Zhou F, ten Dijke P. Signaling interplay between transforming growth factor-beta receptor and PI3K/AKT pathways in cancer. Trends Biochem Sci. 2013;38:612-20.

44. Thuault S, Tan EJ, Peinado H, Cano A, Heldin CH, Moustakas A. HMGA2 and Smads co-regulate SNAIL1 expression during induction of epithelial-to-mesenchymal transition. J Biol Chem. 2008;283:33437-46.

45. Beach S, Tang H, Park S, Dhillon AS, Keller ET, Kolch W, et al. Snail is a repressor of RKIP transcription in metastatic prostate cancer cells. Oncogene. 2008;27:2243-8.

46. Heeboll S, Borre M, Ottosen PD, Dyrskjot L, Orntoft TF, Torring N. Snail1 is over-expressed in prostate cancer. APMIS. 2009;117:196-204.

47. Mak P, Leav I, Pursell B, Bae D, Yang X, Taglienti CA, et al. ERbeta impedes prostate cancer EMT by destabilizing HIF-1alpha and inhibiting VEGF-mediated snail nuclear localization: implications for Gleason grading. Cancer Cell. 2010;17:319-32.

48. Whiteland H, Spencer-Harty S, Thomas DH, Davies C, Morgan C, Kynaston H, et al. Putative prognostic epithelial-to-mesenchymal transition biomarkers for aggressive prostate cancer. Experimental and molecular pathology. 2013;95:220-6.

49. Smith BN, Odero-Marah VA. The role of Snail in prostate cancer. Cell adhesion & migration. 2012;6:433-41.

50. Liu YN, Abou-Kheir W, Yin JJ, Fang L, Hynes P, Casey O, et al. Critical and reciprocal regulation of KLF4 and SLUG in transforming growth factor beta-initiated prostate cancer epithelial-mesenchymal transition. Mol Cell Biol. 2012;32:941-53.

51. Wu Y, Zhou BP. Snail: More than EMT. Cell adhesion & migration. 2010;4:199-203.

52. Qin J, Wu SP, Creighton CJ, Dai F, Xie X, Cheng CM, et al. COUP-TFII inhibits TGF-beta-induced growth barrier to promote prostate tumorigenesis. Nature. 2013;493:236-40.

53. Ding Z, Wu CJ, Chu GC, Xiao Y, Ho D, Zhang J, et al. SMAD4-dependent barrier constrains prostate cancer growth and metastatic progression. Nature. 2011;470:269-73.

54. Li X, Placencio V, Iturregui JM, Uwamariya C, Sharif-Afshar AR, Koyama T, et al. Prostate tumor progression is mediated by a paracrine TGF-beta/Wnt3a signaling axis. Oncogene. 2008;27:7118-30.

55. Yingling JM, Blanchard KL, Sawyer JS. Development of TGF-beta signalling inhibitors for cancer therapy. Nat Rev Drug Discov. 2004;3:1011-22.

56. Schiemann WP. Targeted TGF-beta chemotherapies: friend or foe in treating human malignancies? Expert Rev Anticancer Ther. 2007;7:609-11.

57. Zavadil J, Bitzer M, Liang D, Yang YC, Massimi A, Kneitz S, et al. Genetic programs of epithelial cell plasticity directed by transforming growth factor-beta. Proc Natl Acad Sci U S A. 2001;98:6686-91.

58. Galliher AJ, Neil JR, Schiemann WP. Role of transforming growth factor-beta in cancer progression. Future Oncol. 2006;2:743-63.

59. Ikushima H, Miyazono K. TGFbeta signalling: a complex web in cancer progression. Nat Rev Cancer. 2010;10:415-24.

60. Barron DA, Rowley DR. The reactive stroma microenvironment and prostate cancer progression. Endocr Relat Cancer. 2012;19:R187-204.

61. McKeithen D, Graham T, Chung LW, Odero-Marah V. Snail transcription factor regulates neuroendocrine differentiation in LNCaP prostate cancer cells. The Prostate. 2010;70:982-92.

62. Kim E, Youn H, Kwon T, Son B, Kang J, Yang HJ, et al. PAK1 tyrosine phosphorylation is required to induce epithelial-mesenchymal transition and radioresistance in lung cancer cells. Cancer Res. 2014;74:5520-31.

Chapter 5:

Tracking and functional characterization of epithelial-mesenchymal transition and mesenchymal tumor cells during prostate cancer metastasis

Introduction

Prostate cancer is the most commonly diagnosed male malignancy and the second leading cause of cancer-related death in Western men (1). Although localized prostate cancer is treatable, metastatic, late stage castration-resistant prostate cancer (mCRPC) is currently incurable and represents the major cause of prostate cancer-related death (2). Recent studies have focused on the processes and pathway alterations that cause prostate tumor cells to disseminate and metastasize. We and others have shown that activation of the PI3K/AKT and RAS/MAPK pathways is associated with metastatic prostate cancer, and that activation of both pathways is sufficient to induce distant metastasis and an epithelial-mesenchymal transition (EMT) at the primary tumor site in genetically engineered mouse models (3-5). The acquisition of an EMT phenotype within localized cancer has been demonstrated to be sufficient to trigger lethal metastatic disease (4, 6, 7) and promote CRPC (8-10) in multiple model systems.

EMT, in the context of cancer, allows epithelial cancer cells to acquire migratory and invasive characteristics, as well as overcome senescence, apoptosis, and anoikis, properties that are essential for tumor cell dissemination and distant metastasis (11). Moreover, recent studies have also implicated EMT in the acquisition of stem-like qualities (12-14) and drug resistance properties (15). However, evidence for the role of EMT in cancer stem cell formation and metastasis is mostly based on either *in vitro* manipulation of cultured cell lines to induce EMT or the expression of EMT signature markers in human cancer samples (10). Therefore, a direct role for EMT in prostate tumor progression, dissemination of circulating tumor cells (CTCs) into the blood stream, and seeding of metastases at distant sites remains unclear due to the lack of *in vivo* models that recapitulate the metastatic process.

We previously reported that deletion of the *Pten* tumor suppressor gene and conditional activation of the $Kras^{G12D}$ oncogene in the murine prostate epithelium (Pb-$Cre^{+/-}$;$Pten^{L/L}$;$Kras^{G12D/+}$) leads to 100% penetrable macrometastasis to the lungs and liver, and an EMT phenotype at the primary tumor site (4). Although the Pb-$Cre^{+/-}$;$Pten^{L/L}$;$Kras^{G12D/+}$ (*CPK*) prostate cancer mouse model recapitulates late-stage, metastatic human prostate cancer and associates EMT with prostate cancer metastasis, whether tumor cells that have undergone an EMT contribute directly to tumor progression, dissemination, and distant macrometastasis has yet to be established. In this study, we develop an *in vivo* system that allows tracking of the dynamic EMT program and isolation of cells from the *CPK* prostate cancer model that have either completed (mesenchymal-like) or are transitioning through an EMT for characterization and functional testing. Our *in vivo* analysis suggests that mesenchymal and epithelial states contribute to different stages of the prostate cancer disease, and that EMT tumor cells, which have the plasticity to readily transition between epithelial and mesenchymal lineages, are able to contribute to multiple stages of the metastatic cascade.

Materials and Methods

Mouse strains

Vim-GFP reporter mice were purchased from GENSAT (16). After crossing *Vim-GFP* mice with the $Cre^{+/-};Pten^{L/L};Kras^{G/+}$ model (4), $Pb\text{-}Cre^{+/-};Pten^{L/L};Kras^{+/+};Vim\text{-}GFP$ male mice were crossed with $Pb\text{-}Cre^{-};Pten^{L/L};Kras^{G12D/+}$ female mice to generate the $Cre^{-};Pten^{L/L};Kras^{G/+};Vim\text{-}GFP$ (*V*), $Cre^{+/-};Pten^{L/L};Kras^{+/+};Vim\text{-}GFP$ (*CPV*), and $Cre^{+/-};Pten^{L/L};Kras^{G/+};Vim\text{-}GFP$ (*CPKV*) mouse models. These strains have been maintained on a mixed strain background. All studies with animals were performed under the regulation of the division of Laboratory Animal Medicine at the University of California at Los Angeles (UCLA).

Histology and immunohistochemistry

Immunohistochemistry (IHC) was performed on formalin-fixed, paraffin-embedded tissues. Antigen retrieval was performed by boiling sections in 10mM citrate buffer (pH6) for 30 minutes. The following primary antibodies were used: Vimentin (Cell Signaling; 5741), GFP (Cell Signaling; 2955), E-cadherin (BD Biosciences; 610181), P-S6 (Cell Signaling; 2215), PTEN (Cell Signaling; 9559), Ki67 (Vector Laboratories; VP-RM04), CK5 (Covance; PRB-160P), CK8 (Covance; MMS-162P), Synaptophysin (Dako; A0010), and Pan-Cytokeratin (Sigma; C1801).

Matrigel invasion assay

8μm transwell inserts (BD Biosciences) were coated with Matrigel (300 μg/ml) (BD Biosciences) and placed into 24-well culture plates. 5 X 10^4 sorted cells per population were resuspended in

serum free media in the top chamber, while full serum media (Dulbecco's modified eagle medium (DMEM) with 10% Fetal Bovine Serum (FBS)) was used in the bottom chamber. 24 hours later, invaded cells were fixed with methanol, stained with 0.2% crystal violet, and counted using a light microscope at 10X magnification.

Matrigel sphere assay

The Matrigel sphere assay was carried out as previously described (17). 5 X 10^3 sorted cells from each cell population were plated in triplicate.

BrdU pulse labeling

BrdU pulse labeling was carried out as previously described (18). 2 x 10^4 FACS sorted cells per population were cytospun onto coated cytoslides (Thermo Scientific) at 500 rpm for 5 minutes using Cytospin4 (Thermo Scientific). Cells were fixed with 4% paraformaldehyde for 15 minutes, and stained with a BrdU (BD Biosciences; 563445) primary antibody. 10 fields per slide were counted at 20x magnification.

Subcutaneous tumor regeneration assay

Prostate lobes/regions from *CPKV* mice were separated as described (Fig. 3B), serrated, mixed with Matrigel, and transplanted subcutaneously into *NOD/SCID/IL2Rγ-null* (*NSG*) mice. Once tumors reached 2 cm in size, mice were euthanized, and tumors were again serrated, mixed with Matrigel, and passaged into new recipient hosts.

Orthotopic tumor regeneration assay

5 x 10^3 sorted cells per population were mixed in 50% Matrigel/media, loaded into a 10 µl Hamilton syringe (Microliter), and 2.5 x 10^3 cells were injected into each anterior lobe of the prostates of recipient *NSG* mice.

Tail vein injections

2.5 x 10^4 or 1 x 10^5 sorted cells from each population were resuspended in 200 µl of PBS and injected intravenously into *NSG* hosts. The presence of lung macrometastases was assessed by gross examination of formalin-fixed lung samples under a dissecting microscope.

DNA isolation and genomic PCR

DNA was isolated using the Qiagen AllPrep DNA/RNA Micro Kit. Primer sequences are as follows: *Pb-Cre* F, CGTATAGCCGAAATTGCCAG, R, CAAAACAGGTAGTTATTCGG; *Pte*n F, TCCCAGAGTTCATACCAGGA, R1, GCAATGGCCAGTACTAGTGAAC, R2, AATCTGTGCATGAAGGGAAC; *Kras* F, GTCTTTCCCCAGCACAGTGC, R1, CTCTTGCCTACGCCACCAGCTC, R2, AGCTAGCCACCATGGCTTGAGTAAGTCTGC.

Real time PCR

Total RNA from epithelial, EMT, and mesenchymal-like tumor cells sorted from *CPKV* prostates was isolated using the Qiagen AllPrep DNA/RNA Micro Kit and reverse transcribed into cDNA using the High-Capacity cDNA Reverse Transcription Kit with Multiscribe Reverse Transcriptase (Applied Biosystems). Transcript levels were assessed with quantitative real-time PCR with mouse gene specific RT-PCR primers and iQ™ SYBR® Green Supermix (Bio-Rad) using the CFX Real-Time PCR detection System (Bio-Rad) and normalized against β-actin

expression. The relative expression levels were derived from the delta-delta Ct values using the CFX software (Bio-Rad) and compared to expression levels from epithelial tumor cells. Primer sequences are as follows: *B-Actin* F, GGCTGTATTCCCCTCCATCG, R, CCAGTTGGTAACAATGCCATGT; *Vim* F, CGGCTGCGAGAGAAATTGC, R, CCACTTTCCGTTAAGGTCAAG; *Snai1* F, AAGATGCACATCCGAAGC, R, ATCTCTTCACATCCGAGTGG; *Zeb1* F, CATGTGACCTGTGTGACAAG, R, GCGGTGATTCATGTGTTGAG; *Cdh2* F, CAGGTCTCCTCATGGCTTTGC, R, CTTCCGAAAAGAAGGCTGTCC ; *Mmp2* F, CACCTACACCAAGAACTTCC, R, GAACACAGCCTTCTCCTCCT ; *Cdh1* F, AATGGCGGCAATGCAATCCCAAGA, R, TGCCACAGACCGATTGTGGAGATA; *Sox5* F, GCGATGGGGATCTGTGCTTG, R, CCCGGACTACAAGTACAAGCC; *Sox9* F, GACAAGCGGAGGCCGAA, R, CCAGCTTGCACGTCGGTT; *Sox10* F, CACCGGCACCCAGAAGAAG, R, GAAGTCGATGTGGGGCTTCC; *Sox17* F, TGAAATATGGCCCACTCACA, R, ACAGTAGCGGGTCCAGAATG; *Klf2* F, ACCAAGAGCTCGCACCTAAA, R, GTGGCACTGAAAGGGTCTGT; *Klf4* F, GTGCCCCGACTAACCGTTG, R, GTCGTTGAACTCCTCGGTCT; *Nestin* F,AGCAGGAGAAGCAGGGTCTA, R, CTGGGAACTTCTTCCAGGTG; *Bmi1* F, AATCCCCACCTGATGTGTGT, R, GCTGGTCTCCAGGTAACGAA; *Lrig1* F, CCCCACATACAACAGCACAC, R, GTATGAGACCCATCCGCAGT; *Wnt2* F, CCAACGAAAAATGACCTCGT R, TCATAGCCTCTCCCACAACA; *Wnt10b* F, GAAAACCTGAAGCGGAAGTG R, AGAGTTGCGGTTGTGGGTAT; *Axin2* F, AGGATGCTGAAGGCTCAAAG, R, GCTCAGTCGATCCTCTCCAC; *Wnt5a* F, GGTGCCATGTCTTCCAAGTT, R, ATCACCATGCCAAAGACAGA; *Fzd3* F, AGGGACATCCACACATGCTT, R,

ATGCTGCCGTGAGGTAGTCT; *Notch3* F, CTATGCTAGAGCGGATGCAG, R, TGCCAGGATCAGTGCAGTAG; *Notch4* F, CACCCCACTTCACACTGCT, R, TCTTCAACCAGGTCCTCCAC; *Hey1* F, CACCTGAAAATGCTGCACAC, R, TGGGATGCGTAGTTGTTGAG; *Hey2* F, TGAAGATGCTCCAGGCTACA R, GCACAGGTGCTGAGATGAGA.

Tissue dissociation and single cell suspension.

Single cell suspensions were prepared from prostates of age- and genetic background-matched *V*, *CPV*, and *CPKV* mice at the indicated time points. Prostates were minced in sterile tissue culture dishes, and subjected to collagenase I (1 mg/ml; Invitrogen) digestion overnight at 37°C with constant agitation in Dulbecco's modified eagle medium (DMEM) (Sigma) containing 1% Pen/Strep, 10% Fetal Bovine Serum (FBS) (Omega Scientific), 4 mM L-glutamine (Fisher Scientific), 10mM Hepes, 25 μg /mL bovine pituitary extract, 5 μg /mL insulin (Invitrogen), 6 ng/mL recombinant human EGF (BD Biosciences), and 10 μM Rocki (Y27632; Abcam). Undigested tissue was trypsinized for 5 minutes at 37° C, passed through a 18G and 21G syringe 5 times, and filtered through a 40 μm filter (Fischer Scientific) to facilitate dissociation, followed by washes in PBS and resuspension in DMEM media plus 10% FBS.

FACS analysis and cell sorting

Single-cell suspensions were stained with the following directly conjugated antibodies: CD45-PE (eBioscience; 12-0451-81), CD31-PE (Biolegend; 102407), Ter119-PE (Biolegend; 116207), Epcam-APC-cy7 (Biolegend; 118218), CD49f-Alexa 647 (Biolegend; 313610), Sca-1-PE-cy7

(Biolegend; 122513), and CD44-PE-Cy7 (Biolegend; 103030). 7-AAD (BD Biosciences) was used to gate out dead cell fractions.

Flow cytometric analysis was performed on a FACS Canto II (BD Biosciences) and data were analyzed using BD FACS Diva software (BD Biosciences). For isolation of epithelial, EMT, and mesenchymal-like tumor cells from the prostate and blood of Vim-GFP reporter mouse models, single-cell suspensions were stained with directly conjugated antibodies against CD45, CD31, Ter119, and Epcam, and sorted on a FACSAria (BD Biosciences) as $7AAD^{-}CD45^{-}CD31^{-}Ter119^{-}Epcam^{+}GFP^{-}$, $7AAD^{-}CD45^{-}CD31^{-}Ter119^{-}Epcam^{+}GFP^{+}$, and $7AAD^{-}CD45^{-}CD31^{-}Ter119^{-}Epcam^{-}GFP^{+}$ cell fractions, respectively. LSC^{hi} cells were sorted from $7AAD^{-}CD45^{-}CD31^{-}Ter119^{-}Sca\text{-}1^{+}CD49f^{hi}$ cell fractions. Cells were collected in DMEM plus 50% FBS.

CTC and iCTC isolation

For isolation of CTCs by FACS, 100 µl of peripheral blood was extracted from mice through retro-orbital bleeding and incubated in RBC lysis buffer (Biolegend) for 10 minutes. Cells were then washed with PBS, passaged through a 40 µm filter (Fisher Scientific), and resuspended in DMEM media plus 10% FBS prior to FACS analysis.

For iCTC isolation, 100 µl of blood from each mouse was cultured on a Vita-assay 96-well plate coated with fluorescent red CAM (Vitatex; AR96W) for 10 days as previously described (19). $TRITC^{+}$ iCTCs were quantified by flow cytometry.

Statistical analysis

Graphpad Prism software was used to calculate mean and standard deviation. Student's *t*-test was used to calculate the statistical significance between the two groups of data. $P < 0.05$ is considered significant.

Results

Tracking EMT and mesenchymal-like tumor cells in an endogenous prostate cancer model using a *Vimentin-GFP* reporter line

In order to generate an *in vivo* tracking system to study the role of EMT in prostate cancer progression and metastasis, we crossed *Vimentin-GFP* mice (16) with the *Pb-Cre*$^{+/-}$*;Pten*$^{L/L}$*;Kras*$^{G12D/+}$ (*CPK*) murine model of prostate cancer (4) we recently developed to create the *Pb-Cre*$^{+/-}$*;Pten*$^{L/L}$*;Kras*$^{G12D/+}$;*Vim-GFP* model (*CPKV*). *Vimentin-GFP* reporter mice, in which GFP expression is driven from the endogenous Vimentin promoter on a bacterial artificial chromosome (BAC) (16), were chosen because Vimentin is one of the earliest upregulated genes during the EMT process (20), and its expression is associated with high Gleason scores, disease recurrence, and bone metastasis in human prostate cancers (21, 22).

In 10-12 week old *CPKV* prostates, GFP staining overlaps with endogenous Vimentin expression, which marks EMT regions within the stromal compartment surrounding GFP-negative epithelial glandular structures (Fig. 1A). These EMT regions also contain cells that are PTEN$^-$ and P-S6$^+$, a surrogate marker for PTEN loss and activation of the PI3K pathway, confirming that these cells were originally derived from *Pten*$^{loxp/loxp}$ prostate epithelial cells that underwent Cre recombination (Fig. 1A). As it is possible that endogenous stromal cells in the prostate, including CD45$^+$ leukocytes, also express P-S6$^+$, we stained prostate sections from 4 week old *CPKV* mice, a time-point when these mice have not yet developed invasive prostate tumors or an EMT phenotype, to identify if Vimentin$^+$/GFP$^+$ stromal cells in the prostate normally express P-S6$^+$. Indeed, Vimentin$^+$/GFP$^+$ stromal cells in these prostates were PTEN$^+$ and P-S6$^-$ (Fig. S1A). Moreover, in WT *Vim-GFP* (V) prostates, all Vimentin$^+$ /GFP$^+$ stromal

cells are also P-S6$^-$ (Fig. S1B). These results verify that P-S6 can be used as a marker in our *CPKV* model to distinguish Vimentin$^+$/GFP$^+$/PTEN$^+$ stromal cells from Vimentin$^+$/GFP$^+$/PTEN$^-$ EMT cells derived from the *Pten*$^{-/-}$ prostate epithelium.

In order to isolate and characterize tumor cells with epithelial and mesenchymal characteristics from the prostates of *CPKV* mice, a FACS gating strategy was designed in which the epithelial cell adhesion molecule (EpCAM) was used as an epithelial marker and GFP as a mesenchymal marker (Fig. S1A). Cells from *CPKV* prostates were first negatively selected from CD45$^+$, CD31$^+$, and Ter119$^+$ fractions (referred to as Lin$^-$) in order to avoid contamination from leukocyte, endothelial, and erythrocyte populations, respectively, as these cell types are known to express Vimentin (20). While age-matched WT *Vim-GFP* (*V*) (n=8) and *Pb-Cre*$^{+/-}$*;Pten*$^{L/L}$;Vim-GFP (*CPV*) (n=8) mutant prostates have a very rare population of cells that are EpCAM$^-$/GFP$^+$, which we will refer to as mesenchymal-like (MES-like) tumor cells, *CPKV* mutants (n=13) have a significant induction of the MES-like tumor cell population by 10 weeks of age (Fig. 1B; Fig. S1C). Interestingly, a significant population of cells that co-express both epithelial and mesenchymal markers (EpCAM$^+$GFP$^+$), hereafter referred to as EMT tumor cells, could also be isolated from 10-12 week old *CPKV*, and, to a small extent, *CPV* prostates, but not *V* prostates (Fig. 1B; Fig. S1C). While there was a marginal increase in the percentage of EpCAM$^+$GFP$^-$ epithelial cells within *CPV* and *CPKV* prostates compared to *V* prostates, this change was not significant (Fig. 1B; Fig. S1A). Genomic PCR analysis confirmed that all three FACS isolated tumor cell populations were indeed derived from epithelial cells that initially underwent Cre recombination, as they exhibit *Pten* deletion and *Kras* activation (Fig. S1D).

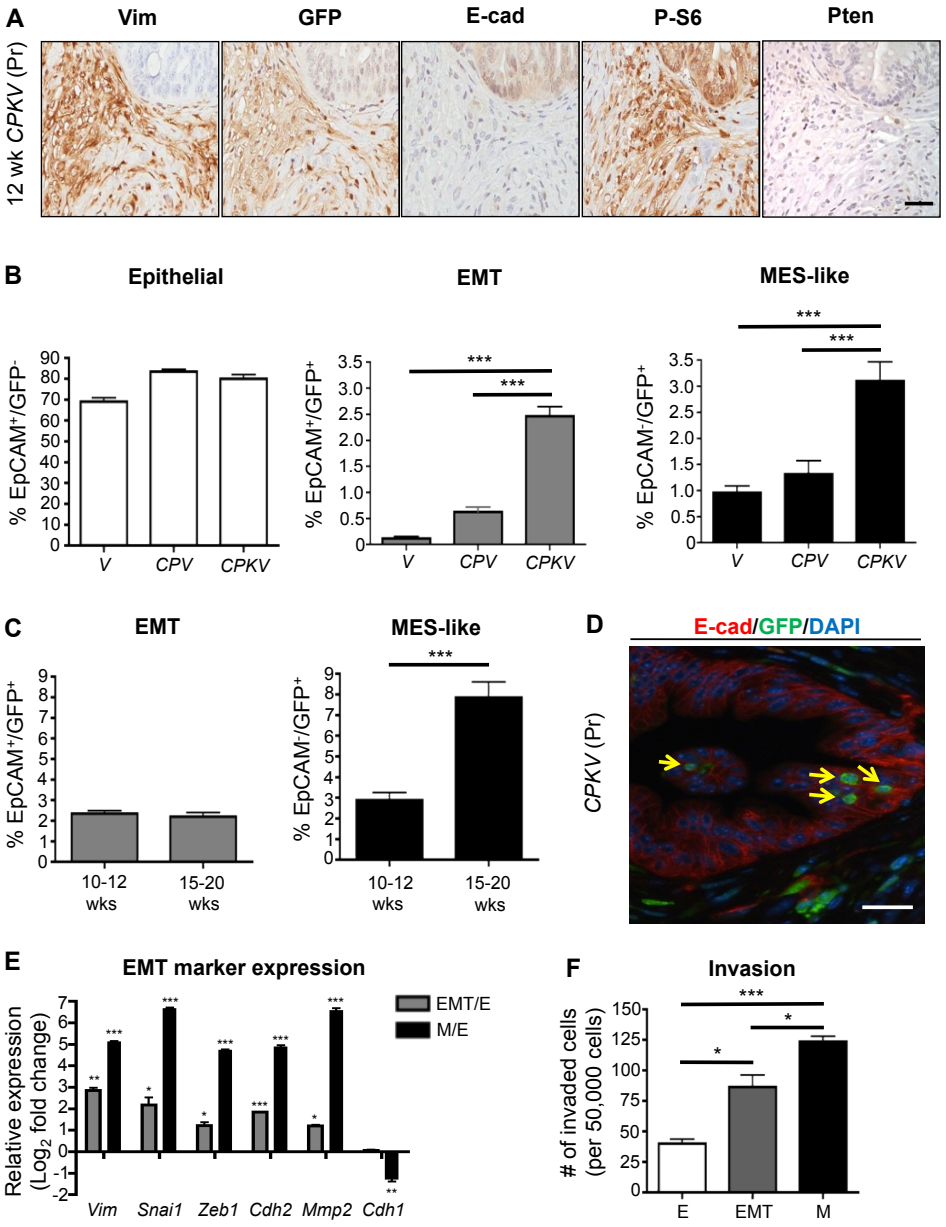

Figure 1. **Tracking EMT and mesenchymal-like tumor cells in an endogenous prostate cancer model using a *Vimentin-GFP* reporter line.** (A) Prostates from *CPKV* mice (12 weeks) display EMT regions that are Vimentin (Vim)/GFP-positive surrounding E-cadherin (E-cad)-positive epithelial glandular structures. P-S6 marks cells that have undergone Cre recombination. (B) Vimentin-GFP (GFP) and EpCAM were used to characterize epithelial ($EpCAM^+/GFP^-$), EMT ($EpCAM^+/GFP^+$), and MES-like ($EpCAM^-/GFP^+$) cell populations from the prostates of various *Vim-GFP* reporter mice (10-12 weeks) by FACS. *CPKV* mice have significant expansion of EMT and MES-like tumor cell populations. (C) Expansion of MES-like tumor cell populations in *CPKV* prostates during late stage tumor progression (15-20 weeks). (D) EMT tumor cells (yellow arrow) that are GFP^+ (green) and E-cadherin $(E\text{-cad})^+$ (red) are found within epithelial glandular structures in *CPKV* prostates (12 weeks). (E) qPCR analysis confirms EMT signature gene expression in EMT and MES-like tumor cells isolated from *CPKV* prostates (10-12 weeks). (F) Matrigel invasion assay reveals that EMT and MES-like tumor cells isolated from *CPKV* prostates (10-12 weeks) are significantly more invasive than epithelial tumor cells. Data in B, C, E, and F are represented as mean ± SEM. Bar, 50 μm. Pr, prostate. Lin^-,$CD45^-/CD31^-/Ter119^-$. *, $p< 0.05$, **, $p< 0.01$. ***, $p< 0.001$.

To assess the association of the EMT and MES-like tumor cell populations with prostate cancer progression, we compared 10-12 week old *CPKV* mutants (n=11), which have begun to develop poorly differentiated EMT morphology, to late stage 15-20 week old mutants (n=9) with sarcomatoid morphology (4). While there was a significant expansion of MES-like tumor cells during tumor progression, there was no change in the percentage of EMT tumor cells in the 15-20 week old mutants (Fig. 1C), indicating that EMT tumor cells may indeed represent a transition stage. Histologically, rare EMT tumor cells that co-expressed both epithelial (E-cadherin; red) and mesenchymal markers (Vim-GFP; Green) were found within epithelial acinar structures, indicating that the early steps of the EMT process do not occur exclusively along the leading edge of the tumor (Fig. 1D, yellow arrows).

Finally, we confirmed that $EpCAM^{+}/GFP^{+}$ and $EpCAM^{-}/GFP^{+}$ cell populations isolated from *CPKV* prostates indeed display EMT signature gene expression by qPCR analysis. While both EMT and MES-like tumor cells had induced expression of EMT signature genes compared to epithelial tumor cells, MES-like prostate tumor cells displayed more dramatically increased expression of the EMT transcription factors *Snail* and *Zeb1*, as well as a switch from E-cadherin (*Cdh1*) to N-cadherin (*Cdh2*) expression (Fig. 1E). MES-like tumor cells were also significantly more invasive *ex vivo* compared to epithelial tumor cells, with EMT tumor cells displaying an intermediate invasive capacity (Fig. 1F). Taken together, we have developed a novel system by using a *Vim-GFP* reporter to faithfully track the dynamics of the EMT program and to isolate and characterize cells undergoing or having undergone an EMT in an endogenous prostate cancer model.

EMT and mesenchymal-like tumor cells have enhanced stemness properties

To explore whether EMT and MES-like tumor cells from an endogenous prostate cancer model have enhanced stemness qualities, tumor cell populations from primary *CPKV* prostates were isolated by FACS and grown in Matrigel cultures to assess their ability to form spheres, an *in vitro* assay used to assess stemness characteristics (17). Indeed, EMT tumor cells could generate significantly more spheres than both epithelial and MES-like tumor cells (Fig. 2A). The EMT tumor cell subpopulation also contained a higher proportion of $Lin^{-}Sca1^{+}CD49f^{high}$ (LSC^{hi}) stem/progenitor cells (Fig. 2B), which have been previously shown to have a basal cell phenotype, high sphere-forming activity, and be sufficient to initiate tumorigenesis and metastasis (4, 23). These findings suggest that EMT tumor cells may represent a subpopulation of tumor cells with enhanced stemness qualities.

Compared to both epithelial and EMT tumor cell populations, MES-like tumor cells had reduced *in vitro* sphere-forming capacity (Fig. 2A). However, MES-like tumor cells had significantly increased expression of genes involved in maintenance of the stem cell state, including the *Sox* family members *Sox5*, *Sox9*, *Sox10*, and *Sox17*, the reprogramming factors *Klf2* and *Klf4*, the self-renewal maintenance factors *Bmi1*, *Nestin*, and *Lrig1*, and members of the WNT and NOTCH developmental pathways, suggesting that MES-like tumor cells may also harbor stemness qualities (Fig. 2C and 2D). One possible explanation for their poor sphere-forming capacity may be that MES-like tumor cells exist in a quiescent state and therefore have less capacity to proliferate and form sphere structures (24, 25). To test this hypothesis, we pulse labeled CPKV mice with 5-bromo-2'-deoxyuridine (BrdU) for 24 hours prior to FACS sorting to assess the percentage of cycling cells in each population. While the epithelial and EMT tumor cell populations had a high percentage of cells in S-phase, the MES-like

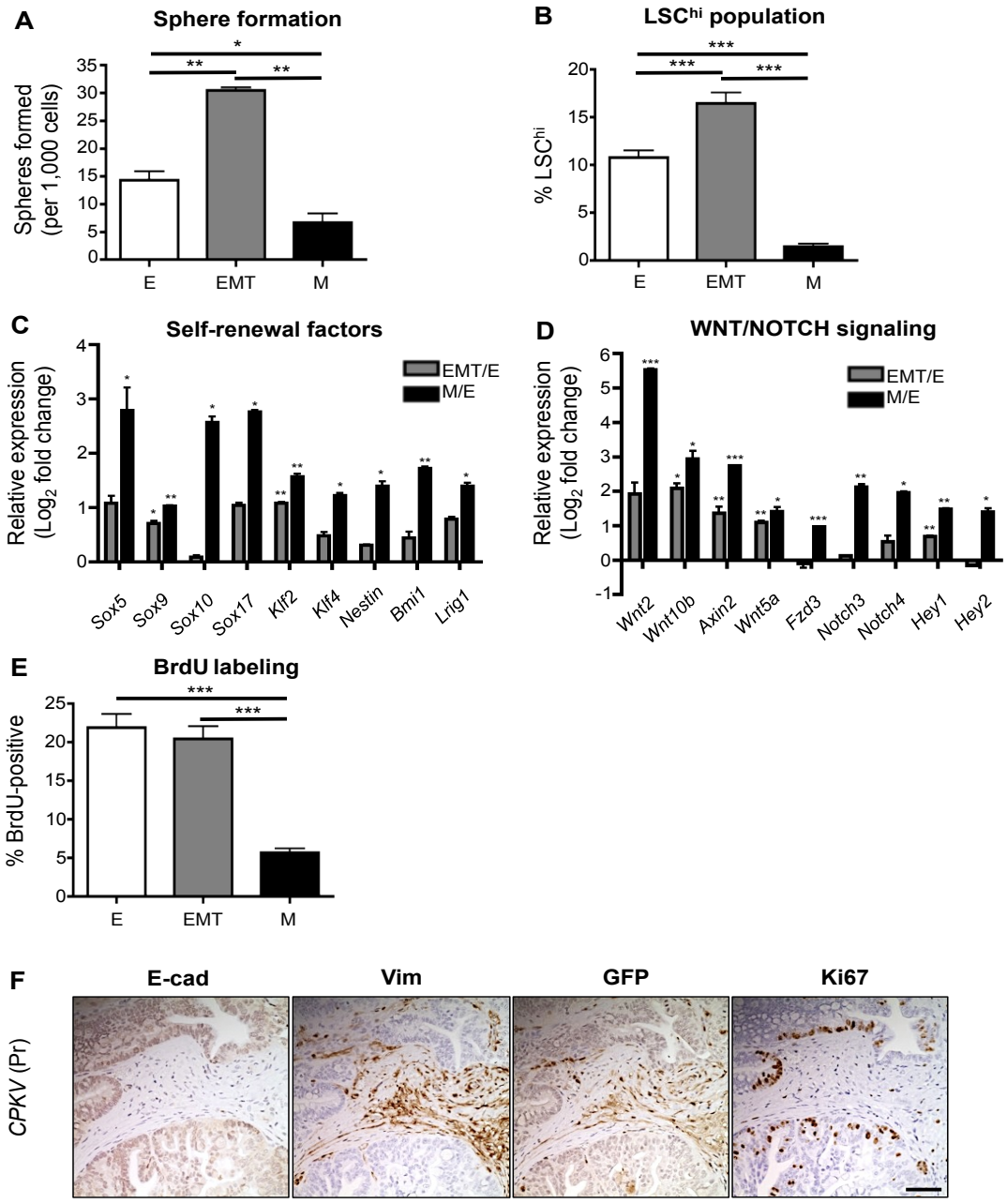

Figure 2. EMT and mesenchymal-like tumor cells have enhanced stemness properties. (A) Matrigel sphere assay reveals that EMT tumor cells sorted from *CPKV* prostates (10-12 weeks) form more spheres than epithelial and MES-like tumor cells after 7 days in culture. (B) EMT tumor cells have a higher LSC^{hi} content compared to epithelial and MES-like tumor cells from *CPKV* prostates (10-12 weeks), as quantified by FACS. (C) EMT and MES-like tumor cells from *CPKV* prostates (10-12 weeks) have enhanced expression of self-renewal and stemness factors compared to epithelial cells. (D) EMT and MES-like tumor cells from *CPKV* prostates (10-12 weeks) have enhanced expression of genes involved in WNT and NOTCH signaling compared to epithelial cells. (E) Epithelial and EMT tumor cells from *CPKV* prostates (10-12 weeks) have a higher percentage of cells in S-phase compared to MES-like tumor cells, as measured by the percentage of $BrdU^{+}$ cells. (F) Ki67-positive cells are found preferentially in E-cadherin (E-cad)-positive glandular structures compared to Vimentin (Vim)/GFP-positive EMT regions in the stroma of *CPKV* prostates (12 weeks). Data in A through E are represented as mean ± SEM. Bar, 100 μm. Pr, prostate. *, $p<0.05$, **, $p<0.01$. ***, $p<0.001$.

tumor cell population had a much lower percentage of cycling cells (Fig. 2E). In support of this finding, our Ki67 immunohistochemical analysis revealed that E-cadherin-positive glandular structures are more proliferative than GFP-positive mesenchymal regions in the stroma (Fig. 2F). In summary, both EMT and MES-like tumor cells from *CPKV* mutants have enhanced stemness characteristics, with EMT tumor cells displaying a proliferative, stem/progenitor cell phenotype, and MES-like tumor cells exhibiting a quiescent stem cell phenotype.

Prostate regions enriched in Vim-GFP$^+$ cells are able to regenerate transplantable tumors *in vivo*

As prostate stem cells have been previously shown to reside in the proximal region of the prostate attached to the urethra (24), we next wanted to ascertain if EMT and MES-like tumor cells were also enriched in this stem cell niche. Gross fluorescent imaging of whole *CPKV* prostates revealed that Vim-GFP expression was most prominent in the proximal anterior lobes, and, interestingly, in the anterior portion of the urethra itself (Fig. 3A). When distinct anatomical regions of the prostate were separated from 10-week old *CPKV* mice with established tumors (Fig. 3B) and subjected to quantitative FACS analysis, the percentage of MES-like tumor cells was significantly higher in the proximal region of the anterior lobes and the anterior portion of the urethra, the regions immediately connected to the proximal region of the prostate, compared to other regions of *CPKV* prostates (Fig. 3C, right panel, n=3). Although the percentage of EMT tumor cells was slightly higher in the proximal region of anterior lobes, the percentage of EMT tumor cells did not change dramatically between the different regions of the prostate (Fig. 3C, left panel, n=3). This data suggests that MES-like tumor cells may indeed have properties of quiescent stem cells, which are localized to specific stem cell niches.

To test whether the regions of *CPKV* prostates with the highest percentage of EMT and MES-like tumor cells also have the highest tumor-initiating capacity, regions/lobes were separated from 10-week old *CPKV* prostates, mixed with matrigel, and implanted subcutaneously into *NOD/SCID/IL2Rγ-null* (*NSG*) mice. Remarkably, the only regions that were able to form subcutaneous tumors *in vivo* were from the proximal region of the anterior gland and anterior portion of the urethra, the same regions with the highest percentage of EMT and MES-like tumor cells (Fig. 3D, n=4). Tumors from both regions were able to be serially passaged, and these passaged tumors contained all 3 prostatic cell lineages ($CK5^+$ basal, $CK8^+$ luminal, and $Synaptophysin^+$ neuroendocrine cells) (Fig. S2), demonstrating that stem cells within these regions have the capacity to regenerate all prostate lineages.

EMT and mesenchymal-like tumor cells have enhanced tumor-initiating capacity and cellular plasticity *in vivo*

In order to directly assess the tumor-initiating capacity of epithelial, EMT, and MES-like tumor cells isolated from *CPKV* mice, 5,000 sorted cells from each population were implanted orthotopically into the anterior lobes of *NSG* mice and allowed to incubate up to 6 months (Fig. 4A). Tumor pathology was defined histologically by the presence of abnormal glandular structures, stromal expansion, and positive staining for P-S6 and Ki67, which should not be present in normal prostate tissue (Fig. 4C and 4D; Fig. S3A). While EMT and MES-like tumor cells have a high tumor-initiating capacity *in vivo*, with 6/9 and 7/9 mice injected with these tumor cells forming prostate tumors, respectively, only 3/13 mice

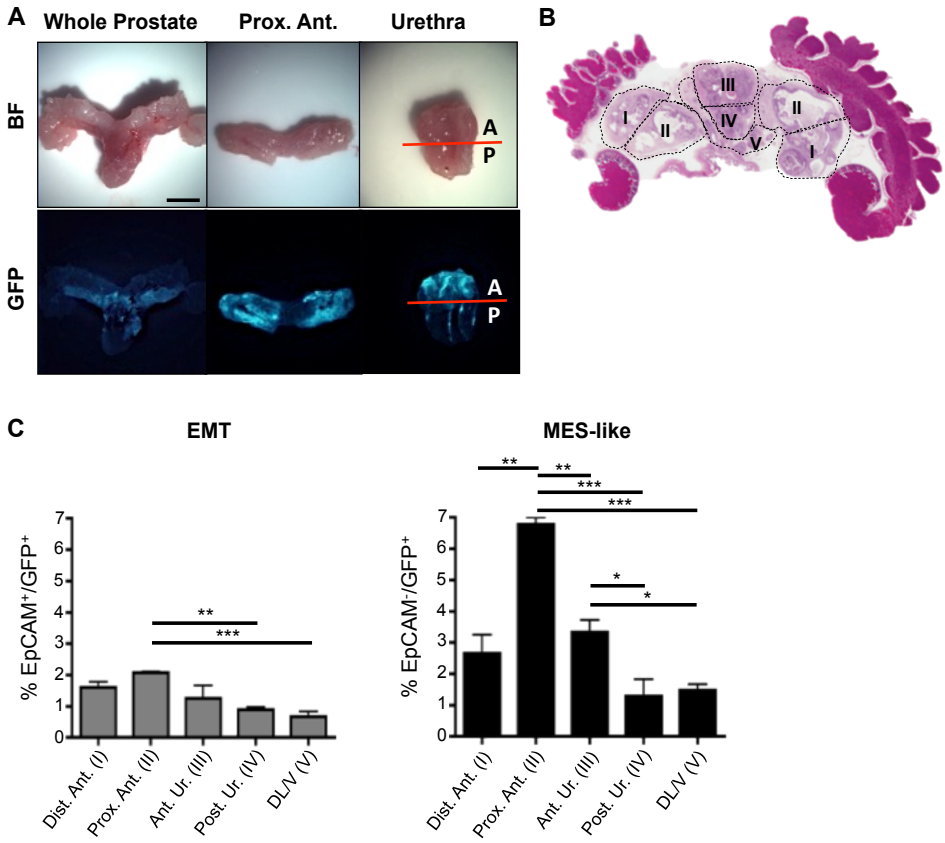

D

Prostate Lobes	P0	P1	P2	P3
Dist. Anterior (I)	-	-	-	-
Prox. Anterior (II)	+	+	+	+
Ant. Urethra (III)	+	+	+	+
Post. Urethra (IV)	-	-	-	-
Dorsolateral/ Ventral (V)	-	-	-	-

Figure 3. Prostate regions enriched in Vim-GFP$^+$ cells are able to regenerate transplantable tumors *in vivo*. (A) Bright-field (BF) and fluorescent images of a whole-mount *CPKV* prostate (10 weeks). GFP expression in *CPKV* prostates is most prominent in the proximal region of the anterior lobes and in the anterior portion of the urethra. (B) Diagram depicting how prostate regions/lobes were separated. I, distal region of the anterior lobe. II, proximal region of the anterior lobe. III, anterior portion of the urethra. IV, posterior portion of the urethra. V, dorsolateral/ventral lobes. (C) FACS analysis demonstrates that the anterior portion of the urethra and proximal region of the anterior lobes express the highest percentage of MES-like cells compared to other regions/lobes from the prostates of *CPKV* mice (10-12 weeks). The percentage of EMT tumor cells was also slightly higher in the proximal region of the anterior lobes compared to other lobes/regions. (D) The only *CPKV* prostate regions/lobes that produced transplantable tumors in *NSG* mice were the proximal region of the anterior lobe and anterior portion of the urethra. Data in C are represented as mean ± SEM. Bar, 4mm. A, anterior. P, posterior. Dist. Ant., distal region of the anterior lobe. Prox. Ant., proximal region of the anterior lobe. Ant. Ur., anterior portion of the urethra. Post. Ur., posterior portion of the urethra. DL/V, dorsolateral/ventral lobes. P0, passage 0. P1, passage 1. P2, passage 2. P3, passage 3. +, tumor. -, no tumor. *, $p<0.05$, **, $p<0.01$. ***, $p<0.001$.

injected with epithelial tumor cells formed tumor pathology *in vivo* (Fig. 4B; Fig. S3A). EMT and MES-like tumor cells also formed tumors as early as 9 weeks and 6 weeks post-transplantation, respectively, whereas the epithelial tumor cells did not form tumors until 24 weeks post-transplantation (Fig. S3B). Tumorigenic areas formed from transplanted epithelial tumor cells were also much less aggressive compared to those formed by EMT and MES-like tumor cells (T; Fig. S3A). EMT and MES-like tumor cells generated tumors with vast regions of EMT morphology that were positive for both Vimentin and P-S6 (Fig. 4C and 4D, bottom panels). Despite initially being injected as GFP^+ cells, EMT and MES-like tumor cells were also remarkably able to regenerate tumorous epithelial acinar structures with prostatic intraepithelial neoplasia (PIN) lesions that were Vimentin-negative and P-S6-positive (Fig. 4C and 4D, top panels), indicating that these cells have the plasticity to switch between mesenchymal and epithelial states. In general, while regenerated epithelial glandular structures were positive for proliferation markers (Ki67), invasive EMT regions were devoid of any proliferation markers in tumors generated from EMT and MES-like tumor cells (Fig. 4C and 4D), mimicking the phenotype seen in primary *CPKV* prostates (Fig. 2F). These results demonstrate that EMT and MES-like tumor cells have enhanced tumor-initiating capacity compared to epithelial tumor cells from the same *CPKV* mice, and that these cells have an inherent plasticity to switch between MES-like and epithelial states, as they are able to form invasive tumor regions that are $P\text{-}S6^+$, $Vimentin^+$, and $Ki67^{lo}$, as well as regenerated glandular structures that are $P\text{-}S6^+$, $Ki67^{int/hi}$, and $Vimentin^-$ (Fig. 4E).

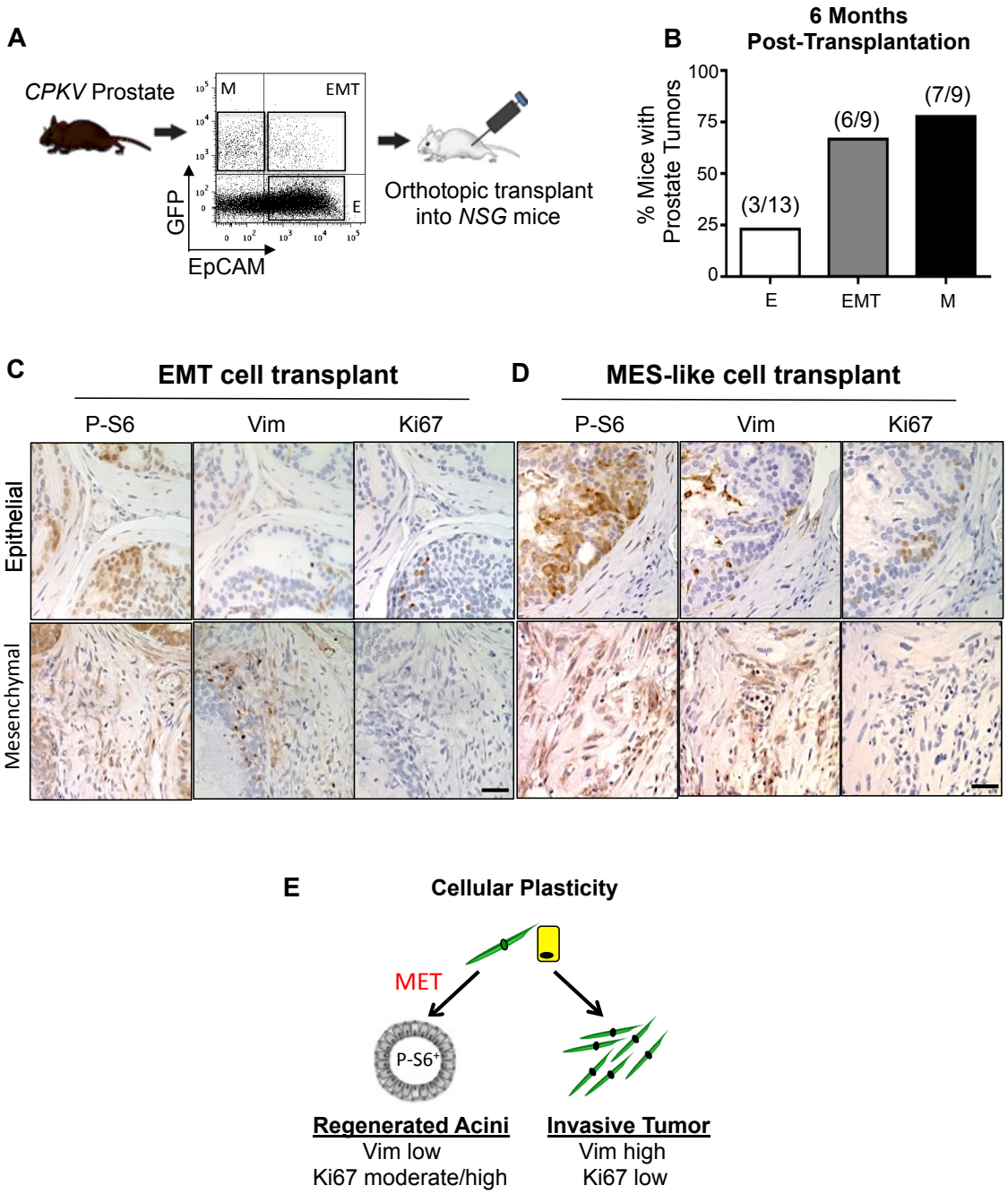

Figure 4. EMT and mesenchymal-like tumor cells have enhanced tumor-initiating capacity and cellular plasticity *in vivo*. (A) Schematic of experimental design for orthotopic transplantations. (B) EMT and MES-like tumor cells form tumors more readily *in vivo* compared to epithelial tumor cells from *CPKV* prostates (10-12 weeks). (C) IHC stains of anterior lobes from an *NSG* mouse transplanted with EMT tumor cells from *CPKV* prostates (10-12 weeks). P-S6 was used to trace transplanted cells, and Vim was used to mark cells with a mesenchymal phenotype. Top panel, transplanted EMT tumor cells form regenerated glandular structures. Bottom panel, transplanted EMT tumor cells form invasive mesenchymal tumor regions. (D) Same as in C, except a prostate section from an *NSG* mouse transplanted with MES-like tumor cells from *CPKV* prostates (10-12 weeks). (E) EMT (yellow) and MES-like (green) tumor cells from *CPKV* prostates have the plasticity to undergo an MET and regenerate epithelial glandular structures, or form invasive mesenchymal-like tumors *in vivo*. Bar, 50 μm.

Increase in CTCs with mesenchymal-like and invasive characteristics during disease progression in *CPKV* mice

Circulating tumor cells (CTCs) represent a surrogate biomarker of metastatic disease and a predictive factor of overall survival in various malignancies, including prostate cancer (26, 27). The current FDA-approved CellSearch method for CTC enumeration uses antibodies against EpCAM to isolate CTCs with epithelial characteristics (28). However, recent studies in human breast and prostate cancer patients have revealed that a significant percentage of CTCs co-express both mesenchymal and epithelial markers or display fully mesenchymal characteristics (22, 29-31), through which they could pass undetected by the CellSearch system.

To determine if we could use the *Vim-GFP* reporter to isolate and characterize CTCs with EMT and mesenchymal-like characteristics at different disease stages, we collected peripheral blood from *CPKV* mutants. CTCs were isolated and characterized from the Lin^- population by FACS analysis in a similar manner to how the primary tumor cell populations were isolated (Fig. S4A). As early as 6 weeks of age and well before the detection of metastatic disease, epithelial, EMT and MES-like CTCs can be detected in the blood of *CPKV* mice (Fig. 5A, left panel, n=7). During the intermediate (10-12 weeks) and late stages (15-20 weeks) of tumor progression, there is a significant expansion of MES-like CTCs and rare EMT CTCs but not epithelial CTCs in *CPKV* mice, suggesting that only MES-like and EMT CTC counts correlate with progression towards metastatic disease (Fig. 5A, middle and right panels, n=10). Supporting this finding, *CPV* mice, which develop micrometastases in the lymph nodes but not distant macrometastasis to the lung or liver (32), show similar epithelial CTC numbers to age-matched *CPKV* mice but have very few CTCs with mesenchymal-like characteristics and no CTCs with EMT traits (Fig. 5A, n=5). This data suggests that 1) dissemination of metastatic tumor cells occurs early on

during tumor initiation, 2) MES-like and EMT CTC counts correlate with metastatic disease, and 3) EMT tumor cells may quickly polarize to a mesenchymal-like or epithelial phenotype upon entering blood circulation.

As it is thought that disseminated cells with metastatic seeding potential must possess stem cell characteristics in order to colonize distant tissues, we looked at expression of CD44, a putative cancer stem cell (CSC) marker (33), in our different CTC subpopulations. Throughout the various stages of disease progression in *CPKV* mice, the majority of CTCs with mesenchymal-like characteristics also expressed CD44, while only a small percentage of epithelial CTCs expressed this CSC marker (Fig. 5B, n=10). Interestingly, 100% of rare EMT CTCs that could be detected were $CD44^+$ (Fig. 5B, n=10).

To further assess metastatic seeding potential of the CTC subpopulations, blood from *CPKV* mutants, as well as *CPV* and *V* mutants, was incubated on Vitatex culture plates, which are coated with a cell-adhesion matrix (CAM) that is used to assess the ability of tumor cells to invade collagen matrices (19, 34). Utilizing a Vitatex plate coated with a fluorescent red CAM, we are able to identify invasive CTCs (iCTCs), which represent CTCs with metastatic potential, by their ability to invade through the matrix and ingest TRITC-labeled CAM (Fig. S4B). After 10 days in culture, blood isolated from *CPKV* mice (n=10) had a significantly larger number of $TRITC^+$ iCTCs compared to blood from *CPV* (n=5) or *V* mice (n=3), supporting the notion that CTCs in *CPKV* mice contain more metastatic seeding potential (Fig. 5C). Moreover, when exploring the phenotype of these iCTCs from *CPKV* mice by FACS analysis, the majority of iCTCs had mesenchymal-like characteristics (Fig. 5D). The *Vim-GFP* reporter can therefore also be utilized for the isolation and characterization of CTC populations during endogenous prostate tumor cell dissemination and metastatic spreading. Our analysis

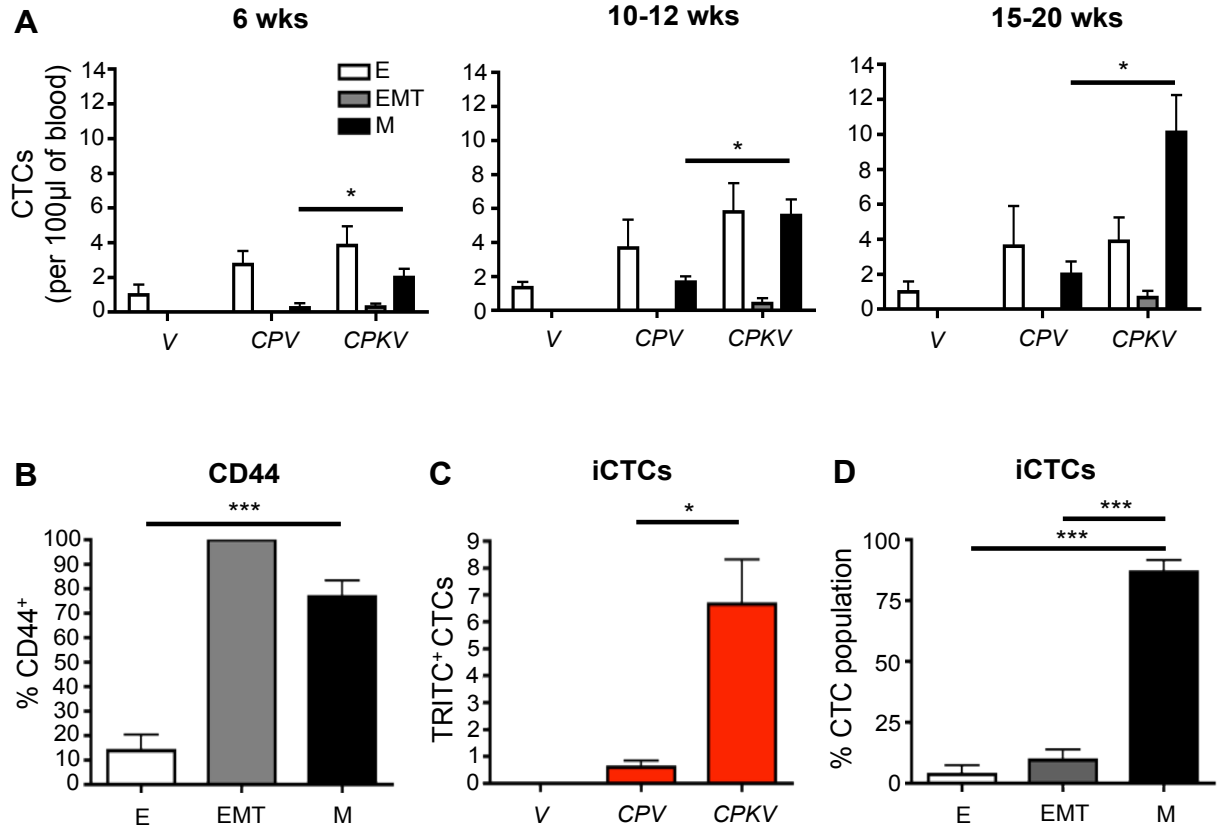

Figure 5. Increase in CTCs with mesenchymal-like and invasive characteristics during disease progression in *CPKV* mice. (A) *CPKV* mice have a significant increase in MES-like and EMT CTCs compared to *CPV* or *V* mice during disease progression. (B) MES-like and EMT CTCs from *CPKV* mice (15-20 weeks) have significantly higher CD44 expression compared to epithelial CTCs. (C) *CPKV* mice have significantly more invasive CTCs (iCTCs) compared to *CPV* and *V* mice (15-20 weeks). (D) The majority of iCTCs have a mesenchymal-like phenotype. Data in A through D are represented as mean $\pm$ SEM. *, $p<0.05$, ***, $p<0.001$.

reveals that *CPKV* mice have a significant increase in EMT and MES-like CTCs, but not epithelial CTCs, during disease progression.

Epithelial tumor cells have enhanced metastatic seeding potential

The observation that metastatic lesions in humans often display an epithelial morphology suggests that tumor cells that have disseminated through an EMT may revert to an epithelial phenotype through a mesenchymal-epithelial transition (MET) in order to form macrometastases (35). To test whether an MET may be required for macroscopic metastasis in *CPKV* mice, we compared epithelial and mesenchymal marker expression in both micrometastases, which remain small, dormant lesions, and actively proliferating macrometastases in the lungs. While micrometastases express high levels of Vimentin and low levels of Pan-Cytokeratin (CK) and Ki67, macrometastases express low levels of Vimentin and high levels of CK and Ki67 (Fig. 6A). This data suggests that a reversion to an epithelial phenotype, marked by high levels of CK, may be required for dormant micrometastases with mesenchymal features to proliferate to form macrometastases.

We next wanted to directly test the metastatic seeding capacity of epithelial, EMT, and MES-like tumor cell populations by injecting these primary tumor cell populations isolated from *CPKV* mice intravenously into *NSG* mice. Remarkably, while MES-like tumor cells were unable to form macrometastases up to 16 weeks post-transplantation, epithelial tumor cells readily formed macrometases when either 25,000 (2/5) or 100,000 (6/6) tumor cells were injected (Fig. 6B and 6C). EMT tumor cells were also able to form metastases (1/5), albeit at a lower efficiency compared to epithelial tumor cells (Fig. 6B and 6C). Upon histological examination of the lungs post-transplantation, the macrometastases formed by both epithelial and EMT tumor

cells were devoid of GFP^+ cells and expressed high levels of CK (Fig. S5), similar to lung macrometastases found in *CPKV* mice (Fig. 6A), confirming that macrometastatic spread requires reversion to an epithelial phenotype. While MES-like tumor cells did not form macrometastases or even small micrometastases in the lungs, solitary GFP^+ cells were found in a quiescent, non-proliferative state ($Ki67^-$) throughout the lungs (Fig. S5). Interestingly, while few tumor cells remained in the circulation of mice transplanted with epithelial and EMT tumor cells 16 weeks post-intravenous injection, those transplanted with MES-like tumor cells had a significantly high number of CTCs with mesenchymal-like characteristics, suggesting that MES-like cells can persist and survive in the blood stream for long periods of time (Fig. 6D, n=4). These findings propose that while MES-like tumor cells are able to survive in the blood, extravasate, and persist as solitary, dormant cells in the lungs over the course of 16 weeks, they are unable to proliferate to generate frank metastases. EMT tumor cells, on the other hand, reside in a transitionary state, and have the capacity to transition to an epithelial state in order to proliferate and form macrometastases. Overall, while both EMT and MES-like prostate tumor cells have enhanced stemness characteristics and tumor-initiating capacity compared to epithelial tumor cells, only EMT tumor cells have the capacity to revert to an epithelial state and proliferate in the lungs to form macrometastases (Fig. 6E).

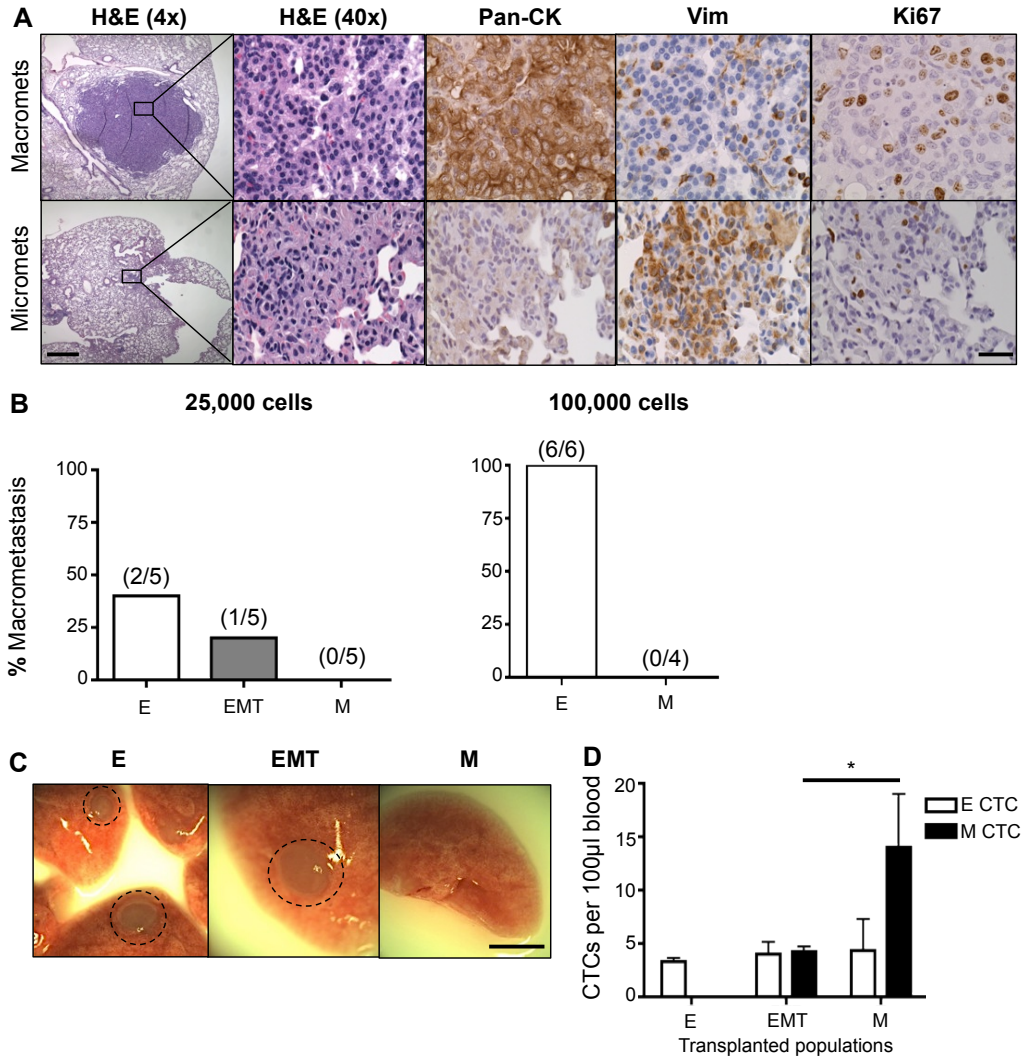

E

	Epithelial	EMT	MES-like
EMT gene expression		++	++++
Sphere Formation	++	++++	+
Stemness gene expression		++	+++
Proliferation	+++	+++	+
Invasive capacity	+	++	++++
Tumor-initiating capacity	+	+++	++++
Metastatic Seeding capacity	++	+	

Figure 6. Epithelial tumor cells have enhanced metastatic seeding potential. (A) IHC analysis of epithelial (Pan-CK), mesenchymal (Vim), and proliferation (Ki67) markers in micrometastases (micromets) and macrometastases (macromets) in primary *CPKV* lungs (18 weeks). Low magnification bar, 500 µm; high magnification bar, 50 µm. (B) Percent of macrometastatic lesions in the lungs of *NSG* mice 16 weeks after intravenous transplantation of either 25,000 or 100,000 epithelial, EMT, or MES-like tumor cells from *CPKV* prostates (10-12 weeks). (C) Whole-mount images of lungs isolated from *NSG* mice transplanted with 25,000 epithelial, EMT, or MES-like tumor cells from *CPKV* prostates (10-12 weeks). Circle, macrometastases. Bar, 4 mm. (D) *NSG* mice transplanted intravenously with MES-like tumor cells (25,000) from *CPKV* prostates (10-12 weeks) contained a significantly higher number of CTCs persisting in the bloodstream compared to mice transplanted with either epithelial or EMT tumor cells 16 weeks post-transplantation. (E) Table summarizing the characteristics of epithelial, EMT, and MES-like tumor cells isolated from *CPKV* prostates. Data in D are represented as mean + SEM. *, $p<0.05$

Discussion

As EMT is a plastic and dynamic process, the study of the EMT process through the *in vitro* manipulation of established cell lines, which often polarizes cells into a fixed mesenchymal state, may overlook much of the biology involved within the transition. Here, we demonstrate for the first time the isolation and characterization of both mesenchymal-like (MES-like) tumor cells that have fully completed an EMT, as well as EMT tumor cells that are in a transitory state between epithelial and mesenchymal programs from an endogenous murine cancer model. While previous studies have suggested that partial but not complete passage of cells into a mesenchymal state is associated with stemness and tumorigenicity (36-38), our study reveals that both EMT and MES-like tumors cells harbor stemness characteristics and tumor-initiating capacity. A striking distinction between these populations is their proliferative capacity, with MES-like tumor cells exhibiting characteristics of quiescent stem cells, and EMT tumor cells exhibiting characteristics of proliferating progenitor cells. Given that MES-like tumor cells localize to the stem cell niche in the proximal region of the prostate, it is likely that they are maintained in a quiescent state by factors in the surrounding microenvironment (25).

While both EMT and MES-like tumor cells demonstrate the plasticity to initiate proliferative epithelial tumor structures in the prostate microenvironment, only EMT cells are able to quickly revert to an epithelial phenotype to form macrometastatic colonies in the lungs. This suggests that MES-like tumor cells may exist in a more fixed state compared to EMT tumor cells, and may require additional stimuli, possibly mediated through paracrine factors secreted from the surrounding microenvironment, in order to acquire an epithelial phenotype and proliferate to form distant metastases. The modeling of dissemination in immunodeficient mice

in our study, as well as by others (36, 39), presents a number of caveats that may affect the rate of successful metastatic colonization. First, *NSG* mice lack mature T cells, B cells, and NK cells, and have documented defects in macrophage activation. This is problematic, as the outgrowth of macrometastases has been shown to rely on the successful recruitment of myeloid and other inflammatory cell types to the metastatic site (40). Second, primary tumors release systemic factors that can educate distant sites in preparation for metastasizing cancer cells and mobilize bone marrow-derived cells to these sites to orchestrate what is termed the "premetastatic niche" (41-43). The lack of both a primary tumor and various immune cell subtypes in our dissemination model may indeed impact the metastatic niche required for colonization. Future studies exploring the contribution of distinct tumor cell populations to metastatic colonization will need to be carried out using lineage-tracing techniques in endogenous mouse models or through transplantation of tumor cells into immunocompetent syngeneic mice to fully recapitulate the role of the tumor microenvironment in metastatic colonization. Finally, as human prostate cancer metastasizes most frequently to the bone, it is plausible that the mesenchymal state, as opposed to the epithelial state, may be favored for metastatic colonization in the bone microenvironment. Indeed, a number of studies have demonstrated that human prostate cancer bone metastases have downregulation of E-cadherin and increased mesenchymal marker expression (44-47).

Given that MES-like CTCs increase in number significantly during disease progression in *CPKV* mice and harbor stemness properties, it is likely that MES-like tumor cells can settle in the distant organ sites and eventually form macrometastases, albeit over long latency periods. It has been well documented in the clinic that disseminated tumor cells (DTCs) can persist in a quiescent state at metastatic sites for decades after surgical removal of the primary tumor and

eventually give rise to macrometastases (48, 49). It is possible that disseminated MES-like tumor cells in our *CPKV* mice model the clinical phenomenon of metastatic dormancy, and that the observation window of our metastasis assay (16 weeks) was not long enough to observe reactivation of these dormant, solitary DTCs to produce growing macrometastases. Moreover, while epithelial tumor cells can readily form metastases in the lung after entering the blood stream, it is unlikely that they can actively disseminate from the primary tumor in the endogenous setting. However, we cannot rule out the possibility that epithelial and MES-like tumor cells dynamically interact at different stages of the invasion-metastasis cascade to produce macrometastatic disease (36, 39). On the other hand, EMT tumor cells, by harboring the plasticity to readily transition between epithelial and mesenchymal states, have the capacity to complete the entirety of the invasion-metastasis cascade on their own. Further understanding of the mechanisms regulating epithelial-mesenchymal plasticity will help to unveil novel therapies that can be used to target tumor cell plasticity and hence inhibit integral steps of the metastastic cascade that ultimately leads to prostate cancer mortality.

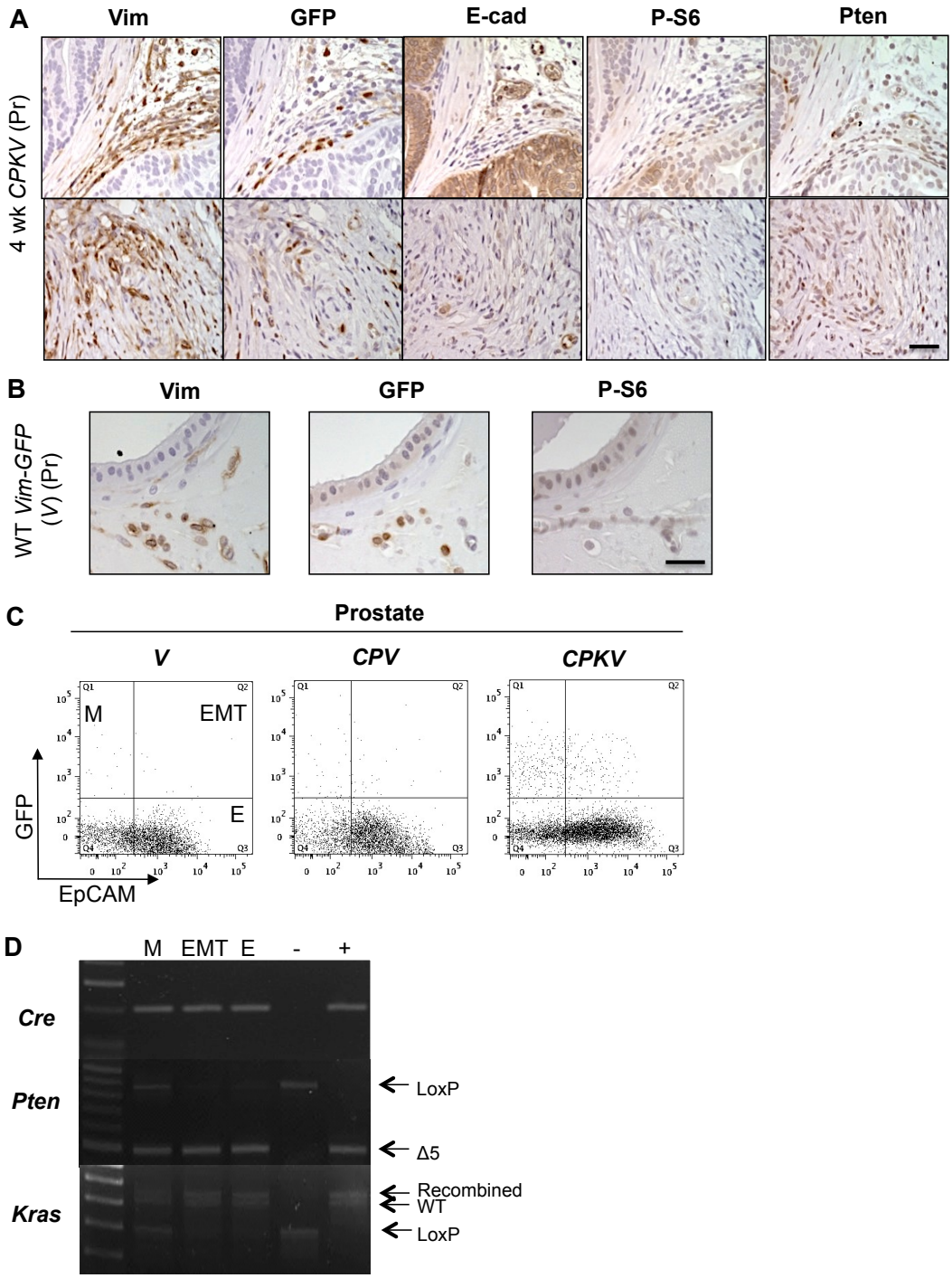

Figure S1. **EMT and mesenchymal-like tumor cell populations from *CPKV* mice are derived from the *Pten*$^{-/-}$ epithelium.** (A) GFP^{+}/Vimentin^{+} stromal cells in 4 week old *CPKV* prostates are PTEN^{+} and P-S6^{-}. (B) GFP^{+}/Vimentin^{+} stromal cells in 10 week old V (*Vim-GFP*) prostates are also PTEN^{+} and P-S6^{-}. (C) Representative FACS plots from single cell suspensions of prostates from *V* (*Vim-GFP*), *CPV* (Pb-Cre$^{+/-}$;*Pten*$^{L/L}$;*Vim-GFP)*, and *CPKV* (Pb-Cre$^{+/-}$;*Pten*$^{L/L}$;*Kras*$^{G12D/+}$;*Vim-GFP*) mice (10-12 weeks). FSC/SCC and lineage depletion (Lin^{-}) gating were performed prior to gating on Epcam and GFP. (D) Genomic PCR confirms that Cre recombination occurred in all cell populations isolated from CPKV prostates (10-12 weeks). Bar, 25 μm. Pr, prostate. Δ5, deletion of exon 5 of *Pten*. -, Cre^{-} control. +, Cre^{+} control.

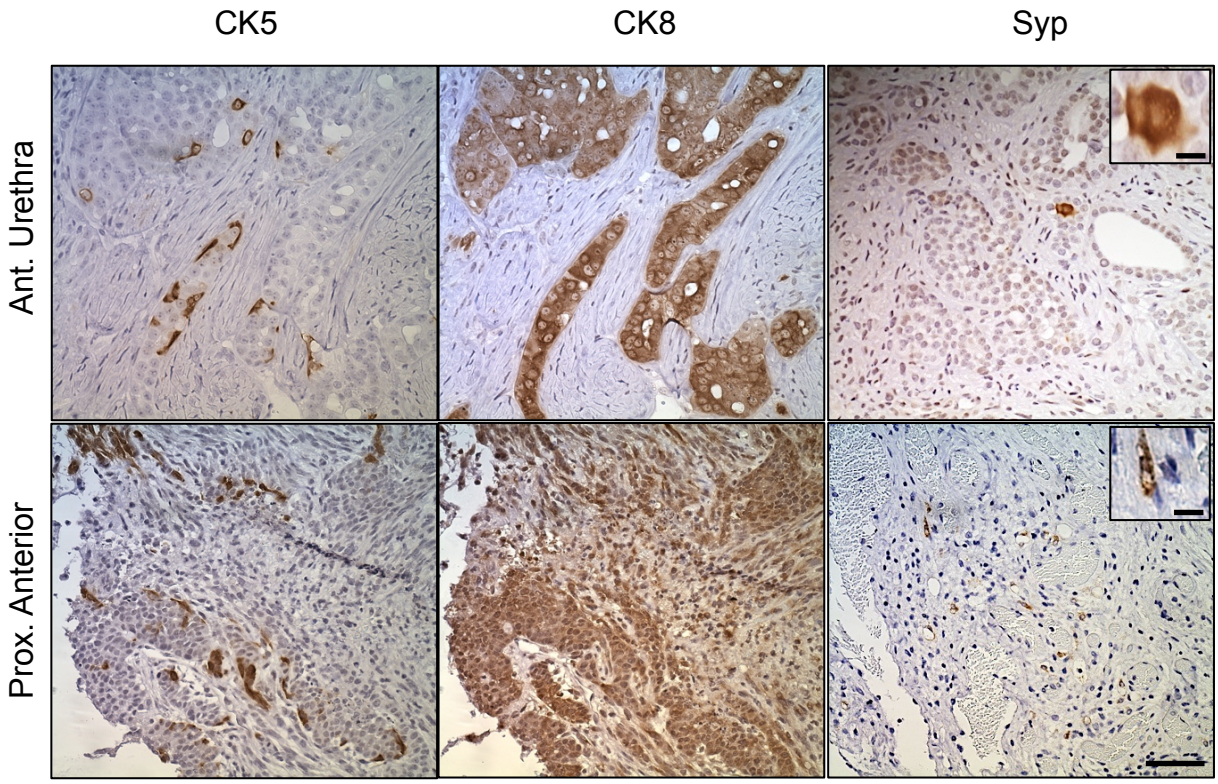

Figure S2. **The anterior portion of the urethra and proximal region of the anterior lobes regenerate tumors containing all three prostate epithelial lineages.** Subcutaneous tumors formed from the anterior portion of the urethra and proximal region of the anterior lobes contain $CK5^+$ basal cells, $CK8^+$ luminal cells, and rare synaptophysin $(Syp)^+$ neuroendocrine cells. Low magnification bar, 100 μm; high magnification bar, 5 μm. Prox. Anterior, proximal region of the anterior lobe. Ant. Urethra, anterior portion of the urethra.

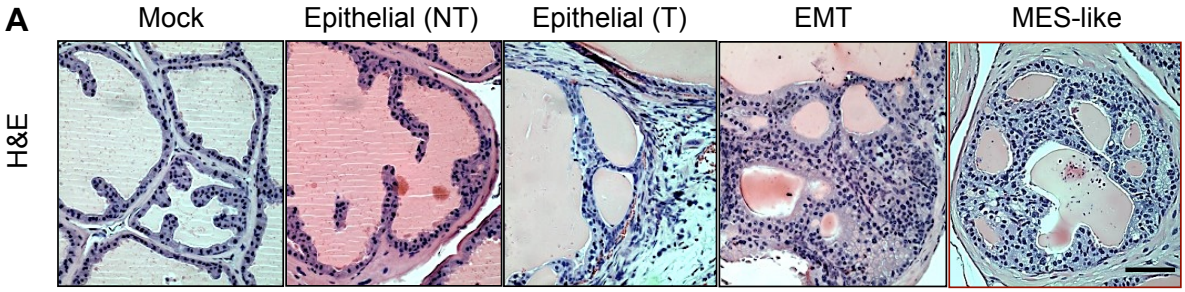

B

Tumor Formation

	6 Weeks	12 Weeks	18 Weeks	24 Weeks
Epithelial	0/2	0/3	0/5	3/13
EMT	0/1	1/2	1/2	6/9
MES-like	1/1	3/3	4/4	7/9

Figure S3. **EMT and mesenchymal-like tumor cells have enhanced tumor-initiating capacity *in vivo.*** (A) H&E images of anterior lobes isolated from *NSG* mice 24 weeks after transplantation with the indicated cell populations from *CPKV* mice. (B) EMT and MES-like tumor cells form tumors at a faster rate compared to epithelial tumor cells. Bar, 100 μm. NT, no tumor. T, tumor. Mock, mock surgery.

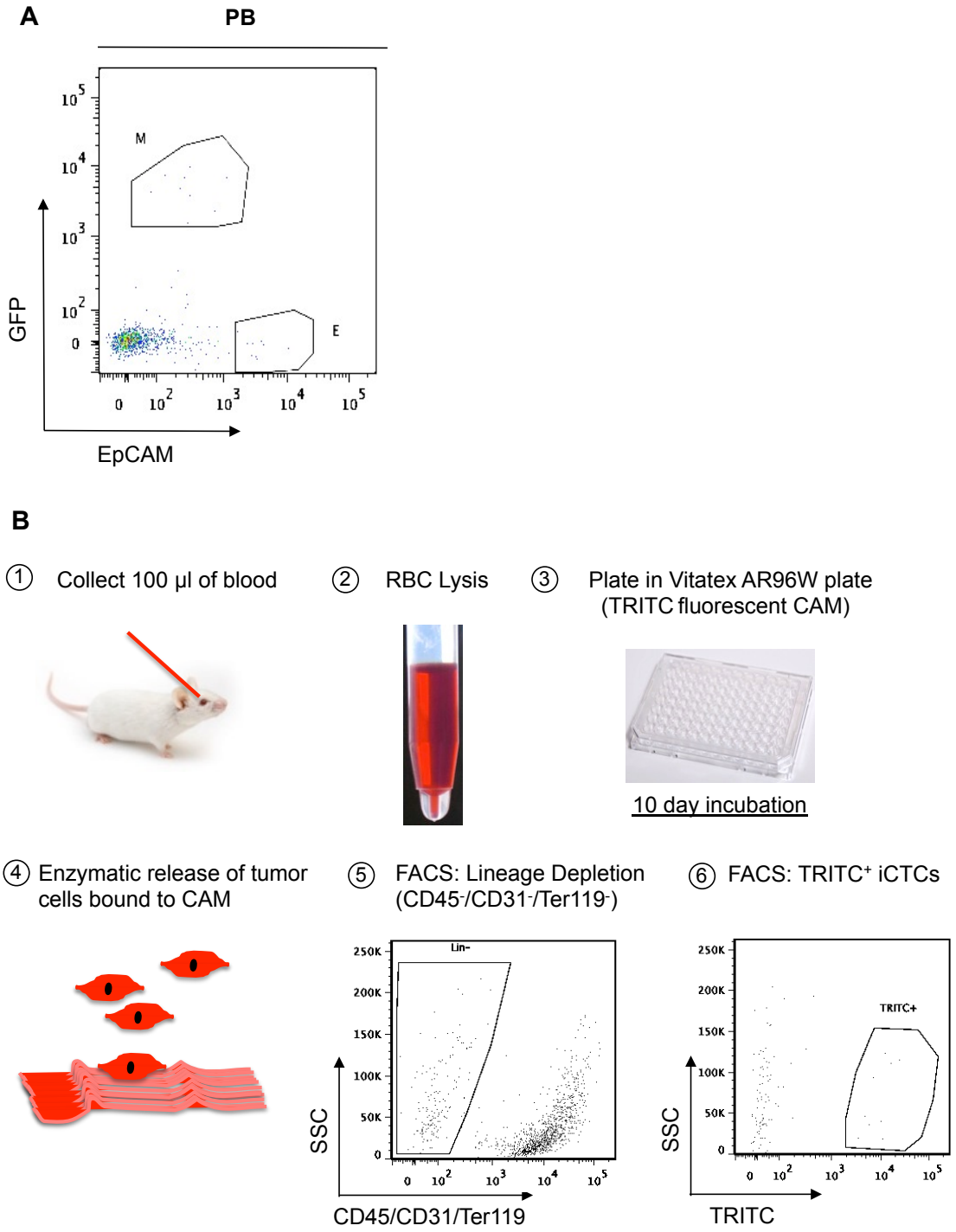

Figure S4. **Characterization of CTCs and iCTCs by FACS analysis.** (A) FACS gating strategy for characterization of CTCs from *CPKV* mice. MES-like CTCs were characterized as 7AAD$^-$CD45$^-$CD31$^-$Ter119$^-$Epcam$^-$GFP$^+$, and epithelial CTCs as 7AAD$^-$CD45$^-$CD31$^-$Ter119$^-$Epcam$^+$GFP$^-$. (B) Schematic outlining the Vitatex Assay used to quantify iCTCs. PB, peripheral blood. RBC, red blood cell. CAM, cell adhesion matrix.

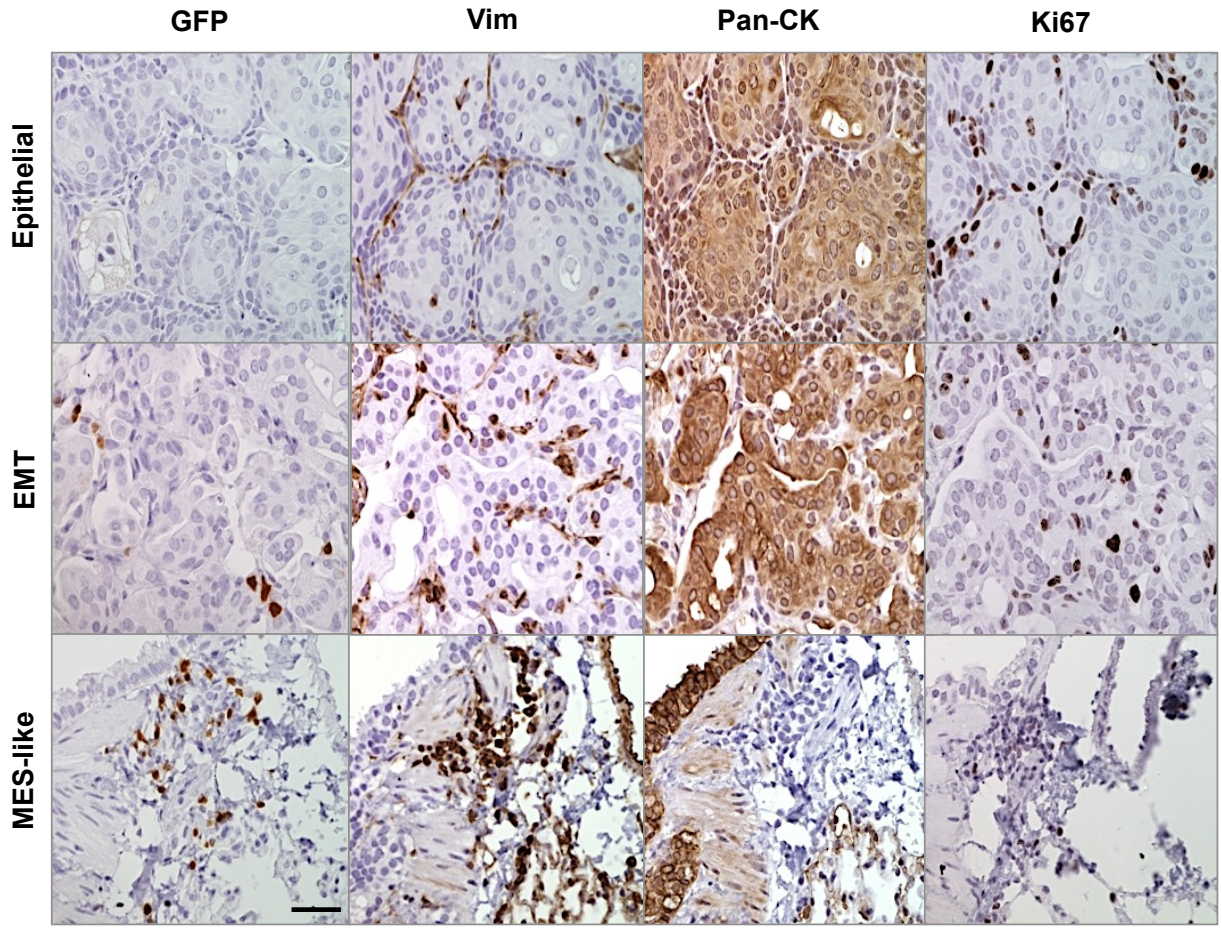

Figure S5. Epithelial and EMT tumor cells form macrometastases with epithelial features, while mesenchymal tumor cells exist as quiescent solitary cells in the lungs. IHC analysis of epithelial (Pan-CK), mesenchymal (GFP, Vim), and proliferation (Ki67) markers in the lungs of *NSG* mice transplanted with epithelial, EMT, and MES-like tumor cells from *CPKV* mice (10-12 weeks). Bar, 50 μm.

References

1. Siegel R, Ma J, Zou Z, Jemal A. Cancer statistics, 2014. CA: a cancer journal for clinicians. 2014;64:9-29.

2. Heidenreich A, Pfister D, Merseburger A, Bartsch G. Castration-resistant prostate cancer: where we stand in 2013 and what urologists should know. European urology. 2013;64:260-5.

3. Taylor BS, Schultz N, Hieronymus H, Gopalan A, Xiao Y, Carver BS, et al. Integrative genomic profiling of human prostate cancer. Cancer cell. 2010;18:11-22.

4. Mulholland DJ, Kobayashi N, Ruscetti M, Zhi A, Tran LM, Huang J, et al. Pten loss and RAS/MAPK activation cooperate to promote EMT and metastasis initiated from prostate cancer stem/progenitor cells. Cancer research. 2012;72:1878-89.

5. Aytes A, Mitrofanova A, Kinkade CW, Lefebvre C, Lei M, Phelan V, et al. ETV4 promotes metastasis in response to activation of PI3-kinase and Ras signaling in a mouse model of advanced prostate cancer. Proceedings of the National Academy of Sciences of the United States of America. 2013;110:E3506-15.

6. Lue HW, Yang X, Wang R, Qian W, Xu RZ, Lyles R, et al. LIV-1 promotes prostate cancer epithelial-to-mesenchymal transition and metastasis through HB-EGF shedding and EGFR-mediated ERK signaling. PloS one. 2011;6:e27720.

7. Josson S, Nomura T, Lin JT, Huang WC, Wu D, Zhau HE, et al. beta2-microglobulin induces epithelial to mesenchymal transition and confers cancer lethality and bone metastasis in human cancer cells. Cancer research. 2011;71:2600-10.

8. Tanaka H, Kono E, Tran CP, Miyazaki H, Yamashiro J, Shimomura T, et al. Monoclonal antibody targeting of N-cadherin inhibits prostate cancer growth, metastasis and castration resistance. Nature medicine. 2010;16:1414-20.

9. Sun Y, Wang BE, Leong KG, Yue P, Li L, Jhunjhunwala S, et al. Androgen deprivation causes epithelial-mesenchymal transition in the prostate: implications for androgen-deprivation therapy. Cancer research. 2012;72:527-36.

10. Nauseef JT, Henry MD. Epithelial-to-mesenchymal transition in prostate cancer: paradigm or puzzle? Nature reviews Urology. 2011;8:428-39.

11. De Craene B, Berx G. Regulatory networks defining EMT during cancer initiation and progression. Nature reviews Cancer. 2013;13:97-110.

12. Mani SA, Guo W, Liao MJ, Eaton EN, Ayyanan A, Zhou AY, et al. The epithelial-mesenchymal transition generates cells with properties of stem cells. Cell. 2008;133:704-15.

13. Morel AP, Lievre M, Thomas C, Hinkal G, Ansieau S, Puisieux A. Generation of breast cancer stem cells through epithelial-mesenchymal transition. PloS one. 2008;3:e2888.

14. Giannoni E, Bianchini F, Masieri L, Serni S, Torre E, Calorini L, et al. Reciprocal activation of prostate cancer cells and cancer-associated fibroblasts stimulates epithelial-mesenchymal transition and cancer stemness. Cancer research. 2010;70:6945-56.

15. Marin-Aguilera M, Codony-Servat J, Reig O, Lozano JJ, Fernandez PL, Pereira MV, et al. Epithelial-to-mesenchymal transition mediates docetaxel resistance and high risk of relapse in prostate cancer. Molecular cancer therapeutics. 2014;13:1270-84.

16. Gong S, Zheng C, Doughty ML, Losos K, Didkovsky N, Schambra UB, et al. A gene expression atlas of the central nervous system based on bacterial artificial chromosomes. Nature. 2003;425:917-25.

17. Lukacs RU, Goldstein AS, Lawson DA, Cheng D, Witte ON. Isolation, cultivation and characterization of adult murine prostate stem cells. Nature protocols. 2010;5:702-13.

18. Garcia AJ, Ruscetti M, Arenzana TL, Tran LM, Bianci-Frias D, Sybert E, et al. Pten Null Prostate Epithelium Promotes Localized Myeloid-Derived Suppressor Cell Expansion and Immune Suppression during Tumor Initiation and Progression. Molecular and cellular biology. 2014;34:2017-28.

19. Friedlander TW, Ngo VT, Dong H, Premasekharan G, Weinberg V, Doty S, et al. Detection and characterization of invasive circulating tumor cells derived from men with metastatic castration-resistant prostate cancer. International journal of cancer Journal international du cancer. 2014;134:2284-93.

20. Satelli A, Li S. Vimentin in cancer and its potential as a molecular target for cancer therapy. Cellular and molecular life sciences : CMLS. 2011;68:3033-46.

21. Zhang Q, Helfand BT, Jang TL, Zhu LJ, Chen L, Yang XJ, et al. Nuclear factor-kappaB-mediated transforming growth factor-beta-induced expression of vimentin is an independent predictor of biochemical recurrence after radical prostatectomy. Clinical cancer research : an official journal of the American Association for Cancer Research. 2009;15:3557-67.

22. Armstrong AJ, Marengo MS, Oltean S, Kemeny G, Bitting RL, Turnbull JD, et al. Circulating tumor cells from patients with advanced prostate and breast cancer display both epithelial and mesenchymal markers. Molecular cancer research : MCR. 2011;9:997-1007.

23. Mulholland DJ, Xin L, Morim A, Lawson D, Witte O, Wu H. Lin-Sca-1+CD49fhigh stem/progenitors are tumor-initiating cells in the Pten-null prostate cancer model. Cancer research. 2009;69:8555-62.

24. Tsujimura A, Koikawa Y, Salm S, Takao T, Coetzee S, Moscatelli D, et al. Proximal location of mouse prostate epithelial stem cells: a model of prostatic homeostasis. The Journal of cell biology. 2002;157:1257-65.

25. Salm SN, Burger PE, Coetzee S, Goto K, Moscatelli D, Wilson EL. TGF-{beta} maintains dormancy of prostatic stem cells in the proximal region of ducts. The Journal of cell biology. 2005;170:81-90.

26. Scher HI, Jia X, de Bono JS, Fleisher M, Pienta KJ, Raghavan D, et al. Circulating tumour cells as prognostic markers in progressive, castration-resistant prostate cancer: a reanalysis of IMMC38 trial data. The lancet oncology. 2009;10:233-9.

27. de Bono JS, Scher HI, Montgomery RB, Parker C, Miller MC, Tissing H, et al. Circulating tumor cells predict survival benefit from treatment in metastatic castration-resistant prostate cancer. Clinical cancer research : an official journal of the American Association for Cancer Research. 2008;14:6302-9.

28. Riethdorf S, Fritsche H, Muller V, Rau T, Schindlbeck C, Rack B, et al. Detection of circulating tumor cells in peripheral blood of patients with metastatic breast cancer: a validation study of the CellSearch system. Clinical cancer research : an official journal of the American Association for Cancer Research. 2007;13:920-8.

29. Yu M, Bardia A, Wittner BS, Stott SL, Smas ME, Ting DT, et al. Circulating breast tumor cells exhibit dynamic changes in epithelial and mesenchymal composition. Science. 2013;339:580-4.

30. Chen CL, Mahalingam D, Osmulski P, Jadhav RR, Wang CM, Leach RJ, et al. Single-cell analysis of circulating tumor cells identifies cumulative expression patterns of EMT-related genes in metastatic prostate cancer. The Prostate. 2013;73:813-26.

31. Kallergi G, Papadaki MA, Politaki E, Mavroudis D, Georgoulias V, Agelaki S. Epithelial to mesenchymal transition markers expressed in circulating tumour cells of early and metastatic breast cancer patients. Breast cancer research : BCR. 2011;13:R59.

32. Wang S, Gao J, Lei Q, Rozengurt N, Pritchard C, Jiao J, et al. Prostate-specific deletion of the murine Pten tumor suppressor gene leads to metastatic prostate cancer. Cancer cell. 2003;4:209-21.

33. Tang DG, Patrawala L, Calhoun T, Bhatia B, Choy G, Schneider-Broussard R, et al. Prostate cancer stem/progenitor cells: identification, characterization, and implications. Molecular carcinogenesis. 2007;46:1-14.

34. Lu J, Fan T, Zhao Q, Zeng W, Zaslavsky E, Chen JJ, et al. Isolation of circulating epithelial and tumor progenitor cells with an invasive phenotype from breast cancer patients. International journal of cancer Journal international du cancer. 2010;126:669-83.

35. Chaffer CL, Weinberg RA. A perspective on cancer cell metastasis. Science. 2011;331:1559-64.

36. Celia-Terrassa T, Meca-Cortes O, Mateo F, de Paz AM, Rubio N, Arnal-Estape A, et al. Epithelial-mesenchymal transition can suppress major attributes of human epithelial tumor-initiating cells. The Journal of clinical investigation. 2012;122:1849-68.

37. Battula VL, Evans KW, Hollier BG, Shi Y, Marini FC, Ayyanan A, et al. Epithelial-mesenchymal transition-derived cells exhibit multilineage differentiation potential similar to mesenchymal stem cells. Stem Cells. 2010;28:1435-45.

38. Shamir ER, Pappalardo E, Jorgens DM, Coutinho K, Tsai WT, Aziz K, et al. Twist1-induced dissemination preserves epithelial identity and requires E-cadherin. The Journal of cell biology. 2014;204:839-56.

39. Tsuji T, Ibaragi S, Shima K, Hu MG, Katsurano M, Sasaki A, et al. Epithelial-mesenchymal transition induced by growth suppressor p12CDK2-AP1 promotes tumor cell local invasion but suppresses distant colony growth. Cancer research. 2008;68:10377-86.

40. Joyce JA, Pollard JW. Microenvironmental regulation of metastasis. Nature reviews Cancer. 2009;9:239-52.

41. Psaila B, Lyden D. The metastatic niche: adapting the foreign soil. Nature reviews Cancer. 2009;9:285-93.

42. Kaplan RN, Riba RD, Zacharoulis S, Bramley AH, Vincent L, Costa C, et al. VEGFR1-positive haematopoietic bone marrow progenitors initiate the pre-metastatic niche. Nature. 2005;438:820-7.

43. Hiratsuka S, Watanabe A, Aburatani H, Maru Y. Tumour-mediated upregulation of chemoattractants and recruitment of myeloid cells predetermines lung metastasis. Nature cell biology. 2006;8:1369-75.

44. Umbas R, Schalken JA, Aalders TW, Carter BS, Karthaus HF, Schaafsma HE, et al. Expression of the cellular adhesion molecule E-cadherin is reduced or absent in high-grade prostate cancer. Cancer research. 1992;52:5104-9.

45. Sethi S, Macoska J, Chen W, Sarkar FH. Molecular signature of epithelial-mesenchymal transition (EMT) in human prostate cancer bone metastasis. American journal of translational research. 2010;3:90-9.

46. Lang SH, Hyde C, Reid IN, Hitchcock IS, Hart CA, Bryden AA, et al. Enhanced expression of vimentin in motile prostate cell lines and in poorly differentiated and metastatic prostate carcinoma. The Prostate. 2002;52:253-63.

47. Kwok WK, Ling MT, Lee TW, Lau TC, Zhou C, Zhang X, et al. Up-regulation of TWIST in prostate cancer and its implication as a therapeutic target. Cancer research. 2005;65:5153-62.

48. Giancotti FG. Mechanisms governing metastatic dormancy and reactivation. Cell. 2013;155:750-64.

49. Aguirre-Ghiso JA. Models, mechanisms and clinical evidence for cancer dormancy. Nature reviews Cancer. 2007;7:834-46.

Chapter 6:

HDAC inhibition effectively impedes HMGA2-controlled epithelial-mesenchymal plasticity and suppresses metastatic, castration-resistant prostate cancer

Introduction

Prostate cancer is the most prevalent malignancy in men and a leading cause of cancer-related death worldwide (1). Nearly all prostate cancer-associated mortality is caused by distant metastasis. The most common treatment for advanced prostate cancer is androgen deprivation therapy (ADT), owing to the central role of androgens and androgen receptor (AR) signaling in normal prostate development and prostate tumor growth. While most men initially respond to ADT, the therapeutic benefits are short-lived, and patients usually succumb to castration-resistant prostate cancer (CRPC) within 18-24 months (2). Treatment of CRPC with new generation androgen signaling inhibitors such as enzalutamide and abiraterone acetate has improved survival outcomes (3, 4); however, CRPC remains incurable, and patients generally die within 2 years (5). Therefore, novel therapies for CRPC, including those that would prevent distant metastasis, are desperately needed.

Genetic and phenotypic heterogeneity within the same prostate tumor is frequently observed despite common underlying pathway alterations (6-10), a finding that suggests a degree of cellular plasticity at the level of RNA and protein expression within a given patient that is uncoupled from mutations and chromosomal abnormalities. There is accumulating evidence that epithelial-mesenchymal plasticity, referring to the reversible processes of the epithelial-mesenchymal transition (EMT) and the mesenchymal-epithelial transition (MET), is induced by ADT and other therapies and plays a role in both treatment resistance and metastatic progression through the acquisition of stemness and invasion programs (11-17). Therefore, co-targeting regulators of epithelial-mesenchymal plasticity may increase the therapeutic efficacy of ADT. However, the molecular mechanisms regulating epithelial-mesenchymal plasticity are poorly understood, and validated biomarkers of epithelial-mesenchymal plasticity are still required.

We and others have previously shown that PI3K/AKT and RAS/MAPK pathway activation is highly associated with metastatic CRPC (mCRPC), and that activation of both pathways in the *Pb-Cre*$^{+/-}$*;Pten*$^{L/L}$*;Kras*$^{G12D/+}$ (*CPK*) mouse model is sufficient to induce an EMT and distant metastasis (7, 17). To study the direct role of EMT in prostate cancer stem cell formation and distant metastasis *in vivo*, we crossed *CPK* mice with *Vim-GFP* reporter mice, as Vimentin is one of the earliest expressed genes during EMT, and generated the *Pb-Cre*$^{+/-}$*;Pten*$^{L/L}$*;Kras*$^{G12D/+}$;*Vim-GFP* (*CPKV*) mouse model (Chapter 5). We demonstrated that epithelial, EMT, and mesenchymal-like (MES-like) prostate tumor cell populations could be isolated from murine prostate tumors of *CPKV* mice using EpCAM and Vim-GFP as markers (Chapter 5). EMT tumor cells, which co-express both epithelial and mesenchymal markers, and mesenchymal-like tumor cells, which are derived from an EMT but have fully lost epithelial marker expression, have enhanced stemness qualities and tumor-initiating capacity compared to epithelial tumor cells (Chapter 5). Fascinatingly, we observed that prostate tumors initiated by EMT and MES-like tumor cells isolated from *CPKV* prostates contained regenerated epithelial glandular structures, indicative of MET *in vivo* (Chapter 5). In the present report, we studied the dynamic regulation of epithelial-mesenchymal plasticity using this genetically defined system. We find that epithelial-mesenchymal plasticity is regulated epigenetically through the activity of the chromatin remodeling protein HMGA2, which is highly upregulated in EMT and MES-like tumor cells, as well as in tumors from men with mCRPC. Importantly, inhibition of HMGA2 activity with the histone deacetylase inhibitor (HDACi) LBH589 is able to eliminate castration-resistant MES-like tumor cells and prevent mCRPC *in vivo*.

Materials and Methods

Mouse strains

The *Cre*$^{-}$;*Pten*$^{L/L}$;*Kras*$^{G/+}$;*Vim-GFP* (V), *Cre*$^{+/-}$;*Pten*$^{L/L}$;*Kras*$^{+/+}$;*Vim-GFP* (CPV), and *Cre*$^{+/-}$;*Pten*$^{L/L}$;*Kras*$^{G/+}$;*Vim-GFP* (CPKV) mouse models were generated as previously described (Chapter 5). These strains have been maintained on a mixed strain background. All studies with animals were performed under the regulation of the division of Laboratory Animal Medicine at the University of California at Los Angeles (UCLA).

Cell lines and reagents

The *PKV* cell line was generated by FACS sorting CD45^{-}CD31^{-}Ter119^{-}EpCAM^{+}GFP^{-} epithelial cells from the prostates of 10 week old *CPKV* mice and culturing them in 0.2% gelatin-coated 10 cm dishes with Dulbecco's modified eagle medium (DMEM) (Sigma) containing 1% Pen/Strep, 10% Fetal Bovine Serum (FBS) (Omega Scientific), 25 μg /mL bovine pituitary extract, 5 μg /mL insulin (Invitrogen), and 6 ng/mL recombinant human EGF (BD Biosciences). LNCaP cells were grown in RPMI-1640 media with 1% Pen/Strep and 10% FBS. For studies carried out in the context of androgen deprivation, media containing 10% charcoal dextran-treated (CDT) FBS (BD Biosciences) was used.

Short hairpin RNA knockdown

To generate the *PKV-shScramble* or *PKV-shHmga2* cell lines, *PKV* cells were transduced with lentivirus containing the pLKO.shHmga2 or pLKO.Scramble plasmids, respectively, for 24 hrs in the presence of 8 μg/ml polybrene. Cells with stable integration of the desired construct were then selected for using puromycin at 4 μg/ml for 5 days. The *PKV-shScramble* or *PKV-shHmga2*

cell lines were subsequently passaged three times before being used for experiments. Stable knockdown of HMGA2 expression was confirmed by Western blot analysis. pLKO.shHmga2 was a gift from Tyler Jacks & Monte Winslow (Addgene plasmid # 32399) (18), and Scramble shRNA was a gift from David Sabatini (Addgene plasmid # 1864) (19).

***In vivo* dissemination model**

500,000 *PKV* cells were resuspended in 200 µl of PBS and transplanted by tail vein injection into 6-8 week old male *NOD/SCID/IL2Rγ-null* (*NSG*) mice. 8 weeks after transplantation, mice were sacrificed, and the presence of lung macrometastases was assessed by gross examination of formalin-fixed lung samples under a dissecting microscope, as well as by examining H&E stained lung sections. Micrometastases were defined as $Ki67^-$ metastases less than 300 µm in diameter.

Drug treatment

For the *in vitro* drug studies, *PKV* cells were treated with PD035901, PKI-587, LBH589 or a combination thereof at the indicated concentrations. Dimethyl Sulfoxide (DMSO) was used as a vehicle control. PD325901 (PF00192513) and PKI-587 (PF05212834) were a generous gift from the Pfizer Pharmaceutical Company, while LBH589 was purchased from LC Laboratories. Live cell counts were assessed using trypan blue exclusion. Percent growth was determined by first assessing the percentage of each cell population by FACS analysis, and then dividing the total cell number of each drug treated cell population by the total cell number of the same populations in vehicle treated cells. Apoptosis was determined by positive staining for 7AAD by FACS analysis.

For the *in vivo* drug studies using intact (non-castrated) *CPKV* mice, 10-week old *CPKV* mice were treated for 2 weeks with either vehicle alone (5.2% Tween 80 and 5.2% PEG 400 in Phosphate buffered saline (PBS)) or LBH589 (10 mg/kg, 3 days/week) by intraperitoneal (i.p.) injection before sacrificing. For the castration studies, 6-week old intact or castrated *CPKV* mice were treated with vehicle or LBH589 for 2 weeks, or until protocol-determined endpoints for morbidity required euthanasia for the survival study. Prostate weight was assessed after removal of the seminal vesicles and bladder from the prostate lobes. For the *in vivo* dissemination assay, *NSG* mice were treated with either vehicle or LBH589 beginning 24 hrs after transplantation of *PKV* cells for a total of 8 weeks.

DNA isolation and genomic PCR

DNA was isolated using the Qiagen AllPrep DNA/RNA Micro Kit. Primer sequences are as follows: *Pb-Cre* F, CGTATAGCCGAAATTGCCAG, R, CAAAACAGGTAGTTATTCGG; *Pte*n F, TCCCAGAGTTCATACCAGGA, R1, GCAATGGCCAGTACTAGTGAAC, R2, AATCTGTGCATGAAGGGAAC; *Kras* F, GTCTTTCCCCAGCACAGTGC, R1, CTCTTGCCTACGCCACCAGCTC, R2, AGCTAGCCACCATGGCTTGAGTAAGTCTGC.

Real time PCR

Total RNA from *PKV* cells or *CPKV* prostates, as well as epithelial, EMT, and MES-like tumor cell populations sorted from *PKV* cells or *CPKV* prostates, was isolated using the Qiagen AllPrep DNA/RNA Micro Kit and reverse transcribed into cDNA using the High-Capacity cDNA Reverse Transcription Kit with Multiscribe Reverse Transcriptase (Applied Biosystems).

Transcript levels were assessed with quantitative real-time PCR with mouse gene specific RT-PCR primers and iQ™ SYBR® Green Supermix (Bio-Rad) using the CFX Real-Time PCR detection System (Bio-Rad) and normalized against β-actin expression. The relative expression levels were derived from the delta-delta Ct values using the CFX software (Bio-Rad) and compared to expression levels from epithelial tumor cells. Primer sequences are as follows: *B-Actin* F, GGCTGTATTCCCCTCCATCG, R, CCAGTTGGTAACAATGCCATGT; *Hmga2* F, GTACCGGTAGAGGCAGTGGT, R, GGGTCTTCCTCTGGGTCTCT; *Vim* F, CGGCTGCGAGAGAAATTGC, R, CCACTTTCCGTTAAGGTCAAG; *Snai1* F, AAGATGCACATCCGAAGC, R, ATCTCTTCACATCCGAGTGG; *Zeb1* F, CATGTGACCTGTGTGACAAG, R, GCGGTGATTCATGTGTTGAG; *Cdh2* F, CAGGTCTCCTCATGGCTTTGC, R, CTTCCGAAAAGAAGGCTGTCC ; *Mmp2* F, CACCTACACCAAGAACTTCC, R, GAACACAGCCTTCTCCTCCT ; *Cdh1* F, AATGGCGGCAATGCAATCCCAAGA, R, TGCCACAGACCGATTGTGGAGATA; *Oct4* F, CACGAGTGGAAAGCAACTCA, R, CCAAGGTGATCCTCTTCTGC; *Sox2* F, AAGAAAGGAGAGAAGTTTGGAGC, R, GAGATCTGGCGGAGAATAGTTGG; *Sox9* F, GACAAGCGGAGGCCGAA, R, CCAGCTTGCACGTCGGTT; *Klf4* F, GTGCCCCGACTAACCGTTG, R, GTCGTTGAACTCCTCGGTCT; *Nestin* F, AGCAGGAGAAGCAGGGTCTA, R, CTGGGAACTTCTTCCAGGTG; *Bmi1* F, AATCCCCACCTGATGTGTGT, R, GCTGGTCTCCAGGTAACGAA; *Ezh2* F, ATCTGAGAAGGGACCGGTTT, R, TGTGCACAGGCTGTATCCTC; *Ar* F, AGACCTATCGAGGAGCGTTC, R, CTGCTGCCTTCGGAGATTAC; *Tmprss2* F, TACGGGAACGTGACGGTATT, R, CAGGGAGCACAGTCAAACAA; *Nkx3-1* F, CCACCAAGTATCCGGCATAG, R , CTACCAGAAAGATGGATGCC; *Fkbp5* F,

AGATCTCCATGTGCCAGAGG, R, CTTCTTCCATGGCCTGACTC; *Slc45a3* F, TGGTGGTAGTGACAGCCTCA, R, AGAGAGCTCCTGGCTTAGGG; *Mdm2* F, AGGTCCCTGTCCTTTGATCC, R, ATCCTGATCCAGGCAATCAC

Tissue dissociation and single cell suspension

Single cell suspensions were prepared from prostates of *CPKV* mice at the indicated time points. Prostates were minced in sterile tissue culture dishes, and subjected to collagenase I (1 mg/ml; Invitrogen) digestion overnight at 37°C with constant agitation in Dulbecco's modified eagle medium (DMEM) (Sigma) containing 1% Pen/Strep, 10% Fetal Bovine Serum (FBS) (Omega Scientific), 4 mM L-glutamine (Fisher Scientific), 10mM Hepes, 25 μg /mL bovine pituitary extract, 5 μg /mL insulin (Invitrogen), 6 ng/mL recombinant human EGF (BD Biosciences), and 10 μM Rocki (Y27632; Abcam). Undigested tissue was trypsinized for 5 minutes at 37° C, passed through a 18G and 21G syringe 5 times, and filtered through a 40 μm filter (Fischer Scientific) to facilitate dissociation, followed by washes in PBS and resuspension in DMEM media plus 10% FBS. Total cell numbers were assessed using trypan blue exclusion.

FACS analysis and cell sorting

Single-cell suspensions were stained with the following directly conjugated antibodies: CD45-PE (eBioscience; 12-0451-81), CD31-PE (Biolegend; 102407), Ter119-PE (Biolegend; 116207), and EpCAM-APC-cy7 (Biolegend; 118218). 7-AAD (BD Biosciences) was used to gate out dead or apoptotic cells.

Flow cytometric analysis was performed on a FACS Canto II (BD Biosciences) and data were analyzed using BD FACS Diva software (BD Biosciences). For isolation and analysis of

epithelial, EMT, and MES-like tumor cells from the prostate and blood of *CPKV* mice, single-cell suspensions were stained with directly conjugated antibodies against CD45, CD31, Ter119, and EpCAM, and sorted on a FACSAria (BD Biosciences) as $7AAD^{-}CD45^{-}CD31^{-}Ter119^{-}EpCAM^{+}GFP^{-}$, $7AAD^{-}CD45^{-}CD31^{-}Ter119^{-}EpCAM^{+}GFP^{+}$, and $7AAD^{-}CD45^{-}CD31^{-}Ter119^{-}EpCAM^{-}GFP^{+}$ cell fractions, respectively. Cells were collected in DMEM plus 50% FBS. Epithelial, EMT, and MES-like tumor cell populations within the *PKV* cell line were analyzed as $7AAD^{-}EpCAM^{+}GFP^{-}$, $7AAD^{-}EpCAM^{+}GFP^{+}$, and $7AAD^{-}EpCAM^{-}GFP^{+}$ cell fractions, respectively.

Histology and immunohistochemistry

Immunohistochemistry (IHC) was performed on formalin-fixed, paraffin-embedded tissues. Antigen retrieval was performed by boiling sections in 10mM citrate buffer (pH6) for 30 minutes. The following primary antibodies were used: HMGA2 (Biocheck; 59170AP), p53 (Vector Laboratories; VP-P956), Ki67 (Vector Laboratories; VP-RM04), H3K27Ac (Abcam; ab4729), GFP (Cell Signaling; 2955), Pan-Cytokeratin (Sigma; C1801), and AR (Santa Cruz; SC-816).

Ki67 proliferation index

The Ki67 proliferation index was calculated by quantifying the percentage of $Ki67^{+}$ cells in 10 fields for each epithelial and stromal region at 40x magnification for every sample.

Western analysis and immunoprecipitation

Protein extracts were prepared by lysing cells in RIPA buffer (Cell Signaling) containing phosphatase inhibitor cocktails 2 and 3 (Sigma Aldrich), 1 mM of PMSF, and complete protease inhibitor cocktails (Roche), followed by brief sonication and 10 minute centrifugation at 20,000 x g at 4^{o}C. 30-50 μg of cleared lysates were resolved by SDS-PAGE, transferred to PVDF membranes, and probed with the following antibodies: β-actin (Sigma; A5441), HMGA2 (Abcam; ab52039), H3K27Ac (Abcam; ab4729), p53 (CalBiochem; OPO3), AR (Santa Cruz; SC-816), and Acetyl Lysine (Ac-Lys) (Millipore; 05-515). Anti-rabbit and anti-mouse HRP-conjugated secondary antibodies and ECL Plus Western Blotting Detection Reagents were used to detect the protein signals (GE Healthcare Amersham). Band densities were quantified using a ChemiDoc XRS+ imager and Image Lab software (Bio-Rad).

To assess AR and p53 acetylation levels, 50 μg of protein was precleared using Protein A/G Plus agarose beads (Santa Cruz; SC-2003) and incubated overnight with AR or p53 antibodies. Samples were washed three times with RIPA buffer, and proteins were eluted by boiling in Laemmli buffer containing β-mercaptoethanol followed by Western blot analysis using an Acetyl Lysine primary antibody.

Matrigel sphere assay

The Matrigel sphere assays were carried out as previously described (20). 5 X 10^3 cells from each cell line were plated in triplicate per experimental condition.

Matrigel invasion assay

8μm transwell inserts (BD Biosciences) were coated with Matrigel (BD Biosciences) at a concentration of 300 μg/ml and placed into 24-well culture plates. 5 X 10^4 sorted cells per population were resuspended in serum free media in the top chamber, while full serum media (Dulbecco's modified eagle medium (DMEM) with 10% Fetal Bovine Serum (FBS)) was used in the bottom chamber. 24 hours later, invaded cells were fixed with methanol, stained with 0.2% crystal violet, and counted using a light microscope at 10x magnification.

Proliferation assay

Cell proliferation was assessed by measuring the conversion of 3-(4,5-dimethylthiazol-2-yl)-2,5-diphenyltetrazolium bromide (MTT; Life Technologies) to formazan. Cells were seeded in 24-well dishes 24 hours before addition of MTT reagent. MTT reagent was added as specified in the manufacturer's protocol and absorbance was read using a Bio-Rad Benchmark microplate spectrophotometer.

CTC isolation

For isolation of CTCs by FACS, 100 μl of peripheral blood was extracted from mice through retro-orbital bleeding and incubated in RBC lysis buffer (Biolegend) for 10 minutes. Cells were then washed with PBS, passaged through a 40 μm filter (Fisher Scientific), and resuspended in DMEM media plus 10% FBS prior to FACS analysis.

Surgical castration

Castration of 6-week old *CPKV* mice was performed as previously described (21).

RNA sequencing and library construction

RNA was extracted from pooled epithelial, EMT and MES-like tumor cells isolated from the prostates of 10-12 week old *CPKV* mice (n=17). Paired-end sequencing data with read lengths of 100 bp were generated by the UCLA Clinical Microarray Core using the Illumina HiSeq2000 system. An average of 75.5 million read pairs per replicate were generated. Total RNA was extracted using the Qiagen AllPrep DNA/RNA Micro Kit. The NEBNext Poly(A) mRNA kit was then used to isolate mRNA, and the KAPA stranded RNA-Seq library preparation kit for library preparation. Reads were mapped to the reference genome mm9 by TopHat (v.2.0.4) (22), allowing 2 mismatches per seed. The differentially expressed genes were calculated using Cuffdiff (v2.2.0) (23), with a false discovery rate less than 0.01.

Laser capture microdissection (LCM) and microarray analysis

LCM and downstream microarray analysis was carried out as previously described (24). Briefly, well-differentiated (epithelial) and poorly differentiated (EMT) tumor regions were isolated from the dorsolateral and anterior lobes of a prostate from a 15-week old *CPK* mouse, and gene expression values were compared to age-matched WT prostates following microarray analysis. H&E stained frozen sections were used to confirm pathological lesions and define well-differentiated tumor regions as cancerous morphology confined to epithelial glandular structures and poorly differentiated tumor regions as EMT regions in the stromal compartment.

Unsupervised hierarchical clustering and Gene Ontology pathway analysis

Unsupervised hierarchical clustering was carried out on both genes and samples. Complete approach was used to stratify genes and samples based on the Euclidean distance. The Gene

Ontology analysis was conducted with DAVID GO (25) in which Fisher's exact test was used to assess enrichment of gene sets in differentially expressed genes. Fisher's exact test was also used to assess enrichment of HMGA2-regulated genes using genes in the dataset derived from the study of Sun et al. (26). P-values were adjusted for multiple tests by using the Benjamini-Hochberg procedure (27) to obtain FDR.

Rank-rank analysis

Rank–rank hypergeometric overlap analysis (RRHO) as carried out as previously described (28) using genes in human datasets derived from the studies of Taylor et al. (7) and Grasso et al. (29). The ranks of genes are ordered by the signed $\log_2$ p-values, where the sign is determined by whether a gene is upregulated or downregulated.

Accession numbers

Gene expression datasets used in this study are available at Gene Expression Omnibus (GEO) under accession numbers GSE67681 and GSE67879.

Statistical analysis

Graphpad Prism software was used to calculate mean and standard deviation. Student's *t*-test was used to calculate the statistical significance between the two groups of data. $P < 0.05$ is considered significant.

Results

Prostate tumor cells with PI3K/AKT and RAS/MAPK co-activation display epithelial-mesenchymal plasticity

To explore whether prostate tumor cells with PI3K/AKT and RAS/MAPK co-activation have an inherent plasticity to switch between epithelial and mesenchymal states, we FACS sorted $EpCAM^{+}GFP^{-}$ epithelial tumor cells from 10-week old *Pb-Cre*$^{+/-}$*;Pten*$^{L/L}$*;Kras*$^{G12D/+}$;*Vim-GFP* (*CPKV*) prostates and cultured them *in vitro* (Figure 1A). After 14 days in culture, epithelial tumor cells that were originally sorted and plated as GFP^{-} cells began to transition into GFP^{+} cells (Figure 1B). FACS analysis conducted on this cell line (hereafter referred to as the *PKV* cell line) revealed the existence of the same epithelial ($EpCAM^{+}GFP^{-}$), EMT ($EpCAM^{+}GFP^{+}$), and mesenchymal-like (MES-like) ($EpCAM^{-}GFP^{+}$) tumor cell populations that could be identified and isolated from primary *CPKV* prostates *in vivo* (Figure 1C) (Chapter 5). Similar to EMT and MES-like tumor cells isolated from *CPKV* prostates, EMT and MES-like tumor cells within the *PKV* cell line were also initially derived from epithelial tumor cells that underwent Cre recombination and harbor *Pten* deletion and *Kras* activation (Figure S1A), as well as exhibit enhanced EMT signature gene expression and invasive capacity compared to epithelial tumor cells (Figures 1D and 1E).

Having shown that epithelial tumor cells have the plasticity to transition into EMT and MES-like tumor cells, we next wanted to determine if EMT and MES-like tumor cells also had

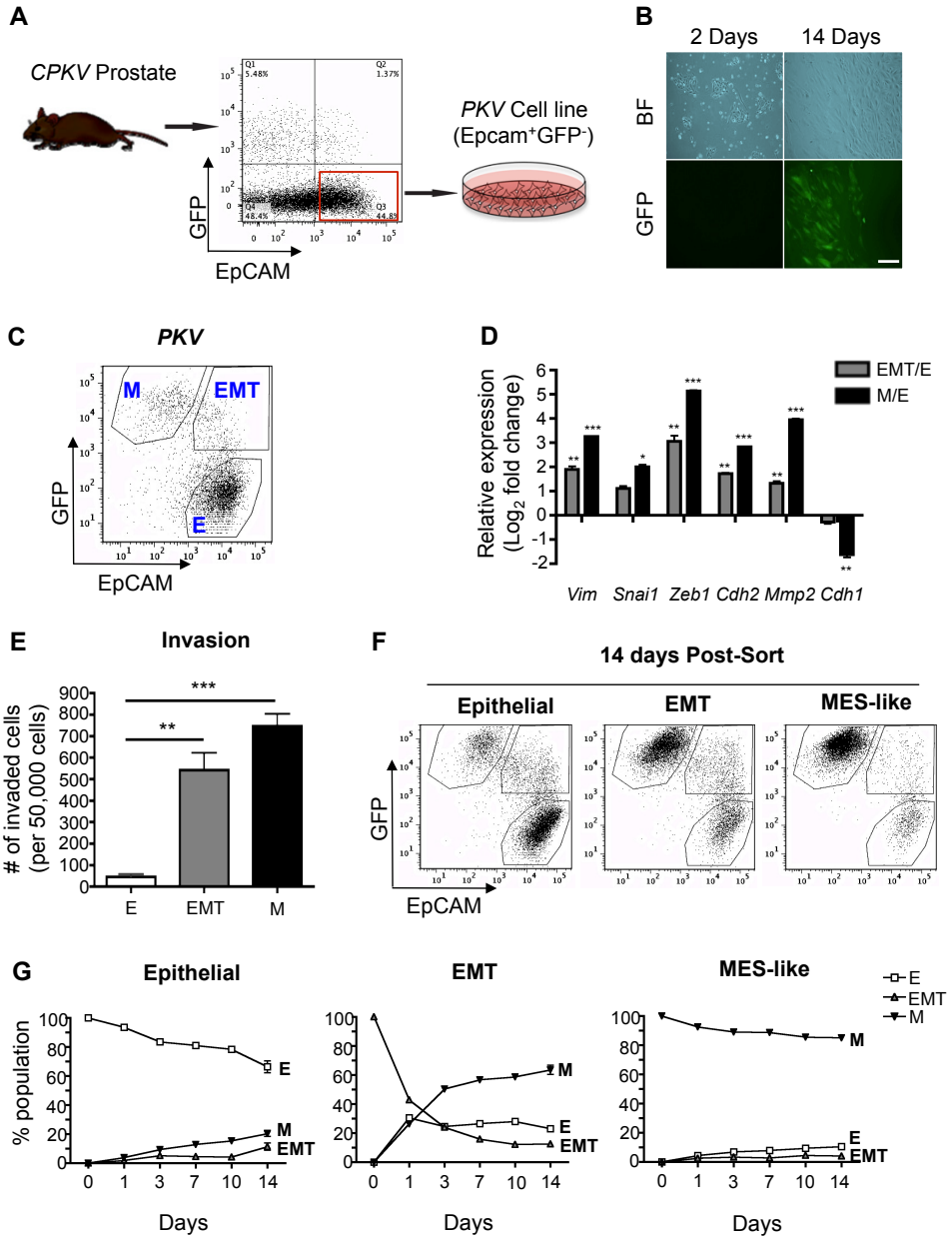

Figure 1. **Prostate tumor cells with PI3K/AKT and RAS/MAPK co-activation display epithelial-mesenchymal plasticity *in vitro*.** (A) Schematic outlining the generation of the *PKV* cell line from EpCAM$^+$/GFP$^-$ epithelial cells FACS sorted from *CPKV* prostates. (B) EpCAM$^+$/GFP$^-$ epithelial cells plated in culture spontaneously undergo EMT and express GFP. Scale bar, 50 μm; BF, brightfield. (C) The *PKV* cell line contains heterogeneous epithelial (E), EMT, and MES-like (M) tumor cell populations as assessed by FACS analysis. (D) qPCR analysis confirms that EMT and MES-like (M) tumor cells from the *PKV* cell line have upregulated EMT signature gene expression compared to epithelial tumor cells. Expression is relative to gene expression values found in epithelial (E) tumor cells. (E) Matrigel invasion assay reveals that EMT and MES-like (M) tumor cells are significantly more invasive than epithelial (E) tumor cells. (F) Each tumor cell population within the *PKV* cell line was isolated by FACS and cultured separately *in vitro*. Representative FACS plots of each cell population 14 days after plating are shown. Each tumor cell population has the plasticity to generate all 3 tumor cell populations. (G) The percentage of each tumor cell population (E, EMT, M) within each individually plated cell type (Epithelial, EMT, MES-like) was assessed by FACS 1, 3, 7, 10, and 14 days post-sort. Data in D, E, and G are represented as mean ± SEM. *, $p<0.05$; **, $p<0.01$; ***, $p<0.001$.

the capacity to generate each of the three tumor cell populations. Epithelial, EMT, and MES-like tumor cell populations were isolated by FACS from the *PKV* line (Figure 1C) and cultured separately. Fourteen days after plating, each population was able to give rise to all three tumor cell populations as determined by FACS analysis and fluorescent imaging (Figures 1F; Figure S1B). Interestingly, while the majority of sorted epithelial and MES-like tumor cells remained in their initial cell state, with small subsets of the other cell populations arising, the majority of EMT tumor cells had transitioned into fully epithelial or MES-like states as early as 24 hours after plating (Figure 1G). Moreover, each sorted cell population maintained a similar percentage of EMT tumor cells 14 days after plating, demonstrating that EMT tumor cells exist in a plastic, transitory state (Figure 1G). Overall, these results demonstrate that prostate tumor cells with PI3K/AKT and RAS/MAPK co-activation have the plasticity to readily transition between epithelial and mesenchymal states through both an EMT and MET.

Epithelial-mesenchymal transition states dictate response to PI3K and MAPK pathway inhibition and differential gene expression profile

The dynamic epithelial-mesenchymal plasticity observed in our genetically defined system raised the issue as to whether such plasticity contributes to the heterogeneous response of prostate cancer cells to targeted therapies, including PI3K and MAPK pathway inhibitors. To address this issue, *PKV* cells were treated with the dual PI3K/mTOR inhibitor PKI-587, the MEK inhibitor PD0325901, or both for 7 days, and the total number of each tumor cell subpopulation remaining after treatment was assessed by FACS and presented as the percentage of each subpopulation compared with vehicle-treated control cells. While the total number of the epithelial and EMT

tumor cells was drastically reduced by treatment with PKI587, PD0325901, or both, the MES-like tumor cell population was relatively unaffected by PI3K and MAPK pathway inhibition (Figure 2A).

As epithelial, EMT, and MES-like tumor cells were all initially derived from Cre^+ prostate epithelial cells harboring *Pten* deletion and *Kras* activation and are in principle genetically identical, we next wanted to ascertain what additional pathways may be altered during the EMT process to account for their differential phenotypes and responses to PI3K/AKT and RAS/MAPK pathway inhibition, especially during the transition of EMT cells to a fully mesenchymal state (EMT-M transition). To this end, we profiled the transcriptomes of epithelial, EMT, and MES-like tumor cells isolated from the prostates of 10-12 week old *CPKV* mice through RNA-sequencing (RNA-seq) analysis. RNA-seq analysis revealed that the epithelial and EMT tumor cell populations (E-EMT transition) had a relatively similar gene expression profile with only 591 differentially expressed genes (DEGs) between the two states; the EMT-M transition, on the other hand, had a dramatically different gene expression profile with 4234 DEGs (Figures 2B and 2C). Gene Ontology (GO) analysis revealed shared pathway alterations between the E-EMT and EMT-M transitions, including changes in focal adhesion, actin cytoskeleton regulation, developmental pathways (urogenital system development, neural crest development) and inflammatory pathways (inflammatory response, cytokine-cytokine receptor, chemokine signaling) (Figures 2D and 2E). However, additional pathway alterations were found during the EMT-M transition, including changes in embryonic morphogenesis, Wnt signaling, apoptosis, and p53 signaling pathways (Figure 2E), which may explain the enhanced *in vivo* tumorigenic potential and stemness activity of mesenchymal-like tumor cells as was reported in

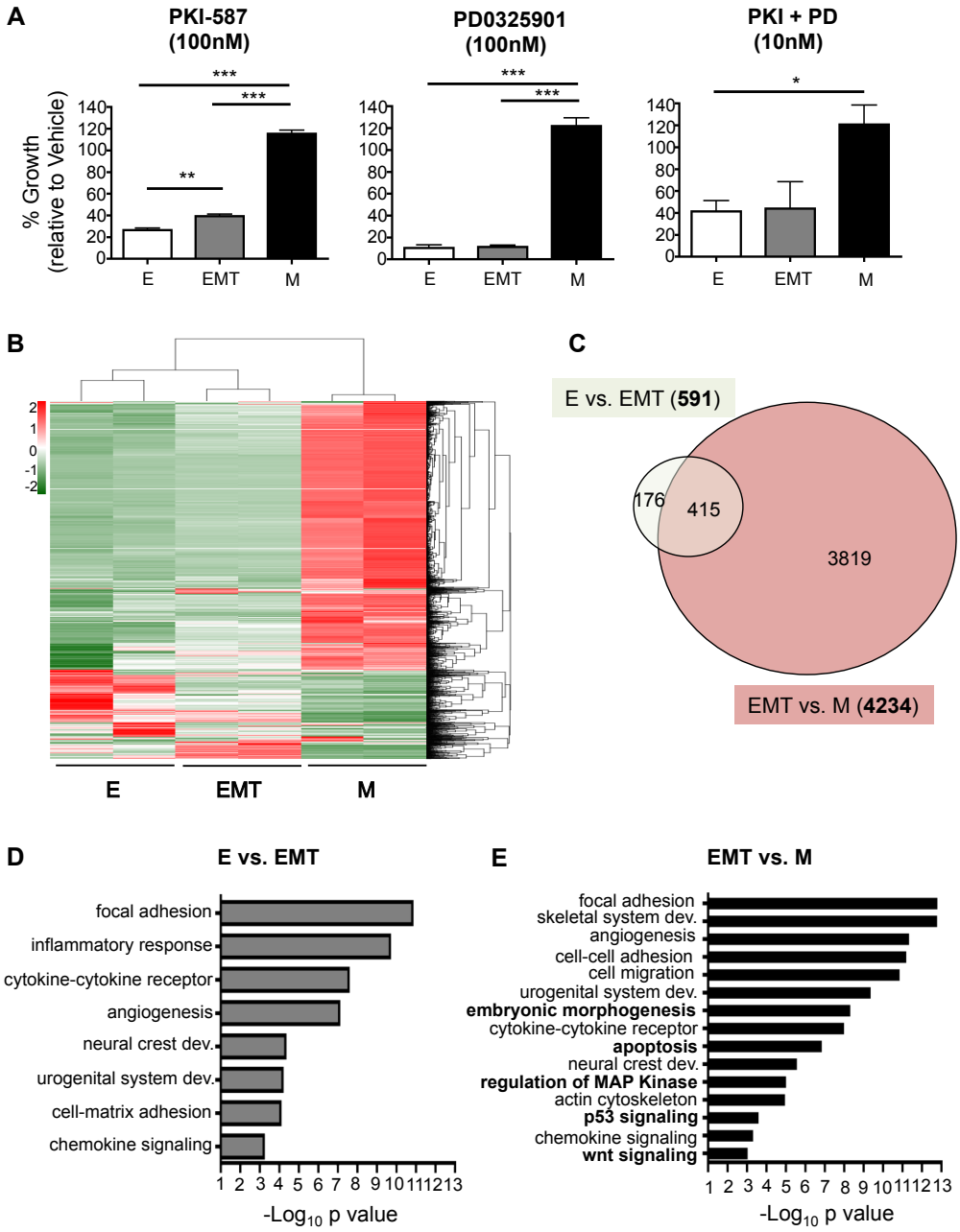

Figure 2. Epithelial-mesenchymal transition states dictate response to PI3K and MAPK pathway inhibition and differential gene expression profile. (A) *PKV* cells were treated with vehicle alone (DMSO), PKI-587 (100nM), PD0325901 (100nM), or both (10nM for each) for 7 days. MES-like (M) tumor cell growth is unaffected by treatment with PI3K and MAPK pathway inhibitors. % growth is relative to vehicle-treated cells. (B) The gene transcription profiles of epithelial (E), EMT, and MES-like (M) tumor cells isolated from the prostates of 10-12 week old *CPKV* mice as assessed by RNA-seq. Heatmap displays mean-centered gene transcription levels of 2190 genes with average FPKM no less than 0.01 and coefficients of variation higher than 0.5. (C) Venn diagram showing the overlap of differentially expressed genes (DEGs) between epithelial vs. EMT (E vs. EMT) and EMT vs. MES-like populations (EMT vs. M). The MES-like tumor cell population has a large number of DEGs compared to the EMT (4234) tumor cell population. (D) Significantly enriched Gene Ontology (GO) items for differentially transcribed genes between epithelial (E) and EMT tumor cell populations. (E) Significantly enriched GO items for differentially transcribed genes between EMT and MES-like (M) tumor cell populations. Items in bold are solely enriched in the EMT-M transition. Data in A is represented as mean ± SEM. *, $p<0.05$; **, $p<0.01$; ***, $p<0.001$.

our recent publication (Chapter 5). Overall, while the early EMT process (E-EMT transition) has relatively few changes in gene expression, the late EMT process (EMT-M transition) is accompanied by a widespread shift in gene expression, including changes in key stem cell, developmental, and cell survival pathways that may ultimately lead to resistance PI3K/AKT and RAS/MAPK pathway inhibition.

EMT signature genes highly expressed in EMT and mesenchymal-like tumor cells are also highly expressed in human metastatic prostate cancer

To determine if EMT-related genes are also expressed in human metastatic prostate cancer samples, we used rank-rank hypergeometric overlap (RRHO) analysis to find those genes that are highly expressed in metastatic tumors in two separate human prostate cancer datasets: 1) the Taylor et al. dataset, which has 29 normal, 131 primary tumor, and 19 metastatic tumor samples (7), and 2) the Grasso et al. dataset, which contains 28 benign, 59 localized cancer, and 34 metastatic CRPC samples (29). As shown in Figure 3A, the two human datasets are very similar to each other. Importantly, a set of EMT signature genes is upregulated in human metastatic prostate tumor samples from both datasets (red circle in Figure 3A). We then analyzed the expression of the EMT signature genes found to be upregulated in human metastatic prostate cancer in two different murine gene expression datasets derived from 1) microarray analysis of laser capture microdissected well-differentiated (epithelial) and poorly differentiated tumor tissue from *CPK* prostates and 2) RNA-seq analysis of epithelial, EMT, and MES-like tumor cells FACS sorted from CPKV prostates. We determined that these EMT signature genes, which include *Snail, Twist1, Foxc2, Fn1, Mmp3, Mmp9, Lox, and Loxl2*, were also upregulated in the

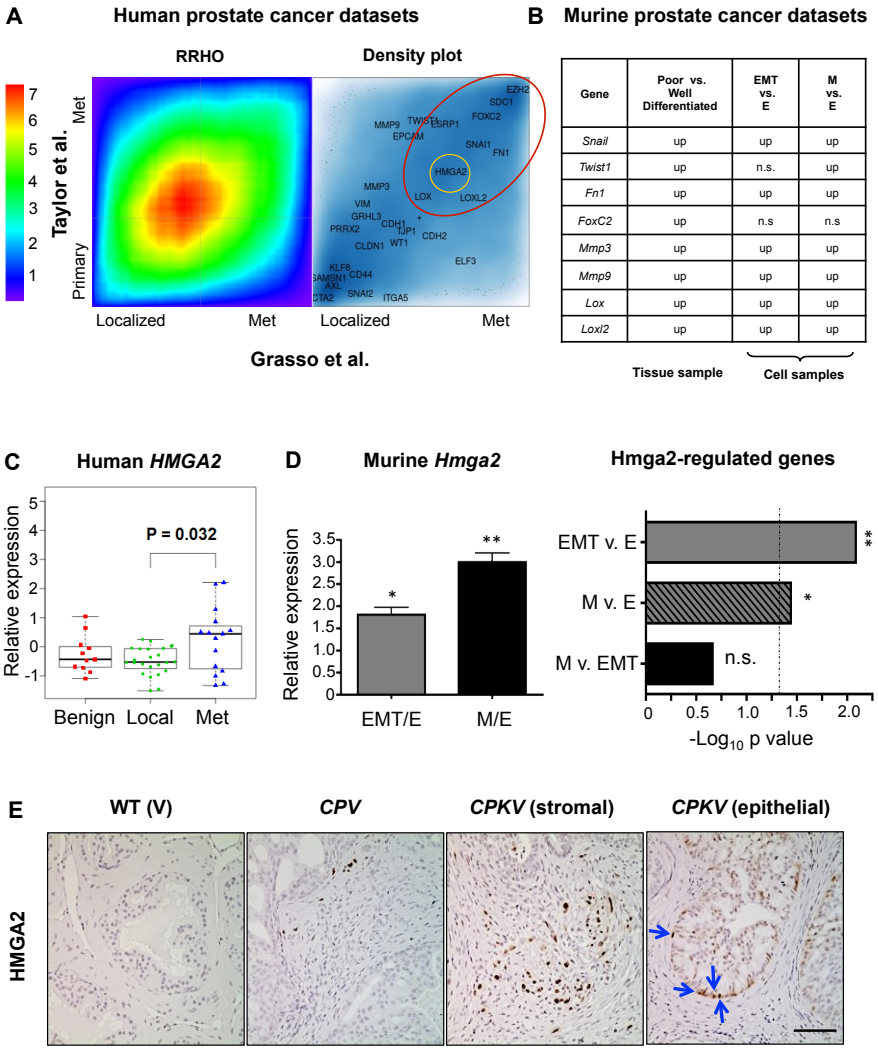

Figure 3. **Hmga2 is highly expressed in human mCRPC and in murine EMT and mesenchymal-like tumor cells.** (A) Heat map comparing the overlap of differentially expressed genes in primary/localized and metastatic (met) prostate tumor specimens from the Taylor et al. and Grasso et al. human prostate cancer datasets based on rank-rank hypergeometric overlap (RRHO) (Left Panel). The color bar indicates the transformed $\log_{10}$ hypergeometric enrichment p-value between two ordered gene sets. Right Panel, selected epithelial and EMT signature genes were plotted corresponding to their signed and logged p-value ranks based on differential expression between metastatic and primary cancer samples. A number of EMT signature genes (large red circle) were consistently ranked at similar positions in both human prostate cancer datasets. *HMGA2* (small yellow circle) was among the group of genes differentially expressed in metastatic prostate cancer in both human datasets. (B) EMT genes upregulated in human metastatic prostate cancer were differentially expressed in murine datasets obtained from 1) laser capture microdissection microarray analysis of prostate tissue samples ($p<0.05$) and 2) RNA-seq analysis of FACS sorted cell populations (FDR<0.05). EMT genes were often upregulated in poorly differentiated prostate tissue and in EMT and MES-like (M) tumor cells. Up, upregulated; n.s., not significant. (C) *HMGA2* expression levels in benign, localized (local), and metastatic CRPC (met) patient samples from Grasso et al. reveals that *HMGA2* expression is significantly upregulated in mCRPC compared to localized disease. (D) *Hmga2* expression is significantly upregulated in EMT and MES-like (M) tumor cells compared to epithelial tumor cells (Left Panel). Right Panel, Fisher's exact test was used to assess enrichment of HMGA2-regulated genes from Sun et al. in differentially expressed genes between the EMT vs. epithelial (EMT v. E) and MES-like vs. epithelial (M v. E) tumor cell populations. Dotted line, p-value= 0.05; n.s, not significant. (E) HMGA2 protein expression is highly induced in both the stroma and epithelium (arrows) of *CPKV* prostates compared to *CPV* and *V* prostates. Scale bar, 50 μm. Data in C and D are represented as mean ± SEM. *, $p<0.05$; **, $p<0.01$.

poorly differentiated murine prostate cancer tissue samples and cells with EMT and MES-like characteristics (Figures 3A and 3B). These data provide evidence that EMT signature gene expression, as defined in our EMT and MES-like tumor cell populations, is associated with metastatic disease and CRPC in the human setting and is therefore likely to have clinical relevance.

The epigenetic regulator Hmga2 is highly expressed in human mCRPC and in murine EMT and mesenchymal-like tumor cells

Recent studies suggest that the master transcriptional regulators of the EMT process depend on epigenetic regulatory mechanisms, particularly those involved in chromatin remodeling, in order to achieve widespread changes in gene expression observed during EMT (30). The massive shift in gene expression between EMT and MES-like tumor cell populations (Figures 2B and 2C) prompted us to hypothesize that epigenetic alterations may play a key role in both initiating and maintaining the mesenchymal state. By surveying those genes that are highly expressed in metastatic tumors in both human datasets based on the RRHO analysis, we identified the epigenetic regulator HMGA2 (yellow circle in 3A), a non-histone chromatin remodeling protein, as a gene strongly associated with human metastatic prostate cancer. HMGA2, through its ability to bind to the minor groove of AT-rich DNA sequences and introduce structural alterations in chromatin that either promote or inhibit the actions of transcriptional enhancers, can alter global gene expression (31). HMGA2 is also known to be associated with embryonic and adult stem-cell states (32-34), and has been previously implicated in 1) modulating the microenvironment to promote prostate tumorigenesis through regulation of Wnt/β-catentin signaling, 2) regulating

Snail expression through TGFβ/SMAD2, and 3) maintaining Ras-induced EMT (35-37). The expression of *HMGA2* is significantly upregulated in human mCRPC compared to localized prostate cancer (29) (Figure 3C). Similarly, *Hmga2* expression is also significantly upregulated in both EMT and MES-like tumor cells compared to epithelial tumor cells (Figure 3D, left panel). In addition to *Hmga2* expression, the Hmga2-regulated transcriptome (26) is also significantly differentially expressed between EMT vs. epithelial and MES-like vs. epithelial tumor cells (Figure 3D, right panel). Compared to WT (*V*) and *Pten null* (*CPV*) prostates, *CPKV* prostates have dramatic induction of HMGA2 protein expression in both the stroma and in a small population of cells within epithelial glandular structures (arrows) (Figure 3E). Hence, these findings suggests that HMGA2 may be an essential factor in modulating epithelial-mesenchymal plasticity, and that *HMGA2* expression could help to stratify human prostate cancer patients that are likely to progress to mCRPC.

Hmga2 regulates stemness and epithelial-mesenchymal plasticity in prostate tumor cells with PI3K/AKT and RAS/MAPK co-activation

To explore the functional role of Hmga2 in our model, we stably knocked down Hmga2 expression in the *PKV* cell line using a short hairpin RNA (shRNA) targeting Hmga2 (Figure 4A). Hmga2 knockdown had no effect on cell proliferation, as *PKV-shHmga2* cells had a similar growth rate compared to *PKV* cells that were stably transduced with a control *shScramble* construct (Figure 4B). In order to investigate the effect of Hmga2 knockdown on the stemness attributes of *PKV* cells, we performed a matrigel sphere formation assay. Compared to control *PKV-shScramble* cells, *PKV-shHmga2* cells had significantly reduced sphere-forming capacity,

indicative of a reduced capacity for anchorage-independent and clonal growth (Figure 4C). Moreover, Hmga2 knockdown significantly reduced the expression of a number of pluripotency factors, including *Oct4, Sox2*, and *Klf4*, as well as other genes known to regulate self-renewal (Figure 4D). These findings demonstrate that Hmga2 activity is important for the maintenance of stemness in *PKV* cells.

Interestingly, compared to the *PKV-shScramble* cell line, the *PKV-shHGMA2* line maintains a relatively reduced percentage of MES-like tumor cells and an increased percentage of EMT tumor cells, suggesting that Hmga2 activity may be required for the EMT-M transition (Figure 4E). To further investigate how Hmga2 regulates epithelial-mesenchymal plasticity, we FACS sorted epithelial, EMT, and MES-like tumor cell populations from *PKV-shScramble* and *PKV-shHGMA2* cells and plated them separately in culture for 7 days. Epithelial, EMT, and MES-like tumor cell populations isolated from *PKV-ShScramble* cells all have the capacity to transition into all three tumor cell states (Figure 4F; Figure S2) with similar kinetics to parental *PKV* cells (Figure 1G). However, in *PKV-shHmga2* cells, sorted epithelial and EMT subpopulations maintained a relatively higher percentage of epithelial cells and a lower percentage of MES-like tumor cells after 7 days in culture compared with control *PKV-shScramble* cells, indicative of a stall in epithelial-mesenchymal plasticity (Figure S2). Importantly, Hmga2 knockdown significantly destabilized the MES-like tumor cell state, as a significantly higher percentage of MES-like tumor cells sorted from the *PKV-shHmga2* line transitioned to both epithelial and EMT states compared to those isolated from control *PKV-shScramble* cells (Figure 4F). From these results, we can conclude that Hmga2 knockdown 1) reduces stemness activity, 2) influences the overall plasticity of epithelial and EMT tumor cells, and 3) destabilizes the MES-like state, enabling MES-like tumor cells to more readily undergo

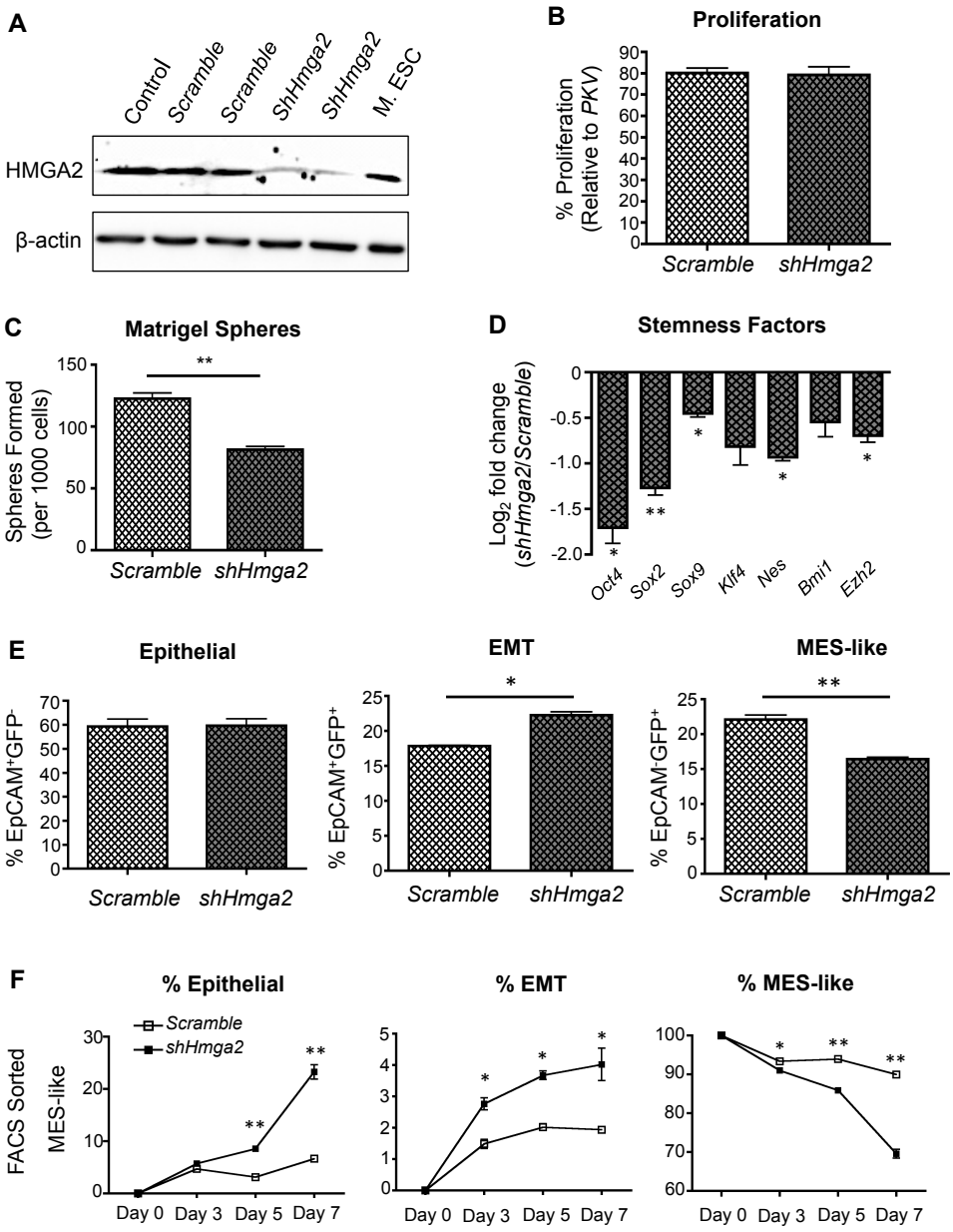

Figure 4. **Hmga2 regulates stemness and epithelial-mesenchymal plasticity in prostate tumor cells with PI3K/AKT and RAS/MAPK co-activation.** (A) ShRNA-targeted knockdown of HMGA2 protein expression in *PKV* cells. Mouse embryonic stem cells (M. ESC) were used as a positive control for HMGA2 expression. β-actin was used as a loading control. Control, *PKV* cells. *Scramble*, *shScramble*. (B) The proliferation of the *PKV-shScramble (Scramble)* and *PKV-shHmga2 (shHMGA2)* cell lines was measured by MTT assay and is presented as % growth compared to control *PKV* cells. (C) *PKV* cells stably expressing *shHmga2* have significantly reduced matrigel sphere-forming capacity compared to control *PKV-shScramble (Scramble)* cells. (D) Hmga2 knockdown reduces the expression of a number pluripotency and self-renewal factors. Expression is relative to gene expression values found in *PKV-shScramble (Scramble)* cells. (E) FACS analysis of the *PKV-shScramble (Scramble)* and *PKV-shHmga2* cell lines revealed that throughout passaging, *PKV-shHmga2* cells maintained a lower percentage of MES-like and higher percentage of EMT tumor cells compared to *PKV-shScramble* cells, indicative of a blockade in the transition of EMT tumor cells into fully MES-like tumor cells. (F) FACS sorted MES-like tumor cell populations from *PKV-shHMGA2* cells have reduced mesenchymal content and increased epithelial and EMT tumor cell numbers compared to control *PKV-shScramble (Scramble)* cells after 7 days in culture. Data in B through F are represented as mean ± SEM. *, $p<0.05$; **, $p<0.01$.

an MET. Therefore, Hmga2 plays an essential role in both the maintenance of stemness qualities, as well as in regulating epithelial-mesenchymal plasticity and the mesenchymal state in our model.

HDACi treatment effectively targets EMT and mesenchymal-like tumor cells through inhibition of HMGA2 activity and induction of p53-mediated apoptosis

As changes in expression of HMGA2 target genes alone cannot account for the more than 4000 DEGs found altered during the EMT-M transition (Figure 2C) (26, 38), we hypothesized that other epigenetic regulators may also be important in regulating such a transition. To examine this hypothesis, we looked at differential expression of various epigenetic regulatory genes among our three tumor cell populations using a recently characterized list of genes associated with epigenetic regulation (39). While there were only 3 epigenetic regulatory genes whose expression were altered between epithelial and EMT tumor cells, 97 epigenetic regulatory genes were differentially expressed between the EMT and MES-like tumor cell states (Figure S3A), including several HDACs that were also found to be significantly overexpressed in human mCRPC (Figure 5A). Since previous studies have demonstrated that histone deacetylase inhibitors (HDACi) can effectively inhibit *HMGA2* expression at the transcriptional level (40, 41), we tested whether HMGA2 expression could be modulated by HDAC activity. When we treated the *PKV* cell line with LBH589 (Panobinostat), a pan-HDACi, LBH589 significantly reduced *Hmga2* gene expression while increasing H3K27 acetylation levels in a dose-dependent manner (Figures 5B and 5G). While low doses of LBH589 (1nM), which did not affect cell proliferation (data not shown) or apoptosis (Figure 5D), had little effect on epithelial and EMT

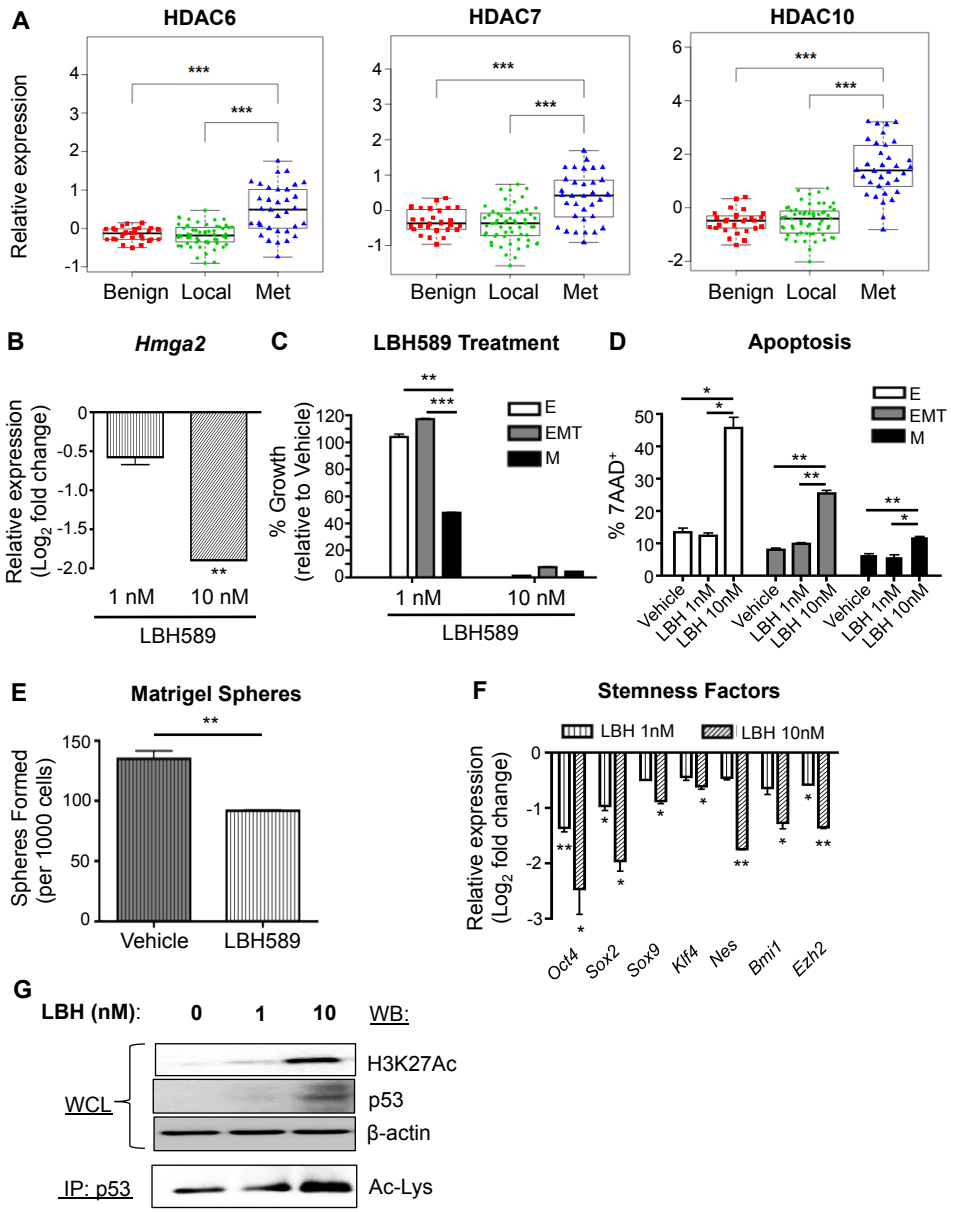

Figure 5. **HDACi treatment effectively targets EMT and mesenchymal-like tumor cells through inhibition of HMGA2 activity and induction of p53-mediated apoptosis.** (A) Analysis of *HDAC* expression levels in benign, localized (local), and metastatic CRPC (met) patient samples from Grasso et al. reveals that *HDAC6, HDAC7,* and *HDAC10* expression is significantly upregulated in mCRPC compared to localized or benign disease. (B) LBH589 treatment (24 hr) of *PKV* cells reduces *Hmga2* expression in a dose-dependent manner. Expression is relative to gene expression values found in vehicle-treated cells. (C) LBH589 treatment (7 day) preferentially reduces MES-like (M) tumor cell numbers at low doses (1nM), and successfully targets all tumor cell populations at higher doses (10nM). % growth is relative to vehicle-treated cells. (D) 7 day treatment of the *PKV* cell line with 10nM LBH589 induces significantly increased levels of apoptosis, as measured by the percentage of $7AAD^+$ cells, in all epithelial (E), EMT, and MES-like (M) tumor cell populations. (E) Low doses of LBH589 (1nM) significantly reduce the sphere-forming capacity of *PKV* cells after 7 days in Matrigel culture (F) LBH589 treatment (24 hr) reduces the expression of various stemness factors in *PKV* cells compared to vehicle alone. (G) LBH589 treatment (6 hr) induces p53 expression and increases H3K27 and p53 acetylation levels in *PKV* cells. β-actin was used as a loading control. IP, immunoprecipitation; WCL, whole cell lysate; WB, Western Blot; Ac-Lys, acetylated lysine antibody. Data in A through F are represented as mean ± SEM. *, $p<0.05$; **, $p<0.01$; ***, $p<0.001$.

tumor cells, it significantly decreased MES-like tumor cell numbers (Figures 5C) and reduced the overall sphere-forming capacity and stem cell-related gene expression of *PKV* cells (Figures 5E and 5F), mirroring the effects observed upon shRNA-mediated Hmga2 knockdown (Figure 4). This suggests that HDACi treatment can indeed inhibit HMGA2 activity and in turn suppress HMGA2-mediated epithelial-mesenchymal plasticity and stemness activity, and, importantly, target a MES-like tumor subpopulation that is relatively insensitive to PI3K and MAPK pathway inhibition (Figure 2).

Higher doses of LBH589 (10nM), on the other hand, were able to induce significant apoptosis and successfully inhibit the growth of all three tumor cell populations (Figures 5C and 5D), suggesting that LBH589 treatment may modulate other factors in addition to its effects on Hmga2 expression. We previously demonstrated that p53 protein levels are greatly reduced in the *CPK* murine prostate cancer model compared to *Pten* null and WT mice (17). We found in our current study that higher concentrations of LBH589 (10nM) significantly increased p53 protein levels (Figure 5G), while *p53* and *Mdm2* mRNA levels remained relatively unchanged (Figure S3B). As p53 acetylation has been shown to enhance its stability, DNA binding affinity, and transcriptional activity associated with cell cycle arrest and apoptosis (42-44), we looked directly at LBH589-induced p53 acetylation, and found that p53 acetylation levels were significantly elevated with increasing concentrations of LBH589 (Figure 5G). P-p53 (Ser15) levels were unaffected by LBH589 treatment (data not shown), suggesting that increased p53 levels in LBH589-treated samples is a consequence of enhanced p53 acetylation rather than altered p53 phosphorylation. Therefore, LBH589-induced p53 acetylation is one mechanism by which LBH589 is able to induce apoptosis in all *PKV* cell populations, including MES-like tumor cells.

HDACi treatment dramatically reduces the primary prostate tumor burden *in vivo*

Given the efficacy of LBH589 in targeting EMT and MES-like tumor cells *in vitro*, we next wanted to assess the impact of HDACi treatment on primary tumor growth *in vivo*. *CPKV* mice were treated with vehicle alone or LBH589 starting at 10 weeks of age, a time point when animals have already developed aggressive prostate tumors with poorly differentiated EMT features (17). After only 2 weeks of treatment with LBH589, there was a dramatic decrease in primary tumor size, most notably in the anterior lobes (Figure 6A, arrows in upper panel). Further histological examination revealed large glandular cysts in the anterior lobes and degenerated, scar-like tissue in the dorsolateral lobes of LBH589-treated mice (Figure S4A), likely resulting from massive cell death. Additionally, there was also a dramatic decrease in the Ki67 proliferation index in both the epithelial and stromal compartments of LBH589-treated mice compared to mice receiving vehicle alone (Figure 6A, lower panel). H3K27 acetylation levels were increased in the prostate epithelium and stroma of *CPKV* mice treated with LBH589 compared to vehicle alone (Figure S4B), verifying that LBH589 was effectively hitting its target. Importantly, FACS analysis revealed a statistically significant decrease in the EMT and MES-like tumor cell populations in the primary tumor site of LBH589-treated mice compared to those treated with vehicle alone, thus confirming the effectiveness of HDACi treatment at inhibiting these populations *in vivo* (Figure 6B). Mirroring our *in vitro* findings, the prostates of LBH589-treated *CPKV* mice also had substantially reduced HMGA2 expression and induction of strong p53 nuclear staining compared vehicle-treated mice (Figure 6C). Therefore, LBH589 treatment effectively reduces primary tumor growth and targets EMT and MES-like tumor cells in *CPKV* mice by modulating HMGA2 and p53 levels.

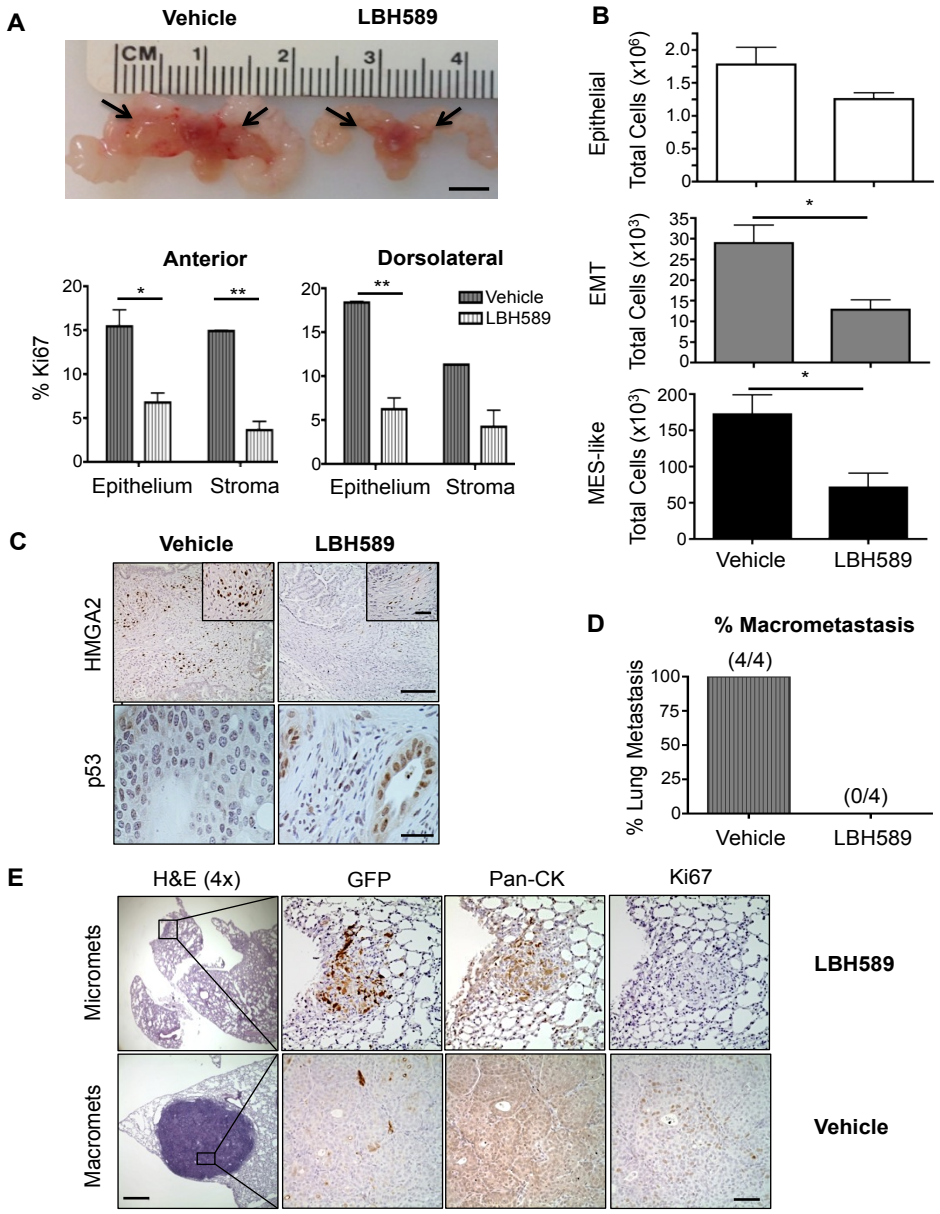

Figure 6. **HDACi treatment inhibits prostate tumor growth, tumor cell dissemination, and metastasis *in vivo*.** (A) 10 wk old *CPKV* mice treated with LBH589 for 2 weeks had dramatically reduced tumor burden, particularly in the anterior lobes (arrows), compared to vehicle-treated mice (Top Panel). Scale Bar, 5 mm. Bottom Panel, the Ki67 proliferation index is significantly reduced in LBH589-treated *CPKV* mice (n=4) compared to *CPKV* mice receiving vehicle alone (n=3). (B) LBH589-treated *CPKV* mice (n=9) have a significant reduction in the EMT and MES-like tumor cell populations compared to vehicle-treated mice (n=6). (C) LBH589 treatment significantly reduces HMGA2 expression (Top Panel) and induces p53 expression (Bottom Panel) in the prostates of *CPKV* mice. Scale bar, top panel, low magnification, 100 μm; top panel, high magnification, 25 μm; bottom panel, 25 μm. (D) LBH589 treatment inhibits the formation of lung macrometastases in *NSG* mice transplanted with *PKV* cells by tail vein injection. (E) Representative lung histology of *NSG* mice 8 weeks after transplantation of *PKV* cells by tail vein injection. While LBH589-treated mice did not develop macrometases (0/4), they did develop small micrometastases that were non-proliferative ($Ki67^-$) and GFP^+ (Top Panel). Bottom Panel, vehicle-treated mice formed large, proliferating ($Ki67^+$) macrometastases that are GFP^- and have strong expression of Pan-Cytokeratin (Pan-CK), indicative of an epithelial phenotype. Scale bar, low magnification, 500 μm; Scale bar, high magnification, 50 μm. Data in A and B are represented as mean ± SEM. *, $p<0.05$. **, $p<0.01$.

HDACi treatment inhibits tumor cell dissemination and distant metastasis *in vivo*

Since *CPKV* mice already have significant tumor cell dissemination into the blood stream at 10 weeks of age (Chapter 5), we wanted to investigate the impact of LBH589 therapy on circulating tumor cell (CTC) numbers and distant metastasis. Peripheral blood was collected from LBH589 and vehicle-treated *CPKV* mice following 2 weeks of treatment. While LBH589 treatment had little effect on the number of $EpCAM^{+}GFP^{-}$ epithelial circulating tumor cells (CTCs) in the blood, treatment dramatically reduced the number of $EpCAM^{-}GFP^{+}$ CTCs with mesenchymal-like features (Figure S4C), further validating the specificity of LBH589 treatment at targeting MES-like tumor cell populations. To determine the effect of LBH589 treatment on metastasis, we developed an *in vivo* dissemination model by transplanting 500,000 *PKV* cells by tail vein injection into *NOD/SCID/IL2Rγ-null* (*NSG)* mice. While 100% of mice treated with vehicle alone (4/4) developed lung macrometastases 8 weeks post-transplantation, LBH589 treatment completely blocked the formation of macrometastases (0/4) (Figure 6D). Although mice receiving LBH589 treatment still developed small, non-proliferative micrometastases in the lungs that maintained GFP expression, they did not develop the proliferative, GFP^{-} macrometastases found in vehicle-treated mice (Figure 6E). Therefore, LBH589 treatment seems to block a rate-limiting step in metastasis: the transition of non-proliferative micrometastases with mesenchymal/EMT features into proliferative macrometastases with epithelial features. Overall, these data demonstrate that HDACi treatment with LBH589 is effective at suppressing primary tumor growth, tumor cell dissemination, and metastasis *in vivo* by inhibiting HMGA2 expression, inducing P53–dependent apoptosis, and subsequently targeting EMT and MES-like tumor cells.

Mesenchymal-like tumor cells are castration-resistant and contribute to early lethality in *CPKV* mice

Recent studies have shown that androgen deprivation therapy (ADT) can induce an EMT in benign and neoplastic prostate epithelium (12), and that EMT contributes to the development of CRPC (11). We therefore wanted to determine if the EMT and MES-like tumor cell populations in our model are further enriched by ADT and could potentially accelerate CRPC development. To test this hypothesis, we castrated *CPKV* mice at 6 weeks of age, and subsequently analyzed the effects of castration on tumor growth and overall animal survival. While *CPKV* prostates initially experience tumor regression, particularly in the anterior lobes at 1 week post-castration, by 2 weeks post-castration, castration-resistant tumors have completely grown back (Figure S5A, black circles), inducing early lethality in *CPKV* mice with a median survival of ~3 weeks post-castration (Figure 7A). Indeed, although the Ki67 proliferation index is reduced in the anterior lobes of *CPKV* mice 1 week post-castration, by 2 weeks post-castration, the proliferation index returned to levels similar to those found in intact (non-castrated) *CPKV* mice (Figure 7B). Such fast regrowth and early lethality are in sharp contrast to our previous study of castration in the *Pten* null model, in which tumors returned to their original sizes 4-8 weeks post-castration and very few animals succumbed to CRPC-related mortality (45, 46).

To investigate the causes for such an early lethality, we compared epithelial, EMT, and MES-like tumor cell numbers before and 2 weeks after castration, and found that while the epithelial and EMT tumor cell populations were significantly decreased in response to castration, the MES-like tumor cell population remained relatively stable (Figure 7C, right panel). RNA-seq analysis revealed that AR expression, along with a number of AR target genes, is significantly

downregulated in the MES-like tumor cell population compared to the epithelial tumor cell population (Figure 7D), which may explain the poor responsiveness of MES-like cells to castration. Indeed, when the *PKV* cell line was treated with media stripped of androgens (charcoal/dextran treated (CDT) FBS), we observed a similar phenotype: while epithelial and EMT tumor cell growth was inhibited, ADT had a minimal effect on MES-like tumor cell growth (Figure 7E). These data suggest that MES-like tumor cells, through downregulation of the AR signaling axis, are inherently castration-resistant, and likely contribute to the early lethality observed in castrated *CPKV* mice.

HDACi treatment can effectively inhibit the development of CRPC by targeting castration-resistant mesenchymal-like tumor cells

Given the substantial effect that HDACi treatment has on MES-like tumor cell growth and survival both *in vitro* and *in vivo* (Figures 5 and 6), we reasoned that HDACi therapy in combination with castration might inhibit castration-resistant disease and in turn improve the overall survival of *CPKV* mice post-castration. At 6 weeks of age, *CPKV* mice were castrated and administered either LBH589 or vehicle alone. *CPKV* mice receiving LBH589 had significantly reduced tumor burden 2 weeks post-castration as determined by decreased anterior lobe size (Figure S5A) and significantly reduced prostate weight (Figure S5B). Remarkably, LBH589 treatment was able to significantly improve the overall survival of castrated *CPKV* mice, nearly doubling the median survival from ~21 days to ~37 days post-castration (Figure 7A). Moreover, castrated mice receiving LBH589 treatment had a significantly diminished Ki67 proliferation index in both the epithelial and stromal compartments compared to mice receiving

vehicle alone (Figure 7B). In sharp contrast to castration alone, LBH589 treatment in combination with castration was able to significantly reduce the number of MES-like tumor cells, as well as further diminish the epithelial and EMT tumor cell populations (Figure 7C, right panel). Therefore, LBH589 treatment can effectively improve the overall survival of castrated *CPKV* mice by targeting castration-resistant MES-like tumor cells.

HDACi treatment induces reactivation of AR signaling and sensitizes mesenchymal-like tumor cells to ADT-induced apoptosis

Finally, we wanted to determine the impact of HDACi treatment on AR signaling *in vivo*. While castration alone led to weaker and more cytoplasmic AR protein expression in the anterior lobes, LBH589 treatment in combination with castration led to restoration of strong nuclear AR staining, similar to that found in intact *CPKV* prostates (Figure 7F, see high powered inserts). As further confirmation of HDACi-induced reactivation of AR signaling, *CPKV* mice treated with LBH589 had significant induction of AR downstream target gene expression, including increased expression of *Tmprss2, Nkx3-1, Fkbp5,* and *Slc45a3* (Figure 7G). Previous studies have suggested that acetylation of AR in its flexible hinge region is required for maximal AR activation and transcriptional activity through its regulation of the DNA binding, nuclear translocation, and transactivation of AR (47, 48). Moreover, HDAC1 has been shown to interact directly with AR and repress AR activity through its effects on AR acetylation (49). As a mechanism behind heightened AR nuclear localization and transcriptional activity following LBH589 treatment, we explored whether AR acetylation itself was enhanced upon LBH589 treatment. As early as 6 hours post-treatment, *PKV* cells treated with LBH589 had dramatically

increased AR acetylation levels compared to cells treated with vehicle alone (Figure S5C). Interestingly, the ratio of acetylated AR to total AR levels after LBH589 treatment is similar to the ratio found in androgen-dependent LNCaP human prostate cancer cells, showing that HDACi treatment with LBH589 leads to AR nuclear localization and increased AR transcriptional activity as would be found in an androgen-dependent context.

To investigate if LBH589 treatment could sensitize MES-like tumor cells to growth inhibition and apoptosis induced by ADT, *PKV* cells were treated with LBH589 in the absence of androgens (CDT FBS). A low concentration of LBH589 (1nM), which by itself only partially reduces MES-like tumor cell numbers, was indeed able to synergize with ADT to sensitize castration-resistant MES-like tumor cells to ADT-induced growth inhibition and significantly reduce MES-like tumor numbers compared to either treatment alone (Figure 7E). Moreover, while androgen withdrawal or 1nM LBH589 treatment alone were unable to induce apoptosis, androgen withdrawal in combination with LBH589 treatment induced significant apoptosis in all three tumor cell populations, including castration-resistant MES-like tumor cells (Figure S5D). These results suggest that HDACi therapy leads to the reactivation of AR signaling in AR-independent MES-like tumor cells, making them sensitive to ADT-induced apoptosis. Overall, while castration leads to expansion of the castration-resistant MES-like tumor cell population and early lethality in CPKV mice, LBH589 treatment in combination with castration significantly prolongs survival by successfully targeting the MES-like tumor cell population and thereby impeding the onset of CRPC.

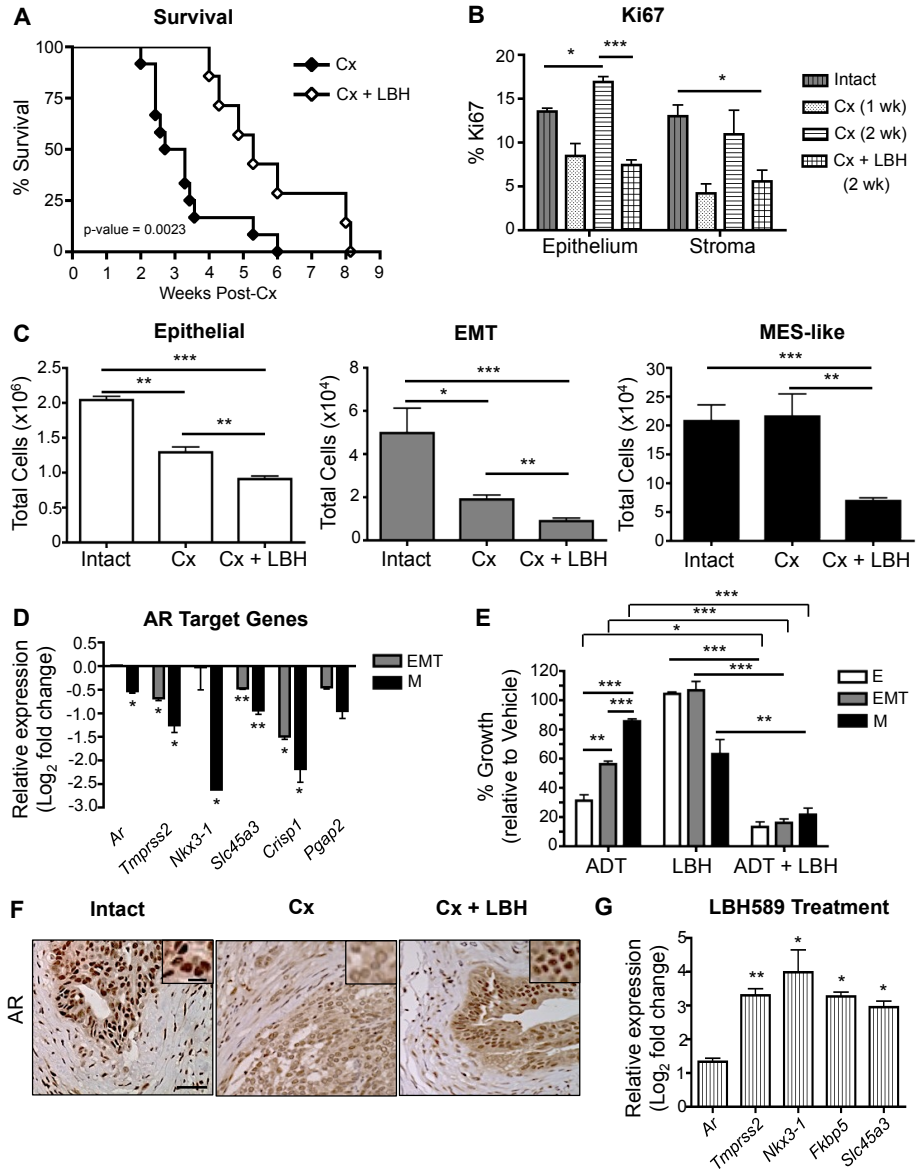

Figure 7. **HDACi treatment can effectively inhibit the development of CRPC by targeting castration-resistant mesenchymal-like tumor cells.** (A) While castration (Cx) of *CPKV* mice (n=12) at 6 weeks of age led to early lethality, LBH589 treatment in combination with Cx (n=7) significantly increased overall survival. (B) LBH589 treatment in combination with Cx significantly lowered the Ki67 proliferation index in *CPKV* prostates. n=3 for Intact and Cx samples; n=4 for Cx + LBH samples. (C) Castrated (Cx) mice (n=4) have no change in MES-like tumor cell numbers compared to intact, vehicle-treated mice (n=3). LBH589 treatment in combination with castration (n=6) successfully targets castration-resistant MES-like tumor cells and further reduces epithelial and EMT tumor cell numbers *in vivo*. (D) AR target gene expression is significantly downregulated in MES-like (M) tumor cells compared to epithelial tumor cells isolated from the prostates of 10-12 week old *CPKV* mice as assessed by RNA-seq analysis. Expression is relative to gene expression values found in epithelial tumor cells. (E) 7 day treatment of *PKV* cells with media lacking androgens (CDT-FBS) significantly impeded the growth of epithelial (E) and EMT but not MES-like (M) tumor cells. Low doses of LBH589 (1nM) in combination with ADT sensitize MES-like (M) tumor cells to androgen withdrawal-induced growth inhibition. (F) LBH589 treatment reestablishes nuclear AR expression after Cx in the anterior lobes of *CPKV* prostates. Scale bar, low magnification, 50 μm; high magnification, 10 μm. (G) LBH589 treatment enhances AR target gene expression in *CPKV* prostates compared to vehicle alone. Expression is relative to gene expression values found in vehicle-treated *CPKV* mice. Data in B, C, D, E, and G is represented as mean ± SEM. *, $p<0.05$; **, $p<0.01$; ***, $p<0.001$.

Discussion

Visualizing epithelial-mesenchymal plasticity has been difficult due to its transient nature and the lack of defined biomarkers of epithelial-mesenchymal plasticity. Here, we created an *in vitro* model system of epithelial-mesenchymal plasticity from the previously described *CPKV* murine prostate cancer model (Chapter 5) that contains epithelial, EMT, and mesenchymal-like tumor cell populations harboring *Pten* deletion and conditional *Kras* activation. Using this system, we uncovered a novel mechanism of regulation of epithelial-mesenchymal plasticity mediated by epigenetic rather than genetic mechanisms through the chromatin remodeling protein Hmga2, and determined an effective therapeutic strategy for inhibiting Hmga2 activity, targeting treatment-resistant mesenchymal-like tumor cells, and preventing mCRPC with the HDACi LBH589. These findings provide some of the first *in vivo* evidence that direct targeting of epithelial-mesenchymal plasticity through epigenetic inhibitors can have therapeutic efficacy at blocking the onset of CRPC and preventing distant metastasis. Importantly, we are also able to identify *HMGA2* and a number of EMT signature genes, including *SNAIL*, *FN1*, and *FOXC2*, as potential biomarkers of epithelial-mesenchymal plasticity and metastatic CRPC in the human setting.

The unexpected finding that MES-like tumor cells, unlike epithelial and EMT tumor cells, are resistant to PI3K and MAPK pathway inhibitors despite uniform *Pten* deletion and *Kras* activation in all cell types has important implications in the clinic, as it suggests that clinicians will need to consider the tumor initiation event (genetic event) as well as the tumor cell state/lineage (epigenetic event) when determining optimal treatment for a given patient. One possible resistance mechanism could be that activation of alternative survival or

developmental/stem cell pathways allows for MES-like tumor cell growth and survival that is independent of PI3K and MAPK signaling (50, 51). Indeed, MES-like tumor cells have a dramatic change in the expression of various developmental, growth-signaling, survival, and stem cell pathways compared to epithelial and EMT tumor cells (Figure 2), and these alterations may contribute to therapeutic resistance.

The large number of epigenetic regulators altered in MES-like tumor cells suggests that epigenetic alterations may play a defining role in the differential transcriptional profile of MES-like tumor cells and their lack of sensitivity to PI3K and MAPK pathway inhibitors. Indeed, we discovered that epigenetic changes mediated by the chromatin remodeling protein HMGA2 are necessary for 1) epithelial-mesenchymal plasticity, 2) preservation of the mesenchymal state, and 3) maintenance of stemness activities. Hence, changes in epigenetic regulation via HMGA2 lead to a more stem-like state where MES-like tumor cells are less susceptible to targeted therapy. As an "architectural transcription factor" with the ability to affect the expression of thousands of genes by altering the structure of chromatin, HMGA2 may have many downstream targets (31), including novel regulators of epithelial-mesenchymal plasticity, which require further elucidation in our model. Our transcriptional profiling analysis of the EMT and MES-like tumor cell populations, combined with the ability to visualize and manipulate epithelial-mesenchymal plasticity *in vitro* with the *PKV* cell line, provides an important platform for uncovering novel regulators of epithelial-mesenchymal plasticity that could be targeted therapeutically. Moreover, as early EMT (E-EMT transition) and late EMT phases (EMT-M transition) can be separated, this system provides a unique model for dissecting and differentiating those alterations that are important for the initiation of EMT versus those that are essential for the maintenance of the mesenchymal state. In addition, it will also be important to unravel the global epigenetic changes

in DNA methylation and histone acetylation/methylation patterns that take place in MES-like tumor cells in order to identify novel regulators of these redefined epigenetic states.

Importantly, we were able to therapeutically inhibit Hmga2 expression and eradicate treatment-resistant MES-like tumor cells with the Pan-HDACi LBH589. Interestingly, we found that LBH589 mediated many of its effects through enhanced acetylation of the nuclear transcription factors p53 and AR, which in turn promotes a more differentiated, androgen-dependent cell state that is re-sensitized to apoptosis. As dysregulated p53 signaling in MES-like tumor cells (Figure 2E) likely contributes to the general resistance of this cell state to therapy-induced apoptosis, a drug such as LBH589 that induces p53 activation is likely to have lasting therapeutic benefit by inducing apoptosis rather than cytostasis. Increased AR activity may also lead to the sensitization of MES-like tumor cells to cell death through its ability to regulate p53, as it has been previously demonstrated that NKX3.1, which is a downstream target of AR, can bind to HDAC1 and subsequently lead to increased p53 acetylation through an MDM2-dependent mechanism (44). In addition to these mechanisms, the effect of LBH589 treatment on histone acetylation, chromatin remodeling, and other epigenetic changes is still worthy of further exploration.

As one major issue with the clinical use of HDACi therapy has been the cytotoxicity and adverse effects associated with treatment (52-54), it will be important to determine which specific HDAC isoforms are responsible for regulating Hmga2, p53, and AR expression and activity so that therapeutics that target specific HDAC isoforms can be designed in order to reduce off-target effects. Moreover, as different doses of HDACi treatment may be required to affect changes in acetylation of histone vs. non-histone protein targets, it will be important to

fully validate the desired molecular target of LBH589 treatment before determining the optimal treatment regimen.

The efficacy of LBH589 (Panobinostat) as a single agent in the treatment of CRPC has not been very promising (52, 55). However, the design of the Phase II study of Panobinostat in CRPC patients specified a protocol-defined response of 50% PSA decline, which 0/34 patients met (55). As our study, in contrast to other preclinical studies, demonstrates that HDACi treatment enhances rather than represses AR activation and signaling in prostate tumor cells (56-58), PSA levels are likely to either remain constant or even potentially rise as a consequence of LBH589 treatment. This suggests that new biomarkers are needed to identify patients with prostate cancer who are responsive to HDAC inhibitors. Our results suggest that HDACi treatment may be effective against a subset of CRPC patients with increased HMGA2 and EMT marker expression. As a previous report has shown that *HMGA2* mRNA could be detected in peripheral blood samples of breast cancer patients by RT-PCR and that patients with *HMGA2* expression had a worse prognosis than those without detectable levels, it will be interesting to see if *HMGA2* mRNA levels in the blood are also predictive of mCRPC development and sensitivity to HDACi therapy (59). Since LBH589 promotes the reactivation of AR signaling and thus facilitates the transition of stem-like, MES-like tumor cells to a more differentiated, AR-dependent state, the combination of ADT or AR-targeted therapies with LBH589 may likely lead to apoptosis and eradication of prostate tumor cell types that are intrinsically castration-resistant. As a test of this concept, the ongoing Phase I/II trial combining LBH589 with bicalutamide therapy in CRPC patients (NCT00878436) will evaluate whether combination therapy improves therapeutic efficacy and has the potential of improving survival outcomes of patients with CRPC, for which there is still no cure.

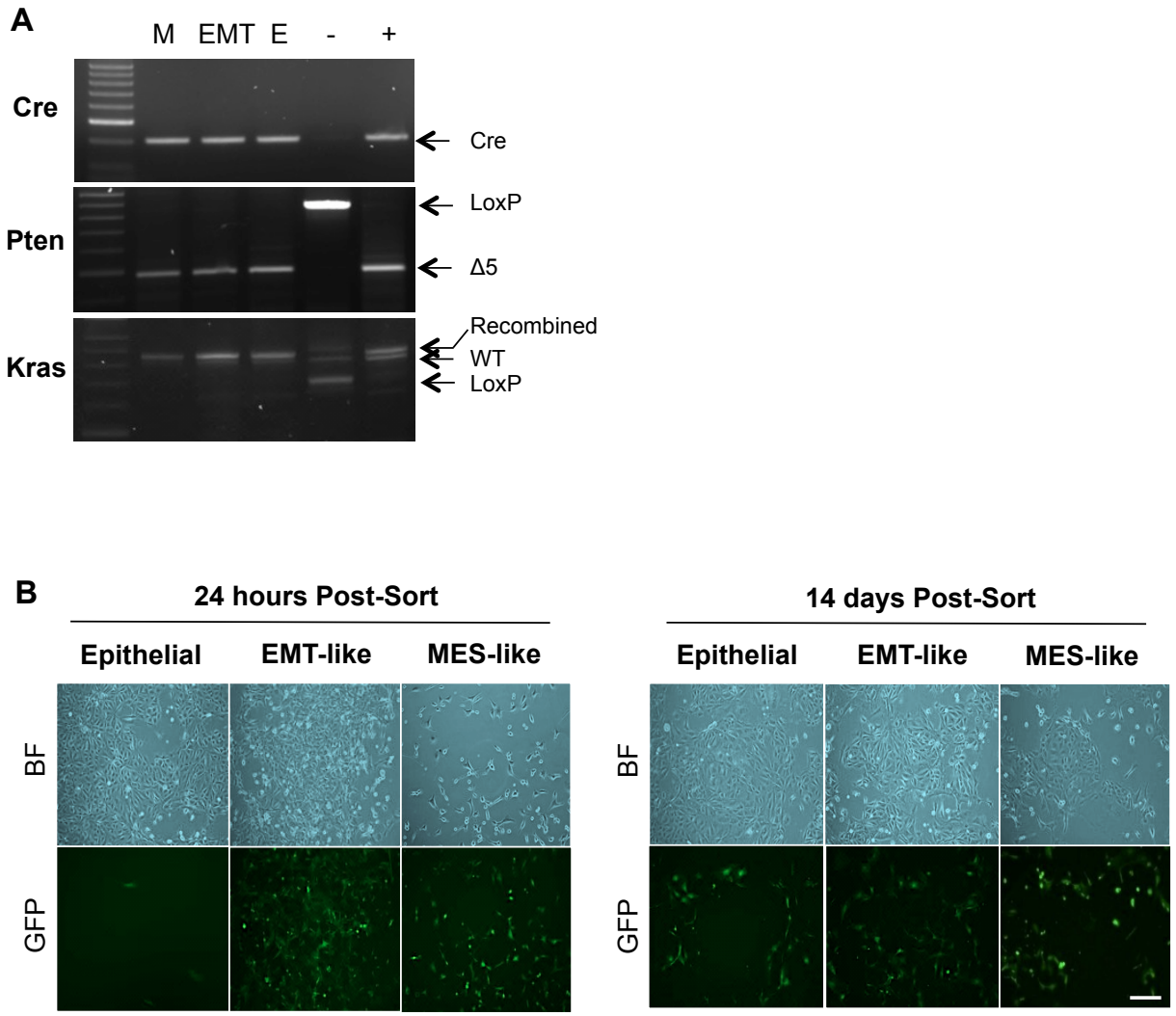

Figure S1. **EMT and mesenchymal-like tumor cells isolated from the *PKV* cell line have undergone Cre recombination and display epithelial-mesenchymal plasticity.** (A) Genomic PCR confirms that Cre recombination occurred in all cell populations isolated from *PKV* cells. Δ5, deletion of exon 5 of *Pten*; -, Cre^- control; +, Cre^+ control. (B) Brightfield (BF) and fluorescent images (GFP) of FACS isolated epithelial, EMT, and MES-like tumor cells 24 hrs (Left Panel) and 14 days (Right Panel) after being plated separately in culture. Scale bar, 50 μm.

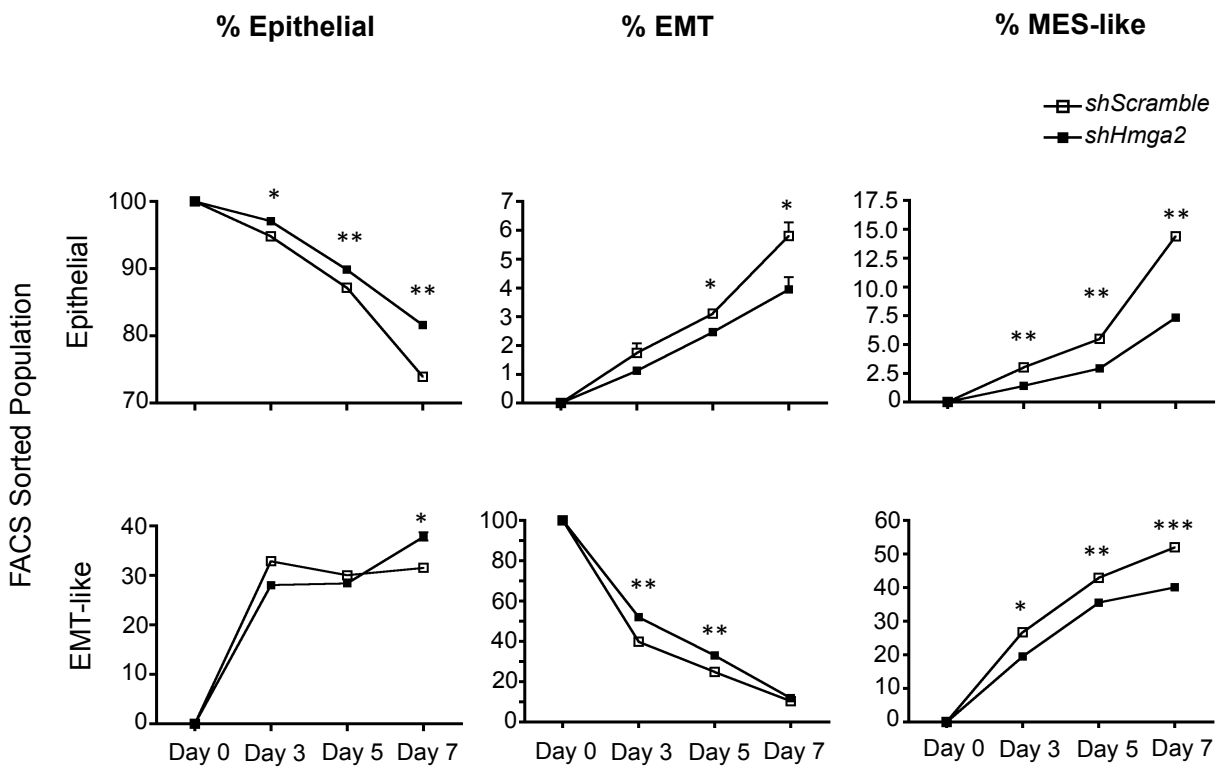

Figure S2. **Hmga2 knockdown inhibits epithelial-mesenchymal plasticity.** FACS sorted epithelial and EMT tumor cell populations from *PKV-shHMGA2* cells plated separately in culture have an increased percentage of epithelial tumor cells and a decreased percentage of MES-like tumor cells compared to control *PKV-shScramble (Scramble)* cells after 7 days in culture. Data is represented as mean $\pm$ SEM. *, $p<0.05$; **, $p<0.01$, ***, $p<0.001$.

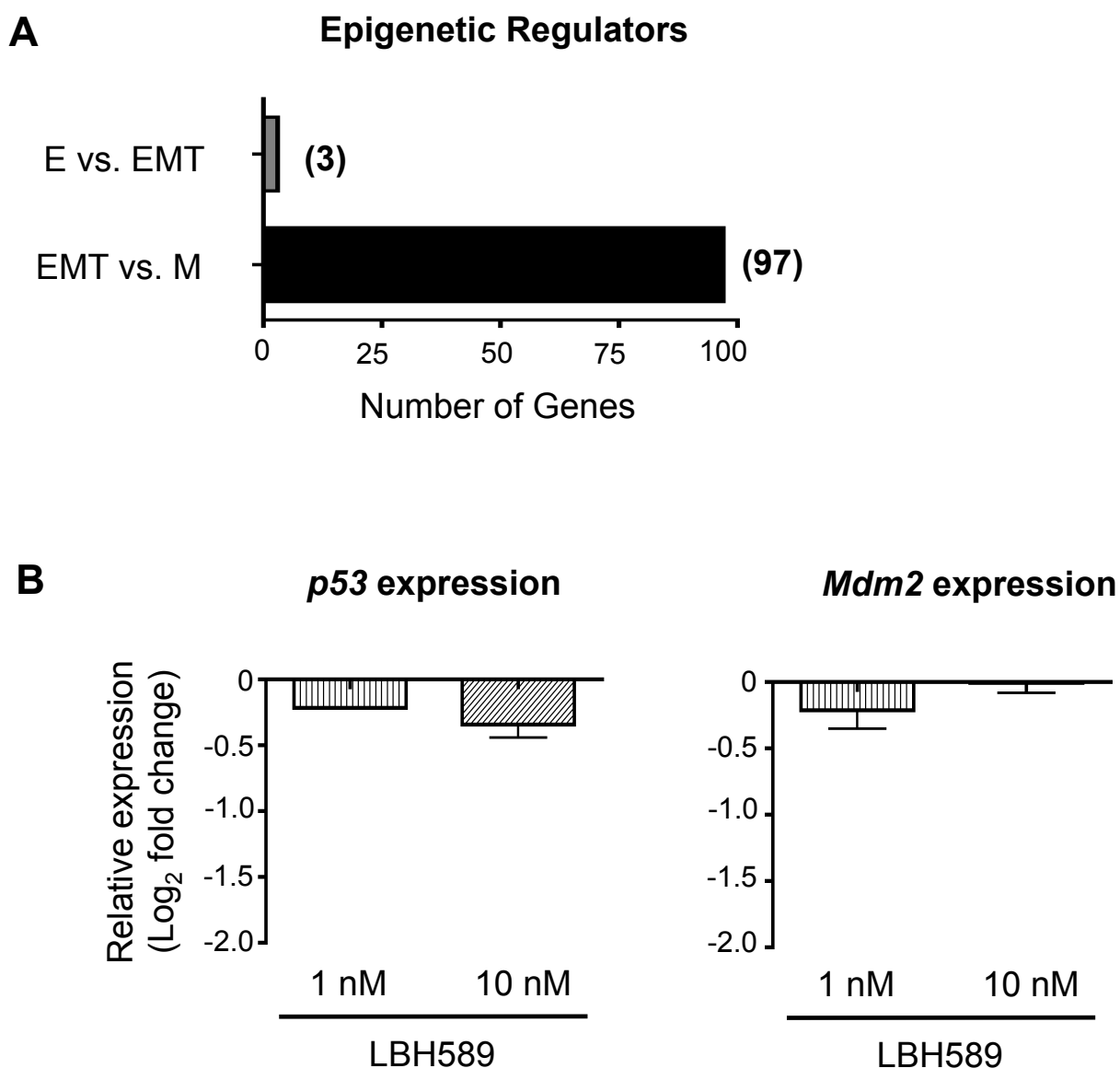

Figure S3. **Differential expression of epigenetic regulators during early and late stages of EMT.** (A) A large number of epigenetic regulatory genes from Gu et al. are differentially expressed in MES-like (M) tumor cells as compared to EMT tumor cells. (B) *p53* and *Mdm2* mRNA expression levels are relatively unaltered in *PKV* cells after LBH589 treatment (24 hr). Expression levels are relative to expression levels found in vehicle-treated *PKV* cells. Data in B is represented as mean ± SEM.

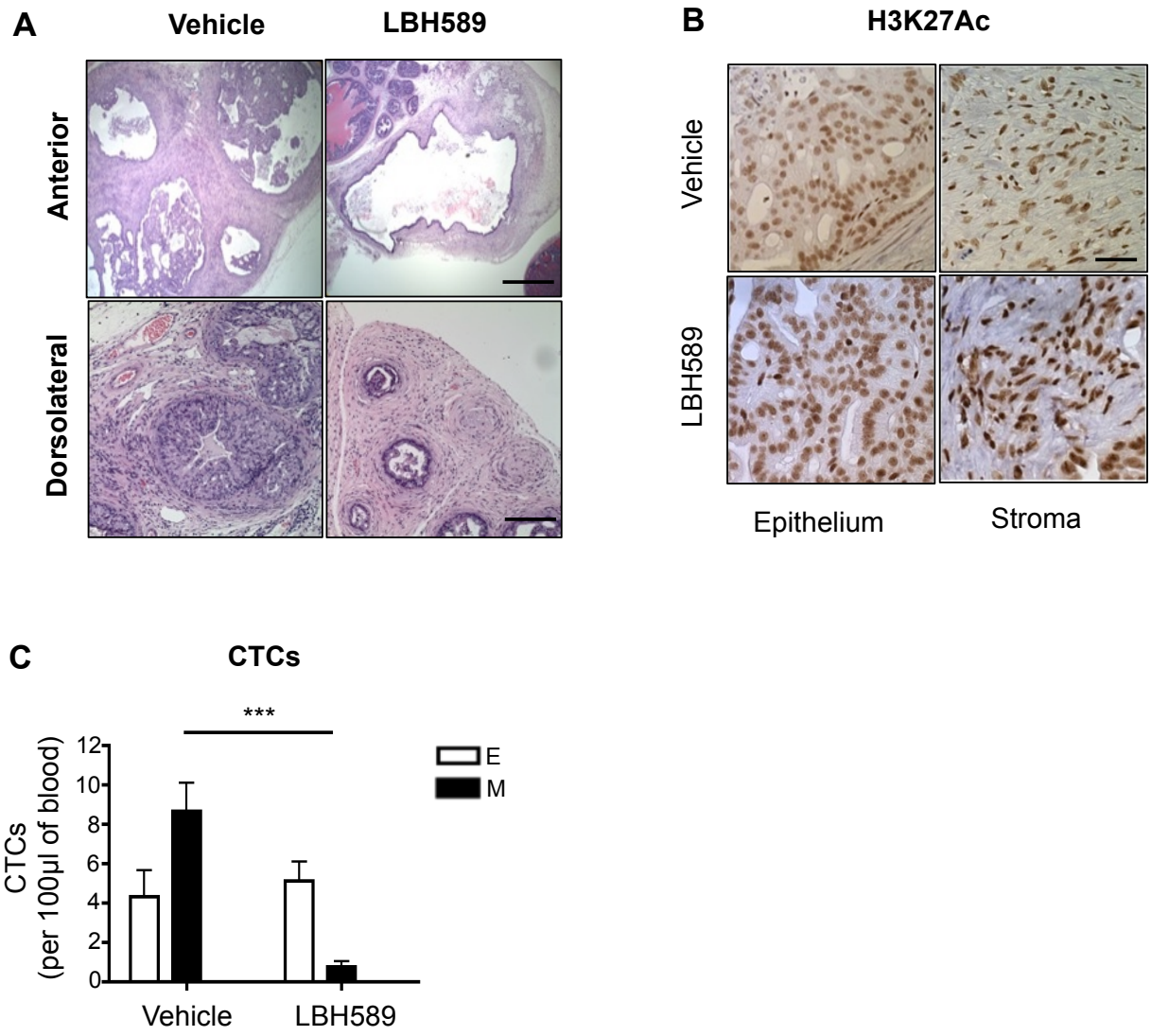

Figure S4. **Effects of LBH589 treatment in *CPKV* mice.** (A) H&E stained *CPKV* prostate sections reveal empty cysts in the anterior lobes (Top Panel) and degenerated glandular structures in the dorsolateral lobes (Bottom Panel) in LBH589-treated mice. Scale bar, top panel, 500 µm; Scale bar, bottom panel, 100 µm. (B) LBH589 treatment induces increased levels of H3K27 acetylation in both the epithelium and stroma of *CPKV* mice compared to vehicle alone. Scale bar, 25 µm. (C) Peripheral blood was collected from LBH589 (n=9) and vehicle-treated (n=4) *CPKV* mice after 2 weeks of treatment. FACS analysis of $EpCAM^{+}GFP^{-}$ epithelial (E) and $EpCAM^{-}GFP^{+}$ MES-like (M) populations revealed that LBH589-treated mice had a dramatically reduced number of MES-like circulating tumor cells (CTCs) compared to vehicle-treated mice. Data in C is represented as mean $\pm$ SEM. *, $p<0.05$; **, $p<0.01$; ***, $p<0.001$.

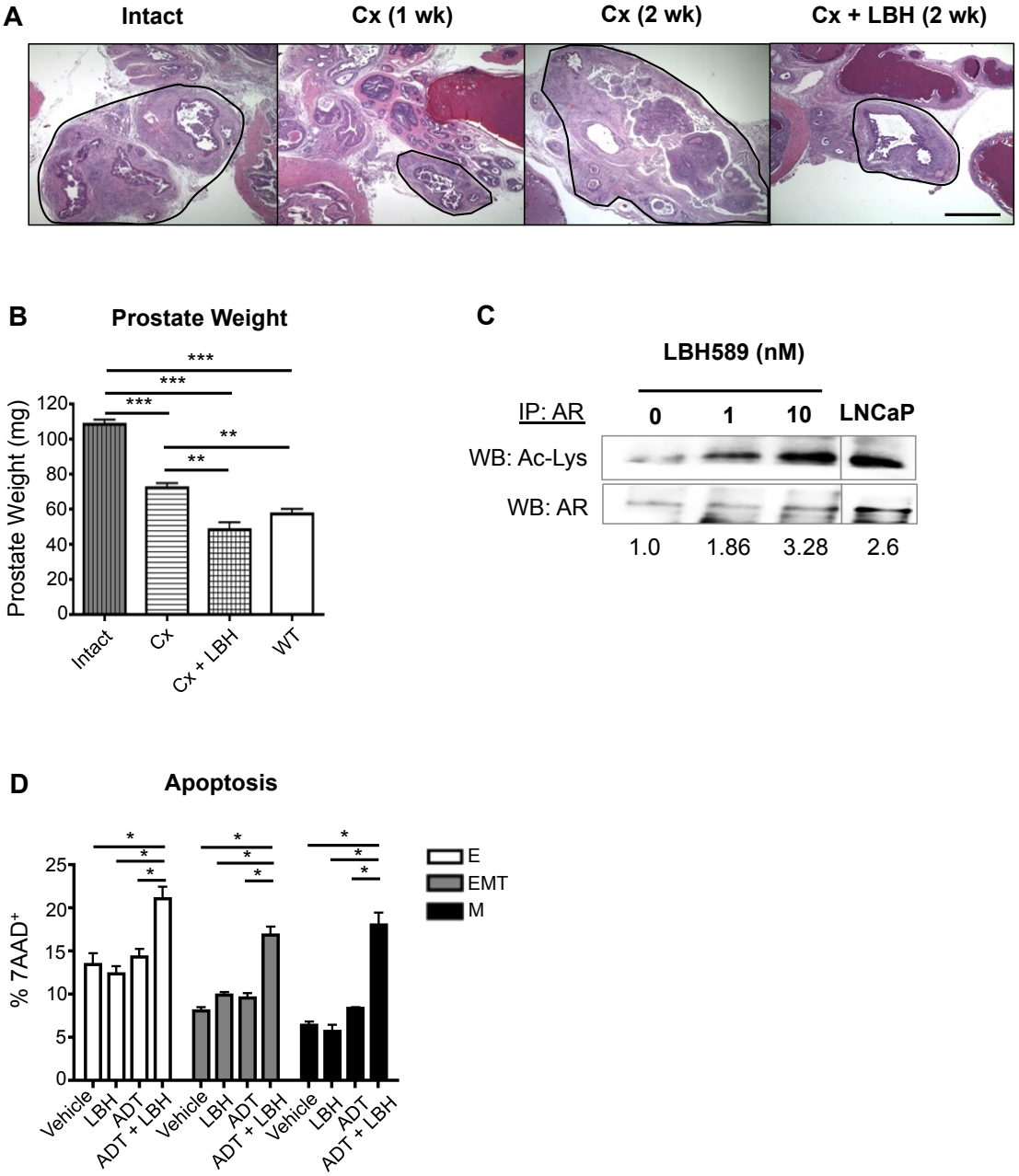

Figure S5. LBH589 treatment in combination with castration reduces the castration-resistant tumor burden and sensitizes all tumor cell populations to androgen withdrawal-induced apoptosis. (A) H&E stained prostate sections reveal that castration-resistant tumor regrowth in the anterior lobes occurs as early as 2 wks post-castration (Cx). Cx + LBH589 impede the onset of CRPC. Black Circle, anterior lobe. Scale bar, 500 μm. (B) *CPKV* mice treated with LBH589 in combination with castration (n=6) had significantly reduced prostate tumor weights compared to intact (n=3) or castrated (n=4) *CPKV* mice that were similar to those of WT prostates (n=7). (C) LBH589 treatment (6 hr) increases AR acetylation levels in *PKV* cells in a dose-dependent manner. LNCaP cells were used as a positive control. Relative AR acetylation levels were quantified by comparing the AR acetylation (Ac-Lys) band intensity to that of the AR band by densitometry. IP, immunoprecipitation; WB, Western Blot; Ac-Lys, acetylated lysine antibody. (D) While neither 1nM LBH589 treatment nor ADT alone induced apoptosis, LBH589 treatment in combination with ADT induced significantly higher levels of apoptosis in all *PKV* cell populations, including castration-resistant MES-like (M) tumor cells, as measured by the percentage of $7AAD^+$ cells. Data in B and D are represented as mean ± SEM. *, $p<0.05$; **, $p<0.01$; ***, $p<0.001$.

References

1. Siegel RL, Miller KD, Jemal A. Cancer statistics, 2015. CA: a cancer journal for clinicians. 2015;65:5-29.

2. Attard G, de Bono JS. Translating scientific advancement into clinical benefit for castration-resistant prostate cancer patients. Clinical cancer research : an official journal of the American Association for Cancer Research. 2011;17:3867-75.

3. de Bono JS, Logothetis CJ, Molina A, Fizazi K, North S, Chu L, et al. Abiraterone and increased survival in metastatic prostate cancer. The New England journal of medicine. 2011;364:1995-2005.

4. Scher HI, Fizazi K, Saad F, Taplin ME, Sternberg CN, Miller K, et al. Increased survival with enzalutamide in prostate cancer after chemotherapy. The New England journal of medicine. 2012;367:1187-97.

5. Rescigno P, Buonerba C, Bellmunt J, Sonpavde G, De Placido S, Di Lorenzo G. New perspectives in the therapy of castration resistant prostate cancer. Current drug targets. 2012;13:1676-86.

6. Shah RB, Mehra R, Chinnaiyan AM, Shen R, Ghosh D, Zhou M, et al. Androgen-independent prostate cancer is a heterogeneous group of diseases: lessons from a rapid autopsy program. Cancer research. 2004;64:9209-16.

7. Taylor BS, Schultz N, Hieronymus H, Gopalan A, Xiao Y, Carver BS, et al. Integrative genomic profiling of human prostate cancer. Cancer cell. 2010;18:11-22.

8. Baca SC, Garraway LA. The genomic landscape of prostate cancer. Frontiers in endocrinology. 2012;3:69.

9. Brannon AR, Sawyers CL. "N of 1" case reports in the era of whole-genome sequencing. The Journal of clinical investigation. 2013;123:4568-70.

10. Haffner MC, Mosbruger T, Esopi DM, Fedor H, Heaphy CM, Walker DA, et al. Tracking the clonal origin of lethal prostate cancer. The Journal of clinical investigation. 2013;123:4918-22.

11. Tanaka H, Kono E, Tran CP, Miyazaki H, Yamashiro J, Shimomura T, et al. Monoclonal antibody targeting of N-cadherin inhibits prostate cancer growth, metastasis and castration resistance. Nature medicine. 2010;16:1414-20.

12. Sun Y, Wang BE, Leong KG, Yue P, Li L, Jhunjhunwala S, et al. Androgen deprivation causes epithelial-mesenchymal transition in the prostate: implications for androgen-deprivation therapy. Cancer research. 2012;72:527-36.

13. Nieto MA. Epithelial plasticity: a common theme in embryonic and cancer cells. Science. 2013;342:1234850.

14. Armstrong AJ, Marengo MS, Oltean S, Kemeny G, Bitting RL, Turnbull JD, et al. Circulating tumor cells from patients with advanced prostate and breast cancer display both epithelial and mesenchymal markers. Molecular cancer research : MCR. 2011;9:997-1007.

15. Bitting RL, Schaeffer D, Somarelli JA, Garcia-Blanco MA, Armstrong AJ. The role of epithelial plasticity in prostate cancer dissemination and treatment resistance. Cancer metastasis reviews. 2014;33:441-68.

16. Marin-Aguilera M, Codony-Servat J, Reig O, Lozano JJ, Fernandez PL, Pereira MV, et al. Epithelial-to-mesenchymal transition mediates docetaxel resistance and high risk of relapse in prostate cancer. Molecular cancer therapeutics. 2014;13:1270-84.

17. Mulholland DJ, Kobayashi N, Ruscetti M, Zhi A, Tran LM, Huang J, et al. Pten loss and RAS/MAPK activation cooperate to promote EMT and metastasis initiated from prostate cancer stem/progenitor cells. Cancer research. 2012;72:1878-89.

18. Winslow MM, Dayton TL, Verhaak RG, Kim-Kiselak C, Snyder EL, Feldser DM, et al. Suppression of lung adenocarcinoma progression by Nkx2-1. Nature. 2011;473:101-4.

19. Sarbassov DD, Guertin DA, Ali SM, Sabatini DM. Phosphorylation and regulation of Akt/PKB by the rictor-mTOR complex. Science. 2005;307:1098-101.

20. Lukacs RU, Goldstein AS, Lawson DA, Cheng D, Witte ON. Isolation, cultivation and characterization of adult murine prostate stem cells. Nature protocols. 2010;5:702-13.

21. Mulholland DJ, Tran LM, Li Y, Cai H, Morim A, Wang S, et al. Cell autonomous role of PTEN in regulating castration-resistant prostate cancer growth. Cancer cell. 2011;19:792-804.

22. Trapnell C, Pachter L, Salzberg SL. TopHat: discovering splice junctions with RNA-Seq. Bioinformatics. 2009;25:1105-11.

23. Trapnell C, Roberts A, Goff L, Pertea G, Kim D, Kelley DR, et al. Differential gene and transcript expression analysis of RNA-seq experiments with TopHat and Cufflinks. Nature protocols. 2012;7:562-78.

24. Garcia AJ, Ruscetti M, Arenzana TL, Tran LM, Bianci-Frias D, Sybert E, et al. Pten Null Prostate Epithelium Promotes Localized Myeloid-Derived Suppressor Cell Expansion and Immune Suppression during Tumor Initiation and Progression. Molecular and cellular biology. 2014;34:2017-28.

25. Huang da W, Sherman BT, Lempicki RA. Systematic and integrative analysis of large gene lists using DAVID bioinformatics resources. Nature protocols. 2009;4:44-57.

26. Sun M, Song CX, Huang H, Frankenberger CA, Sankarasharma D, Gomes S, et al. HMGA2/TET1/HOXA9 signaling pathway regulates breast cancer growth and metastasis. Proceedings of the National Academy of Sciences of the United States of America. 2013;110:9920-5.

27. Benjamini Y, Hochberg Y. Controlling the False Discovery Rate - a Practical and Powerful Approach to Multiple Testing. J Roy Stat Soc B Met. 1995;57:289-300.

28. Plaisier SB, Taschereau R, Wong JA, Graeber TG. Rank-rank hypergeometric overlap: identification of statistically significant overlap between gene-expression signatures. Nucleic acids research. 2010;38:e169.

29. Grasso CS, Wu YM, Robinson DR, Cao X, Dhanasekaran SM, Khan AP, et al. The mutational landscape of lethal castration-resistant prostate cancer. Nature. 2012;487:239-43.

30. Tam WL, Weinberg RA. The epigenetics of epithelial-mesenchymal plasticity in cancer. Nature medicine. 2013;19:1438-49.

31. Fusco A, Fedele M. Roles of HMGA proteins in cancer. Nature reviews Cancer. 2007;7:899-910.

32. Nishino J, Kim I, Chada K, Morrison SJ. Hmga2 promotes neural stem cell self-renewal in young but not old mice by reducing p16Ink4a and p19Arf Expression. Cell. 2008;135:227-39.

33. Li O, Vasudevan D, Davey CA, Droge P. High-level expression of DNA architectural factor HMGA2 and its association with nucleosomes in human embryonic stem cells. Genesis. 2006;44:523-9.

34. Rommel B, Rogalla P, Jox A, Kalle CV, Kazmierczak B, Wolf J, et al. HMGI-C, a member of the high mobility group family of proteins, is expressed in hematopoietic stem cells and in leukemic cells. Leukemia & lymphoma. 1997;26:603-7.

35. Zong Y, Huang J, Sankarasharma D, Morikawa T, Fukayama M, Epstein JI, et al. Stromal epigenetic dysregulation is sufficient to initiate mouse prostate cancer via paracrine Wnt signaling. Proceedings of the National Academy of Sciences of the United States of America. 2012;109:E3395-404.

36. Watanabe S, Ueda Y, Akaboshi S, Hino Y, Sekita Y, Nakao M. HMGA2 maintains oncogenic RAS-induced epithelial-mesenchymal transition in human pancreatic cancer cells. The American journal of pathology. 2009;174:854-68.

37. Luo Y, Li W, Liao H. HMGA2 induces epithelial-to-mesenchymal transition in human hepatocellular carcinoma cells. Oncology letters. 2013;5:1353-6.

38. Zha L, Wang Z, Tang W, Zhang N, Liao G, Huang Z. Genome-wide analysis of HMGA2 transcription factor binding sites by ChIP on chip in gastric carcinoma cells. Molecular and cellular biochemistry. 2012;364:243-51.

39. Gu L, Frommel SC, Oakes CC, Simon R, Grupp K, Gerig CY, et al. BAZ2A (TIP5) is involved in epigenetic alterations in prostate cancer and its overexpression predicts disease recurrence. Nature genetics. 2015;47:22-30.

40. Ferguson M, Henry PA, Currie RA. Histone deacetylase inhibition is associated with transcriptional repression of the Hmga2 gene. Nucleic acids research. 2003;31:3123-33.

41. Lee S, Jung JW, Park SB, Roh K, Lee SY, Kim JH, et al. Histone deacetylase regulates high mobility group A2-targeting microRNAs in human cord blood-derived multipotent stem cell aging. Cellular and molecular life sciences : CMLS. 2011;68:325-36.

42. Luo J, Li M, Tang Y, Laszkowska M, Roeder RG, Gu W. Acetylation of p53 augments its site-specific DNA binding both in vitro and in vivo. Proceedings of the National Academy of Sciences of the United States of America. 2004;101:2259-64.

43. Gu W, Roeder RG. Activation of p53 sequence-specific DNA binding by acetylation of the p53 C-terminal domain. Cell. 1997;90:595-606.

44. Lei Q, Jiao J, Xin L, Chang CJ, Wang S, Gao J, et al. NKX3.1 stabilizes p53, inhibits AKT activation, and blocks prostate cancer initiation caused by PTEN loss. Cancer cell. 2006;9:367-78.

45. Wang S, Gao J, Lei Q, Rozengurt N, Pritchard C, Jiao J, et al. Prostate-specific deletion of the murine Pten tumor suppressor gene leads to metastatic prostate cancer. Cancer cell. 2003;4:209-21.

46. Mulholland DJ, Xin L, Morim A, Lawson D, Witte O, Wu H. Lin-Sca-1+CD49fhigh stem/progenitors are tumor-initiating cells in the Pten-null prostate cancer model. Cancer research. 2009;69:8555-62.

47. Fu M, Rao M, Wang C, Sakamaki T, Wang J, Di Vizio D, et al. Acetylation of androgen receptor enhances coactivator binding and promotes prostate cancer cell growth. Molecular and cellular biology. 2003;23:8563-75.

48. Haelens A, Tanner T, Denayer S, Callewaert L, Claessens F. The hinge region regulates DNA binding, nuclear translocation, and transactivation of the androgen receptor. Cancer research. 2007;67:4514-23.

49. Gaughan L, Logan IR, Cook S, Neal DE, Robson CN. Tip60 and histone deacetylase 1 regulate androgen receptor activity through changes to the acetylation status of the receptor. The Journal of biological chemistry. 2002;277:25904-13.

50. Muranen T, Selfors LM, Worster DT, Iwanicki MP, Song L, Morales FC, et al. Inhibition of PI3K/mTOR leads to adaptive resistance in matrix-attached cancer cells. Cancer cell. 2012;21:227-39.

51. Konieczkowski DJ, Johannessen CM, Abudayyeh O, Kim JW, Cooper ZA, Piris A, et al. A melanoma cell state distinction influences sensitivity to MAPK pathway inhibitors. Cancer discovery. 2014;4:816-27.

52. Rathkopf D, Wong BY, Ross RW, Anand A, Tanaka E, Woo MM, et al. A phase I study of oral panobinostat alone and in combination with docetaxel in patients with castration-resistant prostate cancer. Cancer chemotherapy and pharmacology. 2010;66:181-9.

53. Molife LR, Attard G, Fong PC, Karavasilis V, Reid AH, Patterson S, et al. Phase II, two-stage, single-arm trial of the histone deacetylase inhibitor (HDACi) romidepsin in metastatic castration-resistant prostate cancer (CRPC). Annals of oncology : official journal of the European Society for Medical Oncology / ESMO. 2010;21:109-13.

54. Bradley D, Rathkopf D, Dunn R, Stadler WM, Liu G, Smith DC, et al. Vorinostat in advanced prostate cancer patients progressing on prior chemotherapy (National Cancer Institute Trial 6862): trial results and interleukin-6 analysis: a study by the Department of Defense Prostate Cancer Clinical Trial Consortium and University of Chicago Phase 2 Consortium. Cancer. 2009;115:5541-9.

55. Rathkopf DE, Picus J, Hussain A, Ellard S, Chi KN, Nydam T, et al. A phase 2 study of intravenous panobinostat in patients with castration-resistant prostate cancer. Cancer chemotherapy and pharmacology. 2013;72:537-44.

56. Liu X, Gomez-Pinillos A, Liu X, Johnson EM, Ferrari AC. Induction of bicalutamide sensitivity in prostate cancer cells by an epigenetic Puralpha-mediated decrease in androgen receptor levels. The Prostate. 2010;70:179-89.

57. Frigo DE, McDonnell DP. Differential effects of prostate cancer therapeutics on neuroendocrine transdifferentiation. Molecular cancer therapeutics. 2008;7:659-69.

58. Welsbie DS, Xu J, Chen Y, Borsu L, Scher HI, Rosen N, et al. Histone deacetylases are required for androgen receptor function in hormone-sensitive and castrate-resistant prostate cancer. Cancer research. 2009;69:958-66.

59. Langelotz C, Schmid P, Jakob C, Heider U, Wernecke KD, Possinger K, et al. Expression of high-mobility-group-protein HMGI-C mRNA in the peripheral blood is an independent poor prognostic indicator for survival in metastatic breast cancer. British journal of cancer. 2003;88:1406-10.

Chapter 7:

Concluding Remarks

The promise of immunotherapy for prostate cancer

Prostate cancer is the most prevalent male malignancy in the Western World (1). Using the *Pten* null murine prostate cancer model, which progresses through defined stages of prostate cancer in a manner similar to the human disease, we endeavored to uncover how epithelial-associated tumor-initiating events cross talk with inflammatory cells to orchestrate prostate cancer development. We found that accompanying tumor initiation was a significant expansion of Gr-1^+CD11b$^+$ MDSCs in the prostate, and that MDSC infiltration was associated with inhibition of T cell activation and decreased dendritic cell (DC) and macrophage maturation, resulting in an immune-suppressive microenvironment that establishes a framework for tumor progression. In stark contrast to other studies using transplantation models that reported that MDSC expansion occurs in hematopoietic and nonhematopoietic organs in addition to the tumor site, our study using a spontaneous genetic model demonstrates that immune cell infiltration can occur solely in the localized tumor microenvironment without expansion in other tissue sites. Moreover, Gr-1^+CD11b$^+$ MDSCs from the prostate, but not from other peripheral organs, expressed increased levels of arginase and iNOS and were subsequently able to suppress T cell activation. Our study, therefore, illuminates the important functional differences between Gr-1^+CD11b$^+$ MDSCs that infiltrate tumors and Gr-1^+CD11b$^+$ cells in peripheral tissues. Our findings also emphasize the utility of using spontaneous genetic models, as opposed to xenograft or allograft models, in improving our mechanistic understanding of how tumors create localized immune suppression.

Our results suggest that MDSC infiltration, expansion, and acquisition of immune-suppressive functions are triggered by localized secreted factors from the *Pten* null prostate epithelium. Indeed, localized cytokine release in the form of CSF-1 and IL-1β, as well as other

inflammatory effectors, contributes to the recruitment and maintenance of Gr-1^{+}CD11b^{+} MDSCs. Importantly, treatment with the CSF-1R kinase inhibitor GW2580 was able to interrupt the epithelial-cell associated signaling cascade that drives MDSC infiltration, reverse the immune-suppressive microenvironment, and subsequently delay tumor progression. Therefore, inhibiting MDSC infiltration through the targeting of epithelial-mediated inflammatory signals may benefit prostate cancer patients, as well as augment the efficacy of immunotherapy by permitting a tumor-specific immune response.

Activating the immune system to target tumorigenic tissue has emerged as a promising and personalized way to treat prostate cancer. One recent success has been the FDA approval of Sipuleucel-T, a DC vaccine that uses the *ex vivo* culturing and conditioning of a patient's own peripheral blood mononuclear cells (PBMCs) with tumor-associated antigens and subsequent transfer back into the patient to mount an anti-tumor response (2). The rationale behind using autologous DCs in immunotherapies such as Sipuleucel-T is their efficient activation of tumor antigen-specific T cells to target and eradicate tumor cells. Although phase III clinical trial results showed improved survival when comparing Sipuleucel-T to conventional therapy, disease-free progression was not affected significantly (3, 4). Similarly, ipilimumab, a monoclonal antibody that blocks the activity of the immune checkpoint protein CTLA-4 and thereby prolongs the longevity of the anti-tumor T cell response, demonstrated efficacy at targeting residual metastatic prostate cancer in preclinical models (5), but failed to improve overall survival after radiotherapy of mCRPC patients in a phase III trial (6). Our study suggests that tumor-induced immune suppression mediated by MDSCs within the local tumor environment may prevent more favorable results by inhibiting T cell activation and effective

targeting of tumor cells. Indeed, in advanced melanoma patients, circulating MDSCs have been reported to have a negative impact on survival and inversely correlate with functional antigen-specific T cell responses (7). Moreover, decreased monocytic and granulocytic MDSC activity has been correlated with beneficial therapeutic effects in melanoma patients treated with ipilimumab (8, 9). Our study reveals that targeting tumor-initiated paracrine pathways, as opposed to systemic inflammatory signals, is an effective strategy to inhibit tumor-associated MDSC infiltration and suppressive activities, and that combining CSF-1R inhibitor treatment with immunotherapies such as cancer vaccines (Sipuleucel-T) and immune checkpoint blockade agents (ipilimumab and the anti-PD-1 antibody nivolumab) could greatly benefit the efficacy of immunotherapy.

However, challenges still remain. MDSCs are heterogeneous cells, and while Gr-1 and CD11b can be used as markers to isolate a subset of MDSCs in the murine system, more specific surface markers are needed for the isolation, characterization, and targeting of MDSCs in human cancer patients. Moreover, our understanding of the functional significance and contribution of tumor-infiltrating monocytic and granulocytic MDSCs, as well as macrophages, neutrophils, and Tregs to tumor progression is still at an early stage, and very well may be tumor context dependent. Therefore, preclinical, genetically engineered mouse models (GEMMs) of prostate cancer are needed to better understand how the primary tumor is able to influence the "soil" of the tumor microenvironment and potentiate tumor-immune cell interactions. Future studies in such models will likely uncover additional paracrine and inflammatory pathways that induce MDSC homing and immune-suppressive activities within the tumor microenvironment that can be targeted therapeutically.

PI3K/AKT and RAS/MAPK pathway co-activation induces metastatic prostate cancer

Alteration of the PTEN/PI3K/AKT pathway is found in 42% and 100% of human primary and metastatic tumors, respectively (10). While the *Pten* null murine prostate cancer model mimics the stages of human prostate cancer, including hyperplasia, prostatic intraepithelial neoplasia (PIN), and invasive carcinoma, *Pten* deletion alone fails to induce significant metastatic burden in distant organs. One of several well-known pathways also found to be altered in human prostate cancer is the RAS/RAF/MAPK pathway, showing alterations in 43% and 90% of primary and metastatic lesions, respectively (10). By combining *Pten* deletion with conditional *Kras* activation in the prostate epithelium (*Pb-Cre*$^{+/-}$*;Pten*$^{L/L}$*;Kras*$^{G12D/+}$) (*CPK*) to create a murine prostate cancer model driven by PI3K/AKT and RAS/MAPK pathway co-activation, we developed one of the first metastatic genetically engineered mouse models (GEMMs) of prostate cancer, with 100% penetrance of visceral metastases in the lungs and liver. In addition to the metastatic burden observed in *CPK* mice, a poorly differentiated, EMT morphology was also observed within the primary prostate tumor. As evidence for the role of EMT in cancer stem cell formation and metastasis is mostly based on either *in vitro* manipulation of cultured cell lines to artificially induce an EMT or the expression of EMT signature markers in human cancer samples, this new CPK model provided a unique avenue for studying 1) the direct impact of EMT on prostate cancer progression and metastasis *in vivo* and 2) how the PI3K/AKT and RAS/MAPK pathways converge to induce an EMT. Moreover, as more than 90% of prostate cancer-related mortality is caused by distant metastasis (11), the *CPK* murine prostate cancer model provides an advantageous platform for testing novel therapeutics that may be effective at targeting disseminated, metastatic disease. Indeed, we found that dual treatment with the mTOR

inhibitor rapamycin and the MEK inhibitor PD0325901 was effective at ablating distant metastasis to the lungs *in vivo*. Remarkably, when mice were treated with PD0325901 alone, we observed a nearly complete abolishment of metastasis, indicating that the RAS/MAPK pathway plays a significant role in metastasis. In light of these findings, a trial examining the effect of the MEK inhibitor trametinib in the context of ADT on EMT maker expression (N-cadherin, Vimentin) was recently started at UCLA (NCT01990196).

Although the RAS/MAPK pathway is significantly altered in human metastatic prostate cancer, Ras and Raf mutations (12, 13), as well as Ras fusion events (14), are infrequent in prostate cancer. Therefore, the underlying mechanisms of MAPK activation in prostate cancer remain unclear. One mechanism could be through activation of Braf via chromosomal rearrangements (15). Supporting this notion, mice with *Pten* loss and *Braf* activation in the prostate epithelium (*Nkx3.1*$^{CE2/+}$;*Pten*$^{f/f}$;*Braf*$^{CA/+}$) develop distant macrometastasis similar to *CPK* mice (16). Additionally, downregulation of suppressors of the RAS/MAPK signaling, including the *SPRY1* and *SPRY2* genes (10, 17, 18), as well as the RAS-GAP *DAB2IP* (19), may also contribute to the activation of MAPK signaling in the absence of overt mutations in the pathway. It is also possible that Wild-type RAS and/or RAF are activated as a consequence of autocrine or paracrine growth factor stimulation through growth factor receptors such as EGFR, FGFR, and IGF-1R (20-22). Moreover, as cross-talk between PI3K and RAS signaling has been characterized in certain contexts (23, 24), it is possible that human prostate cancer patients with *PTEN* deletion may also have increased RAS/MAPK activation as a consequence of enhanced PI3K signaling. Approaches that allow for precise quantification of phosphorylation changes in peptides in human metastatic prostate cancer specimens, such as through phosphoproteomic

profiling, may help to improve our understanding of how various growth signaling pathways, including the PI3K/AKT and RAS/MAPK pathways, are regulated and activated during late-stage disease. A major future challenge will be to define how RAS/MAPK signaling is activated in prostate cancer so that the appropriate targets for therapeutic intervention can be identified.

Bone metastasis is a signature of late-stage human prostate cancer; however, most genetically engineered mouse models have failed to recapitulate bone metastasis. Although we detected disseminated tumor cells (DTCs) in the bone marrow by PCR, we were not able to observe overt bone metastases in *CPK* mice. Therefore, additional pathway alterations, especially those that allow for survival or adaptation of disseminated tumor cells to the harsh microenvironment of the bone, seem to be necessary for the formation of bone metastases. Alternatively, it is possible that DTCs in the bone marrow of *CPK* may eventually form metastases, albeit over a long latency that is beyond the lifespan of these mice. This may reflect the phenomenon of clinical dormancy, in which DTCs can exist and persist in metastatic sites for 10-20 years in a stem-like state as dormant cancer stem cells until disease relapse or outgrowth of metastases occur (25, 26). Recent evidence indicates that environmental conditions and crosstalk between tumor cells and other cell types in the host organ are crucial for metastasis (27). While the microenvironment within the lungs may provide sufficient cues for disseminated tumor cells to proliferate and form macrometastases, these same cues may be missing in the bone marrow microenvironment. Future genetically engineered mouse models of prostate cancer should aim to uncover those tumor cell autonomous genetic and pathway alterations, as well as the role of the tumor microenvironment of the bone, in triggering disseminated prostate tumor

cells to 1) home to the bone, 2) survive and overcome an initial dormancy period, and 3) proliferate to seed bone metastases.

A direct role for Snail-mediated EMT in prostate cancer metastasis

To understand the molecular mechanisms underlying the activation of the EMT program by PI3K/AKT and RAS/MAPK pathway co-activation, we measured the expression of a number of EMT transcription factors, and found that SNAIL was the most highly upregulated EMT transcription factor in our model. Mechanistically, co-activation of the PI3K/AKT and RAS/MAPK pathways sensitizes the prostatic epithelium to TGF-β pathway-induced upregulation of *Snail* expression, and also synergistically activates PAK1, which facilitates SNAIL nuclear localization and stability. Using an animal model with genetically defined co-activation of the PI3K/AKT and RAS/MAPK pathways and conditional deletion of *Snail*, we demonstrate that SNAIL is essential for EMT and prostate cancer metastasis. Importantly, we found *SNAIL* to be significantly upregulated in human metastatic prostate cancer samples, and that metastatic prostate cancer patients with high *SNAIL* expression have a poor overall survival after chemotherapy. These findings indicate that *SNAIL* expression can be used to stratify patients that are likely to progress to metastatic disease and have a poor overall outcome. Finally, combined therapy with rapamycin and PD0325901 is able to substantially reduce SNAIL expression, validating the effectiveness of these PI3K and MAPK inhibitors in targeting metastatic prostate disease through their ability to modulate SNAIL levels. Therefore, induction of Snail expression and increased SNAIL activity is one mechanism by which cross-talk between the PI3K/AKT and RAS/MAPK pathways promote prostate cancer metastasis. In all, these

findings provide direct *in vivo* evidence for an essential role of the EMT process in driving metastasis.

Co-activation of PI3K/AKT and RAS/MAPK pathways upregulates SNAIL activity through multiple mechanisms, which include transcriptional activation, as well as post-transcriptional modifications that positively regulate PAK1 activity and negatively regulate GSK3β activity, leading to increased SNAIL nuclear localization and half-life. As direct pharmacological inhibition of SNAIL and other EMT transcription factors has been difficult, it will be valuable to test inhibitors of PAK1 for their potential to treat metastatic disease given the role of PAK1 in regulating SNAIL protein stability and nuclear localization. Moreover, as other EMT transcription factors can induce EMT and metastasis as well, it will be interesting to uncover the role that other EMT regulators play in different stages of the metastatic cascade in our model.

PI3K/AKT and RAS/MAPK pathway co-activation induces epithelial-mesenchymal plasticity

Although our studies using the *CPK* and *CPKS* prostate cancer models demonstrate *in vivo* evidence for the role of EMT in cancer stem cell formation and the metastatic process, we had yet to elucidate the direct contribution of prostate tumor cells with EMT characteristics, in comparison to epithelial tumor cells, to different stages of the metastatic cascade, including tumor progression, invasion, dissemination of circulating tumor cells (CTCs) into the blood stream, and seeding of metastases at distant sites. To address this question, we combined the *Pb-*

Cre$^{+/-}$;*Pten*$^{L/L}$;*Kras*$^{G12D/+}$ prostate cancer model with *Vimentin-GFP* reporter mice (*CPKV*) to mark cells that had undergone an EMT and acquired mesenchymal characteristics. Using the *CPKV* model, we are able to isolate epithelial, EMT, and mesenchymal-like prostate cancer cells based on Vimentin and EpCAM expression. Importantly, in addition to being able to isolate mesenchymal-like tumor cells using this system, we demonstrate for the first time the ability to isolate EMT tumor cells, which harbor both epithelial and mesenchymal characteristics, from an endogenous murine cancer model. EMT and mesenchymal-like tumor cells have enriched tumor-initiating capacity compared to epithelial cells, and are able to regenerate epithelial glandular structures *in vivo*, indicative of epithelial-mesenchymal plasticity. Interestingly, while mesenchymal-like tumor cells are able to persist in circulation and survive in the lung following intravenous injection, only epithelial and EMT tumor cells are able to form macrometastases within our observation time window. This *in vivo* analysis suggests that mesenchymal and epithelial states contribute differentially to tumor initiation and metastatic seeding, respectively, and that EMT tumor cells have the plasticity to contribute to multiple stages of the metastatic cascade.

Unlike previous studies, which rely heavily on *in vitro* manipulation of established cell lines to artificially induce EMT states, the EMT and mesenchymal-like tumor cells that we characterize in our model are derived spontaneously as a consequence of the co-activation of the PI3K/AKT and RAS/MAPK pathways, two pathways we have shown to be highly upregulated in human metastatic prostate cancer patients, and therefore more closely model the impact of EMT on human prostate disease. Moreover, as previous *in vitro* and *in vivo* models of EMT also do not have the capacity to distinguish fully mesenchymal from transitioning EMT tumor cells,

there has been a great deal of discrepancy in the field as to whether tumor cells that undergo an EMT acquire stemness traits, or whether it is the epithelial tumor cells that harbor cancer stem cell qualities (28, 29). We demonstrate that both EMT and mesenchymal-like tumor cells have enhanced stemness traits, with EMT tumor cells exhibiting characteristics of proliferating progenitor cells, and mesenchymal-like tumor cells exhibiting characteristics of quiescent stem cells. Importantly, we also demonstrate that EMT cells, which co-express both epithelial and mesenchymal markers, are able to recapitulate each stage of prostate disease, from tumor initiation through metastasis, through their ability and plasticity to readily transition between epithelial and mesenchymal states. This has important implications for the treatment of late-stage disease, as it supports the use of therapeutics that target tumor cell plasticity in addition to current strategies of specific gene or pathway based therapies. Targeting mesenchymal or EMT-inducing factors alone might be counterproductive in patients with DTCs or dormant micrometastases, since promoting reversion of such cells to an epithelial state could reactivate proliferation and facilitate the formation of metastasis. This may also have important implications for many carcinomas, including prostate cancer, as evidence from previous reports suggests that tumor cells likely disseminate early on from the primary tumor site (30, 31). Indeed, we also demonstrate that CTCs can be isolated during the early stages of tumor development in *CPKV* mice, and that increased mesenchymal-like CTC counts, but not epithelial CTC counts, correlate with disease progression and metastatic disease in our model, providing a potentially useful biomarker for metastatic disease in human prostate cancer patients.

We were initially puzzled when we found that mesenchymal-like tumor cells did not form metastases in our *in vivo* dissemination assay. Our data shows, however, that mesenchymal-

like tumor cells are able to survive in the blood stream and in the lungs for long periods of time post-transplantation. Mesenchymal-like tumor cells are likely unable to form macrometastases in the lung because they are unable to undergo a MET and proliferate to form macrometastatic colonies during the timeframe of this assay. This is why we believe that mesenchymal-like tumor cells may reflect the phenomenon of clinical dormancy. As disseminated mesenchymal-like tumor cells exist in dormant state, it has been postulated that ERK activity, which is downregulated in mesenchymal-like tumor cells (data not shown), must be reactivated in order for these cells to regain proliferative capacity (32, 33). Indeed, while treatment with the MEKi PD0325901 was able to successfully inhibit the formation of macrometastases in *CPK* mice, micrometastases still persisted (34). This finding suggests that a rate-limiting step required for macrometastatic colonization may be the reactivation of MAPK-ERK activity. Reactivation of these mitogenic signals may be dependent on growth factors and cytokines that are naturally present in foreign microenvironment of distant organ sites. Recent studies have provided further evidence that disseminated tumor cells, even when possessing stem-like activity, still require additional alterations in order to effectively colonize distant organs. Therefore, the fact that mesenchymal-like tumor cells do not form metastases during the time window of our study does not necessarily mean that they lack stemness or tumor-initiating qualities, but is rather the consequence of an inability to adapt to foreign microenvironment at distant organ sites, in this case the lungs. Future studies of metastasis should be carried out in immunocompetent hosts in order to truly gauge the effects of the tumor microenvironment on metastasis. Moreover, as human prostate cancer metastasizes most frequently to the bone, it is also possible that the mesenchymal state may be favored for metastatic colonization in the bone marrow microenvironment. A number of studies have demonstrated that human prostate cancer bone

metastases have increased mesenchymal marker expression (35-37). Hence, future research should attempt to compare the metastatic seeding capacity of epithelial and mesenchymal-like tumor cells in the bone, for instance, through direct injection of tumor cells into the bone marrow by intratibial transplantation.

Visualizing epithelial-mesenchymal plasticity has been difficult because of its transient, ephemeral nature. Lineage tracing, as well as intravital imaging modalities, will aid in delineating the spatiotemporal dynamics of the EMT and MET processes *in vivo*. As it is possible that EMT and mesenchymal-like tumor cells arise from different cell types in the prostate (for instance, basal vs. luminal epithelial cells), lineage tracing techniques will be vital in identifying the cell-of-origin of these different tumor cell states. Moreover, such techniques will also help to address whether both EMT and mesenchymal-like tumor cells can be generated stochastically from epithelial cells, or whether mesenchymal-like tumor cells are solely derived from EMT tumor cells in a linear fashion. The *PKV* cell line, which contains epithelial, EMT, and mesenchymal-like tumor cell subpopulations that all retain the capacity to transition into all other cell types, will be a useful tool for understanding the dynamics of epithelial-mesenchymal plasticity, and for identifying novel regulators of the MET process, which are far less understood compared to regulators of the EMT process. Uncovering new factors that are able to potentiate an MET in disseminated mesenchymal-like tumor cells will provide novel targets to prevent distant metastatic colonization in prostate cancer patients.

Epigenetic regulation of epithelial-mesenchymal plasticity and its contribution to metastatic, castration-resistant prostate cancer (mCRPC)

Epithelial-mesenchymal plasticity has been proposed to play a role in progression to metastatic, castration-resistant prostate cancer (mCRPC); however, the molecular mechanisms governing epithelial-mesenchymal plasticity are still poorly understood. To study epithelial-mesenchymal plasticity, we developed a cell line from the *CPKV* murine prostate cancer model that contains genetically identical epithelial, EMT, and mesenchymal-like tumor cell populations. When cultured individually, each population has the plasticity to generate all three populations, implying epigenetic regulation of the EMT program. Among differentially expressed epigenetic regulators, HMGA2 is significantly upregulated in EMT and mesenchymal-like tumors cells, as well as in human metastatic castration-resistant prostate cancer (mCRPC). Functionally, Hmga2 knockdown significantly inhibits epithelial-mesenchymal plasticity and stemness activities. Treatment with the HDAC inhibitor LBH589 suppresses Hmga2 activity, targets treatment-resistant EMT and mesenchymal-like tumor cells, and prevents distant metastasis. Finally, while castration leads to expansion of the castration-resistant mesenchymal-like tumor cells and early lethality in *CPKV* mice, LBH589 treatment in combination with castration significantly prolongs survival by impeding the onset of mCRPC. These findings illustrate that epithelial-mesenchymal plasticity is regulated epigenetically, and that mesenchymal-like tumor cell populations that are resistant to conventional therapies, including androgen deprivation therapy (ADT), can be effectively targeted with epigenetic inhibitors. LBH589 treatment in combination with ADT may therefore be a promising and effective treatment for mCRPC, of which there is currently no cure.

While castrated *Pten* null mice slowly develop CRPC over a two month period but rarely succumb to CRPC-related mortality (38), *CPKV* mice with conditional *Pten* loss and *Kras* activation rapidly develop CRPC and have a median survival of around 3 weeks post-castration.

Previous work from our group has demonstrated that *Pten* loss and subsequent PI3K/AKT activation inhibits AR signaling through a reciprocal feedback loop, indicating that castration resistant growth is an inherent feature of prostate cancer driven by *Pten* inactivation (39). Our present data indicates that the PI3K/AKT and RAS/MAPK pathways converge to promote early lethality in mice following castration by driving epithelial-mesenchymal plasticity to produce stem-like and mesenchymal-like tumor cells that are castration-resistant. The molecular aspects as to why mesenchymal-like tumor cells have reduced AR and AR target gene expression may be partially explained by the fact that these tumor cells have enhanced P-AKT and P-S6 expression compared to androgen-dependent epithelial tumor cells (data not shown), as well as by a previous study elucidating a bidirectional negative feedback loop between AR and the EMT transcription factor Zeb1 (40), which we found to be highly expressed in mesenchymal-like tumor cells in our model. In addition to these AR independent mechanisms of castration-resistance, it has recently been proposed that AR splice variants (ARVs) are highly upregulated in response to ADT and may stimulate EMT through signaling mechanisms that are distinct from canonical AR signaling (41-44). As our RNA-seq analysis revealed a plethora of alternative splicing changes in transcripts from mesenchymal-like tumor cells as compared to those in EMT and epithelial tumor cells (data not shown), it will be interesting to investigate if ARVs exist in mesenchymal-like tumor cells and whether they contribute to castration-resistant disease. Regardless of the molecular mechanisms driving castration-resistance in our model, we demonstrate that by promoting AR reactivation in *CPKV* prostates via differentiation therapy with the HDACi LBH589, we are able to sensitize prostate tumor cells with PI3K/AKT and RAS/MAPK pathway co-activation, including castration-resistant mesenchymal-like tumor cells, to ADT-induced apoptosis. This proof-of-concept drug study suggests that inhibiting the

epigenetic framework that drives epithelial-mesenchymal plasticity promotes the re-differentiation of mesenchymal-like tumor cells and other intrinsically castration-resistant prostate cell populations, making them susceptible to conventional therapies such as ADT. It will be interesting to see if HDACi therapy may also synergize with other conventional cytotoxic and genotoxic therapies for prostate cancer treatment, including chemotherapy and radiotherapy, in a similar manner.

Neuroendocrine differentiation, whereby prostate tumor cells acquire a neuroendocrine/small cell histological phenotype, lose expression of AR and PSA, and subsequently escape the effects of ADT, is another adaptive mechanism that drives the development of CRPC (45). Although an extremely small population of prostate cancer patients present with *de novo* neuroendocrine tumors, neuroendocrine differentiation occurs frequently in response to treatment and is associated with both visceral metastases and an overall poor prognosis (46, 47). Emerging evidence suggests that EMT is associated with and regulates the development of neuroendocrine differentiation (48-50). However, the functional and molecular relationship between these states in the prostate has not been extensively explored. Our RNA-seq analysis revealed a number of neuroendocrine markers to be highly upregulated in mesenchymal-like tumor cells, including *Syp, Chgb, Eno2, Mycn, Sty4, Cdh2, and Crmp1* (data not shown). Therefore, it will be valuable to see if there is a mechanistic link between EMT and neuroendocrine differentiation in our model and in human CRPC, as such a relationship would provide rationale for the use of HDACi therapy for the treatment of neuroendocrine prostate cancer.

While epithelial and EMT tumor cells were sensitive to growth inhibition by PI3K/mTOR and MEK inhibitors, mesenchymal-like tumor cells were resistant to inhibition by both inhibitors. This suggests that both genetic and epigenetic events (governed by the tumor cell state/lineage) play a role in sensitivity to pathway-targeted therapies. Importantly, although we have demonstrated that PD325901 treatment in combination with rapamycin successfully reduces the prostate tumor burden and prevents distant macrometastasis *in vivo*, mesenchymal-like tumor cells are likely to persist after treatment is terminated, and could thereby contribute to disease relapse. One possible resistance mechanism could be that activation of alternative survival or developmental/stem cell pathways allows for mesenchymal-like tumor cell growth and survival that is independent of PI3K and MAPK signaling. Additionally, differential regulation of the PI3K/AKT and RAS/MAPK pathways in mesenchymal-like tumor cells may also contribute to resistance to therapies targeting these pathways. While attenuated RAS/MAPK signaling suggests that mesenchymal-like tumor cell maintenance is independent of this pathway, activation of the PI3K pathway, as assessed by P-S6 and P-AKT levels, is actually enhanced in mesenchymal-like tumor cells (data not shown). Therefore, it remains unclear why mesenchymal-like tumor cells do not respond to PI3K inhibition. It is possible that PI3K signaling in mesenchymal-like tumor cells is mediated by other PI3K isoforms not potently targeted by PKI-587 treatment (51). Interestingly, RNA-seq analysis revealed that mesenchymal-like tumors cells have significantly enhanced expression of the p110δ isoform compared to epithelial (~38 fold) and EMT tumor cells (~7 fold) (data not shown). Further studies are needed to elucidate the complex regulation of the PI3K/AKT and RAS/MAPK signaling pathways in mesenchymal-like tumor cells, particularly in terms of regulation of receptor tyrosine kinases (RTKs) and upstream effectors in the pathways. The inherent drug resistance of mesenchymal-

like tumor cells to both ADT and PI3K/MAPK pathway targeted therapies may be due in large part to their 1) quiescent state, 2) enhanced pro-survival pathway activity, and 3) perturbation of apoptotic pathways, including p53 signaling. Importantly, activation of p53-induced apoptosis through LBH589 treatment is able to successfully target traditionally treatment-resistant tumor cells with EMT characteristics. However, as p53 is commonly mutated in human CRPC (52, 53), attempting to induce p53-mediated apoptosis in the context of p53 loss may not be effective. Hence, additional therapeutic targets may need to be identified in order to target p53 mutant prostate cancers effectively.

HDACi treatment with LBH589 also inhibits epithelial-mesenchymal plasticity in prostate tumor cells with PI3K/AKT and RAS/MAPK pathway co-activation by inhibiting Hmga2 activity, which links the EMT and mesenchymal cell states to a stem-like state. Increased expression of stemness factors likely contributes to the acquisition of epithelial-mesenchymal plasticity in prostate tumor cells with PI3K/AKT and RAS/MAPK activation; however, how specific stemness factors may mechanistically contribute to plasticity requires further experimentation. Notably, the ability of an epigenetic inhibitor such as LBH589 to inhibit both stemness and plasticity and in turn perturb metastatic growth has important implications for the treatment of disseminated, metastatic disease, as it functionally demonstrates the efficacy of utilizing therapeutics that target epithelial-mesenchymal plasticity. In a similar fashion, use of agents that can inhibit Hedgehog, NOTCH, and Wnt signaling (54-57), which we found to be upregulated in the mesenchymal-like tumor cell population, may be another suitable strategy to targeting preexisting metastatic disease, and is worthy of further exploration. As an “architectural transcription factor” with the ability to affect the expression of thousands of genes, HMGA2 may

have many downstream targets (58), including novel regulators of stemness, which require further elucidation in our model.

Our RNA-seq analysis of the EMT and mesenchymal-like tumor cell populations, combined with our ability to visualize and manipulate epithelial-mesenchymal plasticity *in vitro* with the *PKV* cell line, provides an optimal platform for uncovering novel regulators of epithelial-mesenchymal plasticity that could be potentially targeted therapeutically. In addition, it will also be important to unravel the global epigenetic changes in DNA methylation and histone acetylation/methylation patterns that take place in mesenchymal-like tumor cells in order to identify novel regulators of these redefined epigenetic states. For instance, the DNA methyltransferases *Dnmt1* and *Dnmt3l* are highly upregulated in mesenchymal-like tumor cells compared to EMT and epithelial tumor cells (data not shown). Preliminary data using the DNA methyltransferase inhibitor (DNMTi) Decitabine *in vitro* demonstrated that inhibiting DNA methylation may also be an effective strategy for targeting mesenchymal-like tumor cells (data not shown). Methylation analysis by bisulfite sequencing will therefore provide a framework for a deeper understanding of how changes in DNA methylation regulate the mesenchymal state. Moreover, as a total of 18 HDACs have been identified to date, it will be important to determine which specific HDAC isoforms are responsible for regulating HMGA2, AR, and p53 activity so that inhibitors capable of targeting single isoforms can be designed in order to reduce toxicity and off-target effects. In addition to changes in the expression of epigenetic regulators, RNA-seq analysis unveiled a significant number of different alternative splicing events in mesenchymal-like tumor cells compared EMT and epithelial tumor cells, including splicing events in Ras protein signal transduction and the MAPK signaling pathway, as well as differential expression of the epithelial and mesenchymal lineage-specific splicing regulatory proteins ESRP1 and

RBFOX2, respectively (data not shown). How alternative splicing events and epigenetic alterations interact to promote and maintain the mesenchymal state will be pursued in subsequent studies.

Our results suggest that HDACi treatment with LBH589 in combination with ADT could have efficacy in treating human mCRPC. While HDACi therapy has demonstrated efficacy in the clinic as either a monotherapy or in combination with other anticancer drugs in the treatment of hematological malignancies, HDAC inhibitors as single agents have proven less successful for the treatment of solid tumors. Indeed, the efficacy of LBH589 (Panobinostat) as a single agent in the treatment of CRPC in the clinic to date has not been promising (59, 60). However, our research suggests that major flaws with the clinical trial design, including the use of PSA decrease as a protocol-defined response, as well as the absence of patient stratification based on expression of relevant biomarkers that may predict sensitivity to HDAC inhibitors, likely contributed to the lack of efficacy of LBH589 in the treatment of CRPC in the clinic (59). As our study demonstrates that HDACi treatment enhances AR activation and signaling in prostate tumor cells, PSA levels are likely to either remain constant or even potentially rise as a consequence of LBH589 treatment. Hence, in context of HDACi therapy, PSA readout is not a viable biomarker of therapeutic efficacy, and new biomarkers are needed to identify patients who are likely to respond to HDAC inhibitors. Indeed, we show that HDACi therapy may be effective against a subset of CRPC patients with high expression of HMGA2 and other EMT signature genes. Moreover, as our findings show that genetics only provide part of the picture of tumor heterogeneity and drug resistance, it will be important to look at the gene expression and protein levels of specific biomarkers related to CRPC and treatment resistance in addition to genetic

copy number alterations and mutations. Another challenge in the design of clinical trials is the need for highly sensitive and quantitative assays to determine disease burden, assess sensitivity to different therapies, and quantify the impact of a drug on its drug target. As other groups have demonstrated that *HMGA2* mRNA levels can be detected in the blood in a subset of breast cancer patients by quantitative RT-PCR (61), these "liquid biopsies" may be critical in stratifying prostate cancer patients that are likely to be sensitive to HDACi therapy.

Despite the efficacy of LBH589 as a single treatment in our preclinical model, HDACi therapy alone is likely to not have lasting and curative effects on disease in the clinic, as its cellular target is only a minor population of cells with stem-like and EMT characteristics in the prostate, leaving the differentiated bulk of the tumor for the most part unaffected. As LBH589 treatment promotes the reinstatement of AR signaling and forces EMT and mesenchymal-like tumor cells into a more androgen-dependent, differentiated state, these "re-differentiated' tumor cells will now be susceptible to conventional therapies, including ADT, chemotherapy, and radiotherapy. Hence, combination therapies that combine LBH589 treatment with ADT or AR inhibitors will likely have lasting effects on disease burden and prevent disease relapse by eliminating both the differentiated tumor bulk as well as stem-like, mesenchymal-like tumor cells. As a Phase I/II trial combining LBH589 with bicalutamide therapy in CRPC patients is currently ongoing (NCT00878436), it will be exciting to see if combination therapy is able to prevent disease progression in the human CRPC, which still remains incurable.

References

1. Siegel R, Ma J, Zou Z, Jemal A. Cancer statistics, 2014. CA: a cancer journal for clinicians. 2014;64:9-29.

2. Cheever MA, Higano CS. PROVENGE (Sipuleucel-T) in prostate cancer: the first FDA-approved therapeutic cancer vaccine. Clinical cancer research : an official journal of the American Association for Cancer Research. 2011;17:3520-6.

3. Small EJ, Schellhammer PF, Higano CS, Redfern CH, Nemunaitis JJ, Valone FH, et al. Placebo-controlled phase III trial of immunologic therapy with sipuleucel-T (APC8015) in patients with metastatic, asymptomatic hormone refractory prostate cancer. Journal of clinical oncology : official journal of the American Society of Clinical Oncology. 2006;24:3089-94.

4. Higano CS, Schellhammer PF, Small EJ, Burch PA, Nemunaitis J, Yuh L, et al. Integrated data from 2 randomized, double-blind, placebo-controlled, phase 3 trials of active cellular immunotherapy with sipuleucel-T in advanced prostate cancer. Cancer. 2009;115:3670-9.

5. Kwon ED, Foster BA, Hurwitz AA, Madias C, Allison JP, Greenberg NM, et al. Elimination of residual metastatic prostate cancer after surgery and adjunctive cytotoxic T lymphocyte-associated antigen 4 (CTLA-4) blockade immunotherapy. Proceedings of the National Academy of Sciences of the United States of America. 1999;96:15074-9.

6. Kwon ED, Drake CG, Scher HI, Fizazi K, Bossi A, van den Eertwegh AJ, et al. Ipilimumab versus placebo after radiotherapy in patients with metastatic castration-resistant prostate cancer that had progressed after docetaxel chemotherapy (CA184-043): a multicentre, randomised, double-blind, phase 3 trial. The Lancet Oncology. 2014;15:700-12.

7. Weide B, Martens A, Zelba H, Stutz C, Derhovanessian E, Di Giacomo AM, et al. Myeloid-derived suppressor cells predict survival of patients with advanced melanoma: comparison with regulatory T cells and NY-ESO-1- or melan-A-specific T cells. Clinical cancer research : an official journal of the American Association for Cancer Research. 2014;20:1601-9.

8. Pico de Coana Y, Poschke I, Gentilcore G, Mao Y, Nystrom M, Hansson J, et al. Ipilimumab treatment results in an early decrease in the frequency of circulating granulocytic myeloid-derived suppressor cells as well as their Arginase1 production. Cancer immunology research. 2013;1:158-62.

9. Meyer C, Cagnon L, Costa-Nunes CM, Baumgaertner P, Montandon N, Leyvraz L, et al. Frequencies of circulating MDSC correlate with clinical outcome of melanoma patients treated with ipilimumab. Cancer immunology, immunotherapy : CII. 2014;63:247-57.

10. Taylor BS, Schultz N, Hieronymus H, Gopalan A, Xiao Y, Carver BS, et al. Integrative genomic profiling of human prostate cancer. Cancer cell. 2010;18:11-22.

11. Shah RB, Mehra R, Chinnaiyan AM, Shen R, Ghosh D, Zhou M, et al. Androgen-independent prostate cancer is a heterogeneous group of diseases: lessons from a rapid autopsy program. Cancer research. 2004;64:9209-16.

12. Silan F, Gultekin Y, Atik S, Kilinc D, Alan C, Yildiz F, et al. Combined point mutations in codon 12 and 13 of KRAS oncogene in prostate carcinomas. Molecular biology reports. 2012;39:1595-9.

13. Cho NY, Choi M, Kim BH, Cho YM, Moon KC, Kang GH. BRAF and KRAS mutations in prostatic adenocarcinoma. International journal of cancer Journal international du cancer. 2006;119:1858-62.

14. Edgren H, Kangaspeska S, Kallioniemi O. KRAS oncogene rearrangements and gene fusions: unexpected rare encounters in late-stage prostate cancers. Cancer discovery. 2011;1:12-3.

15. Palanisamy N, Ateeq B, Kalyana-Sundaram S, Pflueger D, Ramnarayanan K, Shankar S, et al. Rearrangements of the RAF kinase pathway in prostate cancer, gastric cancer and melanoma. Nature medicine. 2010;16:793-8.

16. Wang J, Kobayashi T, Floc'h N, Kinkade CW, Aytes A, Dankort D, et al. B-Raf activation cooperates with PTEN loss to drive c-Myc expression in advanced prostate cancer. Cancer research. 2012;72:4765-76.

17. Kwabi-Addo B, Wang J, Erdem H, Vaid A, Castro P, Ayala G, et al. The expression of Sprouty1, an inhibitor of fibroblast growth factor signal transduction, is decreased in human prostate cancer. Cancer research. 2004;64:4728-35.

18. McKie AB, Douglas DA, Olijslagers S, Graham J, Omar MM, Heer R, et al. Epigenetic inactivation of the human sprouty2 (hSPRY2) homologue in prostate cancer. Oncogene. 2005;24:2166-74.

19. Xie D, Gore C, Liu J, Pong RC, Mason R, Hao G, et al. Role of DAB2IP in modulating epithelial-to-mesenchymal transition and prostate cancer metastasis. Proceedings of the National Academy of Sciences of the United States of America. 2010;107:2485-90.

20. Shimada K, Nakamura M, Ishida E, Konishi N. Molecular roles of MAP kinases and FADD phosphorylation in prostate cancer. Histology and histopathology. 2006;21:415-22.

21. Papatsoris AG, Karamouzis MV, Papavassiliou AG. Novel insights into the implication of the IGF-1 network in prostate cancer. Trends in molecular medicine. 2005;11:52-5.

22. Kwabi-Addo B, Ozen M, Ittmann M. The role of fibroblast growth factors and their receptors in prostate cancer. Endocrine-related cancer. 2004;11:709-24.

23. Yart A, Chap H, Raynal P. Phosphoinositide 3-kinases in lysophosphatidic acid signaling: regulation and cross-talk with the Ras/mitogen-activated protein kinase pathway. Biochimica et biophysica acta. 2002;1582:107-11.

24. Ebi H, Costa C, Faber AC, Nishtala M, Kotani H, Juric D, et al. PI3K regulates MEK/ERK signaling in breast cancer via the Rac-GEF, P-Rex1. Proceedings of the National Academy of Sciences of the United States of America. 2013;110:21124-9.

25. Aguirre-Ghiso JA. Models, mechanisms and clinical evidence for cancer dormancy. Nature reviews Cancer. 2007;7:834-46.

26. Wan L, Pantel K, Kang Y. Tumor metastasis: moving new biological insights into the clinic. Nature medicine. 2013;19:1450-64.

27. Psaila B, Lyden D. The metastatic niche: adapting the foreign soil. Nature reviews Cancer. 2009;9:285-93.

28. Mani SA, Guo W, Liao MJ, Eaton EN, Ayyanan A, Zhou AY, et al. The epithelial-mesenchymal transition generates cells with properties of stem cells. Cell. 2008;133:704-15.

29. Celia-Terrassa T, Meca-Cortes O, Mateo F, de Paz AM, Rubio N, Arnal-Estape A, et al. Epithelial-mesenchymal transition can suppress major attributes of human epithelial tumor-initiating cells. The Journal of clinical investigation. 2012;122:1849-68.

30. Morgan TM, Lange PH, Porter MP, Lin DW, Ellis WJ, Gallaher IS, et al. Disseminated tumor cells in prostate cancer patients after radical prostatectomy and without evidence of disease predicts biochemical recurrence. Clinical cancer research : an official journal of the American Association for Cancer Research. 2009;15:677-83.

31. Rhim AD, Mirek ET, Aiello NM, Maitra A, Bailey JM, McAllister F, et al. EMT and dissemination precede pancreatic tumor formation. Cell. 2012;148:349-61.

32. Aguirre-Ghiso JA, Estrada Y, Liu D, Ossowski L. ERK(MAPK) activity as a determinant of tumor growth and dormancy; regulation by p38(SAPK). Cancer research. 2003;63:1684-95.

33. Shibue T, Brooks MW, Inan MF, Reinhardt F, Weinberg RA. The outgrowth of micrometastases is enabled by the formation of filopodium-like protrusions. Cancer discovery. 2012;2:706-21.

34. Mulholland DJ, Kobayashi N, Ruscetti M, Zhi A, Tran LM, Huang J, et al. Pten loss and RAS/MAPK activation cooperate to promote EMT and metastasis initiated from prostate cancer stem/progenitor cells. Cancer research. 2012;72:1878-89.

35. Umbas R, Schalken JA, Aalders TW, Carter BS, Karthaus HF, Schaafsma HE, et al. Expression of the cellular adhesion molecule E-cadherin is reduced or absent in high-grade prostate cancer. Cancer research. 1992;52:5104-9.

36. Sethi S, Macoska J, Chen W, Sarkar FH. Molecular signature of epithelial-mesenchymal transition (EMT) in human prostate cancer bone metastasis. American journal of translational research. 2010;3:90-9.

37. Lang SH, Hyde C, Reid IN, Hitchcock IS, Hart CA, Bryden AA, et al. Enhanced expression of vimentin in motile prostate cell lines and in poorly differentiated and metastatic prostate carcinoma. The Prostate. 2002;52:253-63.

38. Wang S, Gao J, Lei Q, Rozengurt N, Pritchard C, Jiao J, et al. Prostate-specific deletion of the murine Pten tumor suppressor gene leads to metastatic prostate cancer. Cancer cell. 2003;4:209-21.

39. Mulholland DJ, Tran LM, Li Y, Cai H, Morim A, Wang S, et al. Cell autonomous role of PTEN in regulating castration-resistant prostate cancer growth. Cancer cell. 2011;19:792-804.

40. Sun Y, Wang BE, Leong KG, Yue P, Li L, Jhunjhunwala S, et al. Androgen deprivation causes epithelial-mesenchymal transition in the prostate: implications for androgen-deprivation therapy. Cancer research. 2012;72:527-36.

41. Cottard F, Asmane I, Erdmann E, Bergerat JP, Kurtz JE, Ceraline J. Constitutively active androgen receptor variants upregulate expression of mesenchymal markers in prostate cancer cells. PloS one. 2013;8:e63466.

42. Liu G, Sprenger C, Sun S, Epilepsia KS, Haugk K, Zhang X, et al. AR variant ARv567es induces carcinogenesis in a novel transgenic mouse model of prostate cancer. Neoplasia. 2013;15:1009-17.

43. Chan SC, Dehm SM. Constitutive activity of the androgen receptor. Adv Pharmacol. 2014;70:327-66.

44. Sun F, Chen HG, Li W, Yang X, Wang X, Jiang R, et al. Androgen receptor splice variant AR3 promotes prostate cancer via modulating expression of autocrine/paracrine factors. The Journal of biological chemistry. 2014;289:1529-39.

45. Terry S, Beltran H. The many faces of neuroendocrine differentiation in prostate cancer progression. Frontiers in oncology. 2014;4:60.

46. Palmgren JS, Karavadia SS, Wakefield MR. Unusual and underappreciated: small cell carcinoma of the prostate. Seminars in oncology. 2007;34:22-9.

47. Wang HT, Yao YH, Li BG, Tang Y, Chang JW, Zhang J. Neuroendocrine Prostate Cancer (NEPC) progressing from conventional prostatic adenocarcinoma: factors associated with time to development of NEPC and survival from NEPC diagnosis-a systematic review and pooled analysis. Journal of clinical oncology : official journal of the American Society of Clinical Oncology. 2014;32:3383-90.

48. McKeithen D, Graham T, Chung LW, Odero-Marah V. Snail transcription factor regulates neuroendocrine differentiation in LNCaP prostate cancer cells. The Prostate. 2010;70:982-92.

49. Salvatori L, Caporuscio F, Verdina A, Starace G, Crispi S, Nicotra MR, et al. Cell-to-cell signaling influences the fate of prostate cancer stem cells and their potential to generate more aggressive tumors. PloS one. 2012;7:e31467.

50. Beltran H, Rickman DS, Park K, Chae SS, Sboner A, MacDonald TY, et al. Molecular characterization of neuroendocrine prostate cancer and identification of new drug targets. Cancer discovery. 2011;1:487-95.

51. Mallon R, Feldberg LR, Lucas J, Chaudhary I, Dehnhardt C, Santos ED, et al. Antitumor efficacy of PKI-587, a highly potent dual PI3K/mTOR kinase inhibitor. Clinical cancer research : an official journal of the American Association for Cancer Research. 2011;17:3193-203.

52. Beltran H, Yelensky R, Frampton GM, Park K, Downing SR, MacDonald TY, et al. Targeted next-generation sequencing of advanced prostate cancer identifies potential therapeutic targets and disease heterogeneity. European urology. 2013;63:920-6.

53. Gao D, Vela I, Sboner A, Iaquinta PJ, Karthaus WR, Gopalan A, et al. Organoid cultures derived from patients with advanced prostate cancer. Cell. 2014;159:176-87.

54. Domingo-Domenech J, Vidal SJ, Rodriguez-Bravo V, Castillo-Martin M, Quinn SA, Rodriguez-Barrueco R, et al. Suppression of acquired docetaxel resistance in prostate cancer through depletion of notch- and hedgehog-dependent tumor-initiating cells. Cancer cell. 2012;22:373-88.

55. Li Y, Maitah MY, Ahmad A, Kong D, Bao B, Sarkar FH. Targeting the Hedgehog signaling pathway for cancer therapy. Expert opinion on therapeutic targets. 2012;16:49-66.

56. Groth C, Fortini ME. Therapeutic approaches to modulating Notch signaling: current challenges and future prospects. Seminars in cell & developmental biology. 2012;23:465-72.

57. Takahashi-Yanaga F, Kahn M. Targeting Wnt signaling: can we safely eradicate cancer stem cells? Clinical cancer research : an official journal of the American Association for Cancer Research. 2010;16:3153-62.

58. Fusco A, Fedele M. Roles of HMGA proteins in cancer. Nature reviews Cancer. 2007;7:899-910.

59. Rathkopf DE, Picus J, Hussain A, Ellard S, Chi KN, Nydam T, et al. A phase 2 study of intravenous panobinostat in patients with castration-resistant prostate cancer. Cancer chemotherapy and pharmacology. 2013;72:537-44.

60. Rathkopf D, Wong BY, Ross RW, Anand A, Tanaka E, Woo MM, et al. A phase I study of oral panobinostat alone and in combination with docetaxel in patients with castration-resistant prostate cancer. Cancer chemotherapy and pharmacology. 2010;66:181-9.

61. Langelotz C, Schmid P, Jakob C, Heider U, Wernecke KD, Possinger K, et al. Expression of high-mobility-group-protein HMGI-C mRNA in the peripheral blood is an independent poor prognostic indicator for survival in metastatic breast cancer. British journal of cancer. 2003;88:1406-10.